

UNIVERSITÀ DEGLI STUDI DI UDINE

---

Facoltà di Ingegneria

Corso di Dottorato di Ricerca in Ingegneria Industriale e dell'Informazione  
Ciclo XXIV

Tesi di Dottorato di Ricerca

ADAPTATION AND OPTIMIZATION IN MULTI-CARRIER  
MODULATION SYSTEMS

Dottorando

SALVATORE D'ALESSANDRO

Nome del Relatore

Prof. ANDREA TONELLO





*to whom that look ahead...*



# Acknowledgements

*As any journey, the Ph.D. course will leave a sign in my life.*

*During these years, I had the opportunity to know many great persons with whom I have collaborated and had interesting discussions. I further had the chance to travel, to know new places, customs and traditions. All these experiences broadened my horizons and made me wiser.*

*The first acknowledgement goes to my tutor, Prof. Andrea Tonello. I'm grateful to him for giving me the possibility to start this journey, for being a great guide, and for the long time he spent teaching me the Art of Research.*

*A second acknowledgement goes to my WiPli Lab colleagues. Staying with them helped in enhancing my research interest and improving my every day life experience. Among them, a special thank goes to my friend Nicola for all the joy he brought in this journey.*

*Finally, I want to thank my family. Without a shadow of a doubt, it is thanks to their love and support that I didn't give up during hard times.*

*Salvatore D'Alessandro*

*Udine, December 2011*



# Contents

<b>List of Tables</b>	<b>ix</b>
<b>List of Figures</b>	<b>xi</b>
<b>List of Acronyms</b>	<b>xvii</b>
<b>Abstract</b>	<b>xxiii</b>
<b>1 Introduction</b>	<b>1</b>
1.1 Multi-Carrier Modulations: State-of-the-Art . . . . .	1
1.1.1 International Communication Standards based on OFDM	2
1.2 Thesis Objectives and Outline . . . . .	7
1.3 Related Publications . . . . .	10
<b>2 Multi-Carrier Modulations</b>	<b>15</b>
2.1 General Architecture of a Multi-Carrier Modulation . . . . .	15
2.2 FMT Overview . . . . .	17
2.3 OFDM Overview . . . . .	18
2.4 PS-OFDM Overview . . . . .	19
2.5 Definition of SINR and Capacity . . . . .	20

<b>3</b>	<b>Parameters Design in OFDM</b>	<b>23</b>
3.1	Introduction . . . . .	23
3.2	System Model . . . . .	26
3.3	Optimization of the CP Length . . . . .	27
3.3.1	Channel Capacity Criterion . . . . .	28
3.3.2	Suboptimal Optimization Metrics . . . . .	29
3.3.3	Simplified Adaptation of the cyclic prefix (CP) Length . . . . .	31
3.4	Bit-Loading and CP-Length Adaptation . . . . .	32
3.4.1	Procedure 1: Different Constellations . . . . .	33
3.4.2	Procedure 2: Uniform Bit-loading . . . . .	34
3.5	Extension to OFDMA . . . . .	37
3.6	Extension to TDMA . . . . .	39
3.7	Numerical Results In-Home Power Line Channels . . . . .	41
3.7.1	PLC Channel Model . . . . .	41
3.7.2	CP-Length Adaptation . . . . .	43
3.7.3	CP-Length Adaptation and Bit-Loading . . . . .	47
3.7.4	CP-Length Adaptation and Resource Allocation in OFDMA . . . . .	51
3.8	Numerical Results in IEEE 802.11n Channels . . . . .	51
3.8.1	IEEE 802.11n Channel Model . . . . .	52
3.8.2	Main Findings . . . . .	54
<b>4</b>	<b>Parameters Design in PS-OFDM</b>	<b>63</b>
4.1	Introduction . . . . .	63
4.2	System Model . . . . .	65
4.2.1	Notching . . . . .	66
4.3	Adaptive Pulse-Shaped OFDM . . . . .	68
4.3.1	Channel Capacity Criterion . . . . .	68
4.3.2	Maximum Rate Criterion . . . . .	70
4.3.3	Simplified Algorithm . . . . .	70
4.4	Limited Adaptation . . . . .	71
4.5	Numerical Results . . . . .	73
4.5.1	Performance with Adaptation . . . . .	75

---

4.5.2	Limited Adaptation . . . . .	78
4.6	Main Findings . . . . .	81
<b>5</b>	<b>Parameters Design in FMT</b>	<b>83</b>
5.1	Introduction . . . . .	83
5.2	System Model . . . . .	85
5.3	Adaptive Overhead: The Single User Case . . . . .	87
5.3.1	Optimal OH Adaptation . . . . .	87
5.3.2	Simplified OH Adaptation . . . . .	89
5.4	Adaptive Overhead: The Multi User Case . . . . .	90
5.4.1	Sub-channels and OH Adaptation . . . . .	91
5.5	Numerical Results . . . . .	92
5.6	Main Findings . . . . .	97
<b>6</b>	<b>On Power Allocation in Adaptive OFDM</b>	<b>99</b>
6.1	Introduction . . . . .	100
6.2	Problem Formulation . . . . .	102
6.3	Sub-optimal Power Allocation . . . . .	104
6.3.1	True Water-Filling . . . . .	104
6.3.2	Constant Power Water-Filling . . . . .	106
6.3.3	Power Allocation with a Constraint on the PSD . . . . .	106
6.3.4	Iterative Water-Filling . . . . .	107
6.4	Numerical Results . . . . .	109
6.4.1	Baseline System . . . . .	109
6.4.2	Simulation Results . . . . .	110
6.5	Main Findings . . . . .	112
<b>7</b>	<b>Adaptation in Hybrid Filter Bank Schemes</b>	<b>115</b>
7.1	Introduction . . . . .	115
7.2	System Model . . . . .	117
7.2.1	Short Orthogonal FMT (SO-FMT) . . . . .	118
7.2.2	Hybrid FMT . . . . .	119
7.3	Power Allocation . . . . .	122

7.4	Numerical Results . . . . .	124
7.5	Main Findings . . . . .	128
<b>8</b>	<b>Time Slot Design in OFDM-TDMA Systems over Time-Variant PLC Channels</b>	<b>129</b>
8.1	Introduction . . . . .	129
8.2	PHY Layer Description . . . . .	131
8.3	Hybrid MAC Models . . . . .	132
8.3.1	Example of Parameters . . . . .	134
8.4	MAC Procedures . . . . .	134
8.4.1	Network State Learning . . . . .	135
8.4.2	Resource Allocation and Scheduling . . . . .	136
8.5	Simplified Optimization Problem . . . . .	138
8.6	Numerical Results . . . . .	139
8.7	Main Findings . . . . .	143
<b>9</b>	<b>Opportunistic Relaying over PLC Networks</b>	<b>147</b>
9.1	Introduction . . . . .	148
9.2	System Model . . . . .	151
9.3	Opportunistic Decode and Forward . . . . .	152
9.3.1	Capacity Improvements with ODF . . . . .	153
9.3.2	Power Saving with ODF . . . . .	154
9.4	Opportunistic Amplify and Forward . . . . .	161
9.4.1	Capacity Improvements with OAF . . . . .	162
9.4.2	Power Saving with OAF . . . . .	164
9.5	In-Home Power Line Application Scenario . . . . .	165
9.5.1	Topology Model . . . . .	165
9.5.2	Statistical Channel Generator . . . . .	168
9.6	Numerical Results . . . . .	168
9.6.1	Capacity Improvements with ODF and OAF . . . . .	169
9.6.2	Power Saving with ODF and OAF . . . . .	172
9.7	Main Findings . . . . .	177

<b>10</b>	<b>Conclusions</b>	<b>179</b>
<b>11</b>	<b>Appendices</b>	<b>183</b>
11.1	Derivation of the Useful and the Interference Power . . . . .	183
11.2	Capacity Bound Criteria . . . . .	185
11.3	Interference Power in OFDM with Uniform Power Distribution	187
11.4	Fourier Transform of the Raised Cosine Window . . . . .	190
11.5	Karush Kuhn Tucker Conditions . . . . .	192
11.5.1	KKT Conditions for Convex Problems . . . . .	194
11.6	Multi-Carrier Power Minimization under a PSD Constraint . .	195
11.7	Power Allocation in DF for Power Minimization . . . . .	199
11.8	Power Allocation in AF for Capacity Maximization . . . . .	202
<b>Bibliography</b>		<b>203</b>



# List of Tables

1.1	(a) Wireless Standards employing OFDM. . . . .	4
1.2	(b) Wireless Standards employing OFDM. . . . .	5
1.3	Narrow band Power Line Standards employing OFDM. . . . .	6
1.4	Broadband Power Line Standards employing OFDM. . . . .	6
3.1	Channel model parameters for channel classes 1, 5 and 9. . . . .	42
4.1	Average bit-rate comparisons: masked case . . . . .	80
4.2	Average bit-rate comparisons: unmasked case . . . . .	80
8.1	Optimal time slot duration in number of OFDM symbols obtained in the 2-user scenario using <i>Procedures B</i> and <i>C</i> . . . . .	144
8.2	Optimal time slot duration in number of OFDM symbols obtained in the 3 and 4 users scenarios using <i>Procedures B</i> and <i>C</i> . . . . .	144
9.1	Average capacity values using ODF and OAF for the various relay configurations. . . . .	171
9.2	Percentage of satisfied links and mean transmitted power for two-sub-topology networks using DT and ODF. . . . .	177



# List of Figures

1.1	Thesis Structure. . . . .	11
2.1	Multicarrier modulation as a filter bank architecture. . . . .	16
2.2	Generation of the $\ell$ -th symbol in PS-OFDM. . . . .	20
3.1	Mean PL for the top-down power line channel generator. . . . .	43
3.2	RMS-DS CDF for the top-down power line channel generator. . . . .	44
3.3	Capacity $C(\mu)$ as a function of the CP length $\mu$ , for different PLC channels. Markers indicate the CP length obtained from the different criteria proposed in Section 3.3. Subplots (A) and (B) show the results for the best case and the worst case channel impulse responses, respectively. . . . .	45
3.4	CDF capacity-optimal CP. . . . .	46
3.5	Capacity $C(\mu)$ for $\mu$ optimized according to the different criteria presented in Section 3.3 as a function of the channel realization belonging to Class 1. For the sake of readability, only realizations 40 to 50 are shown out of 100 realizations. . . . .	48
3.6	Capacity $C(\mu)$ for $\mu$ optimized according to the different criteria presented in Section 3.3 as a function of the channel realization belonging to Class 5. For the sake of readability, only realizations 40 to 50 are shown out of 100 realizations. . . . .	49

3.7 Capacity  $C(\mu)$  for  $\mu$  optimized according to the different criteria presented in Section 3.3 as a function of the channel realization belonging to Class 9. For the sake of readability, only realizations 40 to 50 are shown out of 100 realizations. . . . . 50

3.8 Capacity  $C(\mu)$  for bit loading with Algorithm 1.2 of Section 3.4.1 and  $\mu$  optimized according to the capacity-optimal criterion (3.6) and three different numbers of OFDM sub-channels  $M \in \{384, 768, 1536\}$ . For a comparison,  $C(\mu)$  for bit loading and  $\mu = 209$  (corresponding to 5.57 *mus*) is also included. The channels employed are the BeC channels of the three used classes. 56

3.9 Bit rate  $R(\mu, b)$  from (3.19) as a function of CP length  $\mu$  and constellation size  $2^b$  for uniform bit-loading. Markers are results from Algorithms 2.1 and 2.2 from Section 3.4.2. The BeC channel of Class 5 is assumed. The system uses 384 sub-channels. 57

3.10 Aggregate and single user rate using bit-loading as a function of the CP length. The OFDMA system has  $N_U=4$  users and  $M=384$  sub-channels. The users experience channels belonging to different classes. Markers are results from Algorithm 3 from Section 3.5 with different sets of CP length  $\mathcal{M}$ . . . . . 58

3.11 Capacity as a function of the CP length for 100 class B channel realizations. The distance between transmitter and receiver is set to 10 *m*. . . . . 59

3.12 Optimal CP CDF for channels of class B, C, D, E, and F. The distances between transmitter and receiver are set to 3 *m*, 10 *m*, 30 *m*, and 60 *m*. . . . . 60

3.13 CCDF of capacity using the CP computed with (3.6), with the  $\mu_{99\%}$ , and with a fixed CP equal to 0.8  $\mu s$ . The channel classes used are the B,D, and F. The distances between the transmitter and the receiver are set to 3 *m*, 10 *m*, and 30 *m*. . . . . 61

3.14	CCDF of aggregate network rate obtained using the proposed algorithms for both OFDMA and TDMA. The set of used CPs has been set equal to $\mathbb{P} = \{0.8\mu s\}$ for the baseline system, and equal to $\mathbb{P} = \{\mu_{99\%}^B, \mu_{99\%}^C, \mu_{99\%}^D, \mu_{99\%}^E, \mu_{99\%}^F\}$ for the proposed system. . . . .	62
4.1	Power spectral density mask for the transmitted signal. With a carrier spacing of 24.414 $kHz$ (as in HPAV), the number of sub-channel in 0-37.5 $MHz$ is equal to 1536, of which 619 are notched. . . . .	67
4.2	Search <i>paths</i> to maximize capacity as a function of $(\mu, \alpha)$ . . . . .	72
4.3	(a) Ten channel impulse response realizations, and (b) their frequency responses and the average path loss. . . . .	74
4.4	Cardinality of $\mathbb{K}_{on}$ for the four paths. . . . .	76
4.5	Bit-rate as a function of overhead parameters restricted to the search paths in Fig. 4.2 for 100 channel realizations. The signal to noise ratio (SNR) is equal to 40 dB. . . . .	77
4.6	Bit-rate gain given by the adaptation of the guard interval (GI) and of the roll-off (RO) for 100 channel realizations obtained with the rate maximization criterion along the four paths in Fig. 4.2. The SNR has been set to (a): 20 $dB$ , (b): 40 $dB$ , and (c): 60 $dB$ . The gains have been computed w.r.t. the bit-rate obtained when using the constant values $\mu=5.6 \mu s$ . . . . .	78
4.7	Bit-rate for the Unmasked case using the search <i>path</i> A. (a): OFDM. (b): PS-OFDM. The SNR is equal to 40 dB. . . . .	79
4.8	Guard interval CDF using the search <i>path</i> A. . . . .	81
5.1	Capacity as a function of the OH duration for 100 class B channel realizations using orthogonal frequency division multiplexing (OFDM) (top), and filtered multitone (FMT) (bottom). The distance between transmitter and receiver is set equal to 10 $m$ . . . . .	93

5.2	Optimal OH CDF for FMT considering each single channel class, and all the classes together. The distances between transmitter and receiver are set equal to 3 m, 10 m, 30 m, and 60 m.	94
5.3	Optimal CP CDF for OFDM considering channels of class B, C, D, E, and F. The distances between transmitter and receiver are set equal to 3 m, 10 m, 30 m, and 60 m. . . . .	95
5.4	CCDF of capacity using OFDM and FMT with optimal and limited OH adaptation. The used channel classes are the B,D, and F. The distances between the transmitter and the receiver are set equal to 3 m, 10 m, and 30 m. . . . .	96
5.5	CCDF of the aggregate network rate obtained using the limited overhead (OH) adaptation for both OFDMA and FMT-FDMA. Also plotted are the CCDFs obtained using FMT-FDMA and OFDMA with a fixed OH of 0.8 $\mu s$ . . . . .	97
6.1	Capacities according to the different power allocation algorithms presented in Section 6.3. The SNR is fixed to 6.6 dB. For the sake of readability, only realizations 40 to 50 are shown out of 100. . . . .	111
6.2	Capacities according to the different power allocation algorithms presented in Section 6.3. The SNR is fixed to 26.6 dB. For the sake of readability, only realizations 40 to 50 are shown out of 100. . . . .	112
6.3	Capacities according to the different power allocation algorithms presented in Section 6.3. The SNR is fixed to 46.6 dB. For the sake of readability, only realizations 40 to 50 are shown out of 100. . . . .	113
6.4	Optimal CP CDF for the three proposed power allocation algorithms. The SNR equals {6.6,26.6,46.6} dB. . . . .	114
7.1	Hybrid FMT scheme. . . . .	121

7.2	Achievable rate CCDF obtained using short orthogonal FMT (SO-FMT), adaptive OFDM (A-OFDM), and OFDM with a fixed CP of $0.8 \mu s$ . The employed channel classes are the B,C, and D. The distance between transmitter and receiver is set to $10 m$ , $30 m$ , and $60 m$ . . . . .	126
7.3	CDF of the average transmitted power obtained using the proposed power minimization (PM) algorithm. The comparison is among hybrid FMT (H-FMT) that adopts the optimal and the sub-optimal switching criterion, OFDM with CP equal to $0.8\mu s$ , and A-OFDM. . . . .	127
8.1	Frame Structure. . . . .	133
8.2	Considered network. . . . .	135
8.3	<b>Two users scenario:</b> Aggregate rates for the 4 scheduling Procedures and single user rates for the <i>Procedure C</i> . Labels (a)-(d) denote <i>Procedures A-D</i> respectively . . . . .	140
8.4	<b>Two users scenario:</b> Aggregate rates for the 4 scheduling Procedures and single user rates for the <i>Procedure C</i> . Labels (a)-(d) denote <i>Procedures A-D</i> respectively. . . . .	141
8.5	<b>Three users scenario:</b> Aggregate rates for the 4 scheduling Procedures and single user rates for the <i>Procedure C</i> . Labels (a)-(d) denote <i>Procedures A-D</i> respectively . . . . .	142
8.6	<b>Four users scenario:</b> Aggregate rates for the 4 scheduling Procedures and single user rates for the <i>Procedure C</i> . Labels (a)-(d) denote <i>Procedures A-D</i> respectively. . . . .	143
8.7	Aggregate bit-rate loss for the two-user scenario with <i>Procedures B</i> and <i>C</i> . . . . .	145
8.8	Aggregate bit-rate loss for the three-user scenario with <i>Procedures B</i> and <i>C</i> . . . . .	146
9.1	Cooperative relay system model. . . . .	151
9.2	DT, DF and AF modes and corresponding time slots allocation. . . . .	152

9.3	Illustration of the proposed power allocation algorithm to minimize the power required by DF to reach a target rate $R$ . . . .	159
9.4	Network Architecture with two sub-topologies. . . . .	166
9.5	CCDFs of capacity obtained using opportunistic decode and forward (ODF) with the relay located according to the various described configurations. The CCDF of capacity obtained assuming DT mode when no relay is connected to the network is also reported. $M=1536$ . . . . .	170
9.6	CCDFs of capacity obtained using OAF with the relay located according to the various described configurations. The CCDF of capacity obtained assuming direct transmission (DT) mode when no relay is connected to the network is also reported. $M=1536$ . . . . .	172
9.7	Power required by ODF to achieve a target rate $R$ equal to 20 Mbit/s when using the optimal decode and forward power allocation algorithm and the proposed one. The optimal solution is obtained considering the interior-point algorithms starting from two points, i.e., the power distribution given by the PSD mask and the solution of the proposed algorithm. . . . .	173
9.8	CDF of the total transmitted power using ODF, and the direct transmission. $M=1536$ . . . . .	175
9.9	CDF of the total transmitted power using (left) ODF and (right) OAF. $M=62$ . . . . .	176
11.1	Raised cosine window. . . . .	190
	□	

# List of Acronyms

**ADSL** asymmetric DSL

**AF** amplify and forward

**A-OFDM** adaptive OFDM

**AP** access point

**ARIB** Association of Radio Industries and Businesses

**AWGN** additive white Gaussian noise

**BDB** backbone derivation box

**BPLC** broadband PLC

**CB** circuit breaker

**CCDF** complementary CDF

**CDF** cumulative distribution function

**CCo** central coordinator

**CENELEC** European Committee for Electrotechnical Standardization

**CP** cyclic prefix

- DB** derivation box
- DBPSK** differential binary PSK
- DDB** destination derivation box
- DF** decode and forward
- DFT** discrete Fourier transform
- DMT** discrete multitone
- DQPSK** differential quadrature PSK
- DSL** digital subscriber line
- DT** direct transmission
- DVB** digital video broadcasting
- DWMT** discrete wavelet multi-tone modulation
- EMC** electromagnetic compatibility
- FB** filter bank
- FCC** Federal Communications Commission
- FDD** frequency division duplexing
- FDMA** frequency division multiple access
- FFT** fast Fourier transform
- FMT** filtered multitone
- GI** guard interval
- HDTV** high definition television
- HD-PLC** high definition PLC

- H-FMT** hybrid FMT
- HPGP** HomePlug GP
- HPAV** HomePlug AV
- ICI** inter-carrier interference
- IDFT** inverse discrete Fourier transform
- IF** interpolation factor
- IFFT** inverse fast Fourier transform
- IP** integer programming
- ISI** inter-symbol interference
- ISM** industrial, scientific and medical
- ITU** International Telecommunication Union
- IWF** iterative water-filling
- KKT** Karush-Kuhn-Tucker
- LOS** line of sight
- LP** linear programming
- LPTV** linear periodically time variant
- LTE** long term evolution
- MAC** medium access control
- MC** multi-carrier
- MCM** multi-carrier modulation
- MMSE** minimum mean square error

- MIMO** multiple input multiple output
- MP** main panel
- MPM** main panel multi-sub-topology
- MPS** main panel single sub-topology
- NB** narrow band
- NLOS** non line of sight
- OAF** opportunistic amplify and forward
- ODF** opportunistic decode and forward
- OFDM** orthogonal frequency division multiplexing
- OFDMA** orthogonal frequency division multiple access
- OH** overhead
- ORA** outlet relay arrangement
- PAM** pulse amplitude modulation
- PF** post fix
- PHY** physical
- PL** path loss
- PLC** power line communication
- PM** power minimization
- PRIME** power line intelligent metering evolution
- PS** pulse shaped
- PS-OFDM** pulse shaped OFDM

- PSD** power spectral density
- QAM** quadrature amplitude modulation
- QoS** quality of service
- QPSK** quadrature phase shift keying
- RDB** random derivation box
- RF** radio frequency
- RM** rate maximization
- RO** roll-off
- RRCOS** root-raised-cosine
- SDB** source derivation box
- SINR** signal to interference plus noise ratio
- SIR** signal to interference ratio
- SNR** signal to noise ratio
- SOHO** small office home office
- SO-FMT** short orthogonal FMT
- TDMA** time division multiple access
- UHF** ultra high frequency
- UMTS** universal mobile telecommunications system
- UPA** universal power line association
- VDSL** very high speed digital subscriber lines
- VHF** very high frequency

**WAVE** wireless access in vehicular environments

**WF** water-filling

**WLAN** wireless local area network

**WMAN** wireless metropolitan area network

**WPAN** wireless personal area network

**xDSL** x-digital subscriber line

# Abstract

In recent years, we have assisted to the dawn of many wireless and wire-line communication technologies that have adopted multi-carrier modulation (MCM) at the physical layer.

The basic idea of MCMs is to transmit a high rate data stream by dividing it into low rate streams that are used to generate low rate signals each modulated at a given carrier frequency. The use of MCMs allows for dividing the frequency selective channel into a set of narrow-band sub-channels. Consequently, the transmitted signal experiences, in each sub-channel, a quasi flat frequency response, so that, the equalization task simplifies to a sub-channel filtering.

In addition to the simplification of the equalization task, there are several benefits deriving from the use of MCMs that, in general, depend upon the considered transmission medium. The most important ones are the low complexity digital implementation, and the possibility to use bit and power loading algorithms that allow for nearly achieving channel capacity or for minimizing the transmitted power.

Several MCM schemes have been presented in the literature in the last fifty years. Some examples are: the orthogonal frequency division multiplexing (OFDM); the pulse shaped OFDM (PS-OFDM); the filtered multitone (FMT).

These technologies have to be reliable, namely, they have to be able to work over all the possible conditions (channel realizations) that can occur over a given medium. Consequently, these are designed according to a “worst” case

criterion, i.e., they adopt a set of parameters that allow the system to achieve, also in bad conditions, acceptable performances. However, in some cases, this design criterion is not optimum. In fact, the practice shows that there exist scenarios, where the channel slowly changes, in which the performances can be significantly improved by letting the systems to adapt their parameters to the experienced conditions.

The first topic that we consider in this thesis is the optimization of the parameters and the resource allocation in adaptive-MCM systems whose received signals are affected by interference caused by signaling over a dispersive channel. To be more precise, we propose parameter design criteria for adaptive OFDM, PS-OFDM, and FMT. For these schemes, we also propose resource allocation algorithms that target the achievable rate maximization or the transmitted power minimization. The extension of the parameters adaptation to the multi-user case is also considered. In particular, resource allocation algorithms for the downlink case of networks using frequency division multiple access (FDMA) and time division multiple access (TDMA) is discussed. We also consider the case where the modulation scheme is adapted to the channel condition. More precisely, we make use of a hybrid architecture that depending on the channel conditions wisely switches between adaptive-OFDM and FMT so that the transmitted power is minimized. Extensive numerical results are shown for typical wireless LAN and in-home broadband power line channels.

Besides the use of adaptive MCM schemes, another interesting advanced communication technique that allows for improving the performances of a MCM system is the use of relaying techniques. This is the context where we find the second objective of the thesis, i.e., to propose optimal resource allocation algorithms to provide capacity improvements, power savings, and coverage extension in two hops relay networks where half duplex time division relay protocols are used. More precisely, we consider a network where the communication between the source and the destination node follows an opportunistic protocol, namely, the relay is used whenever it allows w.r.t. the direct transmission (DT): for capacity improvements; or for power saving. Opportunistic decode and forward (ODF), and opportunistic amplify and for-

---

ward (OAF) are considered. At the physical layer, we assume the use of MCM. Under these assumptions, we find the optimal resource allocation, namely, the optimal power and time slot allocation, between the source and the relay nodes that maximizes capacity, or minimizes the total transmitted power for both ODF and OAF. We apply the proposed algorithms to the in-home power line scenario. According to this scenario, the relay can only be placed in accessible points of the network, i.e., in the main panel, or in derivation boxes, or in outlets. For each opportunistic protocol, we also determine the best relay position that maximizes capacity or minimizes the transmitted power.



# Introduction

In this thesis, we focus on the optimization of multi-carrier modulation (MCM) schemes. In particular, we provide parameters design criteria and advanced resource allocation techniques for adaptive MCM schemes considering both the single and the multi user scenarios. We also propose optimal resource allocation algorithms to provide capacity improvements, power savings, and coverage extension in two hops relay networks.

In this chapter, we set the background of the thesis, and we give an overview of its organization. More precisely, in Section 1.1, we introduce the MCM basics, and we glance at the respective state-of-the-art systems. Then, in Section 1.2, we set the objectives of the thesis and we give a brief outline. Finally, in Section 1.3, we list the papers where part of the work of this thesis has been published.

## 1.1 Multi-Carrier Modulations: State-of-the-Art

The basic idea of MCM is to transmit a high rate data stream by dividing it into low rate streams that are used to generate low rate signals each modulated at a given frequency carrier. The idea dates back to the late fifties [1], when Doelz et al. proposed to use MCM to simplify the equalization task for signaling over broadband frequency selective channels. The use of MCM allows in fact for dividing the frequency selective channel into a set of narrow-band sub-channels.

Consequently, the transmitted signal experiences, in each sub-channel, a quasi flat frequency response, so that, when no inter-carrier interference (ICI) is present, the equalization task reduces to sub-channel filtering. In some cases the equalizer consists of a single tap filter.

In addition to the simplification of the equalization task, there are several benefits deriving from the use of MCMs that, in general, depend upon the considered transmission medium. We can, however, say that the most important ones are the low complexity digital implementation, and the possibility to use bit and power loading algorithms that allow for nearly achieving channel capacity or for minimizing the transmitted power required to grant a certain target rate.

Several MCM schemes have been presented in the literature in the last fifty years. Some examples are [2, Ch. 5]: orthogonal frequency division multiplexing (OFDM) [3]; pulse shaped OFDM (PS-OFDM) [4]; filtered multi-tone (FMT) [5]; discrete wavelet multi-tone modulation (DWMT) [6].

OFDM is certainly the most used MCM scheme since, in 1971, Weinstein and Ebert presented its efficient implementation through the use of a discrete Fourier transform (DFT), and simple single tap zero forcing sub-channel equalization [3]. In 1989, Kalet showed that the optimal power distribution in an OFDM like system is given by the water-filling distribution, furthermore, he showed that the use of M-quadrature amplitude modulation (QAM) constellations could allow the system to achieve bit-rate values close to channel capacity (9 dB far). From then on, OFDM has been adopted in several communication standards. In the following, we list them.

### **1.1.1 International Communication Standards based on OFDM**

#### **Wireless Communication Standards**

Wireless communication devices are nowadays pervasively deployed to offer a broad variety of services, e.g., mobile communications, area and sensor networking, terrestrial video broadcasting, and so on. Wireless devices used for non commercial applications can work in the frequency bands internationally

reserved for industrial, scientific and medical (ISM) purposes other than communication [7].

It is well known that wireless channels are harsh media inasmuch they are strongly frequency selective and, in general, they are also time variant. Due to these characteristics, OFDM has been adopted in several high bit-rate wireless communications standards. It has been used as one of the modulation schemes of the IEEE 802.11 [8] standard, which has been conceived for wireless local area network (WLAN) communications. Furthermore, it has been also adopted for: wireless metropolitan area networks (WMANs), in the IEEE 802.16 standard [9] - also known as WiMax; wireless private area networks (WPANs), in the IEEE 802.15.3c [10] (also known as 60 GHz communications), and in the WiMedia [10] standard; cellular communications, in the 3GPP long term evolution (LTE) standard [11]; digital video broadcasting (DVB), in the ETSI EN 302755 standard [12, 13]; wireless access in vehicular environments (WAVE), in the IEEE 802.11p standard [14]. Tables 1.1 and 1.2 reports some physical layer information of the standards listed above. The acronyms used in the table are defined in page xiii.

## **Wireline Communication Standards**

We restrict the description of the wireline communication devices that adopt MCM to the ones that work over power lines and copper telephone lines.

Power line communications (PLCs) make use of the existing power line grid to transmit data signals. There is a broad range of applications for which PLCs have been or are being used, e.g., remote metering, command and control of domestic systems, small office home office (SOHO) communication, and recently, smart grid applications. Essentially, the PLC devices can be grouped into two categories, i.e., narrow band (NB) and broadband (B) PLC devices, according to the bit-rate that they can achieve. The NB-PLC devices have been developed with the scope of offering indoor (home automation, e.g., command and control as, heating, lighting, security, and in general all the household devices) and outdoor (smart grid, e.g., the safe integration and the management of renewable energy sources, the management of plug-in electric vehicles, the

Table 1.1: (a) Wireless Standards employing OFDM.

	<b>WiMedia</b>	<b>IEEE 802.15.3c</b>	<b>IEEE 802.11</b>	<b>IEEE 802.16</b>
<b>Modulation</b>	Multiband OFDM in 3.1-10.6 GHz	Multiband OFDM in 58.3-64.8 GHz	OFDM	OFDM
<b>Bandwidth</b>	14 bands of 528 MHz	4 bands of 2.592 GHz	20, 40 MHz	5, 10 MHz
<b>Carriers</b>	128 per band	512 per band	64 128	512 1024
<b>RF</b>	function of used band	function of used band	2.4, 5 GHz	2.4 GHz
<b>CP</b>	303 ns	24.69, 49.38 $\mu$ s	0.8, 0.4 $\mu$ s	1/32 1/16 1/8 1/4 carriers
<b>Constellation</b>	QPSK	QPSK, 16-QAM 64-QAM	2, 4, 16, 64 QAM	QPSK 16-QAM 64-QAM
<b>Bit-rate</b>	53-480 Mbit/s	59 Mbit/s to 6.3 Gbit/s	11-600 Mbit/s	up to 70 Mbit/s
<b>MIMO</b>	NO	NO	up to 4 antennas	up to 4 antennas
<b>Range</b>	<10 m	<10 m	<100 m	some Km

management of demand side and demand response to allow the customers to collaborate in order to adapt the production and the delivery of electricity and to achieve energy efficiency and saving) command and control services. The frequency bands dedicated from standardization organizations to NB-PLC devices vary among the continents. In the EU, the European Committee for Electrotechnical Standardization (CENELEC) issued the standard EN 50065 that specifies four frequency bands for communications over PL networks [2]. The band A (3–95 kHz) is reserved exclusively to power utilities. The band B (95–125 kHz) can be used for any application. The band C (125–140 kHz) is dedicated to in-home networking systems. The band D (140–148.5 kHz) is reserved to alarm and security systems. In the US and Asia, the regulation is different. Federal Communications Commission (FCC) and Association of Radio Industries and Businesses (ARIB) allow PLC devices to work in the band 3–500 kHz. Nowadays, there are two NB-PLC technologies developed

Table 1.2: (b) Wireless Standards employing OFDM.

	<b>DVB</b>	<b>3GPP LTE</b>	<b>IEEE 802.11p</b>
<b>Modulation</b>	OFDM	OFDM	OFDM
<b>Bandwidth</b> [MHz]	6, 7, 8	1.25 up 20	10, 20
<b>Carriers</b>	2048 8192	128 2048	32 64
<b>RF</b>	VHF/UHF	2.6 GHz	5.9 GHz
<b>CP</b>	1/32 1/16 1/8 1/4 carriers	4.9-16.67 $\mu$ s	-
<b>Constellation</b>	QPSK 16-QAM 64-QAM	QPSK 16-QAM 64-QAM	2, 4, 16, 64 QAM
<b>Bit-rate</b> [Mbit/s]	4-32	up to 100	3-54
<b>MIMO</b>	NO	4x2, 2x2 2x1, 1x1	-
<b>Range</b>	some Km	up to 30 Km	up to 1 Km

for smart grid applications whose physical (PHY) layer is based on OFDM. These are the ERDF G3 PLC [15], and the power line intelligent metering evolution (PRIME) [16]. As one of the earlier NB-PLC technologies developed before G3-PLC and PRIME is the DLC 2000 by iAd GmbH (see references in [17]). It is interesting to note that both G3-PLC and PRIME solutions have been selected as baseline technologies for the PHY layer specification of the upcoming IEEE P1901.2 and International Telecommunication Union (ITU)-T G.hnem NB-PLC standards. In Table 1.3, we report the OFDM NB-PLC technologies developed for smart grid applications.

BPLC devices have been developed with the aim of offering SOHO and multimedia services. Essentially, broadband PLC (BPLC) devices work on the frequency band 2-30 MHz. The most relevant examples of commercial devices are the ones compliant with the HomePlug AV (HPAV) [18] and the high definition PLC (HD-PLC) [2, Chapter 7] industry standards. It is interesting to note that both solutions, i.e., HPAV and HD-PLC, have been used as baseline for the PHY layer specification of the IEEE P1901 standard [19], which has been released in December 2010. Finally, we note that also ITU is delivering

Table 1.3: Narrow band Power Line Standards employing OFDM.

	<b>G3-PLC</b>	<b>G3-PLC/(FCC)</b>	<b>PRIME</b>
<b>Modulation &amp; band</b>	OFDM CENELEC A 3-95 kHz	OFDM FCC 3-500 kHz	OFDM CENELEC A 3-95 kHz
<b>Carriers</b>	128	128	256
<b>CP</b>	75 $\mu$ s	25 $\mu$ s	192 $\mu$ s
<b>Constellation</b>	DQPSK DBPSK	DQPSK DBPSK	D8PSK DQPSK DBPSK
<b>Bit-rate (up-to)</b>	34 kbit/s	240 kbit/s	128 kbit/s

the ITU-T G.hn standard for in-home communications over power lines, coax, and phone lines [20]. Table 1.4 summarizes the PHY layer characteristics of OFDM based BPLC devices.

Table 1.4: Broadband Power Line Standards employing OFDM.

	<b>HPAV</b>	<b>HD-PLC</b>	<b>IEEE P1901</b>	<b>ITU T G.hn</b>
<b>Modulation &amp; band</b>	OFDM 2-30 MHz	WOFDM (DWMT) 2-28 MHz	OFDM WOFDM (DWMT) 2-28, 2-60 MHz	OFDM up to 100 MHz
<b>Carriers</b>	1536	512	OFDM: 1536, 3072 WOFDM: 512, 1024	up to 4096
<b>CP</b>	5.56, 7.56 $\mu$ s	0	OFDM: 5.56, 7.56 $\mu$ s WOFDM: 0	8 values
<b>Constellation</b>	bit-loading up to 1024-QAM	bit-loading up to 32-PAM	bit-loading OFDM: up to 4096-QAM WOFDM: up to 32-PAM	bit-loading up to 4096-QAM
<b>Bit-rate (up-to)</b>	200 Mbit/s	190 Mbit/s	540 Mbit/s	1 Gbit/s

As it is well known, copper telephone lines of the access network are used to

offer Internet connectivity between a central office and the houses. There is a family of technologies referred to as x-digital subscriber lines (xDSLs) that have been conceived to solve the last mile problem. These are specified by the ITU G.99x family standard. Essentially, all the xDSL technologies adopt OFDM<sup>1</sup> at the physical layer. Among the xDSL technologies, asymmetric DSL (ADSL) is certainly the most known inasmuch it is used to deliver Internet connectivity to residential consumers. ADSL devices work in the frequency band 0-1.1 MHz (up to 2.2 MHz in ADSL2+) and use 256 sub-channels (512 in ADSL2+). Furthermore, they adopt bit-loading (up to 15 bits per QAM symbol) and spectrum balancing algorithms. Depending on the the employed technology, and on the channel characteristics - e.g. cable length, bundle size, and so on - ADSL modems offer variable bit-rate from 1 to 24 Mbit/s in downstream, and from 1 up to 3.3 Mbit/s in upstream. The duplexing is accomplished via frequency division duplexing (FDD). The interested reader can refer to [21,22] for further information regarding DSL.

## 1.2 Thesis Objectives and Outline

As we have seen in the previous section, many communication technologies adopt MCM to transmit data over channels that are frequency selective and/or time variant. These technologies have to be reliable, namely, they have to be able to work over all the possible conditions (channel realizations) that can occur over a given medium. Consequently, these are designed according to a “worst” case criterion, i.e., they adopt a set of parameters that allow the system to achieve acceptable performances also in bad conditions. However, in some cases, this design criterion is not optimum. In fact, the practice shows that there exist scenarios where the performances can be significantly improved by letting the system to adapt its parameters to the experienced conditions. In this context, we can find a first objective of the thesis, i.e., provide design criteria and advanced resource allocation algorithms for adaptive MCM schemes for both the single and the multi user scenarios.

---

<sup>1</sup>To be precise, xDSL technologies adopt discrete multitone (DMT) modulation. Roughly speaking, it differs from OFDM only for the digital implementation.

Besides the use of adaptive MCM schemes, another interesting advanced communication technique that allows for improving the performances of a MCM system is the use of cooperative schemes based on relaying. In this context, we find the second objective of the thesis, i.e., to propose optimal resource allocation algorithms that provide capacity improvements, power savings, and coverage extension in two hops relay networks.

An outline of the thesis follows.

## **Adaptive MCMs**

A MCM can be viewed as a filter bank (FB) scheme where, at the transmitter, a set of  $M$  parallel data signals, each transmitted with a certain power, is interpolated by a factor  $N$ , filtered by a prototype pulse, modulated and transmitted over the channel. The receiver can be viewed as an analysis FB where the signals are demodulated, filtered by a prototype pulse, sampled, and finally equalized. The prototype pulses and the modulation functions, e.g., exponential or cosine, lead to the various forms of multi-carrier modulation, e.g., OFDM, PS-OFDM, FMT. From the previous description, it is evident that, for each MCM scheme, to obtain a given target - i.e., the achievable rate maximization or the transmitted power minimization - it is possible to optimally allocate the resources, namely, to optimize its physical layer parameters, e.g., number of carriers, interpolation factor, transmitted power distribution, and so on. When the optimization is done in the setup phase of the modems, and it is updated according to the channel condition, the MCM becomes adaptive. It is worth noting that, in general, when the system works over dispersive channels, the received signal will be affected by interference. In such a case, the resource allocation becomes complex inasmuch the corresponding optimization problem is generally not convex. In these cases, a simplified solution is desirable to make it feasible in real conditions.

The first topic that we consider in this thesis is the resource allocation problem when the MCM system is affected by interference caused by signaling over a dispersive channel. The discussion is organized as follows. In Chapter 2, we describe the general MCM system model through a FB architecture, and

we derive OFDM, PS-OFDM and FMT. Then, in Chapters 3-5, we discuss optimal and simplified solutions for the adaptation of the parameters. More precisely, in Chapter 3, we focus on adaptive-OFDM, whereas in Chapters 4 and 5, we respectively focus on adaptive-PS-OFDM and on adaptive-FMT. The extension of the parameters adaptation to the multi-user case is also considered. In particular, resource allocation algorithms for the downlink case of networks using FDMA and TDMA is discussed. In Chapters 3-5, we suppose to uniformly transmit the power across the MCM sub-channels. The only constraint we consider regards the power spectral density (PSD) mask. This is a practical assumption since it represents what it is done over commercial systems. Nevertheless, in Chapter 6, we consider the general case where the previous assumption is relaxed. In Chapter 7, we extend the adaptation to the modulation scheme. To be more precise, we make use of a hybrid architecture that depending on the channel conditions wisely switches between adaptive-OFDM and FMT to minimize the total transmitted power.

Differently from Chapters 3-7, where we consider the resource allocation problem in stationary channels, in Chapter 8, we consider cyclostationary channel and noise. In such a scenario, we compute the optimal time slot duration assuming an OFDM-TDMA system. It is determined for various amounts of overhead required by the PHY layer.

Each chapter contains extensive numerical results that compare the performances of the baseline systems (the ones specified by some communication standards) with the ones of the proposed solutions. The numerical results are obtained employing WLAN or BPLC channel models.

## **Relaying Techniques**

The second topic that we consider in this thesis is the resource allocation in networks that make use of a relay to improve the point to point communication performance. More precisely, in Chapter 9, we investigate the use half duplex time division relay protocols to provide capacity improvements, power savings, and coverage extension in home power line communication (PLC) networks. We consider a network where the communication between the source

and the destination node follows an opportunistic protocol, namely, the relay is used whenever it allows w.r.t. the direct transmission (DT): for capacity improvements; or for power saving. Opportunistic decode and forward (ODF), and opportunistic amplify and forward (OAF) are considered. At the physical layer, we assume the use of multi-carrier modulation. Under these assumptions, we find the optimal resource allocation, namely, the optimal power and time slot allocation, between the source and the relay nodes that maximizes capacity, or minimizes the total transmitted power for both ODF and OAF. Furthermore, since over in-home PLC networks, the relay can only be placed in accessible points of the network, i.e., in the main panel, or in derivation boxes, or in outlets, for each opportunistic protocol, we also determine the best relay position that maximizes capacity or minimizes the transmitted power. Finally, the conclusions follow in Chapter 10. Fig. 1.1 summarizes the thesis structure.

### 1.3 Related Publications

The main results of the work presented in this thesis have been the subject of publications. Some of the papers in the list present extensions of the application of the algorithms described in this thesis.

#### Journal Papers

- [J-1] S. D'Alessandro, A. Tonello, "Capacity Improvements and Power Saving for Multi-Carrier Schemes through Opportunistic Relaying in Home Power Line Networks," *submitted to IEEE Trans. on Commun.*, Jul. 2011.
- [J-2] S. D'Alessandro, A. Tonello, L. Lampe, "Adaptive Pulse-Shaped OFDM with Application to In-Home Power Line Communications", *Telecommunication Systems Journal*, Springer, DOI 10.1007/s11235-010-9410-3, Jan. 2011.
- [J-3] A. Tonello, S. D'Alessandro, L. Lampe, "Cyclic Prefix Design and Allocation in Bit-Loaded OFDM over Power Line Communication Channels,"

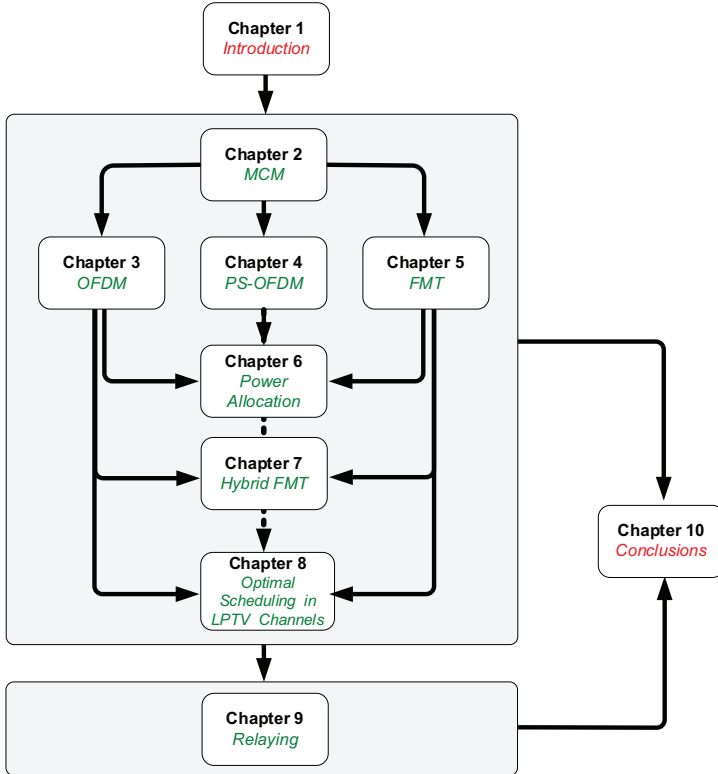


Figure 1.1: Thesis Structure.

*IEEE Trans. on Commun.*, vol. 58, no. 11, pp. 3265 - 3276, Nov. 2010.

## Conference Papers

[C-1] A. M. Tonello, S. D'Alessandro, F. Versolatto, "Comparison of Narrow-Band OFDM PLC Solutions and I-UWB Modulation over Distribution Grids," *proc. of IEEE Smart Grid Commun. Conf.*, Bruxelles, Belgium, Oct. 2011.

[C-2] A. M. Tonello, M. Antoniali, F. Versolatto, and S. D'Alessandro, "Power

- Line Communications for In-Car Application: Advanced Transmission Techniques,” *proc. of the 5th Biennial Workshop on DSP for In-Vehicle Systems*, Kiel, Germany, Sep. 2011.
- [C-3] S. D’Alessandro, A. M. Tonello, F. Versolatto, “Power Savings with Opportunistic Decode and Forward over In-Home PLC Networks,” *proc. of IEEE Int. Sym. on Power Line Commun. and Its App.*(ISPLC 2011), Udine, Italy, Apr. 2011.
- [C-4] N. Moret, S. D’Alessandro, A. M. Tonello, “Performance of FMT with Time Confined and Frequency Confined Pulses over Indoor Radio Channels,” *proc. of IEEE IFIP Wireless Days* (WD 2010), Venice, Italy, Oct. 2010.
- [C-5] S. D’Alessandro, N. Moret, A. M. Tonello, “Green Hybrid FMT for WLAN Applications,” *proc. of IEEE IFIP Wireless Days* (WD 2010), Venice, Italy, Oct. 2010.
- [C-6] A. M. Tonello, F. Versolatto, S. D’Alessandro, “Opportunistic Relaying in In-Home PLC Networks,” *proc. of IEEE Global Commun. Conf.* (GLOBECOM 2010), Miami, Florida, Dec. 2010.
- [C-7] S. D’Alessandro, N. Moret, A. M. Tonello, “Hybrid Filtered Multitone Architecture for WLAN Applications,” *proc. of IEEE Personal, Indoor and Mobile Radio Commun. Conf.* (PIMRC 2010), Istanbul, Turkey, Sep. 2010.
- [C-8] S. D’Alessandro and A. M. Tonello, “Adaptive Filter Bank Modulation for Next Generation Wireless in Home Networks,” *proc. of ICST MOBILIGHT 2010*, Barcelona, Spain, Jun. 2010.
- [C-9] S. D’Alessandro, A. M. Tonello, L. Lampe, “On Power Allocation in Adaptive Cyclic Prefix OFDM,” *proc. of IEEE Int. Sym. on Power Line Commun. and Its App.* (ISPLC 2010), Rio de Janeiro, Brazil, Mar. 2010.

- [C-10] S. D'Alessandro, A. M. Tonello, L. Lampe, "Improving WLAN Capacity Via OFDMA and Cyclic Prefix Adaptation," *proc. of IEEE IFIP Wireless Days (WD 2009)*, Paris, France, Dec. 2009.
- [C-11] P. Pagani, M. Tlich, A. Zeddani, A. Tonello, F. Pecile, S. D'Alessandro, G. Mijic, K. Kriznar, "PLC Transfer Function for the OMEGA ICT Project," *proc. of ICT Mobile Summit 2009*, Santander, Spain, Jun. 2009.
- [C-12] A. M. Tonello, J.A. Cortés, S. D'Alessandro, "Optimal Time Slot Design in an OFDM-TDMA System over Power-Line Time-Variant Channels," *proc. of IEEE Int. Sym. on Power Line Commun. and Its App. (ISPLC 2009)*, Dresden, Germany, Mar. 2009.
- [C-13] S. D'Alessandro, A. M. Tonello, L. Lampe, "Bit-Loading Algorithms for OFDM with Adaptive Cyclic Prefix Length in PLC Channels," *proc. of IEEE Int. Sym. on Power Line Commun. and Its App. (ISPLC 2009)*, Dresden, Germany, Mar. 2009.
- [C-14] A. M. Tonello, S. D'Alessandro, L. Lampe, "Bit, Tone and Cyclic Prefix Allocation in OFDM with Application to In-Home PLC," *IEEE IFIP Wireless Days (WD 2008)*, Dubai, United Emirates, Dec. 2008.

### **Contribution to the EU-FP7 Omega Project Deliverables**

- [D-1] Seventh Framework Programme: Theme 3 ICT-213311 OMEGA, Deliverable D3.1, "State-of-the-Art, Application Scenario and Specific Requirements for PLC," Mar. 2008.
- [D-2] Seventh Framework Programme: Theme 3 ICT-213311 OMEGA, Deliverable D3.2, "PLC Channel Characterization and Modelling," Jan. 2009.
- [D-3] Seventh Framework Programme: Theme 3 ICT-213311 OMEGA, Deliverable D3.4, "Performance Report of Optimized PHY Algorithms," May 2010.

- [D-4] Seventh Framework Programme: Theme 3 ICT-213311 OMEGA, Deliverable D3.5, “Optimized MAC Algorithms and Performance Report,” May 2010.
- [D-5] Seventh Framework Programme: Theme 3 ICT-213311 OMEGA, Deliverable D2.6, “Performance Report of Cross Layer Mechanisms,” Dec. 2009.

The previous deliverables can be downloaded from  
[www.ict-omega.eu/publications.html](http://www.ict-omega.eu/publications.html).

## Multi-Carrier Modulations

In this chapter, we offer a review of a general multi-carrier (MC) modulation system looking at it as a FB architecture. The presented scheme will be used in the rest of the thesis as the MC system model. Following the approach in [2, Ch. 5], from the general scheme, we derive three MC modulation architectures, namely, the filtered multitone (FMT), the orthogonal frequency division multiplexing (OFDM), and the PS-OFDM. We glance at their efficient implementation, and we compute the signal to interference plus noise ratio (SINR) that is experienced at the receiver side when the signal is transmitted over a dispersive channel. Finally, we define the system capacity.

### 2.1 General Architecture of a Multi-Carrier Modulation

We consider a complex baseband MCM scheme. In MC modulations, a high data rate signal is split into  $M$  parallel signals  $a^{(k)}(\ell N)$ , where  $k$  is the sub-channel index ( $k = 0, \dots, M - 1$ ), and  $N$  is the symbol period in samples. The symbol period in seconds is given by  $NT$ , where  $T$  is the sampling period (see Fig. 2.1)<sup>1</sup>. The parallel signals, which in general are streams of data symbols belonging to a complex constellation, e.g.,  $M$ -ary QAM, are interpolated by a factor  $N$ , namely  $N-1$  zeros are introduced, filtered with a sub-channel

---

<sup>1</sup>In order to simplify the notation, through this work, we omit the dependence of the signals from  $T$

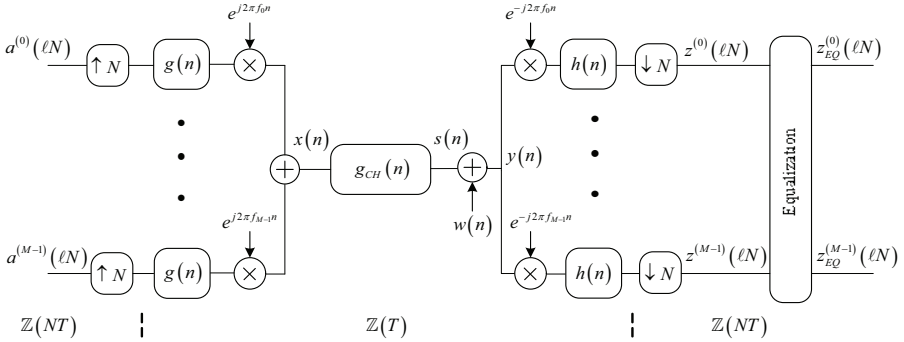


Figure 2.1: Multicarrier modulation as a filter bank architecture.

pulse  $g(n)$ , exponentially modulated, summed and transmitted over the channel. The transmitted signal can be therefore expressed as the output of the synthesis FB as follows

$$x(n) = \sum_{k=0}^{M-1} \sum_{\ell \in \mathbb{Z}} a^{(k)}(\ell N) g(n - \ell N) e^{j2\pi f_k n}, \quad (2.1)$$

where  $f_k = k/M$  is the normalized frequency at which the sub-channel signal is modulated. The interpolation factor  $N$  is equal to  $M + \beta$  samples, where  $\beta$  denotes the OH factor. When  $N = M$  the bank is critically sampled, whereas the bank is non-critically sampled when  $N > M$ .

The signal is transmitted over a channel with impulse response

$$g_{CH}(n) = \sum_{p=0}^{v-1} \alpha_p \delta(n - p), \quad (2.2)$$

where  $\alpha_p$  denote the complex channel gains, and  $\delta(n) = 1$  for  $n = 0$ , and zero otherwise.

From Fig. 2.1, we note that the additive noise is denoted as  $w(n)$ , and the received signal as  $y(n)$ . The receiver consists of an analysis FB with sub-channel pulse  $h(n)$ . Before the equalization block, the FB outputs are sampled

at rate  $1/N$  to obtain

$$\begin{aligned} z^{(k)}(\ell N + \Delta) &= \sum_{n \in \mathbb{Z}} y(n) h(\ell N + \Delta - n) e^{-j \frac{2\pi k n}{M}} \\ &= H^{(k)}(\beta, \Delta) a^{(k)}(\ell N) + I^{(k)}(\beta, \ell N + \Delta) + \eta^{(k)}(\ell N + \Delta), \end{aligned} \quad (2.3)$$

where  $-\mu \leq \Delta \leq \mu$  is the synchronization time phase. Furthermore,  $H^{(k)}(\beta, \Delta)$  is the amplitude of the data of interest,  $I^{(k)}(\beta, \ell N + \Delta)$  is the overall interference that includes the inter-symbol interference (ISI) and the ICI. ISI and ICI occur when transmitting over a frequency-selective channel, or the FB is not orthogonal. As discussed in the following, the factor  $H^{(k)}(\beta, \Delta)$  and the interference term  $I^{(k)}(\beta, \ell N + \Delta)$  are functions of the OH factor  $\beta$ . Finally,  $\eta^{(k)}(\ell N + \Delta)$  represents the noise contribution.

In [2, Ch. 5], it is shown that the FB implementation can be realized in an efficient way, i.e., the transmitter consists of an inverse fast Fourier transform (IFFT) followed by a cyclic extension and a low rate sub-channel filtering with pulses that are obtained by polyphase decomposition of the synthesis prototype pulse, whereas the receiver consists of a filtering by an interpolation pulse that is obtained by a polyphase decomposition of the analysis prototype pulse, a periodic repetition stage and an  $M$ -point fast Fourier transform (FFT).

In the following, we briefly show that several MC schemes can be derived from the FB architecture of Fig. 2.1. More precisely, in Sections 2.2, 2.3, and 2.4, we respectively derive the FMT, the OFDM, and the PS-OFDM systems.

## 2.2 FMT Overview

FMT is a discrete time implementation of a multi-carrier system where sub-carriers are uniformly spaced and the sub-channel pulses are identical. FMT modulation has been proposed for transmission over broadband frequency selective channels in very high speed digital subscriber lines (VDSL) [5], in wireless [23, 24] and in power line [25, 26] scenarios. In FMT the sub-channel period  $N \geq M$  and the analysis pulse is matched to the synthesis pulse. An important characteristic of FMT is that the prototype pulse is designed to

obtain high frequency confinement. A conventional choice is to use a root-raised-cosine (RRCOS) prototype pulse with roll-off equal to  $\alpha$  [27], so that the modulated sub-channel pulse is

$$g(n) = rrcos\left(\frac{n}{N}\right) = \frac{N}{4} \text{sinc}\left(\alpha \frac{n}{N} + 0.25\right) \text{sinc}\left(\pi \left(\frac{n}{N} - 0.25\right)\right) + \frac{N}{4} \text{sinc}\left(\alpha \frac{n}{N} - 0.25\right) \text{sinc}\left(\pi \left(\frac{n}{N} + 0.25\right)\right), \quad (2.4)$$

where  $\text{sinc}(n) = \sin(\pi n)/(\pi n)$ .

### 2.3 OFDM Overview

OFDM can be viewed as an FMT where the synthesis and the analysis pulses are rectangular windows respectively defined as

$$g(n) = \text{rect}\left(\frac{n}{N}\right), \quad h(n) = \text{rect}\left(-\frac{n + \mu}{M}\right), \quad (2.5)$$

where  $\text{rect}(n/A) = 1$  for  $n = 0, \dots, A - 1$  and zero otherwise. The synthesis window has duration  $N = M + \mu$  samples. Therefore, the OH factor is equal to  $\beta = \mu$  samples.

The efficient implementation of OFDM [3] at the transmitter comprises the following steps: compute an  $M$ -point IFFT of the block of data symbols  $a^{(k)}$  ( $\ell N$ ) for  $k = 0, \dots, M - 1$ ; then, add a guard interval in the form of a CP that equals the last  $\mu$  IFFT output coefficients. At the receiver: acquire symbol synchronization, discard the CP, and apply an  $M$ -point FFT on the remaining  $M$  samples.

As it is well known, if the length of the channel impulse response does not exceed the CP length by more than one, i.e.,  $\mu \geq \nu - 1$ , the system will be orthogonal such that the received symbol will be neither affected by ISI nor by ICI [28], and therefore the equalization reduces to a simple single tap sub-channel equalizer. Nevertheless, this advantage has to be paid in terms of an SNR penalty, because of the discard of the CP samples at the receiver, and a raw transmission rate loss that is equal to  $M/(M + \mu)$ .

Another drawback with OFDM is that the sub-channels have a sinc frequency response that decays as  $1/f$  and has the first side lobe only 13 dB down compared to the main lobe. This translates in poor sub-channel confinement, and consequently, in a large transmission rate penalty when notching is required to enable coexistence with other systems. An example is given by BPLC devices that work in the frequency band 2-30 MHz. This frequency band also contains sub-bands dedicated to other communication systems, as for example amateur radio. Hence, in order to allow coexistence a number of sub-channels have to be switched off such that the transmitted signal occupies a certain spectrum with notches, and thus there is a transmission rate loss.

## 2.4 PS-OFDM Overview

To overcome the poor sub-channel frequency confinement, a window better than the rectangular window can be deployed. The scheme is referred to as pulse shaped OFDM (PS-OFDM) [4]. In PS-OFDM the synthesis prototype pulse is a Nyquist window. A common choice is to use a raised cosine window with roll-off  $\alpha$  samples [4]. It can be defined as follows

$$g(n) = \begin{cases} \frac{1}{2} + \frac{1}{2} \cos\left(\frac{\pi}{\alpha} (|n - n_1| - n_2)\right), & n \in [0, \alpha] \cup [N, N + \alpha], \\ 1 & n \in ]\alpha, N[, \\ 0 & \textit{otherwise}, \end{cases} \quad (2.6)$$

with  $n_1 = (N + \alpha)/2$  and  $n_2 = n_1 - \alpha$ . With  $\alpha = 0$ , we obtain the conventional OFDM scheme. In PS-OFDM, the symbol period increases by  $\alpha$  samples w.r.t. OFDM assuming that we still deploy a guard interval of length  $\mu$  samples, i.e.,  $N = M + \mu + \alpha$ . Consequently, the OH factor is equal to  $\beta = \mu + \alpha$ , and the transmission rate loss is equal to  $M/(M + \mu + \alpha)$  that turns out to be higher than that of OFDM.

It can be shown [2, Ch. 5] that the efficient implementation of PS-OFDM comprises an  $M$ -point IFFT, followed by a CP extension of  $\mu + \alpha$  samples, and a cyclic post fix (PF) extension of  $\alpha$  samples. Then a windowing with a window of duration  $N + \alpha$  samples is applied. Finally, the signal to be

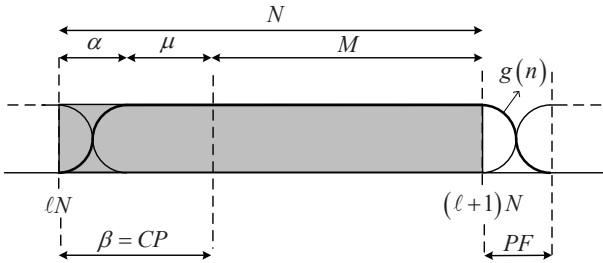


Figure 2.2: Generation of the  $\ell$ -th symbol in PS-OFDM.

transmitted is obtained by overlapping and adding the first  $\alpha$  samples of each symbol with the last  $\alpha$  samples of the preceding symbol (see Fig. 2.2).

In PS-OFDM, the analysis pulse is a rectangular window of duration  $M$  samples that is defined as

$$h(n) = \text{rect}\left(-\frac{n + \beta}{M}\right). \quad (2.7)$$

Again, if  $\mu \geq \nu - 1$  the system will be orthogonal.

## 2.5 Definition of SINR and Capacity

Looking at (2.3), we can express the signal to interference plus noise ratio (SINR) in the  $k$ -th sub-channel output of a MCM scheme, for a given channel realization, as follows

$$\text{SINR}^{(k)}(\beta, \Delta) = \frac{P_U^{(k)}(\beta, \Delta)}{P_\eta^{(k)} + P_I^{(k)}(\beta, \Delta)}, \quad (2.8)$$

with

$$P_U^{(k)}(\beta, \Delta) = \left|H^{(k)}(\beta, \Delta)\right|^2 E\left[\left|a^{(k)}(\ell N)\right|^2\right] = \left|H^{(k)}(\beta, \Delta)\right|^2 P_a^{(k)}, \quad (2.9)$$

$$P_I^{(k)}(\beta, \Delta) = E \left[ \left| I^{(k)}(\beta, \ell N + \Delta) \right|^2 \right], \quad (2.10)$$

$$P_\eta^{(k)} = E \left[ \left| \eta^{(k)}(\ell N + \Delta) \right|^2 \right]. \quad (2.11)$$

The relations (2.9)-(2.11), respectively, denote the useful, the interference, and the noise power terms on sub-channel  $k$ , and  $E[\cdot]$  is the expectation operator. Furthermore, in (2.9),  $P_a^{(k)}$  represents the statistical power of the signal transmitted on sub-channel  $k$ , i.e.,  $P_a^{(k)} = E \left[ \left| a^{(k)}(\ell N) \right|^2 \right]$ . A detailed derivation of the power terms can be found in the Appendix 11.1.

In order to evaluate the performance of a MCM system, we evaluate the capacity<sup>2</sup> assuming single tap sub-channel equalization and using the formula for parallel Gaussian channels, i.e., the noise and the input signals are independent and Gaussian distributed such that the interference signals are also Gaussian [29].

Therefore, if  $K_{ON}(\beta)$  is the set of active sub-channels that allows fulfilling a certain transmission mask, the capacity in bit/s is

$$C(\beta, \Delta) = \frac{1}{(M + \beta)T} \sum_{k \in K_{ON}(\beta)} \log_2 \left( 1 + \frac{SINR^{(k)}(\beta, \Delta)}{\Gamma} \right), \quad (2.12)$$

where  $\Gamma$  represents a gap factor to take into account practical implementation constraints [30], [31]. It should be noted that the set  $K_{ON}(\beta)$  depends on the OH parameter inasmuch also the prototype filters rely on it.

From (2.12), it is important to note that to maximize the capacity of a multi-carrier system, if we set the prototype pulse and thus the modulation scheme, we need to optimize several parameters, i.e., the OH factor, the synchronization time phase  $\Delta$ , the transmitted power distribution  $P_a^{(k)}$  with  $k = 0, \dots, M - 1$ , and the number of sub-channels  $M$ .

In the following chapters we will focus on the parameters optimization of OFDM (Chapters 3), of PS-OFDM (Chapter 4), and of FMT (Chapter 5).

---

<sup>2</sup>In this work, the term ‘‘capacity’’ is used to denote the maximal data rate achievable under some typical system constraints, e.g., a power spectral density constraint.



## Parameters Design in OFDM

The usual approach when designing an orthogonal frequency division multiplexing (OFDM) system, is to dimension the length of the cyclic prefix (CP) equal to the length of a typical “bad” (i.e., long) channel impulse response, so that both inter-symbol and inter-carrier interference are avoided for all channel realizations. However, such an approach does not maximize system capacity. It (a) wastes channel resources for relatively short channel impulse response realizations and (b) it is not necessarily optimal to completely eliminate interference. In this chapter, we study the problem of designing the CP length for OFDM systems in a capacity-optimal way. To this end, we first present optimal and simplified metrics suitable to maximize capacity. Then, we apply those metrics and propose practical resource (bit-loading) algorithms that include CP-length adaptation. We present numerical results for in-home broadband PLC (BPLC) and IEEE 802.11n channels. These show that significant gains can be obtained considering the CP-length adaptation w.r.t. a system that deploys a fixed value of CP. Finally, extensions to the multi-user scenario with frequency and time division multiplexing access are also considered.

### 3.1 Introduction

OFDM has become the most popular transmission technology for communication over wide band channels that exhibit frequency selectivity. It has been

adopted for many wireless, subscriber line, and PLC systems. The key feature of OFDM is the orthogonalization of the frequency selective channel into parallel sub-channels (each described by a scalar gain) through the use of a CP and DFT operations [3]. Thus, simple one-tap equalization per sub-channel can be used at the receiver, and channel capacity can be approached by practical implementation of the water-filling principle using bit and power loading of OFDM sub-channels [30]. Furthermore, the partition of sub-channels among multiple users realizes a form of multiple access known as orthogonal frequency division multiple access (OFDMA) [32].

To maximize system performance, resources have to be optimally allocated. Assuming the use of finite size constellations, the resource allocation problem in OFDM(A) is also known as the bit, power, and sub-channel allocation problem [30–34]. The optimization and adaptation of the CP is usually not considered. Instead, the conventional approach is to use a fixed CP that is longer than the maximum channel duration such that neither inter-symbol interference (ISI) nor inter-carrier interference (ICI) occurs at the receiver side. However, this approach is power and bandwidth inefficient. The insertion of the CP requires additional transmission energy and introduces a loss in transmission rate of  $M/(M+\mu)$ , where  $M$  is the number of OFDM sub-channels and  $\mu$  is the CP length in number of samples. Since the channel impulse response realizations may be different for different links and/or may vary with time, adaptation of  $\mu$  to the specific channel realization is beneficial. Furthermore, the CP length does not necessarily need to be equal to the channel duration to maximize capacity. That is, allowing for a controlled amount of ISI and ICI in order to reduce  $\mu$ , we may overall improve performance. It is therefore reasonable to consider the optimization of the CP length.

The case of a CP shorter than the channel impulse response has been considered in a number of early and more recent works on OFDM, cf. e.g. [35] and references therein. Viterbo and Fazel [36] compute the interference power due to channel echoes exceeding the CP and consider the application of per sub-channel equalization and coding to mitigate the effect of interference in a digital terrestrial TV broadcasting setting. Following this work, Seoane et

al. [29] provide simulative evidence that interference can well be modeled as additive white Gaussian noise (AWGN), and study the performance degradation due to interference using the suburban hilly universal mobile telecommunications system (UMTS) channel model. In [35], the effect of CP length on OFDM capacity is studied for single-user wireless OFDM systems using 20 MHz bandwidth and operating at 3.7 GHz in urban and suburban environments. However, the mentioned works do not consider CP adaptation to the channel realizations. CP adaptation has been investigated in [37] for OFDM-based WLAN systems. It is suggested to choose the CP length twice the channel delay spread. As we will show in this work, this criterion is not reliable unless the channel attenuation, and therefore the receiver-side signal to noise ratio (SNR), is taken into account.

In this chapter we report a comprehensive analysis of the CP-length optimization problem. In particular, we consider joint CP-length, bit, and sub-channel allocation for single user and multi-user OFDM systems. For numerical examples we choose PLC and WLAN scenarios and consider parameters according to state-of-the-art systems, e.g., the PLC HomePlug AV (HPAV) or universal power line association (UPA) [18,19,38] and the wireless IEEE 802.11 standards. Due to the electromagnetic compatibility (EMC) normative [8,39], these systems transmit signals with a constant power spectral density (PSD) level in the used frequency band. This assumption is also made in this chapter. Note that, even though PLC transceivers are static, similarly to the WLAN environment, the PLC channel between two nodes is time-varying due to load-impedance variations and loads being plugged into or removed from the power grid. Hence, different channel realizations are experienced even for a fixed pair of nodes, and CP-length adaption is potentially beneficial. This said, we expect significant channel variations not being frequent with respect to data rates, and thus adaptation of the CP length is deemed practically feasible. As it will be clarified in the following, the previous observation holds also true for WLAN devices that work in a certain scenario e.g., small office or large open space. This is because, as it will be explained in the following, a given scenario is represented by a channel class and it is sufficient to adapt the CP

to the channel class.

The chapter is organized as follows. After recalling the system model in Section 3.2, we first show, in Section 3.3.1, that assuming a power spectral density constraint at the transmitter side and signaling over a frequency selective channel, the achievable rate (capacity) is a function of the CP length. Therefore, the optimal CP length can be determined by maximizing the capacity. We consider other simplified metrics in Section 3.3.2, namely two metrics derived from an upper and a lower capacity bound and a metric based on the channel delay spread. Then, in Section 3.3.3, we propose to adapt the CP length by choosing it from a finite set of values. The set of CP values is pre-computed from the statistical analysis of the channel, specifically the analysis of the cumulative distribution function (CDF) for the optimal CP length. In Section 3.4, the joint bit-loading and CP-length adaptation problem is addressed. We consider both bit-loading with distinct constellations and uniform bit-loading (identical constellations) on all the sub-channels. In Sections 3.5 and 3.6, we extend the idea of optimizing the CP length to the multiuser OFDMA and TDMA scenarios. Extensive numerical results for an HPAV like [18] and for 802.11 OFDM systems are reported in Sections 3.7 and 3.8 respectively. They show that significant gains can be obtained by the appropriate adaptation of the CP length to the channel conditions. Finally, Section 3.8.2 summarizes the main findings.

## 3.2 System Model

We assume an OFDM scheme (see Section 2.3)) with  $M$  sub-channels (or tones), and a CP length of  $\mu = N - M$  samples, where  $N$  is the normalized sub-channel symbol period (OFDM symbol duration in samples) assuming a sampling period  $T$ . The normalized sub-carrier frequencies are defined as  $f_k = k/M$ , for  $k = 0, 1, \dots, M - 1$ . According to equation (2.2), the OFDM signal is transmitted over a channel that has an equivalent discrete time complex impulse response of duration of  $\nu$  samples. We assume that  $\nu \leq M$ , so that the channel is not longer than the useful OFDM symbol duration. However, the channel duration may exceed the CP length. As a result, according to formula

(2.8), assuming perfect symbol synchronization, we have that the SINR for sub-channel  $k$  is equal to

$$\text{SINR}^{(k)}(\mu) = \frac{P_{\text{U}}^{(k)}(\mu)}{P_{\eta}^{(k)} + P_{\text{I}}^{(k)}(\mu)}, \quad (3.1)$$

As shown in Appendix 11.1, assuming i.i.d. zero mean data symbols, and perfect synchronization ( $\Delta = 0$ ), the useful signal power and the interference power can be expressed as

$$P_{\text{U}}^{(k)}(\mu) = P_a^{(k)} \left| \sum_{p=0}^{\nu-1} \alpha_p r_{gh}^{(k,k)}(-p) \right|^2, \quad (3.2)$$

$$P_{\text{I}}^{(k)}(\mu) = P_{\text{tot}}^{(k)}(\mu) - P_{\text{U}}^{(k)}(\mu), \quad (3.3)$$

$$P_{\text{tot}}^{(k)}(\mu) = \sum_{q \in \mathbb{Z}} \sum_{i \in \mathbb{K}_{\text{on}}} P_a^{(i)} \left| \sum_{p=0}^{\nu-1} \alpha_p r_{gh}^{(i,k)}(qN - p) \right|^2, \quad (3.4)$$

where  $P_a^{(k)}$  is the power of the constellation in sub-channel  $k$  and  $\mathbb{K}_{\text{on}} \subseteq \{0, \dots, M-1\}$  is the set of indexes associated to the active sub-channels, i.e.,  $P_a^{(k)} > 0$  for  $k \in \mathbb{K}_{\text{on}}$ . To evaluate the expressions in (3.2)-(3.4), we make the usual assumption that rectangular windows of length  $N$  and  $M$  are used as OFDM synthesis and analysis prototype pulses (see eq. (2.5)). It follows directly from (3.2)-(3.4) that if the CP is longer than the channel duration, i.e.,  $\mu \geq \nu - 1$ , the interference power is null and the useful power term corresponds to the absolute square value of the  $k$ -th DFT output of the channel response multiplied by the power of the constellation. Therefore, increasing the CP length beyond the channel length does not increase the SINR since the interference is zero for  $\mu \geq \nu - 1$ .

### 3.3 Optimization of the CP Length

In this section, we present criteria for the optimization of the CP length. Throughout this chapter, we assume the application of a PSD mask constraint for the transmitted signal. The PSD mask determines the set of active OFDM

sub-channels  $\mathbb{K}_{\text{on}}$ , while the remaining sub-channels are switched off (notched) in order to fulfill regulations and coexistence norms [19, 39, 40]. Furthermore, the PSD mask is such that the transmitted power is uniformly distributed over the sub-channels in  $\mathbb{K}_{\text{on}}$ , i.e.,  $P_a^{(k)} = P_a, \forall k \in \mathbb{K}_{\text{on}}$ .

We start with the criterion for capacity-optimal CP length (Section 3.3.1). Since the evaluation of this criterion turns out to be computationally complex, we then propose three sub-optimal metrics to select the CP length (Section 3.3.2). Furthermore, we propose a method to design a small set of CP values over which we perform adaptation (Section 3.3.3).

### 3.3.1 Channel Capacity Criterion

In order to evaluate the impact of the CP length on the system performance we consider the achievable data rate assuming parallel Gaussian channels. That is, we assume independent and Gaussian distributed input signals, which renders ISI and ICI also Gaussian (see also [29]). Furthermore, we stipulate the use of single tap sub-channel equalization, i.e., no attempt is made to suppress ISI and ICI, which is the very reason for the widespread use of OFDM. Then, the maximal data rate is

$$C(\mu) = \frac{1}{(M + \mu)T} \sum_{k \in \mathbb{K}_{\text{on}}} \log_2 \left( 1 + \frac{\text{SINR}^{(k)}(\mu)}{\Gamma} \right) \text{ [bit/s]}, \quad (3.5)$$

where  $\Gamma$  represents a gap factor accounting for practical modulation and channel coding [30, 31]. For  $\Gamma = 1$ ,  $C(\mu)$  is the system capacity, and, in slight abuse of notation, we refer to the CP design such that (3.5) is maximized for any given  $\Gamma \geq 1$  as capacity-optimal CP. That is, the capacity-optimal CP length (in number of samples) is given by

$$\mu_{\text{opt}} = \underset{0 \leq \mu < \nu}{\text{argmax}} \{C(\mu)\} . \quad (3.6)$$

The evaluation of the argument of (3.6) is computationally demanding because it requires the SINR and a sum-log computation for each CP value. Therefore, lower-complexity solutions are desirable.

### 3.3.2 Suboptimal Optimization Metrics

We introduce three suboptimal metrics suitable to adjust the CP length.

#### Capacity Bound Criteria

The first two simplifications for the optimization of the CP length are obtained by lower and upper bounding the capacity in (3.5). For this purpose, we assume white noise with  $P_\eta^{(k)} = P_\eta$ . Details of the derivations are provided in Appendix 11.2.

The capacity can be lower bounded by

$$C(\mu) > \frac{M_{\text{on}}}{(M + \nu)T} \log_2 \left( \frac{P_{\text{U},\min}}{P_\eta} \right) - \frac{M_{\text{on}}}{(M + \nu)T} \log_2 \left( \frac{(M + \mu)\Gamma}{(M + \nu)M_{\text{on}}} \sum_{k \in \mathbb{K}_{\text{on}}} \left( 1 + \frac{P_1^{(k)}(\mu)}{P_\eta} \right) \right), \quad (3.7)$$

where  $M_{\text{on}} = |\mathbb{K}_{\text{on}}|$  is the cardinality of  $\mathbb{K}_{\text{on}}$  and  $P_{\text{U},\min} = \min_{k \in \mathbb{K}_{\text{on}}, \mu} \{P_{\text{U}}^{(k)}(\mu)\}$ . The corresponding optimal CP length is given by

$$\mu_{\text{opt}} = \underset{0 \leq \mu < \nu}{\text{argmin}} \{ (M + \mu) (M_{\text{on}} P_\eta + P_1(\mu)) \}, \quad (3.8)$$

where  $P_1(\mu) = \sum_{k \in \mathbb{K}_{\text{on}}} P_1^{(k)}(\mu)$  denotes the total interference power.

Although the bound on capacity is not necessarily tight, metric (3.8), derived from this bound, yields performance close to that achieved with the optimal metric (3.6) as shown by numerical results in Section 3.7.

A capacity upper bound can be found as

$$C(\mu) \leq \frac{M_{\text{on}}}{\Gamma(M + \mu)T} \log_2(e) \overline{\text{SINR}}(\mu), \quad (3.9)$$

where the average SINR

$$\overline{\text{SINR}}(\mu) = \frac{1}{M_{\text{on}}} \sum_{k \in \mathbb{K}_{\text{on}}} \text{SINR}^{(k)}(\mu) \quad (3.10)$$

has been used. The resulting CP-length criterion is

$$\mu_{\text{opt}} = \underset{0 \leq \mu < \nu}{\operatorname{argmax}} \left\{ \frac{\overline{\text{SINR}}(\mu)}{M + \mu} \right\}. \quad (3.11)$$

The suboptimal criteria (3.8) and (3.11) have a computational advantage over (3.6). First, the computation of the logarithm is avoided. Second, (3.8) only requires the evaluation of the interference power for different values of  $\mu$  instead of the computation of the SINRs as metric (3.6). When all  $M$  sub-channels are used, metric (3.8) is simple to compute since the total interference power can be evaluated as (see Appendix 11.3)

$$P_I(\mu) = NP_a \sum_{p=0}^{\nu-1} |\alpha_p|^2 \left[ M - \frac{(M - (p - \mu) S_{p-\mu})^2}{M} \right], \quad (3.12)$$

with  $S_i = 1$  for  $i \geq 0$  and zero otherwise.

### Delay Spread Criterion

The third simplification that we propose for the adjustment of the CP length is based on the evaluation of the root mean square (rms) delay spread  $\sigma_{\text{ch}}$  for a given channel realization  $g_{\text{ch}}(n)$ , which is given by [41, pp. 77-78]

$$\sigma_{\text{ch}} = \sqrt{\frac{\sum_{p=0}^{\nu-1} (pT - m_{\text{ch}})^2 \alpha_p^2}{\sum_{p=0}^{\nu-1} \alpha_p^2}}, \quad (3.13)$$

where

$$m_{\text{ch}} = T \frac{\sum_{p=0}^{\nu-1} p \alpha_p^2}{\sum_{p=0}^{\nu-1} \alpha_p^2}. \quad (3.14)$$

Considering that the significant fraction of energy of the channel impulse response is captured within  $\theta \sigma_{\text{ch}}$  for some  $\theta > 0$  [41], the CP length can be adjusted according to

$$\mu_{\text{opt}} = \theta \sigma_{\text{ch}} / T. \quad (3.15)$$

This approach is very attractive for its computational simplicity. In fact,  $\mu_{\text{opt}} = 2\lceil\sigma_{\text{ch}}/T\rceil$  ( $\lceil.\rceil$  denotes the ceiling operator) has been used in [37] for CP-length adjustment for IEEE 802.11a OFDM systems. Nevertheless, as it is discussed in more detail in the next subsection, the factor  $\theta$  should be adapted as a function of SNR and thus of the attenuation introduced by the channel, in order to balance the contributions from interference (ISI and ICI) and background noise to the overall SINR.

### 3.3.3 Simplified Adaptation of the CP Length

The adaptation of the CP requires that for each channel realization the receiver computes the CP length according to one of the criteria above described and feeds back the selected value to the transmitter. One attractive possibility to reduce computational cost and the amount of feedback is to choose the CP length from a small set of pre-determined values. Several OFDM specifications, e.g., the power line HPAV standard [18], have opted for such an approach. To determine an appropriate set of CP values, we propose a method based on the evaluation of the CDF of the capacity-optimal CP length according to (3.6).

Considering the PLC or the wireless IEEE 802.11 channel model (more details follow in Sections 3.7.1, 3.8.1), which classify channels according to different classes, it is found that the optimal CP length varies relatively little for members of the same class, but significantly between members of different classes. Hence, we propose, for a given channel class, to choose a single value of CP length for all channel realizations.

The specific lengths are chosen to be the value of  $\mu$  for which the CDF of (3.6) is 99%. We denote these values as  $\mu_{\text{opt,CLASS}}^{(99\%)}$ , i.e., the 99th percentile of the capacity-optimal  $\mu_{\text{opt}}$  (3.6).

Also the adaptation of  $\theta$  in metric (3.15) can be based on the CDF for  $\mu_{\text{opt}}$ . That is, for each channel class, we propose to relate  $\theta$  to the average delay spread  $\bar{\sigma}_{\text{ch,CLASS}} = \mathcal{E}\{\sigma_{\text{ch,CLASS}}\}$  via

$$\theta_{\text{CLASS}} = T \frac{\mu_{\text{opt,CLASS}}^{(99\%)}}{\bar{\sigma}_{\text{ch,CLASS}}}. \quad (3.16)$$

Since  $\mu_{\text{opt,CLASS}}^{(99\%)}$  is defined as a function of the class, also the weighting factor  $\theta_{\text{CLASS}}$  depends on the channel class. The computation of the  $\mu_{\text{opt,CLASS}}^{(99\%)}$  and the corresponding  $\theta_{\text{CLASS}}$  when applying (3.15) is done off-line, and the values are stored in a look-up table. However, to apply (3.15) using (3.16), we need to know the channel class under which the system is operating. This could be obtained through the SNR estimation.

We would like to emphasize that both suggested methods, i.e., (3.15) using (3.16) and  $\mu_{\text{opt,CLASS}}^{(99\%)}$ , require reliable statistical channel models being available for the specific application example.

### 3.4 Bit-Loading and CP-Length Adaptation

In this section we propose two resource allocation procedures that combine bit-loading with CP-length adaptation according to the criteria previously introduced. The procedures that we consider take into account different practical constraints. In the first one, we assume that the signal constellations can vary across the sub-channels, but a constraint on the constellation size is considered. In the second one, we assume that a single constellation is used across all OFDM sub-channels (uniform bit-loading). This constraint is often applied for adaptive modulation with low-rate feedback channels, cf. e.g. [42, 43].

In addition to bit-loading, OFDM also enables adaptation of the transmit powers for the sub-channels. As we have previously discussed, we assume to transmit with a constant PSD level given by the PSD constraint over the active sub-channels  $\mathbb{K}_{\text{on}}$ , while the other sub-channels are switched off for coexistence purposes. The adaptation of the transmit powers for adaptive OFDM is treated in Chapter 6.

We note that different from conventional bit-loading for the case of an orthogonal system, notching has an effect on loading of other sub-channels in the case of CP-length adaptation, since the interference power and thus the SINR in those sub-channels changes. Likewise, if the SINR on a given sub-channel is too low for transmission and this sub-channel is switched off, the SINRs on the remaining sub-channels change. A search for which sub-channels should be switched off would be required for optimal bit-loading,

which is infeasible. Therefore, for both non-uniform and uniform bit-loading we present two algorithms which take sub-channel activity into account and where the set  $\mathbb{K}_{\text{on}}$  and the SINRs are updated via two bit-loading iterations. The first algorithm jointly computes the optimal CP length and bit-loading such that achievable rate is maximized. The second algorithm determines the CP length using one of the proposed criteria introduced in Section 3.3 and then it runs the bit-loading for only this CP length. Hence, it enjoys a significantly lower complexity.

### 3.4.1 Procedure 1: Different Constellations

We consider bit-loading with varying signal constellations across the sub-channels. The available constellation sizes are given by  $2^b$ , where  $b = 1, \dots, b_{\text{max}}$ .

#### Algorithm 1.1

The first practical algorithm reads as follows.

1. Initialize the sets of used sub-channels  $\mathbb{K}_{\text{on}}(\mu) \subseteq \{0, \dots, M - 1\}$  for  $\mu \in \{0, \dots, \nu - 1\}$  according to the transmission mask and uniformly distribute the power among these sub-channels to meet the PSD constraint.
2. *for*  $\mu = 0 : \nu - 1$ 
  - (a) Compute the  $\text{SINR}^{(k)}(\mu)$  for  $k \in \mathbb{K}_{\text{on}}(\mu)$ , assuming the set of active sub-channels  $\mathbb{K}_{\text{on}}(\mu)$ .
  - (b) Determine the bit-loading on sub-channel  $k$  from

$$b^{(k)}(\mu) = \min \left\{ c^{(k)}(\mu), b_{\text{max}} \right\},$$

where  $c^{(k)}(\mu) = \left\lfloor \left\lceil \log_2 \left( 1 + \frac{\text{SINR}^{(k)}(\mu)}{\Gamma} \right) \right\rceil \right\rfloor$ , and  $\lfloor \cdot \rfloor$  denotes the operation of rounding the number of bits to that associated to the nearest available constellation towards zero.

- (c) if  $(b^{(k)}(\mu) == 0)$  for some  $k \in \mathbb{K}_{\text{on}}(\mu)$   
 Update the set of active sub-channels  $\mathbb{K}_{\text{on}}(\mu)$ , i.e.,  
 $\mathbb{K}_{\text{on}}(\mu) = \{k : b^{(k)}(\mu) > 0\}$ .  
 Goto 2a).  
*end*  
*end*

3. Compute the optimal CP as

$$\mu_{\text{opt}} = \underset{\mu \in \{0, \dots, \nu-1\}}{\text{argmax}} \left\{ \frac{1}{M + \mu} \sum_{k \in \mathbb{K}_{\text{on}}(\mu)} b^{(k)}(\mu) \right\}. \quad (3.17)$$

### Algorithm 1.2

The pseudo-code for the simplified algorithm reads as follows.

1. Initialize the set of used sub-channels  $\mathbb{K}_{\text{on}} \subseteq \{0, \dots, M-1\}$  according to the transmission mask and uniformly distribute the power among these sub-channels to meet the PSD constraint.
2. Optimize the CP-length according to (3.6), (3.8), (3.11), (3.15), or via table look-up (cf. Section 3.3.3). This step returns  $\mu_{\text{opt}}$ .
3. Run steps 2a – 2c of Algorithm 1.1 assuming  $\mu = \mu_{\text{opt}}$ .

We note that since the SINRs of active sub-channels can only increase when other sub-channels are switched off, only one update of the sub-channel SINRs and active sub-channel set  $\mathbb{K}_{\text{on}}$  is needed in Algorithms 1.1 and 1.2 (step 2c). Furthermore, Algorithm 1.2 has a significantly lower complexity than Algorithm 1.1 because the SINR computation is only required for one value of CP length.

### 3.4.2 Procedure 2: Uniform Bit-loading

We now consider an OFDM system with identical constellations for all sub-channels.

### Algorithm 2.1

The pseudo-code for the first practical algorithm reads as follows.

1. Initialize the sets of used sub-channels  $\mathbb{K}_{\text{on}}(\mu, b) \subseteq \{0, \dots, M-1\}$  for  $\mu \in \{0, \dots, \nu-1\}$  and  $b \in \mathbb{B} = \{1, \dots, b_{\text{max}}\}$  according to the transmission mask, and uniformly distribute the power among these sub-channels to meet the PSD constraint.
2. *for*  $\mu = 0 : \nu - 1$ 
  - (a) Set  $\mathbb{K}_{\text{on}}(\mu, 0) = \mathbb{K}_{\text{on}}(\mu, 1)$ .
  - (b) *for*  $b \in \mathbb{B}$ 
    - i. Set  $\mathbb{K}_{\text{on}}(\mu, b) = \mathbb{K}_{\text{on}}(\mu, b-1)$ .
    - ii. Compute the SINR<sup>(k)</sup>( $\mu, b$ ) for  $k \in \mathbb{K}_{\text{on}}(\mu, b)$ , assuming the set of used sub-channels  $\mathbb{K}_{\text{on}}(\mu, b)$ .
    - iii. Determine the maximum number of bits that can be transmitted on sub-channel  $k$  as

$$b^{(k)} = \min \left\{ c^{(k)}(\mu, b), b_{\text{max}} \right\}, \text{ where}$$

$$c^{(k)}(\mu, b) = \left\lceil \left\lfloor \log_2 \left( 1 + \frac{\text{SINR}^{(k)}(\mu, b)}{\Gamma} \right) \right\rfloor \right\rceil.$$

- iv. Update the set of active sub-channels  $\mathbb{K}_{\text{on}}(\mu, b) = \{k : b^{(k)} \geq b\}$ .

*end*

*end*

3. Compute the optimal CP and the bits associated to the optimal constellation to be used as

$$(b_{\text{opt}}, \mu_{\text{opt}}) = \underset{(b, \mu) \in \{1, \dots, b_{\text{max}}\} \times \{0, \dots, \nu-1\}}{\text{argmax}} \{R(\mu, b)\}. \quad (3.18)$$

where  $R(\mu, b)$  is the bit-rate that can be achieved using a CP equal to  $\mu$  samples and  $b$  bits per QAM symbol, i.e.,

$$R(\mu, b) = b \cdot |\mathbb{K}_{\text{on}}(\mu, b)|. \quad (3.19)$$

### Algorithm 2.2

The pseudo-code for the simplified uniform bit-loading algorithm reads as follows.

1. Initialize the sets of used sub-channels  $\mathbb{K}_{\text{on}}(b) \subseteq \{0, \dots, M - 1\}$  for  $b \in \mathbb{B} = \{1, \dots, b_{\text{max}}\}$  according to the transmission mask, and uniformly distribute the power among these sub-channels to meet the PSD constraint.
2. Optimize the CP-length according to (3.6), (3.8), (3.11), (3.15), or via table look-up (cf. Section 3.3.3). This step returns  $\mu_{\text{opt}}$ .
3. Set  $\mathbb{K}_{\text{on}}(\mu_{\text{opt}}, b) = \mathbb{K}_{\text{on}}(b)$  and run steps 2a and 2b of Algorithm 2.1 for  $\mu = \mu_{\text{opt}}$ .
4. Compute the optimal constellation to be used as

$$b_{\text{opt}} = \underset{b \in \{1, \dots, b_{\text{max}}\}}{\text{argmax}} \{b \cdot |\mathbb{K}_{\text{on}}(\mu_{\text{opt}}, b)|\}. \quad (3.20)$$

Algorithms 2.1 and 2.2 take into account the fact that the set of sub-channels that are switched off for a certain constellation (because they cannot sustain the associated bit-rate) necessarily contains the set of sub-channels that are switched off for the constellation of immediately lower order. Therefore, the algorithms require only to update the set of active sub-channels in the event that more sub-channels need to be switched off. Again, Algorithm 2.2, which makes use of the CP-length criteria from Section 3.3 has considerably lower computational complexity than Algorithm 2.1.

### 3.5 Extension to OFDMA

In this section, we extend the idea of optimizing the CP length to the multiuser context. We assume a network where a central coordinator (CCo) allocates resources by collecting information regarding the network state, i.e., number of users, channel conditions of each user, rate requirement from each user request, etc. Once the CCo has collected all the information needed, it dynamically allocates the resources among the users. We focus on the downlink channel from the CCo to the  $N_U$  users of the network. Multiplexing is accomplished by partitioning the sub-channels among the users realizing OFDMA. Since the channels experienced by the users are different, the CCo allocates the sub-channels and sub-channel bits, and adjusts the CP length according to a fair principle based on maximizing aggregate rate and ensuring that all users exceed a minimum rate.

We follow the capacity-optimal approach in Section 3.3.1. In OFDMA the capacity of the  $k$ -th sub-channel of user  $u$ , for a certain CP length, is given by

$$C^{(u,k)}(\mu) = \frac{1}{(M + \mu)T} \log_2 \left( 1 + \frac{\text{SINR}^{(u,k)}(\mu)}{\Gamma} \right) \text{ [bit/s]}, \quad (3.21)$$

where  $\text{SINR}^{(u,k)}(\mu) = \frac{P_U^{(u,k)}(\mu)}{P_\eta^{(u,k)} + P_I^{(u,k)}(\mu)}$ , and  $P_U^{(u,k)}(\mu)$ ,  $P_\eta^{(u,k)}(\mu)$ , and  $P_I^{(u,k)}(\mu)$  respectively are the useful, the noise and the interference power experienced by  $u$ -th user in the  $k$ -th sub-channel.

In order to allocate resources to the users, for a given CP length, the central coordinator can solve the following optimization problem:

$$\begin{aligned} AR(\mu) &= \max_{\underline{\alpha}} \sum_{u=1}^{N_U} \sum_{k \in \mathbb{K}_{\text{on}}} \alpha^{(u,k)} C^{(u,k)}(\mu), \\ \underline{\alpha} &= \left\{ \alpha^{(u,k)}, \text{ for } k \in \mathbb{K}_{\text{on}}, \text{ and } u = 1, \dots, N_U \right\}, \\ \text{subject to } & \sum_{u=1}^{N_U} \alpha^{(u,k)} = 1, \quad k \in \mathbb{K}_{\text{on}} \end{aligned} \quad (3.22)$$

$$\sum_{k \in \mathbb{K}_{\text{on}}} \alpha^{(u,k)} C^{(u,k)}(\mu) \geq \frac{p^{(u)}}{100} \sum_{k \in \mathbb{K}_{\text{on}}} C^{(u,k)}(\mu),$$

$$u = 1, \dots, N_U,$$

where  $\alpha^{(u,k)} \in \{0, 1\}$  denotes the binary sub-channel index, which is equal to 1 if sub-channel  $k$  is allocated to user  $u$ , and zero otherwise,  $p^{(u)}$  is the percentage of the bit-rate that the  $u$ -th user has to achieve with respect to the one that it would achieve in a single user scenario, and  $AR(\mu)$  is the aggregate network rate. (3.22) is a binary integer programming problem. To reduce the problem complexity we consider the relaxed problem for  $\alpha^{(u,k)} \in [0, 1]$ , which can be solved using linear programming (LP) [44]. The solution returned by LP is rounded towards the closest integer. The optimal CP is obtained via a discrete search for  $\mu \in \{0, \dots, \nu - 1\}$  that maximizes the aggregate rate  $AR(\mu)$ .

Starting from the formulation in (3.22), a practical bit-loading algorithm for OFDMA is given by the following pseudo-code.

### Algorithm 3

1. Initialize the set of used sub-channels  $\mathbb{K}_{\text{on}} \subseteq \{0, \dots, M - 1\}$  according to the transmission mask and uniformly distribute the power among these sub-channels to meet the PSD constraint.
2. Determine a set  $\mathcal{M} \subseteq \{0, \dots, \nu - 1\}$  of CP lengths to be considered.
3. *for*  $\mu \in \mathcal{M}$ 
  - (a) For each user, compute the SINRs according to (3.1).
  - (b) Solve (3.22) using LP.
  - (c) Round the coefficients given by LP, i.e.,  $\xi^{(u,k)}(\mu) = \lceil \alpha^{(u,k)} \rceil$ , to partition the sub-channels among the users.
  - (d) Load the bits to each user according to

$$b^{(u,k)}(\mu) = \min \left\{ \xi^{(u,k)}(\mu) c^{(u,k)}(\mu), b_{\max} \right\},$$

for  $u = 1, \dots, N_U$ ,  $k \in \mathbb{K}_{\text{on}}$ , where

$$c^{(u,k)}(\mu) = \left\lceil \left\lfloor \log_2 \left( 1 + \frac{\text{SINR}^{(u,k)}(\mu)}{\Gamma} \right) \right\rfloor \right\rceil.$$

- (e) If there exist at least one sub-channel  $k$  that is switched off, i.e.,  $b^{(u,k)}(\mu) = 0 \forall u$ , do another bit-loading iteration as follows
- i. Define  $\mathbb{K}_{\text{OFF}}(\mu) = \{k \in \mathbb{K}_{\text{on}} : b^{(u,k)}(\mu) = 0 \forall u = 1, \dots, N_U\}$ .
  - ii. For  $k \in \mathbb{K}_{\text{OFF}}(\mu)$ , set  $\xi^{(u,k)}(\mu) = 0 \forall u$ .
  - iii. Recompute the SINRs and load the bits according to d) on the sub-channels that are switched on.
- (f) Compute the aggregate network rate:
- $$R(\mu) = \frac{1}{(M+\mu)T} \sum_{u=1}^{N_U} \sum_{k \in \mathbb{K}_{\text{on}}} b^{(u,k)}(\mu).$$

*end*

4. Compute the optimal CP length as  $\mu_{\text{opt}} = \operatorname{argmax}_{\mu \in \mathcal{M}} \{R(\mu)\}$ . The final sub-channel allocation is given by  $\xi^{(u,k)}(\mu_{\text{opt}})$ , for  $u = 1, \dots, N_U$ ,  $k \in \mathbb{K}_{\text{on}}$ .

It is worth noting that this algorithm requires only one update of the SINRs and the set of active sub-channels, similar to Algorithms 1.1 and 1.2. This is because the set of active sub-channels is defined at the first step, while at the second step the SINRs on the remaining sub-channels can only increase so that no more sub-channels can be switched off. The choice for  $\mathcal{M}$  is not obvious in general. One possibility is full enumeration, i.e.,  $\mathcal{M} = \{0, 1, \dots, \nu - 1\}$ , which entails relatively high complexity. The criteria from Section 3.3 are not immediately applicable as  $N_U$  different channels need to be dealt with. However, the simplified adaptation via table look-up (cf. Section 3.3.3) is perhaps best suited. The numerical results presented in Section 3.7 confirm this suggestion.

### 3.6 Extension to TDMA

As done in the previous section for OFDMA, in this section, we extend the idea of optimizing the CP length to the multi-user context where the channel

access is managed through TDMA. In particular, we assume a network where a CCo dynamically allocates the resources among the  $N_U$  network users.

We consider the downlink case, where the CCo signals to the  $N_U$  network users. Since we are interested in finding the optimal CP duration for the whole network, we assume an idealistic case where the resources, i.e., the number of slots in a TDMA frame, are infinite. Under the previous assumptions, the resource allocation problem consists in assigning the time slots to the network users in such way that the aggregate network rate is maximized. Therefore, for a certain value of  $\mu$ , we can solve the following optimization problem

$$\begin{aligned}
 AR_T(\mu) = \max_{\underline{t}} \quad & \sum_{u=1}^{N_U} \sum_{k \in \mathbb{K}_{\text{on}}} t^{(u)} C^{(u,k)}(\mu); \quad \underline{t} = [t^{(1)}, \dots, t^{(N_U)}] \\
 \text{s.t.} \quad & \sum_{u=1}^{N_U} t^{(u)} = 1, \\
 & t^{(u)} \sum_{k \in \mathbb{K}_{\text{on}}} C^{(u,k)} \geq p^{(u)} \sum_{k \in \mathbb{K}_{\text{on}}} C^{(u,k)}, \quad u = 1, \dots, N_U,
 \end{aligned} \tag{3.23}$$

where  $AR_T(\mu)$  denotes the aggregate network rate, and  $p^{(u)}$  the percentage of the bit-rate that the  $u$ -th user has to achieve with respect to the one that it would achieve in the correspondent single user scenario. Also in this case, the solution of (3.23) can be obtained using LP [44].

Then, to obtain the optimal CP and channel occupation time allocation, the CCo solves (3.23) exhaustively for  $\mu = 0, \dots, \nu - 1$  and chooses the CP that maximizes the aggregate network rate.

The exhaustive search of CP values renders the algorithm complexity relatively high. A significant simplification is obtained if we solve (3.23) with LP only for a finite set  $\mathcal{M}$  of CP values, e.g., the set of  $\mu_{\text{opt,CLASS}}^{(99\%)}$  pre-determined in the single user case according to the criterion of Section 3.3.3. Clearly, once the network coordinator knows the scenario, namely the channel class, in which the device is working, the set  $\mathcal{M}$  reduces to one value of CP.

### 3.7 Numerical Results In-Home Power Line Channels

In this section, we present and discuss numerical results that illustrate the performance of OFDM transmission using CP-length adaptation and quantify the gains achievable with the proposed metrics. We assume a constant transmit PSD mask equal to  $-50$  dBm/Hz in the 2-28 MHz range, and zero outside as it is used in the HPAV system [18] to comply with EMC rules [39]. The AWGN has a PSD of  $-110$  dBm/Hz which is typical for indoor PLC scenarios [45]. The considered channel model (for in-home PLC applications) is described in detail in Section 3.7.1. In Section 3.7.2, we first report results for CP-length adaptation using the metrics from Section 3.3. It will be seen that the adaptation of the CP to the channel realization yields significant improvements in the system performance. Then, in Section 3.7.3, we show that also in the case of bit-loaded OFDM large gains are attained from CP optimization. Finally, results for the OFDMA multiuser case are presented in Section 3.7.4.

#### 3.7.1 PLC Channel Model

In-home PLC channels exhibit a relatively large range of signal attenuation and delay spread. Based on the results of a measurement campaign it has been proposed to categorize transmission channels into nine classes [45]. Each class is characterized by a specific average frequency dependent path loss (PL), which has significant impact on the corresponding channel capacity. To generate statistically representative channel frequency responses according to this classification, we herein use the channel model from [46] that it is based on a multipath model with a finite number of components (cf. e.g. [47, 48]). According to this model, the channel frequency response can be expressed as

$$G_{\text{ch}}(f) = \sum_{i=1}^{N_p} (A_0 g_i + A_1 h_i f^{K_2}) e^{-(\gamma_0 + \gamma_1 f^{K_1}) d_i} e^{-j2\pi f \frac{d_i}{v_p}},$$

$$0 \leq f \leq 37.5 \text{ MHz}, \quad (3.24)$$

Table 3.1: Channel model parameters for channel classes 1, 5 and 9.

Parameter [unit]	Class 1	Class 5	Class 9
$L_{max}$ [m]	580	280	130
$\Lambda$ [path/m]	0.2	0.2	0.2
$v_p$ [m/s]	2e8	2e8	2e8
$\gamma_0$ [m <sup>-1</sup> ]	-0.0064	-0.0179	-0.0281
$\gamma_1$ [s·m <sup>-1</sup> ]	9.9240e-27	1.9962e-5	2.4875e-20
$K$	2.9843	0.3654	2.2005
$K_2$	0.4039	-	0.3415
$A_0$	2.1763e-5	0.0016	0.0108
$A_1$ [s <sup>-1</sup> ]	2.6116e-8	0	1.62e-5

where the number of components  $N_p$  is drawn from a Poisson process with average path rate per unit length  $\Lambda = 0.2$  path/m,  $g_i$  and  $h_i$  are two independent uniformly distributed random variables in  $[-1,1]$ . The variable  $h_i$  models the frequency dependent coupling that may exist between lines in the network. The path lengths  $d_i$  follow an Erlang distribution of parameter  $\Lambda$  and index  $i$ . The maximum path length in the network is set to  $L_{max}$ , i.e.,  $d_{N_p} \leq L_{max}$ . The speed of propagation in the medium is  $v_p$ . The constant parameters have been chosen to generate three channel classes, denoted Classes 1, 5, and 9 according to [45], in the frequency band 0-37.5 MHz and the values are reported in Table 3.1. Fig. 3.1 shows the average path loss profiles and three exemplary channel frequency responses for Classes 1, 5, and 9. Class 9 channels cause relatively little signal attenuation (the average SNR is 53.6 dB), Class 5 channels show medium attenuation (the average SNR is 35.7 dB), and Class 1 channels represent scenarios with strong signal attenuation (the average SNR is 8.8 dB).

The lengths of the channel responses are truncated to 209 samples, which is about 5.57  $\mu$ s and identical to the CP length used in HPAV [18]. Fig. 3.2 shows the CDF of the rms delay spread for the three classes. We notice that the average values for the rms delay spread indicated in Fig. 3.2 are similar to

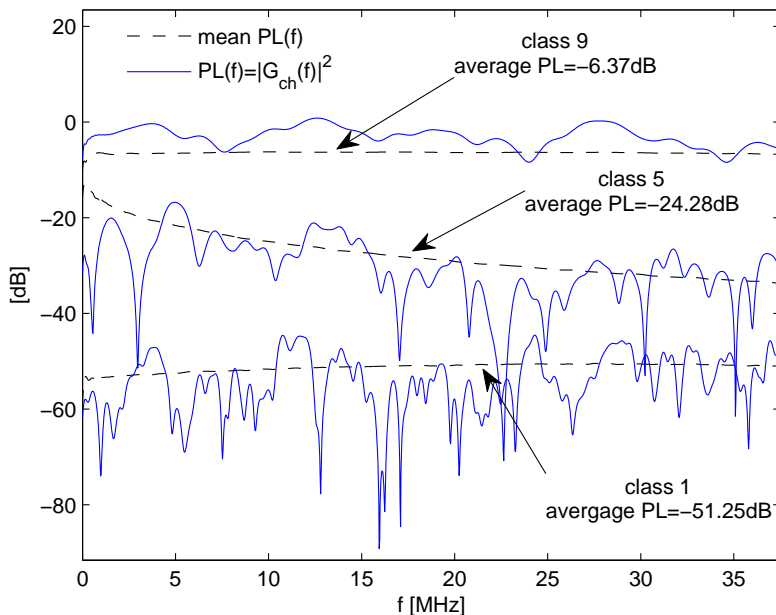


Figure 3.1: Mean path loss (PL) and sample frequency response realizations for the three modeled channel classes.

the ones obtained from measurements in [45].

### 3.7.2 CP-Length Adaptation

The OFDM system uses  $M=384$  sub-channels<sup>1</sup> in the  $37.5$  MHz band. To satisfy the PSD mask, 266 sub-channels are active and the sub-channels at the band edges are switched off. The SNR gap  $\Gamma$  is fixed to  $9$  dB for all simulations.

Fig. 3.3 shows the capacity  $C(\mu)$  (3.5) as a function of the CP length for different channel realizations that are representative, in terms of capacity, of

<sup>1</sup>This is a quarter of the number of sub-channels used in HPAV. The effect of different  $M$  will be addressed in Section 3.7.3.

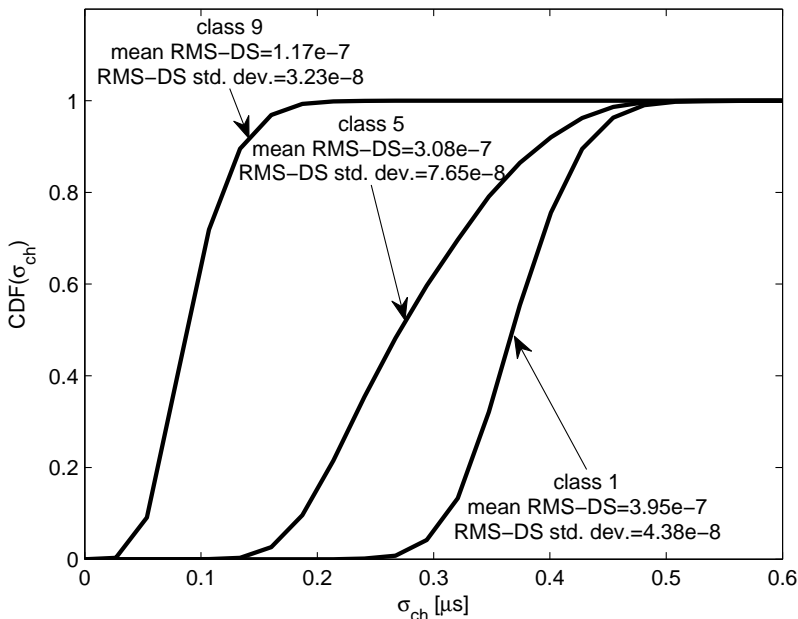


Figure 3.2: CDF of the rms delay spread (RMS-DS) for the three modeled channel classes.

the best (subplot A) and of the worst (subplot B) realization of each channel class (selected from a total of 100 realizations for each class). We also report with markers the CP lengths and the corresponding capacities obtained with the criteria proposed in Section 3.3. We observe that, although  $\text{SINR}(\mu)$  monotonically increases with  $\mu$ , the capacity  $C(\mu)$  attains its maximum at  $\mu_{\text{opt}} < \max\{\mu\} = 209$  samples. Furthermore, the higher the channel attenuation (therefore the lower the SNR) the higher the value for  $\mu_{\text{opt}}$  that maximizes capacity. This behavior is explained by the fact that for high SNR the performance is dominated by interference, whose mitigation requires a relatively long CP. Therefore, the capacity gains from CP shortening are expected to be more pronounced in the low SNR region, when the system is noise limited.

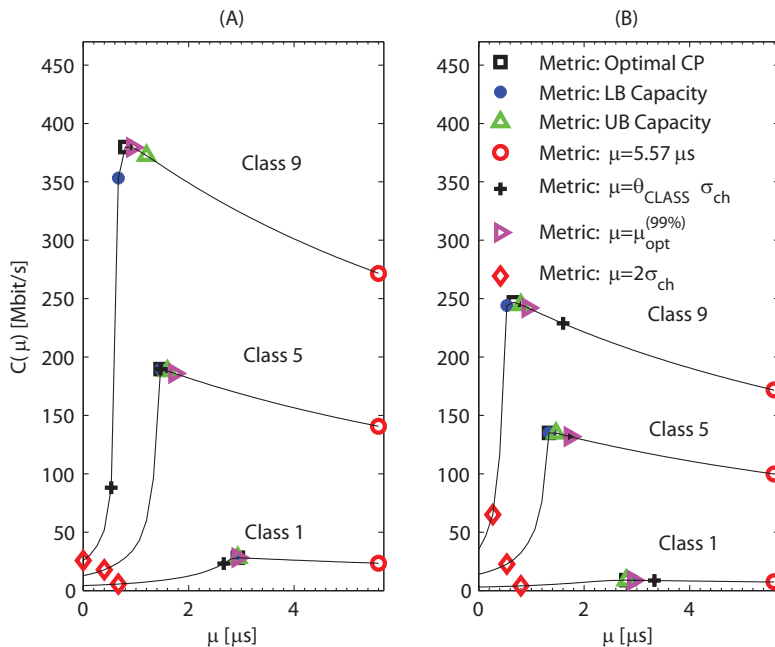


Figure 3.3: Capacity  $C(\mu)$  as a function of the CP length  $\mu$ , for different PLC channels. Markers indicate the CP length obtained from the different criteria proposed in Section 3.3. Subplots (A) and (B) show the results for the best case and the worst case channel impulse responses, respectively.

Metrics (3.8) and (3.11) based on capacity bounds give results that are very similar to those achieved with the optimal metric. Also the adaptation based on the simplified approach described in Section 3.3.3 that uses  $\mu_{\text{opt,CLASS}}^{(99\%)}$  performs close to optimum. In this case, we used fixed values for the CP length as derived below.

When adaptation to the channel class is performed using the delay spread criterion (3.15), we observe that choosing a fixed value of  $\theta$  as it was advocated in [37] results in a consistently poor performance. The suggested adaptation according to (3.16) (the specific values for  $\theta$  are given below) leads to significant

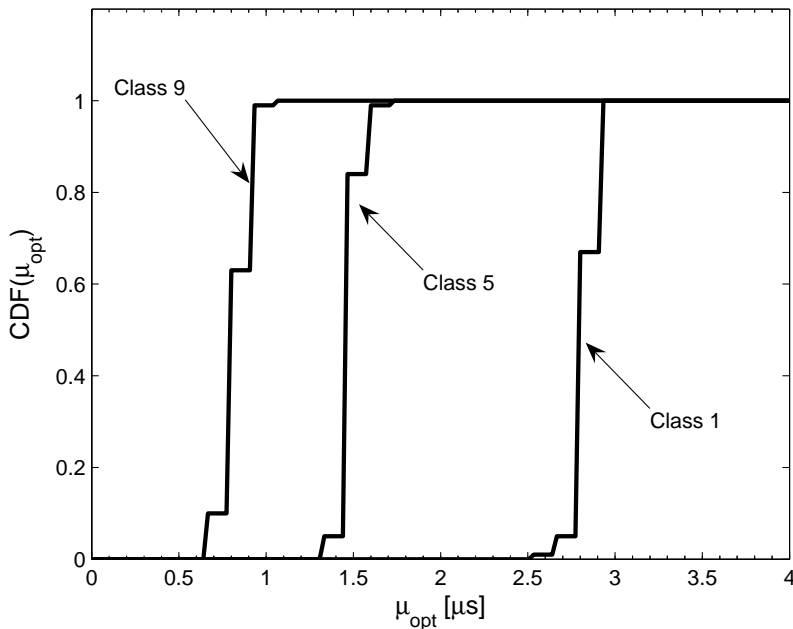


Figure 3.4: CDF of capacity-optimal CP length measured for 100 channel realizations belonging to Classes 1, 5, and 9.

performance improvements. In particular, the achievable rate is close to the optimal one except for the best-case impulse response for Class 9, which is due to the rather step shape of the rate curve in this case.

Finally, a comparison of the results in Figs. 3.3(A) and (B) reveals that the optimal CP length is a function of both the channel class and the specific channel impulse response. Next, we consider a set of 100 channel realizations. Fig. 3.4 shows the measured CDF of the capacity-optimal CP length according to (3.6). We notice that for Class 9, the optimal CP is shorter than  $0.93 \mu\text{s}$  (or 35 samples) in 99% of the cases. This value increases to  $1.73 \mu\text{s}$  (or 65 samples) for the channel class 5, and to  $2.93 \mu\text{s}$  (or 110 samples) for the channel class 1. Hence, we set  $\mu_{\text{opt},9}^{(99\%)}=35$  for Class 9 channels,  $\mu_{\text{opt},5}^{(99\%)}=65$  for Class 5

channels, and  $\mu_{\text{opt},1}^{(99\%)}=110$  for Class 1 channels. Furthermore, since the average rms delay spread  $\bar{\sigma}_{\text{ch,CLASS}}$  for the Classes 1, 5, and 9 is respectively equal to 14.84, 11.50, and 4.42 samples, we obtain the scaling parameters  $\theta_1=7.41$ ,  $\theta_5=5.65$ , and  $\theta_9=7.92$ , according to rule (3.16).

Given those parameters, Figs. 3.5, 3.6, and 3.7 provide a comparison of the various CP-length criteria from Section 3.3. We also include the capacity obtained setting the CP length equal to  $5.57 \mu\text{s}$ . As we can see, for all channel classes, the adaptation of the CP length yields significant gains compared to a fixed CP length of  $5.57 \mu\text{s}$ . For channel classes 1, 5, and 9, the capacity-optimal CP (3.6) respectively increases the average (over the 100 channel realizations) achievable rate by 20.7%, 32.9%, and 39.3%. Very similar results are obtained when using lower (20.5%, 31.3%, and 32.0%) and upper (20.7%, 27.6%, and 32.2%) capacity bound criteria. The delay-spread criterion (3.15) increases the rate by 16.6%, 18.3%, and 33.0%. Notably, the simplified adaptation with  $\mu_{\text{opt,CLASS}}^{(99\%)}$  results in close-to-optimal rate gains of 20.2%, 30.7%, and 38.6% for the three channel classes.

We note that the gains depend on the number of OFDM sub-channels used for data transmission. More specifically, the larger  $M$  the lower is the impact of the CP length. This aspect will be addressed in the next section.

### 3.7.3 CP-Length Adaptation and Bit-Loading

We now turn our attention to the combination of CP-length adaptation with bit-loading. In addition to the system parameters specified above, we consider different number of OFDM sub-channels, namely,  $M \in \{384, 768, 1536\}$  in the 0-37.5 MHz band. The number of used tones such that the PSD mask is met, follows as  $M_{\text{on}} \in \{266, 532, 1065\}$ , which defines  $\mathbb{K}_{\text{on}}$  at the initial step of bit-loading. The constellations employed are 2-PAM and  $\{4, 8, 16, 64, 256, 1024\}$ -QAM, and we consider the best case (BeC) channel realizations for the three considered classes (cf. Fig. 3.3(A)). The baseline OFDM system uses a fixed CP length of  $5.57 \mu\text{s}$ .

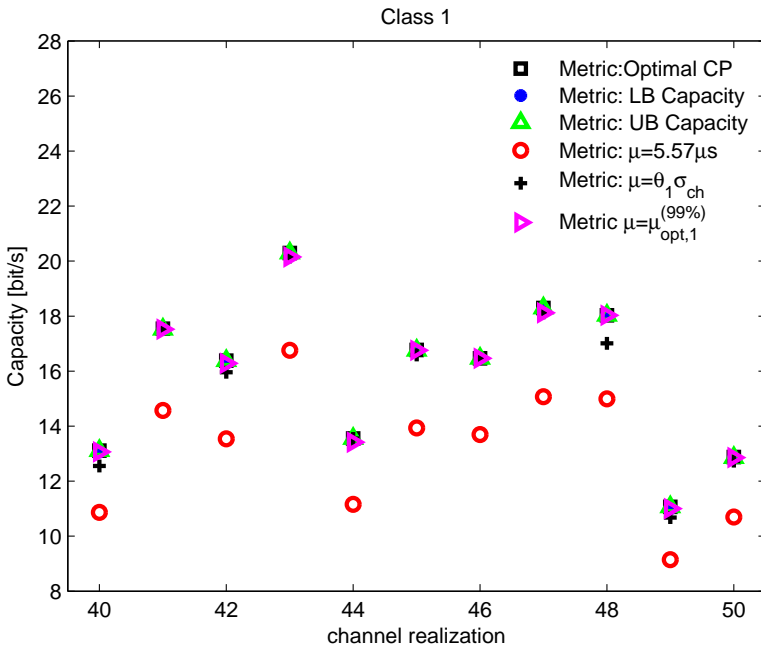


Figure 3.5: Capacity  $C(\mu)$  for  $\mu$  optimized according to the different criteria presented in Section 3.3 as a function of the channel realization belonging to Class 1. For the sake of readability, only realizations 40 to 50 are shown out of 100 realizations.

### Allocation of Different Constellations

Fig. 3.8 shows the data rate achieved with Algorithm 1.2 as a function of the number of OFDM sub-channels  $M$  for the BeC channels. For brevity, we assume CP optimization only using the capacity-optimal criterion (3.6). However, we note that very similar results are obtained with the simplified CP metrics (3.8), (3.11) and (3.15), as we have seen in the previous section. We observe that data rate gains range between 4 Mbit/s and 70 Mbit/s with  $M = 384$  and between about 4 Mbit/s and 25 Mbit/s with  $M = 1536$ , which translates into significant relative rate improvements of between 6% and 39%.

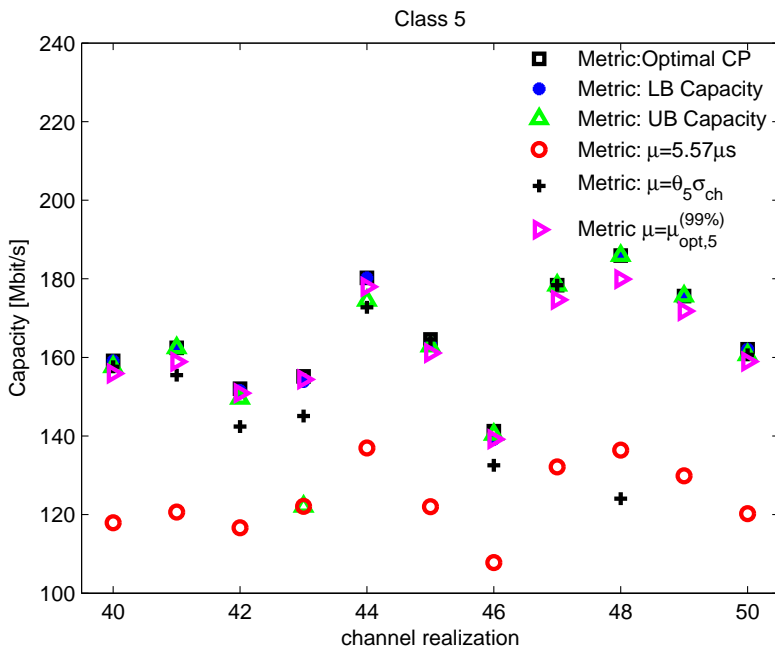


Figure 3.6: Capacity  $C(\mu)$  for  $\mu$  optimized according to the different criteria presented in Section 3.3 as a function of the channel realization belonging to Class 5. For the sake of readability, only realizations 40 to 50 are shown out of 100 realizations.

The smaller gains for larger  $M$  are due to a reduced impact of the CP length on data rate. It is also interesting to note that the rate for  $M=384$  and CP-length adaptation is the same or higher than the rate for  $M=1536$  and  $\mu=5.57\mu\text{s}$ . Therefore, CP-length adaptation is a suitable way of lowering the implementation complexity in terms of DFT size of an OFDM system without sacrificing data rate.

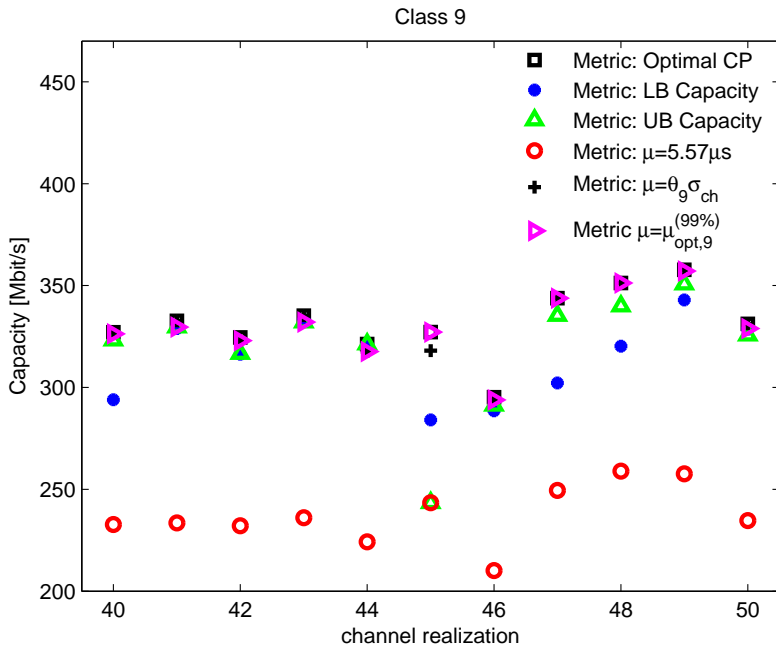


Figure 3.7: Capacity  $C(\mu)$  for  $\mu$  optimized according to the different criteria presented in Section 3.3 as a function of the channel realization belonging to Class 9. For the sake of readability, only realizations 40 to 50 are shown out of 100 realizations.

### Uniform Bit-loading

Fig. 3.9 shows the bit rate  $R(\mu, b)$  (3.19) as a function of the CP length and the constellation used for an OFDM system with 384 sub-channels. The employed channel is the BeC channel of Class 5. In this example, we restrict the possible QAM constellations to  $b \in \{1, 2, 4, 6\}$  bits per constellation point. As we can see in Fig. 3.9, the jointly optimized CP length and constellation size obtained with Algorithm 2.1 are  $\mu_{\text{opt}}=55$  and  $b_{\text{opt}}=4$ , for which a considerably enhanced rate relative to the standard choice of a CP equal to the channel length is achieved. The gain obtained with Algorithm 2.1 equals 36%. The

bit rate obtained with Algorithm 2.2 and a CP length computed using the optimal metric (3.6) and via table look-up (cf. Section 3.3.3) is essentially equal and very close to that from Algorithm 2.1. This is quite remarkable and renders the low-complexity Algorithm 2.2, as well as Algorithm 1.2, attractive solutions for practical implementations. Finally, comparing the performance of Algorithm 2.2 in Fig. 3.9 with that of Algorithm 1.2 in Fig. 3.8, we observe that uniform bit-loading provides lower bit rate than full bit-loading.

### 3.7.4 CP-Length Adaptation and Resource Allocation in OFDMA

Finally, we consider OFDMA for a network of  $N_U=4$  users with a proportionally fair resource allocation, i.e.,  $p^{(u)}=25$  for all users, and  $M=384$ . Four different channel realizations belonging to the three channel classes presented in Section 3.7.1 are used for the four users. The other system parameters are the same as for the single user scenario in Section 3.7.3. We have applied Algorithm 3 for sub-channel allocation, bit-loading, and CP-length selection. Fig. 3.10 shows the per-user and the aggregate data rate as a function of the CP length. It can be seen that the rate-maximizing CP length for the multiuser OFDMA scenario is markedly different from the default CP length of  $5.57 \mu\text{s}$ . For the presented scenario, the maximal gain in aggregate rate due CP adaptation compared to a fixed CP of length  $5.57 \mu\text{s}$  is 44%, which has been obtained using Algorithm 3 with full enumeration of  $\mathcal{M} = \{0, 1, \dots, \nu - 1\}$ . Remarkably, almost the full gain (36%) is retained if  $\mathcal{M} = \{\mu_{\text{opt},1}^{(99\%)}, \mu_{\text{opt},5}^{(99\%)}, \mu_{\text{opt},9}^{(99\%)}\}$  is used, which is a promising result towards devising low-complexity resource allocation algorithms for OFDMA with CP adaption.

## 3.8 Numerical Results in IEEE 802.11n Channels

The idea of adapting the CP length to the channel condition can be also exploited for WLAN applications. As it will be shown in the following, although the WLAN channels are time variant, it is possible to obtain near maximal achievable rate choosing the CP from a small set of values, one for each scenario in which the devices are working, i.e., we will show that the temporal

variation of the channel within a given scenario (e.g., a small office, a large open space, and so on) does not significantly affect the statistics of the optimal CP, and consequently it is possible to set a value of “globally optimal” CP for a given scenario.

To obtain numerical results, we have chosen the following system parameters that are essentially those of the IEEE 802.11 standard [8]. The OFDM system uses  $M=64$  sub-channels with a transmission bandwidth of 20 MHz. The signal is transmitted with a constant PSD of -53 dBm/Hz. At the receiver side, we add white Gaussian noise with PSD equal to -168 dBm/Hz, which is the typical level in radio scenario. Thus, the SNR, without path loss and fading, on each sub-channel is 115 dB. The baseline system uses a CP of 0.8  $\mu$ s that corresponds to the value employed in the IEEE 802.11 standard [8].

### 3.8.1 IEEE 802.11n Channel Model

We use the IEEE 802.11 TGn [49] channel model. This model generates channels belonging to five classes labeled with B,C,D,E,F. Each class is representative of a certain environment, e.g., small office, large open space/office with line of sight (LOS) and non line of sight (NLOS) propagation, and so on. Both small scale multipath fading and large scale path loss fading as a function of distance are taken into account. Doppler effects from movement are also considered. Although the model allows considering multiple input multiple output (MIMO) channels, we restrict ourselves to the case of single-transmit/single-receive antenna. For a detailed description of the model, please see [49] and references therein. Therefore, the continuous time complex impulse response provided by such a model (with slow fading) can be written as

$$\hat{g}_{\text{ch}}^{(u)}(t, d) = A^{(u)}(d) \sum_{p=0}^{\nu^{(u)}-1} \alpha^{(u)}(p) \delta(t - \tau_p^{(u)}), \quad (3.25)$$

where  $A^{(u)}(d)$  is the attenuation due to path-loss when the access point (AP) and the receiver  $u$  are at distance  $d$ . The number of multipath components is denoted with  $\nu^{(u)}$ . Depending on the distance and on the channel class the

path-loss is deterministically computed or is drawn from a log-normal shadow fading distribution.  $\alpha^{(u)}(p)$  denote the complex channel coefficients whose amplitude can be Rayleigh or Ricean distributed depending on the channel class and the associated time delay  $\tau_p^{(u)}$ . To obtain the equivalent discrete time channel impulse response, we use a low pass filter followed by sampling with frequency  $1/T$  that is equal to the system transmission bandwidth.

Fig. 3.11 shows the capacity (3.5) as a function of the CP length for 100 class B channel realizations. The distance between transmitter and receiver equals  $10\text{ m}$ . As we can see, an optimal CP length that maximizes the capacity (3.5) can be found for each channel realization. Some variability on the optimal CP length as the channel changes is present. We can also see that the adaptation of the CP to the channel realization can appreciably improve the system performance w.r.t. the baseline system that uses a CP equal to  $0.8\text{ }\mu\text{s}$ .

Now, in Fig. 3.12 we show the CDF of the optimal CP (3.6) for each channel class and for different distances between transmitter and receiver. We can see that the distribution of the optimal CP depends both on the distance and on the channel class. However, the dependence on the class is stronger than the one on the distance. Furthermore, from Fig. 3.11 we see that the achievable rate curves are relatively flat around the optimal CP value, thus, if we choose a CP near to the optimal one, the achieved capacity will not dramatically change compared to the choice of the optimal CP value. These observations justify our proposal to design the CP according to its CDF. The set of CP values found according to the analysis of its distribution is  $\mathcal{M} = \{\mu_{99\%}^B = 0.4\text{ }\mu\text{s}, \mu_{99\%}^C = 0.5\text{ }\mu\text{s}, \mu_{99\%}^D = 0.6\text{ }\mu\text{s}, \mu_{99\%}^E = 0.9\text{ }\mu\text{s}, \mu_{99\%}^F = 1.1\text{ }\mu\text{s}\}$ . It should be noted that for class B the CP is half the standard CP value of  $0.8\text{ }\mu\text{s}$  while for class F it is longer than the standard one.

Fig. 3.13 shows the complementary CDF (CCDF) of capacity computed for the channel classes B,D,F choosing the CP with the optimal metric (3.6), with limiting the CP values to those associated to the classes, and simply setting the CP equal to  $0.8\text{ }\mu\text{s}$  (baseline system). The distances have been set to  $3\text{ m}$ ,  $10\text{ m}$ , and  $30\text{ m}$ . The choice of the CP with the distribution criterion gives results very close to the optimal criterion (3.6). Furthermore, both the

proposed criteria provide significant gains w.r.t. the baseline choice of a CP equal to  $0.8 \mu s$ . Finally, Fig. 3.14 shows the complementary distribution of the aggregate network rate that has been obtained using OFDMA and TDMA. The resource allocation and the CP adaptation has been done solving problems (3.22) and (3.23) for OFDMA and TDMA respectively. Furthermore, the set of CP values among which we adapt is  $\mathcal{M} = \{\mu_{99\%}^B = 0.4 \mu s, \mu_{99\%}^C = 0.5 \mu s, \mu_{99\%}^D = 0.6 \mu s, \mu_{99\%}^E = 0.9 \mu s, \mu_{99\%}^F = 1.1 \mu s\}$ . As a comparison we also show the performance without any adaptation, but simply setting the CP equal to  $0.8 \mu s$ . The network is composed of  $N_U = 4$  users. The coefficients  $p^{(u)}$  are set to 25% (fair allocation). The users have channels belonging the same class, the channel class is randomly selected among the possible ones, and the distance between each user and the AP is drawn randomly between  $3 m$  and  $60 m$ . As we can see, the proposed algorithms improve the aggregate network rate w.r.t. the baseline system in both OFDMA and TDMA. Furthermore, OFDMA significantly outperforms TDMA. This is because the use of OFDMA allows each user to optimally exploit the channel frequency selectivity, i.e., each user transmits in those sub-channels that allow for carrying more information. For example at a CCDF of 90%, the proposed limited CP adaptation yields a rate gain of about 8% in both TDMA and OFDMA. OFDMA provides a rate gain that exceeds 18% over TDMA.

### 3.8.2 Main Findings

We have investigated the problem of CP-length adaptation in OFDM(A) transmission systems. We have argued that the use of a CP length adjusted to the current channel conditions is beneficial in terms of achievable data rate. The underlying rationale is that the level of self-interference can be raised in noise-limited systems. We have considered constrained capacity as the pertinent figure of merit, and suggested a number of related, simplified criteria to select the CP length. Furthermore, we have presented four practical single-user bit-loading algorithms that take into account the CP optimization, and we have outlined extensions to the multiuser transmission scenario using OFDMA and TDMA. Numerical results for typical indoor power line and WLAN channels

have shown significant gains due to CP-length adaptation. These gains come from (i) adjusting the CP length according to the instantaneous channel impulse response and (ii) allowing for a controlled amount of self-interference using the proposed optimization criteria.

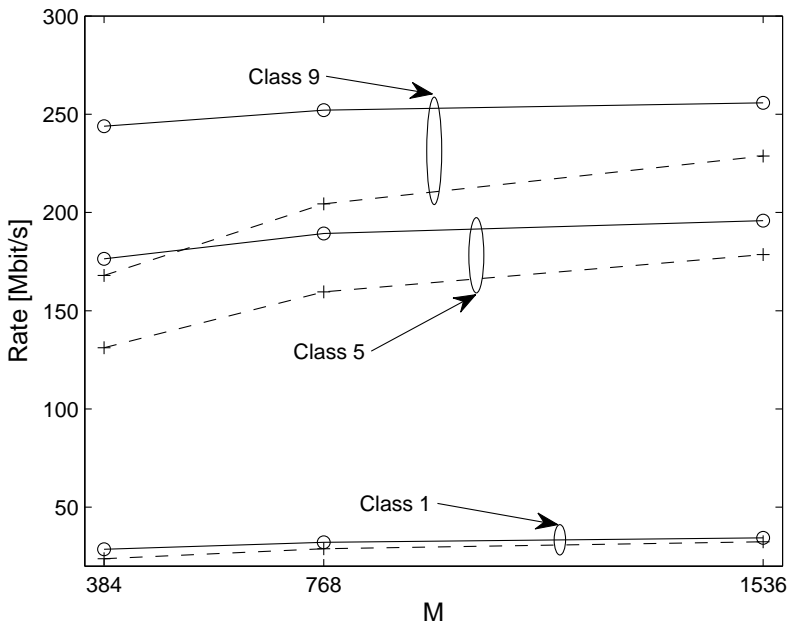


Figure 3.8: Capacity  $C(\mu)$  for bit loading with Algorithm 1.2 of Section 3.4.1 and  $\mu$  optimized according to the capacity-optimal criterion (3.6) and three different numbers of OFDM sub-channels  $M \in \{384, 768, 1536\}$ . For a comparison,  $C(\mu)$  for bit loading and  $\mu = 209$  (corresponding to 5.57  $\mu s$ ) is also included. The channels employed are the BeC channels of the three used classes.

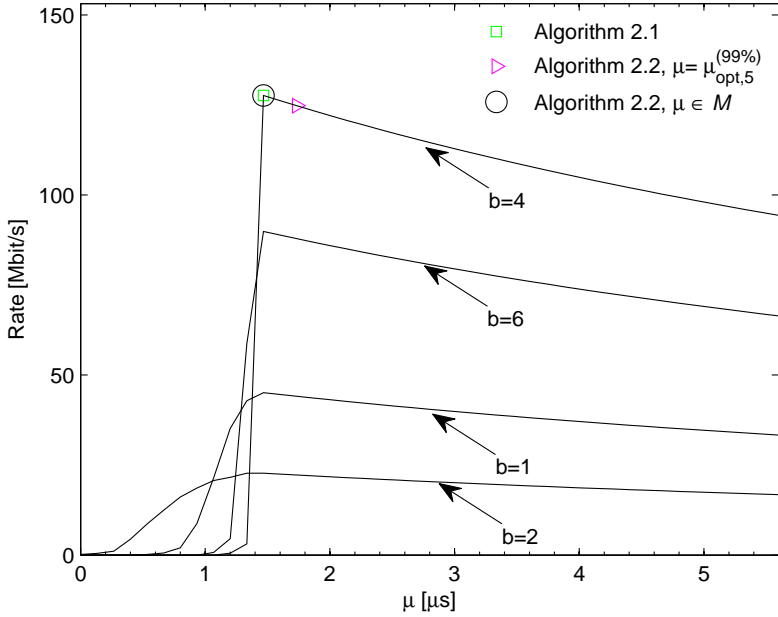


Figure 3.9: Bit rate  $R(\mu, b)$  from (3.19) as a function of CP length  $\mu$  and constellation size  $2^b$  for uniform bit-loading. Markers are results from Algorithms 2.1 and 2.2 from Section 3.4.2. The BeC channel of Class 5 is assumed. The system uses 384 sub-channels.

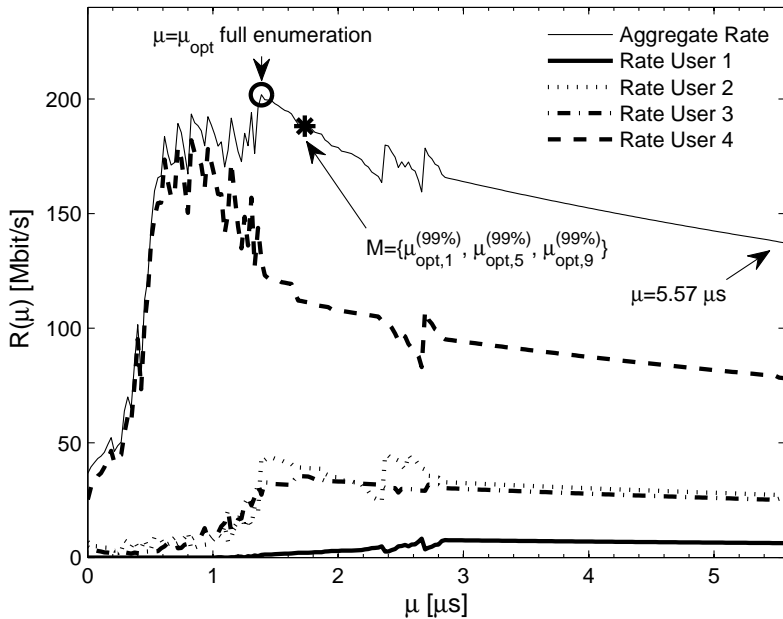


Figure 3.10: Aggregate and single user rate using bit-loading as a function of the CP length. The OFDMA system has  $N_U=4$  users and  $M=384$  sub-channels. The users experience channels belonging to different classes. Markers are results from Algorithm 3 from Section 3.5 with different sets of CP length  $\mathcal{M}$ .

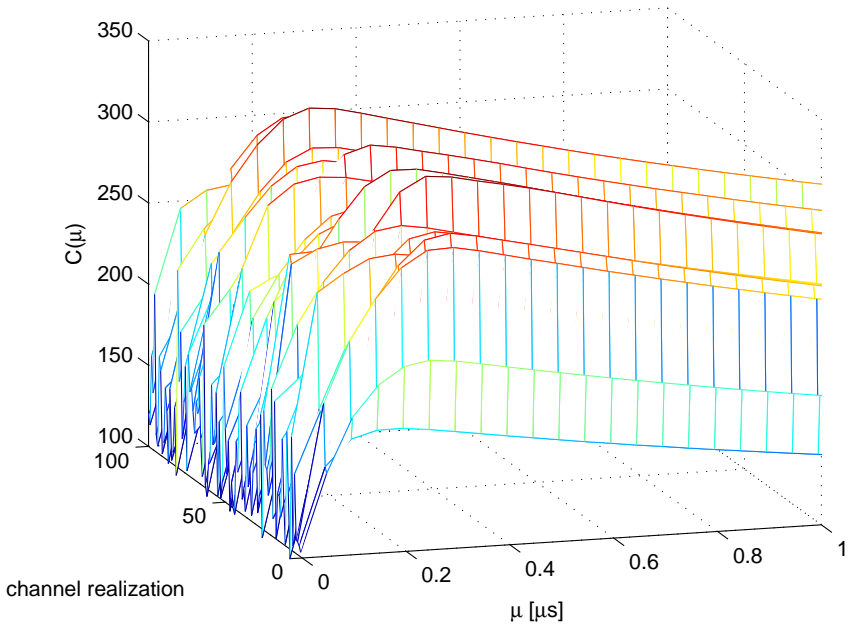


Figure 3.11: Capacity as a function of the CP length for 100 class B channel realizations. The distance between transmitter and receiver is set to 10  $m$ .

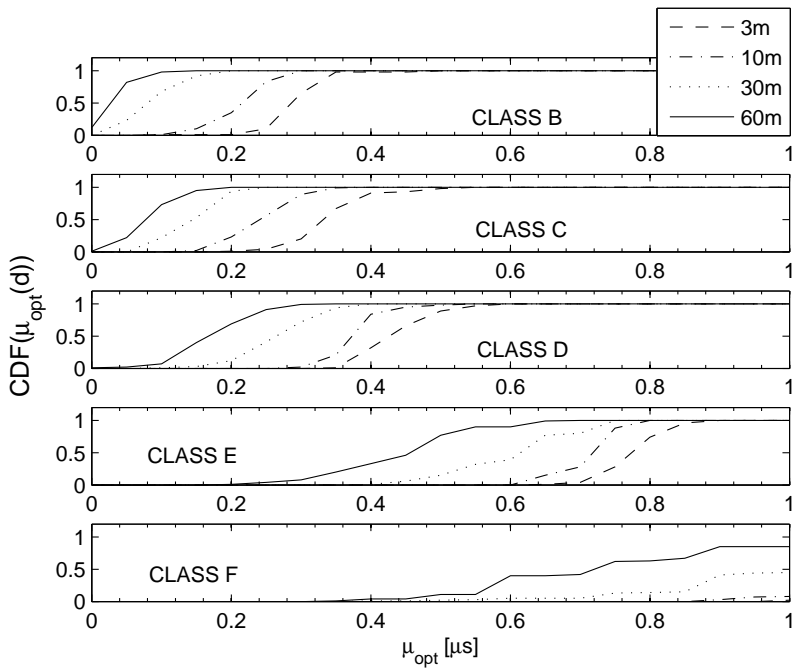


Figure 3.12: Optimal CP CDF for channels of class B, C, D, E, and F. The distances between transmitter and receiver are set to 3 m, 10 m, 30 m, and 60 m.

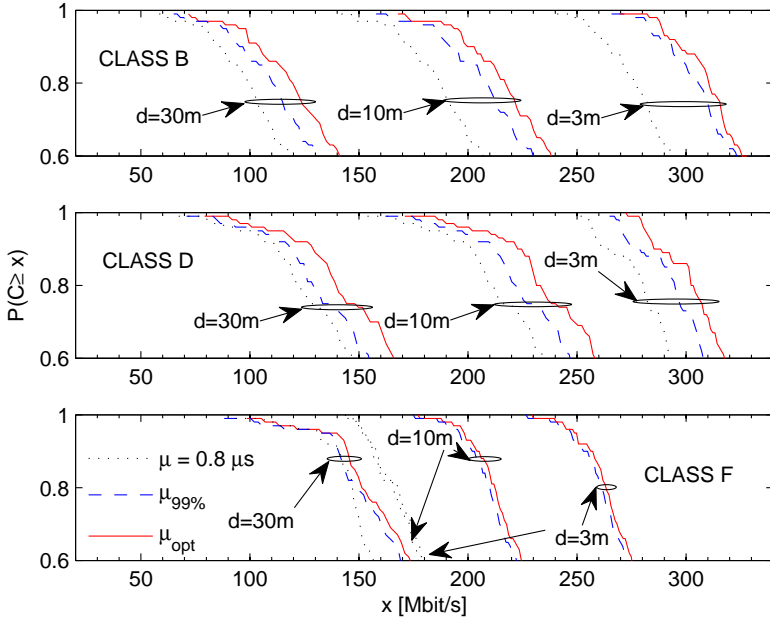


Figure 3.13: CCDF of capacity using the CP computed with (3.6), with the  $\mu_{99\%}$ , and with a fixed CP equal to  $0.8 \mu s$ . The channel classes used are the B, D, and F. The distances between the transmitter and the receiver are set to  $3 m$ ,  $10 m$ , and  $30 m$ .

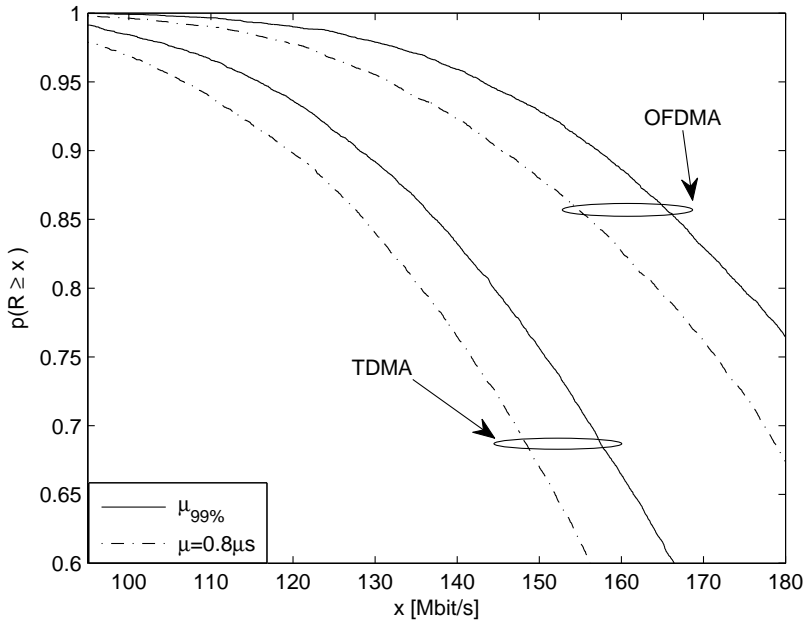


Figure 3.14: CCDF of aggregate network rate obtained using the proposed algorithms for both OFDMA and TDMA. The set of used CPs has been set equal to  $\mathbb{P} = \{0.8\mu s\}$  for the baseline system, and equal to  $\mathbb{P} = \{\mu_{99\%}^B, \mu_{99\%}^C, \mu_{99\%}^D, \mu_{99\%}^E, \mu_{99\%}^F\}$  for the proposed system.

## Parameters Design in PS-OFDM

In this chapter, we study the parameters design for the adaptive pulse shaped OFDM (PS-OFDM) scheme where the overhead and active sub-channels are adapted to jointly maximize capacity and fulfill the notching mask for coexistence with other devices operating in the same spectrum. In PS-OFDM the overhead includes the guard interval to partly compensate the channel dispersion, and the roll-off factor used by the shaping window. We show that significant gains are obtained compared to the case of using a fixed guard interval and roll-off factor. To simplify the implementation complexity we also propose to limit the amount of adaptation by deploying a finite set of overhead parameters. Numerical results are reported for typical wideband power line communication indoor channels.

### 4.1 Introduction

As we have seen in Chapter 2, PS-OFDM uses a Nyquist window to provide better sub-channel confinement than OFDM. PS-OFDM is in fact employed in the FFT-OFDM physical layer modality of the IEEE P1901 standard which operates in the band 2-30 *MHz* and grants backward compatibility with the HomePlug AV (HPAV) standard [19, 50], [2, Ch. 7]. This frequency band contains also sub-bands dedicated to other communication systems, as for example amateur radio. Hence, in order to allow coexistence a number of sub-

channels are switched off such that the transmitted signal occupies a certain spectrum with notches. Since PS-OFDM has a better sub-channel spectral containment it is capable of respecting the mask by switching off a lower number of sub-channels than OFDM.

As in OFDM, also in PS-OFDM the use of the guard interval (GI) when signaling over dispersive channels permits the orthogonalization of the system such that simple one-tap equalization per sub-channel can be used. The conventional choice is to use a GI of  $\mu$  samples that is longer than the channel duration [28]. Clearly, as for OFDM, this advantage has to be paid in terms of both a transmission rate loss and a signal-to-noise ratio penalty [29].

Since PS-OFDM uses a pulse shaping window with a roll-off (RO) equal to  $\alpha$  samples, it introduces an overhead (OH) equal to  $\alpha + \mu$  samples which yields a loss in transmission rate equal to  $M/(M + \mu + \alpha)$  where  $M$  is the number of sub-channels.

In this chapter, we address the problem of optimizing the system parameters  $\alpha$  and  $\mu$ . We propose to adapt the OH parameters  $\alpha$  and  $\mu$  to the channel realization such that we jointly maximize capacity and fulfill the notching mask for coexistence with other devices operating in the same spectrum. This realizes an adaptive PS-OFDM scheme.

To lower the computational cost, we also propose to limit the amount of adaptation, i.e., to use a finite set of OH parameters. The OH parameters can be computed from the analysis of their distribution function in statistically representative channels. Since a significant change of the OH parameters is determined by a significant change in the signal to noise ratio (SNR), we consider the design of the OH parameters for a low, a medium, and a high SNR scenario assuming a certain target notching mask. Thus, the adaptation is limited to the computation of the SNR at the receiver, followed by feedback to the transmitter of the best OH parameters for such an SNR.

This chapter is organized as follows. In Section 4.2, we briefly recall the system model. In Section 4.3, adaptive PS-OFDM is considered and the problem of optimizing the system parameters is discussed. Limited adaptation is proposed in Section 4.4. The numerical results for indoor wideband power line

channels are reported in Section 4.5. Finally, the main findings are summarized in Section 4.6.

## 4.2 System Model

We assume to employ the OFDM and the PS-OFDM system models presented in Section 2.1. Therefore, the received signal can in general be affected by interference.

In the following we briefly recall the OFDM and PS-OFDM MCM systems.

### OFDM

In OFDM the synthesis and the analysis pulses are rectangular windows with duration respectively equal to  $N = M + \mu$  and  $M$  samples. Therefore, the OH factor  $\beta$  is equal to  $\mu$  samples that corresponds to the CP length.

As we have seen in the previous chapters, if the length of the channel impulse response does not exceed the CP length by more than one, i.e.,  $\mu \geq \nu - 1$ , the system will be orthogonal such that the received symbol will be neither affected by ISI nor by ICI. This advantage has to be paid in terms of an SNR penalty and a raw transmission rate loss that is equal to  $M/(M + \mu)$ . Another drawback with OFDM is that the sub-channels have a sinc frequency response that decays as  $1/f$  and has the first side lobe only 13 dB down compared to the main lobe. This translates in poor sub-channel confinement, and consequently, in a large transmission rate penalty when notching is required to enable coexistence with other systems. In fact, to fulfill stringent notching masks a large number of sub-channels has to be switched off.

### Pulse-Shaped OFDM

To overcome the poor sub-channel frequency confinement, a window better than the rectangular window can be deployed. The scheme is referred to as PS-OFDM. In PS-OFDM the synthesis prototype pulse is a Nyquist window. A common choice is to use a raised cosine window with roll-off  $\alpha$  samples (see (2.6)). The analysis pulse corresponds to that of OFDM.

In PS-OFDM the symbol period increases by  $\alpha$  samples w.r.t. OFDM assuming that we still deploy a guard interval of length  $\mu$  samples, i.e.,  $N = M + \mu + \alpha$ . Consequently, the OH factor is equal to  $\beta = \mu + \alpha$ , and the transmission rate loss is equal to  $M/(M + \mu + \alpha)$  that turns out to be higher than in OFDM (see Fig. 2.2).

Again, if  $\mu \geq \nu - 1$  the system will be orthogonal.

### 4.2.1 Notching

State-of-the-art broadband PLC (BPLC) systems operate in the band 2-30  $MHz$  and optionally even above 30  $MHz$  [2]. This frequency band also contains sub-bands dedicated to other communication systems, as for example amateur radio. Furthermore, above 30  $MHz$  the limits for radiated emissions are much more stringent than those in the band below 30  $MHz$ . Hence, in order to allow the coexistence with other systems, the PLC modem has to be capable of respecting a flexible notching mask. In Fig. 4.1, we show a representative example of PSD mask which is similar to the one employed in the HPAV system [50]. The PSD of the transmitted signal is set at -50  $dBm/Hz$ , while the notched portions of the spectrum are set at -80  $dBm/Hz$ . The transmitted signal PSD can be computed as follows [51]

$$P_x(f) = \frac{P_a}{NT} \sum_{k \in K_{ON}(\alpha, \mu)} |G(f - f_k)|^2, \quad f \in [0, B], \quad (4.1)$$

if we assume the data symbols to be i.i.d. with zero mean and power  $P_a^{(k)} = P_a \forall k \in \mathbb{K}_{on}(\alpha, \mu)$ . Further,  $T$  is the sampling period in the system,  $B = 1/T$  is the system transmission band,  $G(f)$  is the discrete time Fourier transform of  $g(n)$ , and  $K_{ON}(\alpha, \mu)$  is the set of tones that are switched on. It is a function of the OH parameters  $\alpha$  and  $\mu$ , and for a certain choice of them, the set of active tones is determined to satisfy a target PSD mask  $P_{MASK}(f)$ , as follows

$$P_x(f) \leq P_{MASK}(f), \quad f \in [0, B]. \quad (4.2)$$

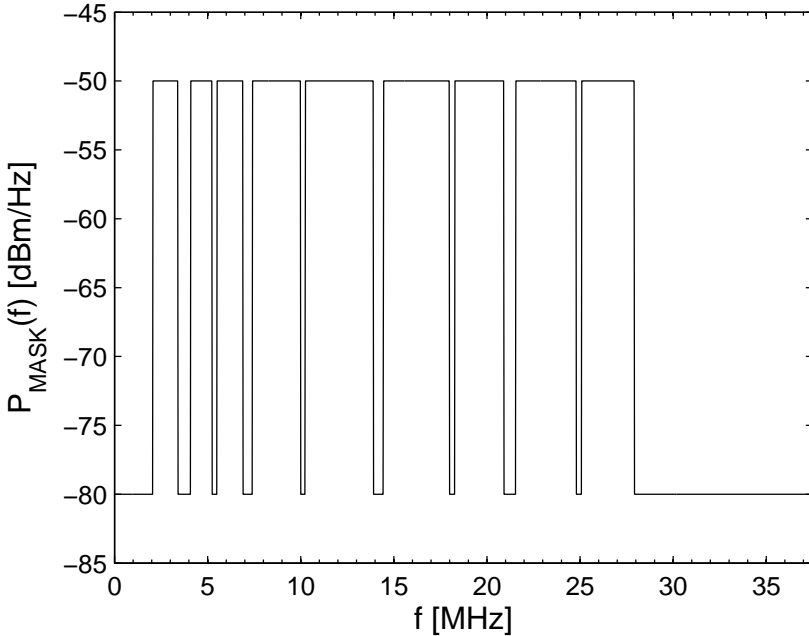


Figure 4.1: Power spectral density mask for the transmitted signal. With a carrier spacing of  $24.414 \text{ kHz}$  (as in HPAV), the number of sub-channel in  $0\text{-}37.5 \text{ MHz}$  is equal to 1536, of which 619 are notched.

For the raised cosine window of eq. (2.6),  $G(f)$  is equal to (details on the derivation are provided in Appendix 11.4):

$$G_{rcos}(f) = \frac{N}{1 - (2\alpha T f)^2} \text{sinc}(fNT) \cos(\pi f \alpha T) e^{-j\pi f(N+\alpha)T}. \quad (4.3)$$

Since PS-OFDM has a better sub-channel spectral containment, it is capable of respecting the mask by switching off a smaller number of sub-channels than OFDM. In other words, the set of used sub-channels in PS-OFDM has a cardinality that is greater than the one of OFDM when notching has to be taken into account. Therefore, although PS-OFDM requires a higher OH factor than OFDM, it may be able to transmit at a higher rate when notching

has to be taken into account. As done for OFDM in Chapter 3, in the next section, we propose a system design criterion for PS-OFDM based on the maximization of the capacity. More precisely, we propose to choose the OH factor such that maximum capacity is achieved.

### 4.3 Adaptive Pulse-Shaped OFDM

As discussed for OFDM, it is reasonable to adapt the system OH, namely the roll-off factor and the guard interval in PS-OFDM, to the specific channel realization. Furthermore, the notching mask is not necessarily static. That is, adaptive notching can be implemented to avoid parts of the spectrum in which the presence of another signal has been detected such as a radio frequency (RF) signal captured by the PLC network. This realizes a form of cognitive PLC system.

In the following, Subsection 4.3.1 describes a criterion to adapt the OH based on the capacity maximization. As it will be explained, this method is computationally complex. Therefore, we also propose a simpler suboptimal method that limits the amount of adaptation in Subsection 4.3.2.

#### 4.3.1 Channel Capacity Criterion

As shown in equation (2.3), the FB sub-channel output may experience not only noise, but also ISI and ICI. If the guard interval is sufficiently long ( $\mu \geq \nu - 1$ ), then both OFDM and PS-OFDM are orthogonal, and neither ISI nor ICI is present. However, if the guard interval is too short, the interference will occur. We can express the SINR in the  $k$ -th sub-channel output (2.3), for a certain channel realization, as follows

$$SINR^{(k)}(\mu, \alpha, \Delta) = \frac{P_U^{(k)}(\mu, \alpha, \Delta)}{P_\eta^{(k)} + P_I^{(k)}(\mu, \alpha, \Delta)}, \quad (4.4)$$

with  $P_U^{(k)}(\mu, \alpha, \Delta)$ ,  $P_I^{(k)}(\mu, \alpha, \Delta)$ , and  $P_\eta^{(k)}$  denoting the useful, the interference, and the noise power term in sub-channel  $k$ . They are defined as in equations (2.9), (2.10), and (2.11). A detailed derivation can be found in Appendix 11.1.

In order to evaluate the impact of the OH length on the PS-OFDM system performance we evaluate capacity assuming single tap sub-channel equalization and using the formula for parallel Gaussian channels, i.e., the noise and the input signals are independent and Gaussian distributed such that the interference signals from an insufficient OH are also Gaussian. We further assume a PSD constraint such that the power is uniformly distributed across the used sub-channels (see Fig. 4.1).

Therefore, if  $K_{ON}(\mu, \alpha)$  is the set of active tones indices that allows fulfilling the transmission mask, the capacity in bit/s is

$$C(\mu, \alpha, \Delta) = \frac{1}{(M + \beta)T} \sum_{k \in K_{ON}(\mu, \alpha)} \log_2 \left( 1 + \frac{SINR^{(k)}(\mu, \alpha, \Delta)}{\Gamma} \right), \quad (4.5)$$

where  $\Gamma$  represents a gap factor to take into account practical implementation constraints [30], [31]. It should be noted that the set  $K_{ON}(\mu, \alpha)$  depends on the OH parameters. As it will be shown in the numerical results section, for a fixed number of sub-channels  $M$ , as the OH increases both the cardinality of the set of active sub-channel  $|K_{ON}|$  and the SINR increase, whereas the raw transmission rate decreases. Furthermore, we point out that the capacity is a function not only of the OH but also of the synchronization phase  $\Delta$ . Therefore, the optimal OH and synchronization phase can be chosen so that (4.5) is maximized as follows

$$(\mu_{OPT}, \alpha_{OPT}, \Delta_{OPT}) = \arg \max_{\mu, \alpha, \Delta} \{C(\mu, \alpha, \Delta)\}. \quad (4.6)$$

Finding the optimal solution of (4.6) is a complex problem since it requires the full search of the three parameters  $(\mu, \alpha, \Delta)$ . To simplify it, we propose to first set the synchronization phase with a simple criterion. That is, the capacity criterion is used only for the search of the pair of parameters  $(\alpha, \mu)$  as follows

$$(\mu_{OPT}, \alpha_{OPT}) = \arg \max_{\mu, \alpha} \left\{ C(\mu, \alpha, \hat{\Delta}) \right\}, \quad (4.7)$$

where  $\hat{\Delta}$  is the synchronization phase initially determined. The approach that

we use is to determine the optimal synchronization phase when  $\mu = \nu - 1$ . In this case the interference is null, therefore  $\hat{\Delta} = 0$  is the optimal time phase [52], [53] and the receiver DFT is applied immediately after the overhead samples.

It is worth noting that with the maximum capacity criterion we optimize not only the OH parameters and adapt them to a specific channel realization, but we also adapt the set of tones that are switched off to allow the transmitted signal to respect a given PSD mask. We refer to the resulting scheme as adaptive PS-OFDM.

### 4.3.2 Maximum Rate Criterion

If we assume to use finite size constellations, under the assumption that the interference is still Gaussian, which is practically the case for a high number of tones [29], we can modify the criterion (4.7) as follows

$$(\mu_{OPT}, \alpha_{OPT}) = \arg \max_{\mu, \alpha} \left\{ R(\mu, \alpha, \hat{\Delta}) \right\}, \quad (4.8)$$

where

$$R(\mu, \alpha, \hat{\Delta}) = \frac{1}{(M + \beta)T} \sum_{k \in K_{ON}(\mu, \alpha)} b^{(k)}(\mu, \alpha, \hat{\Delta}), \quad (4.9)$$

$$b^{(k)}(\mu, \alpha, \hat{\Delta}) = \left\lfloor \left\lfloor \log_2 \left( 1 + \frac{SINR^{(k)}(\mu, \alpha, \hat{\Delta})}{\Gamma} \right) \right\rfloor \right\rfloor. \quad (4.10)$$

In (4.10), the operator  $\lfloor \bullet \rfloor$  denotes the operation of rounding the number of bits to that associated to the nearest available constellation towards zero.

### 4.3.3 Simplified Algorithm

Both the maximization problems in (4.7) and (4.8) are complex because they require to compute the set of active tones  $K_{ON}(\mu, \alpha)$  for each pair of values  $(\alpha, \mu)$  and the evaluation of the capacity (rate). To simplify the problem we propose to limit the domain of the pair of values  $(\alpha, \mu)$ . Firstly, we limit the guard interval to the channel length, i.e.,  $\mu \leq \nu - 1$ . Secondly, simulation results show that if we set  $\mu_{MAX} = \nu - 1$ , a value  $\alpha_{MAX}$  will exist beyond

which the cardinality of the set of active tones  $K_{ON}$  does not appreciably increase. Consequently, we define the domain of the capacity function as  $D = \{(\mu, \alpha) : 0 \leq \mu \leq \mu_{MAX} \wedge 0 \leq \alpha \leq \alpha_{MAX}\}$ .

To further reduce the computational complexity, we propose to limit the search of the solution in four sub-domains (search *paths*)  $D_s \subset D$  that are defined below. The sub-domains identify a certain path within the domain  $D$ . Fig. 4.2 depicts the four *paths*.

**Path A:** The roll-off  $\alpha$  is set equal to  $\alpha_{MAX}$  while  $\mu$  varies between 0 and  $\mu_{MAX}$ . Therefore,  $D_A = \{(\mu, \alpha) : 0 \leq \mu \leq \mu_{MAX} \wedge \alpha = \alpha_{MAX}\}$ . The pair  $(\alpha, \mu)$  given by the solution of (4.8) is denoted with  $(\alpha_{OPT,A}, \mu_{OPT,A})$ .

**Path B:** The guard interval  $\mu$  is set to  $\mu_{MAX}$  and  $\alpha$  varies between 0 and  $\alpha_{MAX}$ . Therefore,  $D_B = \{(\mu, \alpha) : \mu = \mu_{MAX} \wedge 0 \leq \alpha \leq \alpha_{MAX}\}$ . The pair  $(\alpha, \mu)$  given by the solution of (4.8) is denoted with  $(\alpha_{OPT,B}, \mu_{OPT,B})$ .

**Path C:** In this case we move along the diagonal of  $D$ , i.e.,  $\alpha = \mu$ , and we vary  $\mu$  between 0 and  $\mu_{MAX}$ . Therefore,  $D_C = \{(\mu, \alpha) : 0 \leq \mu \leq \mu_{MAX} \wedge \alpha = \mu\}$ . The pair  $(\alpha, \mu)$  given by the solution of (4.8) is denoted with  $(\alpha_{OPT,C}, \mu_{OPT,C})$ .

**Path D:** The guard interval  $\mu$  is set to the optimal value  $\mu_{OPT,C}$  obtained using *path C*. Then,  $\alpha$  varies from zero to  $\alpha_{MAX}$ . Therefore,  $D_D = \{(\mu, \alpha) : \mu = \mu_{OPT,C} \wedge 0 \leq \alpha \leq \alpha_{MAX}\}$ . The pair  $(\alpha, \mu)$  given by the solution of (4.8) is denoted with  $(\alpha_{OPT,D}, \mu_{OPT,C})$ .

#### 4.4 Limited Adaptation

The adaptation of the OH requires that the receiver computes the pair  $(\alpha, \mu)$  for each channel realization. A significant simplification will be obtained if the OH parameters are chosen from a small set of pre-stored values. As an example, the IEEE P1901 and the HPAV standards [19, 50], [2, Ch. 7] also specify a finite set of guard interval lengths (and a single roll-off length).

As done for OFDM in Chapter 3, herein, we propose an approach to determine the set of values based on the evaluation of the OH parameters cumulative distribution function (CDF). To obtain the OH CDF we apply the statistical PLC channel model from [48] that is also summarized in the next section.

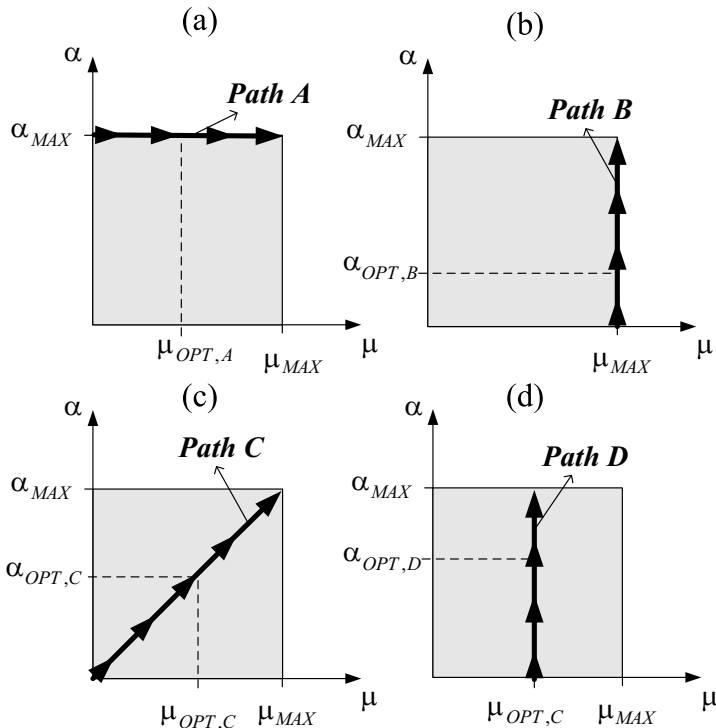


Figure 4.2: Search *paths* to maximize capacity as a function of  $(\mu, \alpha)$ .

Now, PLC channels can be partitioned into classes according to their capacity [54]. Each class is characterized by an average path loss profile and an average SNR.<sup>1</sup>

For a given channel, the capacity surface as a function of the two OH parameters (see Section 4.3) exhibits a flat shape around the optimal OH value (see Section 4.5), i.e, it does not significantly change around the optimal values. Furthermore, for the channels that belong to a given class, the optimal OH parameters have similar value. In contrast to this, significant changes of

<sup>1</sup>Assuming white additive background noise with PSD  $N_0$ , we can define the average SNR as  $\overline{SNR} = \int_0^B P_x(f) P_L(f) df / N_0 / B$  where  $P_L(f) = E[|G_{CH}(f)|^2]$  is the channel average path loss.

the optimal parameter values are found for channels that belong to different classes and that correspond to a notable SNR change. Therefore, we propose to use a unique pair  $(\alpha, \mu)$  for all channel realizations that belong to a given average SNR class. Furthermore, we reduce the number of pairs  $(\alpha, \mu)$  by considering three values of SNR, i.e., a low, a medium, and a high SNR. This induces a partition of the channels into three classes, only.

For a given average SNR, say  $SNR_{low}$ , we determine the joint cumulative distribution function of the optimal pair  $(\alpha, \mu)$  (obtained from the realizations of the channel belonging to the given class) that maximizes capacity. We denote with  $(\alpha, \mu)_{95\%}$  the pair that yields a CDF of 0.95. Then,  $(\alpha, \mu)_{95\%}$  is the OH pair used for all channel realizations belonging to the given SNR class. If the pair of OH values for which the CDF is equal to 0.95 is not unique, we choose that for which the OH  $\beta = \alpha + \mu$  is minimum.

It has to be said that the numerical computation of the joint CDF is a rather time consuming process. To simplify it, we can limit the computation by considering the sub-domains defined by the *paths A-D*. In this case, since there is only one degree of freedom, the CDF is a function of only one parameter. Thus, we determine  $\alpha_{95\%}(SNR)$  or  $\mu_{95\%}(SNR)$  as the parameter that achieves the 95th-percentile of the CDF.

We emphasize that with this method we limit the amount of adaptation. The algorithm reduces itself to the identification of the channel class and the selection of the pair  $(\alpha, \mu)_{95\%}$  from a look-up table. The identification is done by evaluating the average SNR since in our channel model there is a one-to-one correspondence between the SNR and the channel class. Certainly, the approach of adapting the CP to the specific channel realization is more robust, and it does not rely on a channel model. However, it is more complex.

## 4.5 Numerical Results

To obtain numerical results, we consider the statistical PLC channel model presented in Section 3.7.1, whose parameters are adjusted in such way that the average PL at zero frequency equals  $\{30, 50, 70\}$  dB. Fig. 4.3 shows a number of realizations of the channel responses as well as the average path

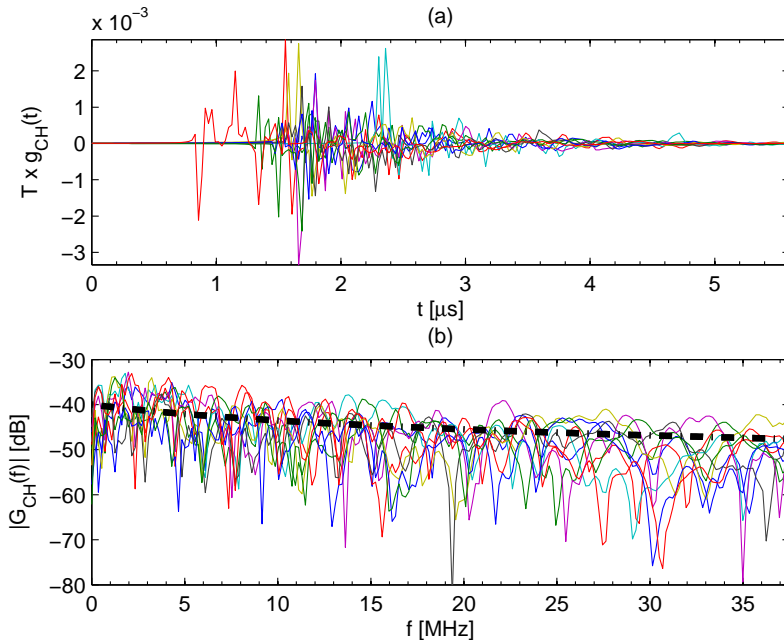


Figure 4.3: (a) Ten channel impulse response realizations, and (b) their frequency responses and the average path loss.

loss.

The signal is transmitted with a power spectral density  $P_x(f) = P_x$  equal to  $-50 \text{ dBm/Hz}$  such that the PSD of Fig. 4.1 is respected. The background noise is assumed to be white Gaussian with a PSD equal to  $-140 \text{ dBm/Hz}$  [55]. We consider three channel classes with different average SNR, the channel is normalized such that the average path loss at zero frequency is equal to 70, 50 and 30 dB. Therefore the average SNR at zero frequency<sup>2</sup> is respectively equal to 20, 40, and 60 dB. The average SNR at zero frequency is used to label the performance curves. The average  $\overline{SNR}$  is respectively equal to 16.7 dB, 36.7 dB and 56.7 dB.

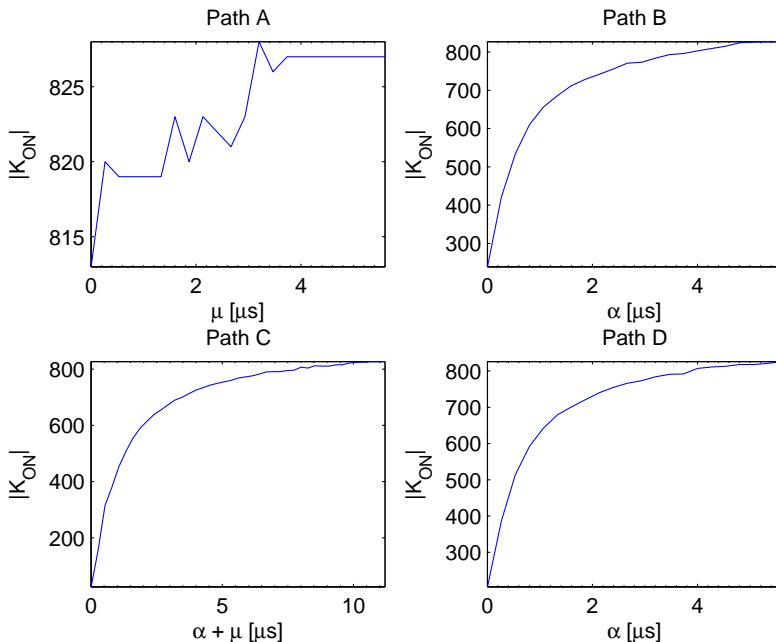
<sup>2</sup>Assuming a constant transmitted PSD  $P_x$ , the average SNR at zero frequency can be defined as  $SNR = P_x P_L(0) / N_0$ .

For the transmitter, we choose parameters similar to those employed in HPAV [18]. The number of sub-channels is  $M = 1536$  in the band  $0\text{-}37.5\text{ MHz}$ . The interested reader can find results of adaptive PS-OFDM system that works in the frequency band  $2\text{-}100\text{ MHz}$  in [56]. The transmission window is either rectangular or raised cosine. The OH parameters can assume the maximum values  $\mu_{MAX} = \alpha_{MAX} = 5.6\ \mu\text{s}$ . The QAM constellations that we deploy for bit-loading have size  $2^c$  with  $c = [1, 2, 4, 6, 8, 10]$ . The gap factor is set to  $\Gamma = 9\text{ dB}$ . Finally, we let the parameters  $\mu$  and  $\alpha$  vary in steps of 10 samples ( $0.267\ \mu\text{s}$ ).

#### 4.5.1 Performance with Adaptation

As discussed, both  $\mu$  and  $\alpha$  have an effect on the sub-channel frequency response in PS-OFDM. In turn, this affects the number of tones that need to be switched off to fulfill a certain notching mask. Let us consider the notching mask of Fig. 4.1. As we can see from Fig. 4.4, for the *path A*, where we set the roll-off equal to  $\alpha = 5.6\ \mu\text{s}$ , the increase of the guard interval does not appreciably increase the number of active sub-channels. In other words, the guard interval does not significantly affect the signal PSD once the roll-off is set to  $5.6\ \mu\text{s}$ . In contrast to this, for the other *paths* the number of active sub-channels increases significantly by increasing the roll-off factor up to  $\alpha_{MAX}$ . For all the *paths*, the maximum number of active tones is equal to 827. In Fig. 4.5, we show the bit-rate (4.9) that is obtained when the search of the OH parameters is done moving through the four *paths* in Fig. 4.2 for an SNR equal to  $40\text{ dB}$ . We observe that an optimal pair  $(\alpha, \mu)$  can be found for each of the 100 channel realization herein considered. The rate-optimal OH values depend on the search *path*, and the achievable-rate varies significantly as a function of  $(\alpha, \mu)$ .

To determine the achievable gains, we deploy, as a baseline, the system that uses a constant value for both the guard interval and the roll factor that are equal to the channel length of  $5.6\ \mu\text{s}$ . Fig. 4.6 shows the bit-rate gains obtained adapting the GI and the RO to the channel condition using the rate maximization criterion (4.8) along the four *paths*. The gains are computed

Figure 4.4: Cardinality of  $\mathbb{K}_{\text{on}}$  for the four paths.

w.r.t. to the baseline system that uses a constant OH. The gains are reported for 100 channel realizations assuming an SNR equal to 20 dB, 40 dB and 60 dB. As we can see, *path A* gives the best results for all SNR cases and for all channel realizations. For this path the gains range between 5% and 11%.

It is interesting to note that high gains are obtained for low SNRs. This can be explained by observing that for low SNRs the noise dominates the interference. Thus, in the rate formula (4.9), the rate loss given by the factor  $M/(M+\beta)$  outweighs the rate gain from the SINR increase due to an increase of the OH and in particular of the GI.

In Table 4.1, we report the average bit-rate that is obtained with the rate maximization criterion with the search *path A*, and the bit-rate that we will obtain if we set both the GI and the RO equal to 5.6  $\mu\text{s}$  (baseline system).

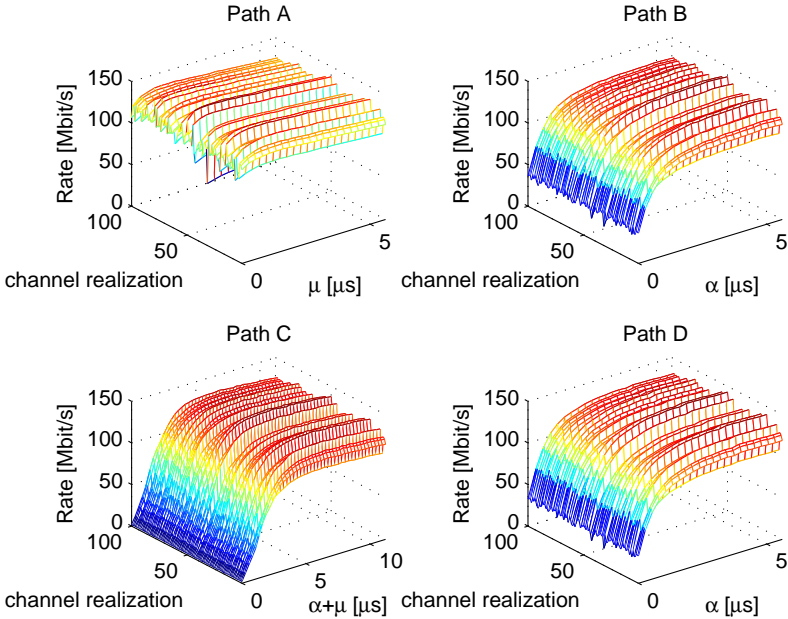


Figure 4.5: Bit-rate as a function of overhead parameters restricted to the search paths in Fig. 4.2 for 100 channel realizations. The SNR is equal to 40 dB.

Table 4.1 also lists the bit-rate obtained using limited adaptation as discussed in the next subsection.

Now, in Fig. 4.7, we show the bit-rate that is achieved when no notching is required. A comparison with OFDM is also reported. The figure shows that the rate curves have a more pronounced convex shape than those in Fig. 4.5. OFDM achieves a higher rate than PS-OFDM that uses a fixed  $\alpha = 5.6 \mu\text{s}$ . However, it should be noted that if we adapted the roll-off factor, then PS-OFDM would use a roll-off equal to zero, thus, falling back to OFDM. However, although not shown here, we note that OFDM has poor performance when notching is required.

Finally, Table 4.2 summarizes the results in terms of average bit-rate for

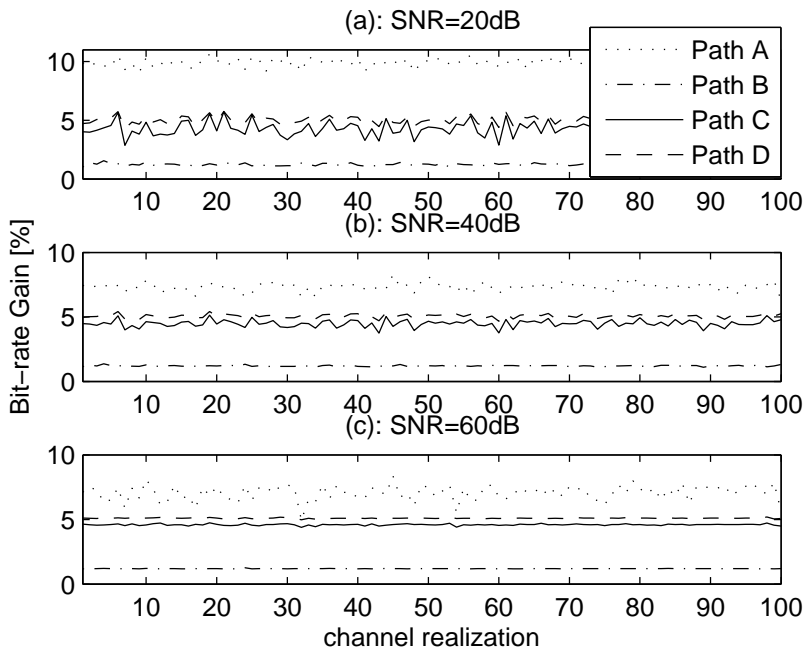


Figure 4.6: Bit-rate gain given by the adaptation of the GI and of the RO for 100 channel realizations obtained with the rate maximization criterion along the four paths in Fig. 4.2. The SNR has been set to (a): 20 dB, (b): 40 dB, and (c): 60 dB. The gains have been computed w.r.t. the bit-rate obtained when using the constant values  $\mu=5.6 \mu\text{s}$ .

OFDM and PS-OFDM without notching.

#### 4.5.2 Limited Adaptation

As discussed in the previous subsection, solving (4.8) along *path A* gives the best results for the channels and notching mask that we have considered. Nevertheless, it is worth noting that the bit-rate curves (Fig. 4.5) show that the bit-rate will not dramatically change if we choose an OH close but not exactly identical to the optimal one. This observation justifies the idea of limiting the adaptation, in particular the idea of using the OH CDF to find the finite set

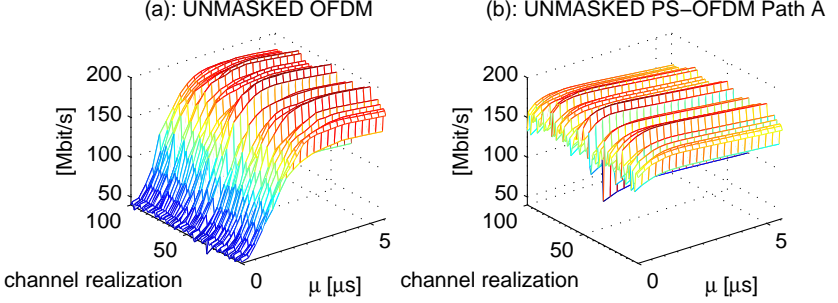


Figure 4.7: Bit-rate for the Unmasked case using the search *path A*. (a): OFDM. (b): PS-OFDM. The SNR is equal to 40 dB.

of OHs as described in Section 4.4.

In Fig. 4.8, we show the guard interval CDF obtained solving (4.8) when the search is done along *path A*. The guard intervals that yield a CDF equal to 0.95 are:  $\mu_{95\%}(20\text{dB}) = 0.25 \mu\text{s}$ ,  $\mu_{95\%}(40\text{dB}) = 1.6 \mu\text{s}$ ,  $\mu_{95\%}(60\text{dB}) = 2 \mu\text{s}$ . Recalling that the roll-off for *path A* is equal to  $\alpha_{OPT,A} = 5.6 \mu\text{s}$ , we can compute the OH values as  $\beta(SNR) = \alpha_{OPT,A} + \mu_{95\%}(SNR)$ . They are equal to  $\beta(20\text{dB}) = 5.85 \mu\text{s}$ ,  $\beta(40\text{dB}) = 7.2 \mu\text{s}$ , and  $\beta(60\text{dB}) = 7.6 \mu\text{s}$ .

HPAV specifies a very large value of OH that is used for the synchronization channel, and two OH values that are used during normal transmission [2]. The latter two OH values are equal to  $5.56 \mu\text{s}$ , and  $7.56 \mu\text{s}$ . Further, the RO is set to  $4.96 \mu\text{s}$ . These values are close to the ones that we have computed with the proposed method. The roll-off duration of HPAV is smaller than the one we obtained. It has however to be said that HPAV uses a piece wise linear window [57].

Finally, in Table 4.1 and 4.2, we summarize the performance results in terms of average bit-rate. The main remarks are the following:

1. When notching is not required, the optimal roll-off is equal to zero, i.e., PS-OFDM becomes identical to OFDM. In such a case the average gains

Table 4.1: Average bit-rate comparisons: masked case

PS-OFDM			
SNR [dB]	Avg. Rate [Mbit/s] $\alpha = 5.6 \mu\text{s}$ $\mu$ -adap.	Avg. Rate [Mbit/s] $\alpha = 5.6 \mu\text{s}$	Avg. Rate [Mbit/s] $\alpha = 5.6 \mu\text{s}$ $\mu = 5.6 \mu\text{s}$
20	34.7	34.7 $\mu_{95\%} = 0.25 \mu\text{s}$	31.5
40	126.3	126.2 $\mu_{95\%} = 1.6 \mu\text{s}$	117.7
60	169	168 $\mu_{95\%} = 2 \mu\text{s}$	157.8

Table 4.2: Average bit-rate comparisons: unmasked case

SNR [dB]	OFDM		PS-OFDM	
	Avg. Rate [Mbit/s] $\alpha = 0$ $\mu$ -adap.	Avg. Rate [Mbit/s] $\alpha = 0$ $\mu = 5.56 \mu\text{s}$	Avg. Rate [Mbit/s] $\alpha = 5.6 \mu\text{s}$ $\mu$ -adap.	Avg. Rate [Mbit/s] $\alpha = 5.6 \mu\text{s}$ $\mu = 5.6 \mu\text{s}$
20	49.3	46.1	45.7	41.2
40	176.1	170.6	164.1	152.3
60	234.4	227.7	218.1	203.2

obtained by adapting the GI w.r.t. to using a constant GI as long as the channel, span between 3% and 7%;

2. The search path A yields the highest bit-rate among the four search paths considered, when we use the HPAV notching mask of Fig. 4.1. In such a case the roll-off factor is equal to  $5.6 \mu\text{s}$  and the adaptation of the GI yields gains, w.r.t. a GI equal to the channel length, that range between 5% and 11%;
3. The limited adaptation of the GI based on the CDF criterion gives an

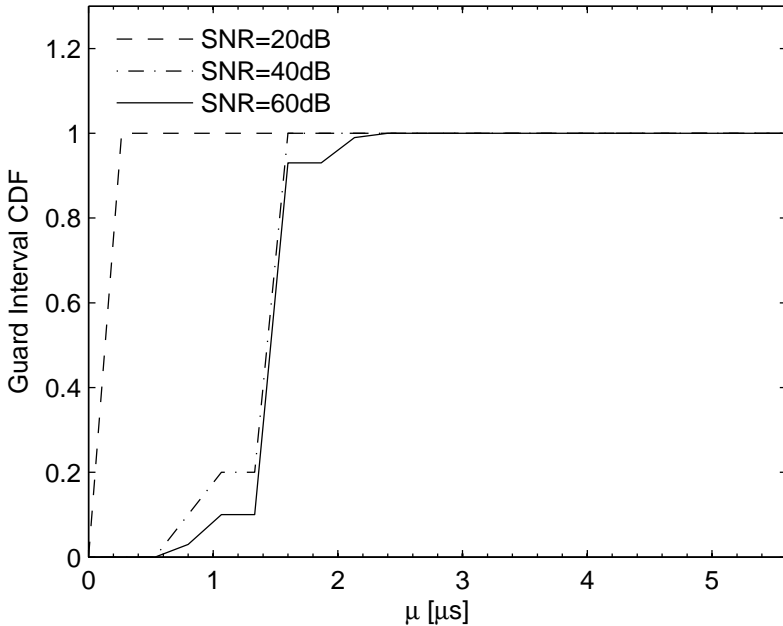


Figure 4.8: Guard interval CDF using the search *path A*.

average bit-rate very close to the one that we achieve if we fully adapt the GI.

## 4.6 Main Findings

We have proposed an adaptive pulse-shaped OFDM scheme where the OH parameters (guard interval and roll-off factor) are adapted to jointly maximize capacity and fulfill a desired notching mask. The adaptation can be done when the channel response and/or the notching mask changes. This realizes a form of cognitive PLC system if the notching mask is adapted according to the presence or absence of interferers in the transmission spectrum.

To lower the computational cost, we have also proposed to limit the amount of adaptation, i.e., to use a finite set of OH parameters. The OH values can be

pre-computed from the analysis of their distribution function in statistically representative channels. Since a significant change of the OH parameters is caused by a significant change in the SNR, we have considered the design of the OH parameters for a low, a medium, and a high SNR scenario assuming a certain target notching mask. Thus, the adaptation is limited to the computation of the SNR at the receiver, and feedback to the transmitter of the best OH parameters for such an SNR.

Several performance results show that both the full adaptation and the limited adaptation provide notable gains compared to the case of using constant suboptimal OH parameters, i.e., a RO that minimizes the number of switched off tones and a GI as long as the channel.

## Parameters Design in FMT

In this chapter, we consider the design of the parameters in filtered multitone (FMT) modulation. In particular, we consider the adaptation of the overhead factor of FMT to the channel condition. Optimal and sub-optimal approaches are described. Comparisons with orthogonal frequency division multiplexing (OFDM) are also presented. Both, the single user and the multi user (based on frequency division multiplexing) cases are considered. Through extended numerical results over typical WLAN channels we show that the use of adaptive FMT could further improve the WLAN standard achievable rate w.r.t. the use of adaptive OFDM.

### 5.1 Introduction

As we have seen in Chapter 2, a multi-carrier modulation (MCM) system can be described using a filter bank architecture. In such a case, at the transmitter side, the  $M$  parallel data signals are interpolated by a factor  $N = M + \beta$ , filtered with a modulated prototype pulse and transmitted over the channel. The interpolation factor (IF)  $N$ , or equally the OH  $\beta$ , and the modulated prototype pulse determine the type of MCM scheme, e.g., OFDM or FMT. On the other hand, the IF also affects the achievable rate of the system. As an example, in OFDM, the IF determines the duration of the cyclic prefix (CP). As discussed in previous chapters, if the CP is longer than the channel duration,

the received signal will be neither affected by inter-carrier interference (ICI) nor by inter-symbol interference (ISI) [29]. Nevertheless, this benefit is paid in terms of a loss in achievable rate and in SNR of a factor  $M/(M + \beta)$ , with  $\beta$  equal to the CP duration.

In Chapter 3, we have found that over typical WLAN channels, the CP does not need to be long as the channel duration to maximize the achievable rate, or with an abuse of terminology, to maximize capacity. Furthermore, for each channel class of the IEEE 802.11n WLAN channel model [49], we have found a near optimal value of CP designed according to the statistic of the capacity-optimal CP duration. We have shown that capacity improvements for the WLAN standard are attainable adapting the CP to the experienced channel class, this is true for both the single and the multi user cases. Moreover, for the multi user case, we have found that the CP adaptation to the channel class improves the aggregate network rate both with the use of OFDMA and with the use of TDMA.

In [26], it has been shown that for the single user case, over typical power line channels, FMT provides significant gains in terms of achievable rate w.r.t. OFDM, but its digital implementation is more complex than that of OFDM. This statement is true considering both FMT and OFDM with OH adapted to the channel conditions.

Inspired by the above results, in this chapter, we are interested on extending to FMT the approach followed in Section 3.3.3 to design the OH in OFDM. That is, we want to find a limited set of OH values for FMT using the statistic of the capacity-optimal OH. The set of OH values is used to adapt the system to the channel conditions. We call such a system adaptive-FMT. We compare adaptive-FMT with the adaptive-OFDM presented in Section 3.3.3, and we show that further capacity improvements to the IEEE 802.11 standard could be obtained adopting the former scheme, although it requires a higher computational complexity to be implemented.

Regarding the multi user case, we focus on the downlink channel where the network coordinator signals to the  $N_U$  users of the network. Considering this scenario, we propose for FMT-FDMA a sub-channel allocation algorithm

jointly with the adaptation of the OH duration. We then compare adaptive-FMT-FDMA with adaptive-OFDMA (presented in Section 3.5) and we show that the former scheme significantly outperforms the latter.

The chapter is organized as follows. In Section 5.2, we briefly recall the system model. Thus, considering a single user scenario, in Section 5.3, we compute the optimal and the sub-optimal OHs for FMT, and we review the results obtained in Section 3.8 for OFDM. In Section 5.4, we extend the OH adaptation to the multi user case, namely, to FMT-FDMA.

Extensive numerical results that compare FMT and OFDM in both single and multi user cases are presented in Section 5.5. Finally, the main conclusions follow.

## 5.2 System Model

We consider the system model presented in Chapter 2. Furthermore, we assume the signal to be transmitted from the access point to the user  $u$  over a channel that has an equivalent complex impulse response  $g_{ch}^{(u)}(n, d)$ , where  $d$  denotes the distance between the transmitter and the receiver. As it was assumed in Section 3.8, we here use the IEEE 802.11 TGn channel model [49]. We just recall that this model generates channels belonging to five classes labeled with B,C,D,E,F, and that each class is representative of a certain environment, e.g., small office, large open space/office with line of sight (LOS) and NLOS propagation, and so on.

The received signal  $y^{(u)}(n) = x^{(u)}(n) * g_{ch}^{(u)}(n, d)$  is analyzed with a filter bank having sub-channel pulses  $h(n)$ . The outputs are sampled with period  $N$ . Therefore, before equalization, the signal received by user  $u$  in the  $k$ -th sub-channel is given by

$$z^{(u,k)}(\ell N) = a^{(u,k)}(\ell N)g_{TOT}^{(u,k)}(0) + ISI^{(u,k)}(\ell N) + ICI^{(u,k)}(\ell N) + \eta^{(u,k)}(\ell N). \quad (5.1)$$

In (5.1),  $g_{TOT}^{(u,k)}(0)$  denotes the complex amplitude of the data of interest, whereas,  $ISI^{(u,k)}(\ell N)$ ,  $ICI^{(u,k)}(\ell N)$ , and  $\eta^{(u,k)}(\ell N)$  respectively denote the ISI, the ICI and the noise term experienced by user  $u$  in sub-channel  $k$ . The in-

interference terms are in general present when transmitting through a frequency selective channel. They can be mitigated with some form of equalization. The filter bank design aims at reaching a tradeoff between ISI and ICI. While the presence of both ISI and ICI requires a multi-channel equalizer, the presence of only ISI allows for using sub-channel equalization. In our analysis, we consider the use of sub-channel equalization only. Therefore, the signal after the sub-channel equalization can be written as

$$z_{EQ}^{(u,k)}(\ell N) = a^{(u,k)}(\ell N)g_{EQ}^{(u,k)}(0) + ISI_{EQ}^{(u,k)}(\ell N) + ICI_{EQ}^{(u,k)}(\ell N) + \eta_{EQ}^{(u,k)}(\ell N), \quad (5.2)$$

where we use the subscript EQ to denote the dependence from the equalizer. The terms  $g_{EQ}^{(u,k)}(0)$ ,  $\eta_{EQ}^{(u,k)}(\ell N)$ ,  $ISI_{EQ}^{(u,k)}(\ell N)$  and  $ICI_{EQ}^{(u,k)}(\ell N)$ , respectively denote the peak of the overall impulse response, the noise term and the interference terms at the  $k$ -th sub-channel equalizer output.

**OFDM.** The OFDM scheme can be obtained setting the synthesis and the analysis pulses respectively equal to rectangular pulses of duration  $N = M + \beta$  and  $M$  samples (see Section 2.3). The factor  $\beta$  denotes the length of the CP. As previously said, when the length of the CP is greater than the channel duration, the received signal (5.1) is neither affected by ISI nor by ICI [29]. In such a case the equalization task reduces to a simple single tap zero forcing sub-channel equalizer. Through this chapter, when showing numerical results for OFDM, we assume the use of a simple single tap sub-channel equalizer. That is, each sub-channel equalizer multiplies the received signal (5.1) by  $\left(g_{TOT}^{(u,k)}(0)\right)^{-1}$ . We make this choice to maintain simple the OFDM implementation.

**FMT.** In FMT (see Section 2.2), the sub-channel symbol period is  $N$  and the analysis pulse is matched to the synthesis pulse, i.e.,  $h(n) = g^{(*)}(-n)$ . A distinctive characteristic of FMT is that the prototype pulse is designed to obtain high frequency confinement [5]. Therefore, qualitatively we can say that in FMT the ICI term is negligible, and thus the equalization task focuses on

deleting the ISI term. This observation justifies our assumption of considering only sub-channel equalization.

When showing numerical results for FMT, we consider minimum mean square error (MMSE) fractionally spaced sub-channel equalization [51]. Furthermore we deploy a truncated root-raised-cosine pulse with rolloff equal to  $(N - M)/M$ , and length 10 symbols to obtain good frequency confinement.

### 5.3 Adaptive Overhead: The Single User Case

In Chapter 3, we have seen that an optimal criterion for the design of the cyclic prefix in OFDM is based on the capacity maximization. The same idea can be used to optimize the overhead factor  $\beta$  of FMT. In this section, we first present the optimal approach to design the OH factor of FMT, we then present a simplified approach that is based on the evaluation of the optimal OH CDF.

#### 5.3.1 Optimal OH Adaptation

To evaluate the impact of the OH duration on the FMT performance, we can follow the same procedure used for the CP optimization of OFDM. We can compute the capacity assuming parallel Gaussian channels. That is, we assume additive white Gaussian noise, independent and Gaussian distributed input signals, which renders ISI and ICI also Gaussian (cf. e.g. [29]). Therefore, the capacity in bit/s for the link of user  $u$  and for a given channel realization is given by

$$C^{(u)}(\beta) = \sum_{k \in \mathbb{K}_{\text{on}}^{(u)}} C^{(u,k)}(\beta), \quad (5.3)$$

with

$$C^{(u,k)}(\beta) = \frac{1}{(M + \beta)T} \log_2 \left( 1 + \text{SINR}_{EQ}^{(u,k)}(\beta) \right), \quad (5.4)$$

where  $\text{SINR}_{EQ}^{(u,k)}(\beta)$  denotes the signal over interference plus noise ratio, after sub-channel equalization, experienced by user  $u$  in sub-channel  $k$  when we transmit using an OH of  $\beta$  samples. Details on its computation, can be found

in Section 2.5 for OFDM, and in [58] for FMT. In (5.3),  $\mathbb{K}_{\text{on}}^{(u)}$  denotes the set of sub-channels used by user  $u$ .

In (5.3), the factor  $T$  denotes the system sampling period. Through this chapter we assume to transmit power across sub-channels at a constant level given by a constraint on the power spectral density (PSD).

From (5.3), we can see that the capacity of both OFDM and FMT is a function of the OH duration  $\beta$ . Therefore, considering a single user communication, an optimal approach to adapt the OH to the channel realization is to choose  $\beta$  as the value that maximizes capacity (5.3), i.e.,

$$\beta_{\text{opt}}^{(1)} = \underset{0 \leq \beta < \nu^{(1)}}{\operatorname{argmax}} \left\{ C^{(1)}(\beta) \right\}, \quad (5.5)$$

where we have denoted with  $\nu^{(1)}$  the channel duration in samples. The choice of considering  $\beta$  shorter than the channel duration is dictated by two reasons. First, in OFDM the SINR does not increase for a value of OH, or equally of CP, greater than the channel duration, and thus the capacity only decreases for higher OH values. Second, in FMT, numerical results show that the optimal OH is always shorter than the channel duration.

Since the argument of (5.5) is generally not convex, the implementation of the optimal approach requires an exhaustive search which is complex and maybe unfeasible over typical WLAN channels that change in time, for complexity/time issues. Clearly, there are situations where this approach can be adopted, as for instance, the case where two fixed laptops are wirelessly connected and exchange data. In this case the channel can be consider quasi static.

A significant simplification that assures the feasibility of the OH adaptation to the channel realization, is to pre-compute a limited amount of OH values, and then adapt the OH over this small set of values. This is discussed in the next sub-section.

### 5.3.2 Simplified OH Adaptation

In this section, we are interested at finding a finite set of OH values over which perform adaptation. The method that we use is based on the evaluation of the statistics of the capacity-optimal OH (5.5). As it will be clarified in the following, since the statistics of the capacity-optimal OH depends on the used MCM scheme, in the following we distinctly describe the simplified OH adaptation for OFDM and FMT.

**Simplified OH Adaptation in OFDM.** To determine the limited set of CP values for OFDM, in Section 3.3.3, we have proposed an approach based on the evaluation of the cumulative distribution function (CDF) of the capacity-optimal CP (5.5). As it has been shown in Section 3.8, the capacity-optimal CP value depends on the specific channel realization and therefore, in general, it relies on the channel class and on the distance between the access point (AP) and the user. However, we have noted that the CP value variations are more pronounced among classes than within a given class. That is, the variation of the CP for the channel realizations of a given class for various distances is not as significant as if we draw channels from different classes. Hence, we have proposed to choose a single value of CP for all channel realizations that belong to a certain channel class. For a given class and distance, the specific CP length is chosen to be the value of  $\beta$  for which the CDF of (5.5) is 99%. Then, to obtain a single CP value associated to that class we pick the largest CP among those obtained for the considered set of distances, say from  $3 m$  to  $60 m$ . The set of the obtained CP values for the five classes is denoted with  $\mathcal{M}_{OFDM} = \left\{ \beta_{B,OFDM}^{(99\%)}, \beta_{C,OFDM}^{(99\%)}, \beta_{D,OFDM}^{(99\%)}, \beta_{E,OFDM}^{(99\%)}, \beta_{F,OFDM}^{(99\%)} \right\}$ .

Clearly, once the devices know the scenario in which they are working, or equivalently the experienced channel class, the CP adaptation reduces to pick the corresponding value of CP from the set  $\mathcal{M}_{OFDM}$ .

**Simplified OH Adaptation in FMT.** To determine the limited set of OH values for FMT, we use a method similar to the one above described for OFDM.

Looking at the capacity-optimal OH CDFs of FMT (see Section 5.5), we notice that its variations are more pronounced within a given class than among different classes. In other words, the capacity-optimal OH CDF of FMT strongly relies on the distance between transmitter and receiver. Whereas, for a given distance, the dependence among classes is negligible. Therefore, for FMT we choose to define the limited set of OH values based on the distance between transmitter and receiver. In order to have a limited set of OH values, we compute the capacity-optimal OH CDF only for four values of distances, i.e.,  $3 m$ ,  $10 m$ ,  $30 m$ ,  $60 m$ . Now, for each value of distance, we choose a near optimal OH as the value of OH that renders the corresponding capacity-optimal OH CDF equal to 99%. The corresponding set of OH values is  $\mathcal{M}_{FMT} = \left\{ \beta_{3,FMT}^{(99\%)}, \beta_{10,FMT}^{(99\%)}, \beta_{30,FMT}^{(99\%)}, \beta_{60,FMT}^{(99\%)} \right\}$ .

It is worth noting that for FMT, if we chose for each channel class, the smallest value of  $\beta$  such that all the OH CDFs are lower than 0.99, as we did for OFDM, we would obtain the same OH value for all the channel classes. Thus, this method could be used to design a single value of OH in FMT.

## 5.4 Adaptive Overhead: The Multi User Case

Since we have already shown in Section 3.8 that OFDMA outperforms OFDM that deploys time division multiple access, to assess the performance of multiuser FMT we consider a network where multiplexing is accomplished via FDMA. We focus on the downlink channel from the access point (AP) to the  $N_U$  users of the network. Since the channels experienced by the users are different, the AP allocates the sub-channels and the OH according to a fair principle based on maximizing the aggregate network rate but assuring that all users exceed a minimum rate.

In the following, we extend to FMT-FDMA the optimal and the sub-optimal OH and sub-channels allocation algorithms that we have described in Section 3.5 for OFDMA.

### 5.4.1 Sub-channels and OH Adaptation

In order to allocate the sub-channels to the network users, for a certain value of  $\beta$ , the AP can solve the following optimization problem

$$\begin{aligned}
 R(\beta) = \max_{\underline{\alpha}} \quad & \sum_{u=1}^{N_U} \sum_{k \in \mathbb{K}_{\text{on}}} \alpha^{(u,k)} C^{(u,k)}(\beta), \\
 \text{s.t.} \quad & \sum_{u=1}^{N_U} \alpha^{(u,k)} = 1, \quad k \in \mathbb{K}_{\text{on}}, \\
 & \sum_{k \in \mathbb{K}_{\text{on}}} \alpha^{(u,k)} C^{(u,k)}(\beta) \geq p^{(u)} \sum_{k \in \mathbb{K}_{\text{on}}} C^{(u,k)}(\beta), \quad u = 1, \dots, N_U.
 \end{aligned} \tag{5.6}$$

In (5.6),  $\alpha^{(u,k)}$  denotes the binary sub-channel coefficient equal to 1 if sub-channel  $k$  is allocated to user  $u$ , and to zero otherwise, and  $\underline{\alpha} = \{\alpha^{(u,k)}, \text{ for } u = 1, \dots, N_U; \text{ and } k \in \mathbb{K}_{\text{on}}\}$ .  $p^{(u)}$  are quality of service coefficients, each denotes the percentage of achievable rate that the  $u$ -th user has to achieve w.r.t. the one that it would achieve in the corresponding single user scenario.  $R(\beta)$  denotes the aggregate network rate when deploying an OH of  $\beta$  samples.  $\mathbb{K}_{\text{on}}$  denotes the set of available sub-channels, e.g., for the WLAN standard [8], it corresponds to  $M = 64$  sub-channels deployed in a frequency band of  $20 \text{ MHz}$ . Problem (5.6) can be solved using integer programming (IP) [44]. In order to diminish the computational complexity, we solve (5.6) via linear programming (LP) followed by rounding the coefficients  $\alpha^{(u,k)}$  to the nearest zero or one integer. Consequently, for each value of  $\beta$  the set of sub-channels assigned to user  $u$  is given by  $\mathbb{K}_{\text{on}}^{(u)} = \{k : \alpha^{(u,k)} = 1\}$ . The optimal value of  $\beta$  is obtained by the maximization:  $\text{argmax}_{\beta} \{R(\beta)\}$ .

The exhaustive search of the OH values renders the algorithm complexity relatively high. A significant simplification is obtained if we solve (5.6) with LP only for the finite set of OH values that has been pre-determined in the single user case according to the criteria of Section 5.3.2. That is, the optimal OH is respectively given by  $\beta_{\text{opt}}^{\text{OFDMA}} = \text{argmax}_{\beta \in \mathcal{M}_{\text{OFDMA}}} \{R(\beta)\}$  for OFDMA, and by  $\beta_{\text{opt}}^{\text{FMT-FDMA}} = \text{argmax}_{\beta \in \mathcal{M}_{\text{FMT}}} \{R(\beta)\}$  for FMT-FDMA.

It is worth noting that for the case of OFDMA, if the environment where

the devices operate is known, or in other words, the AP knows the channel class of its network, the set  $\mathcal{M}_{OFDM}$  of the CPs reduces to one value. Therefore, for OFDMA, the allocation of sub-channels to the network users consists in solving (5.6) only for a single value of  $\beta$ .

## 5.5 Numerical Results

To obtain numerical results, we have chosen the following system parameters that, considering OFDM, are essentially those of the IEEE 802.11 standard [8]. The MCM systems use  $M = 64$  sub-channels with a transmission bandwidth of  $20\text{ MHz}$ . The signal is transmitted with a constant PSD of  $-53\text{ dBm/Hz}$ . At the receiver side, we add white Gaussian noise with PSD equal to  $-168\text{ dBm/Hz}$ . Thus, the SNR, without path loss and fading, on each sub-channel is  $115\text{ dB}$ . The baseline systems use an OH of  $0.8\text{ }\mu\text{s}$  that corresponds to the value of CP employed in the IEEE 802.11 standard [8]. Fig. 5.1 shows the capacity (5.3) as a function of the OH duration for both OFDM and FMT for 100 class B channel realizations. The distance between transmitter and receiver equals  $10\text{ m}$ . As we can see in both cases an optimal OH that maximizes the capacity (5.3) can be found for each channel realization. Furthermore, we can see that the capacity curves are relatively flat around the optimal OH value. Therefore, the choice of an OH close to the optimal one will not dramatically change the capacity value w.r.t. the maximum. These observations justify our proposal to design the OH according to the capacity-optimal OH CDF as described in Section 5.3.2. From Fig. 5.1, we can also notice that the OH adaptation significantly improves the system performance w.r.t. the baseline system that deploys an OH of  $0.8\text{ }\mu\text{s}$ . Figs. 5.2, 5.3 respectively show the capacity-optimal OH CDFs for FMT and for OFDM for each channel class and for different distances between transmitter and receiver. From Fig. 5.2 (see the first 5 sub-plots starting from the top), we can see that for FMT the optimal OH CDF does not appreciably depend on the experienced channel class but it shows a strong dependence on the distance between transmitter and receiver. Thus, as explained in Section 5.3.2, for each distance value, we choose a near optimal OH value that renders the

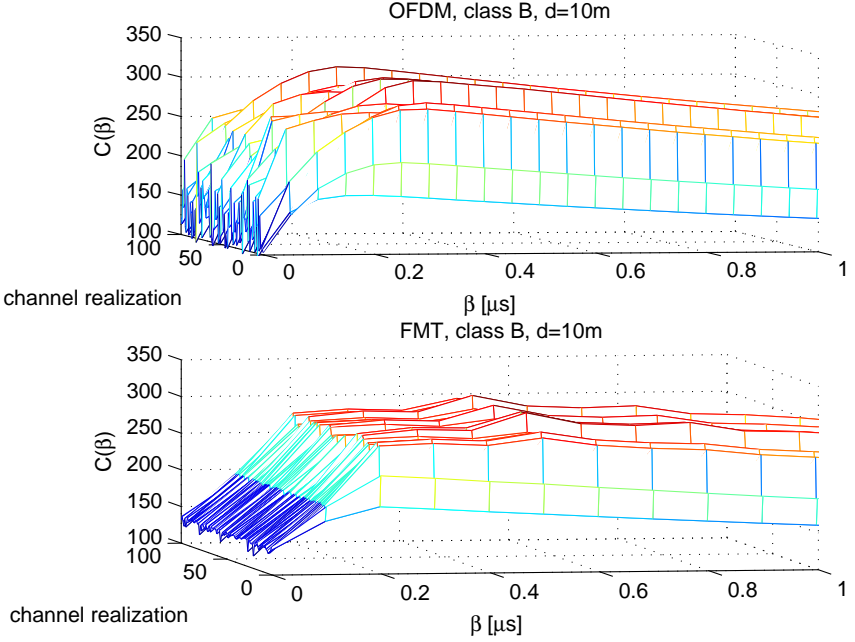


Figure 5.1: Capacity as a function of the OH duration for 100 class B channel realizations using OFDM (top), and FMT (bottom). The distance between transmitter and receiver is set equal to 10  $m$ .

optimal OH CDF equal to 0.99 (obtained averaging the data across all the channel classes, see the last sub-plot of Fig. 5.2). The corresponding set of OH values is  $\mathcal{M}_{FMT} = \{\beta_{3,FMT}^{(99\%)} = 0.8\mu s, \beta_{10,FMT}^{(99\%)} = 0.5\mu s, \beta_{30,FMT}^{(99\%)} = 0.2\mu s, \beta_{60,FMT}^{(99\%)} = 0.2\mu s\}$ .

Regarding Fig. 5.3, we can see that for OFDM the optimal OH CDF depends more on the channel class than on the distance. Thus, as assumed in Section 3.8, for each channel class, we choose a near optimal value of OH (or equally CP) that renders the optimal OH CDF (obtained averaging the data over the distances) equal to 0.99. The corresponding set of OH values is  $\mathcal{M}_{OFDM} = \{\beta_{B,OFDM}^{(99\%)} = 0.4\mu s, \beta_{C,OFDM}^{(99\%)} = 0.5\mu s, \beta_{D,OFDM}^{(99\%)} = 0.6\mu s, \beta_{E,OFDM}^{(99\%)} = 0.9\mu s, \beta_{F,OFDM}^{(99\%)} = 1.1\mu s\}$ . It is worth noting that the applica-

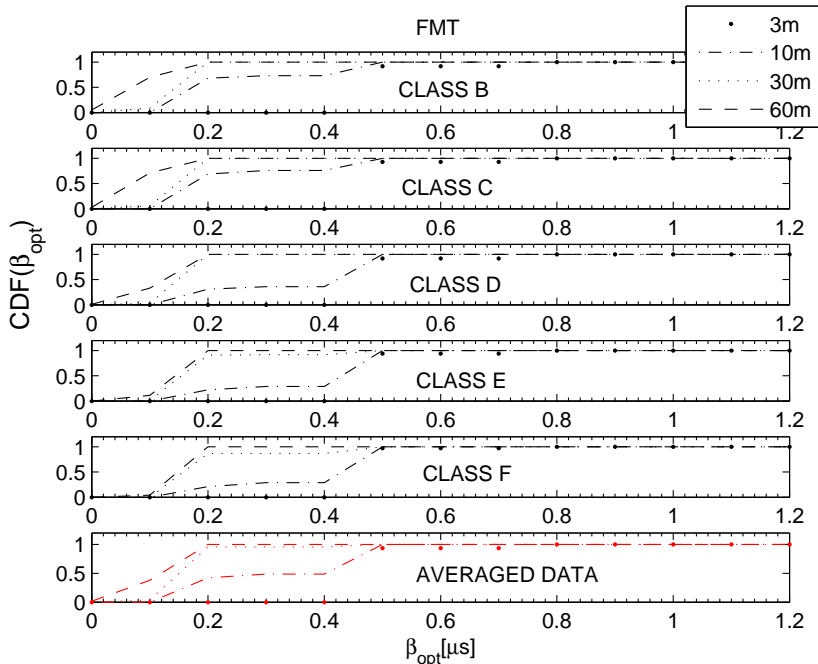


Figure 5.2: Optimal OH CDF for FMT considering each single channel class, and all the classes together. The distances between transmitter and receiver are set equal to 3 m, 10 m, 30 m, and 60 m.

tion to FMT of the criterion used to compute the limited set  $\mathcal{M}_{OFDM}$  for OFDM, would return a single value of OH equal to  $0.8 \mu s$ . This is because, as shown in Fig. 5.2, the optimal OH of FMT does not depend on the channel class. Thus, for all the channel classes we would obtain the same value of  $\beta$  that renders all the CDFs equal to 0.99. This criterion could be adopted to design a globally “optimal” value of OH for FMT.

The different behavior of the optimal OH CDFs for FMT and OFDM is due to the use of different sub-channel pulses and equalization scheme. In FMT the ICI is minimized via the design of the OH factor together with the sub-channel pulse, while the ISI is mitigated with the use of the sub-channel equalizer. In OFDM since we deploy a single tap equalizer, the OH

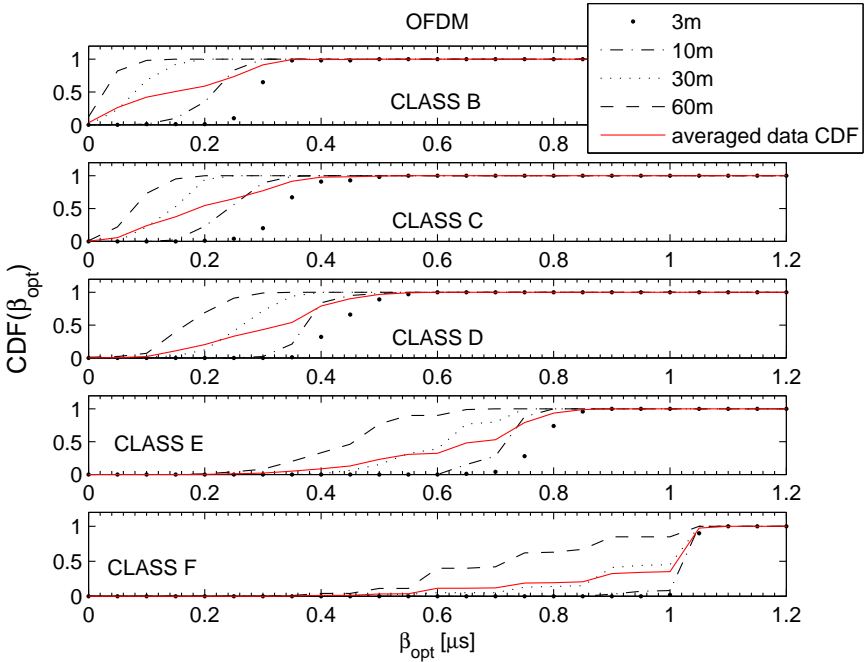


Figure 5.3: Optimal CP CDF for OFDM considering channels of class B, C, D, E, and F. The distances between transmitter and receiver are set equal to 3 m, 10 m, 30 m, and 60 m.

(cyclic prefix) has to be designed such that we tradeoff between ISI+ICI and noise. Indeed, multichannel equalization is in principle applicable in OFDM in order to mitigate the ICI with a CP shorter than the channel response, which however, significantly increases the complexity [59].

Now, in Fig. 5.4 we report the CCDF of the capacity (5.3) obtained for FMT and OFDM with both the optimal OH value (5.5) and the sub-optimal ones listed above. The used channel classes are B, D, and F. The distance between transmitter and receiver is set equal to 3 m, 10 m and 30 m. As we can see, in almost all cases, FMT with OH optimized outperforms OFDM with OH optimized. This is true either using the optimal OH adaptation (5.5) based on the exhaustive search, or the simplified OH adaptation based on the

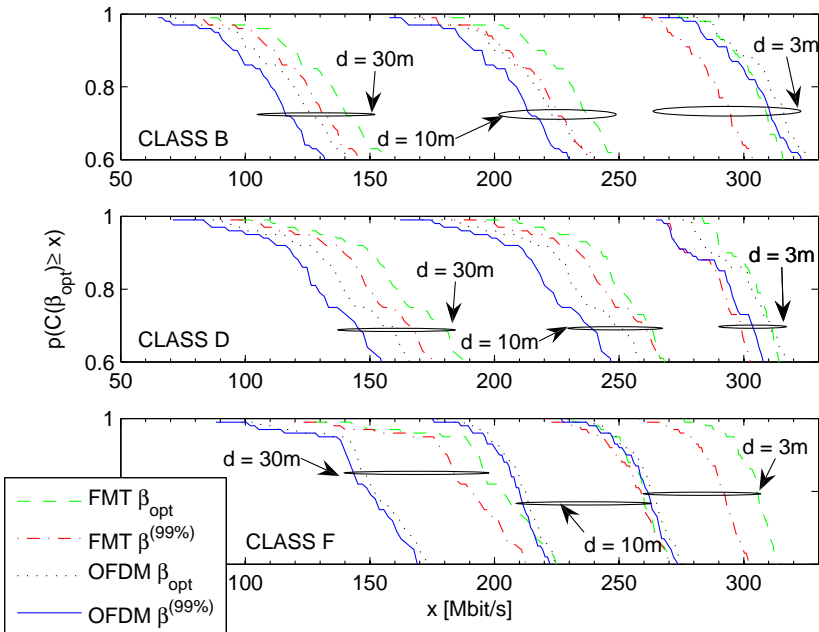


Figure 5.4: CCDF of capacity using OFDM and FMT with optimal and limited OH adaptation. The used channel classes are the B,D, and F. The distances between the transmitter and the receiver are set equal to 3 m, 10 m, and 30 m.

limited search over the sets  $\mathcal{M}_{OFDM}$  and  $\mathcal{M}_{FMT}$ . Finally, in Fig. 5.5 we show the CCDF of the aggregate network rate obtained using the algorithm described in Section 5.4 for both FMT-FDMA and OFDMA. The CCDF obtained using the baseline systems that deploy an OH equal to  $0.8 \mu\text{s}$  are also shown. The network is composed by 4 users. The weights  $p^{(u)}$  are equal to 0.25. Therefore, we have considered a proportional fair resource allocation. The users experience channels belonging to the same class, the channel class is randomly selected, and the distance between each user and the AP is randomly drawn between 3 m and 60 m. As we can see, the limited OH adaptation to the channel condition improves the performances of both FMT-FDMA and OFDMA w.r.t. the baseline system that deploys an OH equal to  $0.8 \mu\text{s}$ . More

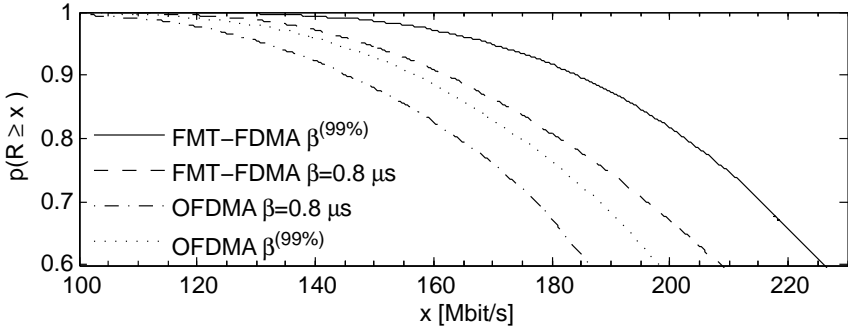


Figure 5.5: CCDF of the aggregate network rate obtained using the limited OH adaptation for both OFDMA and FMT-FDMA. Also plotted are the CCDFs obtained using FMT-FDMA and OFDMA with a fixed OH of  $0.8 \mu\text{s}$ .

precisely, with probability equal to 0.9, the limited OH adaptation respectively improves the aggregate network rate of about 7% for OFDMA, and of about 12% for FMT-FDMA. From Fig. 5.5, we also notice that the use of adaptive FMT-FDMA, with probability equal to 0.9, improves the aggregate network rate of about 27% w.r.t. the use of OFDMA with a fixed CP value equal to  $0.8 \mu\text{s}$ . Note that a fair comparison between FMT and OFDM should also take into account the implementation complexity. In this work we were however interested in showing that theoretically the WLAN capacity can significantly be improved at expense of complexity. However, in Chapter 7, we will consider a simplified OFDM/FMT adaptation scheme where single tap equalization is also used for FMT.

## 5.6 Main Findings

At expense of complexity, the use of adaptive FMT could further improve the WLAN standard achievable rate w.r.t. the use of adaptive OFDM. This is true for both the single user case and the multi user case that deploys FDMA.



## On Power Allocation in Adaptive OFDM

In the previous chapters, we have assumed to transmit OFDM signals with an uniform power distribution over the sub-channels. This power allocation maximizes the achievable rate of multi-carrier systems not affected by interference and constrained by a flat power spectral density (PSD) mask.

In this chapter, we consider a more general problem that consists in the joint allocation of power and cyclic prefix (CP) duration to maximize the achievable rate of OFDM. In particular, we relax the constraint on the PSD mask, and we consider the interference as a function of the transmitted power distribution. A closed form solution to the problem does not exist and the exhaustive search of the optimal values is practically unfeasible. Therefore, we propose a sub-optimal iterative power allocation algorithm jointly with the CP adaptation to see whether capacity improvements can be obtained w.r.t. the conventional choice of a uniform power distribution over the sub-channels and a predetermined long CP value.

Through numerical results, obtained over broadband PLC channels, we show that the use of the proposed iterative power allocation algorithm together with the adaption of the CP can improve the OFDM system capacity for the low SNR region. We further shown that the optimal CP length does not strongly depends on the power distribution.

## 6.1 Introduction

As we have argued in the previous chapters, if OFDM deploys a CP longer than the channel duration, the received signal will be neither affected by ISI nor by ICI [3]. In such a case, assuming additive Gaussian noise, the system input-output mutual information with a total power constraint is maximized by Gaussian input signals whose power is computed with the water-filling algorithm [30, 60]. However, we have seen that the system capacity can be increased with the usage of a CP shorter than the channel duration since the CP introduces a loss in transmission rate by a factor  $M/(M + \mu)$ , where  $M$  and  $\mu$  respectively denote the number of sub-channels and the CP length in samples.

When the CP is shorter than the channel duration, the OFDM system can be modeled as a Gaussian interference channel. In the previous chapter we have considered single tap sub-channel equalization and uniform power distribution across the sub-channels. Then, we have evaluated the capacity improvements via adaptation of the CP to the channel realization. Although uniform power allocation over the sub-channels at a certain level is simple and allows fulfilling a PSD mask requirement for coexistence, it is interesting to investigate whether further capacity improvements are attainable with a non-uniform power allocation.

As stated above, for a certain CP, the system can be viewed as a Gaussian interference channel with  $M$  total interferers. Both cross-talk ICI and ISI are present in the system. To the authors' knowledge the capacity of an interference channel either with a total power constraint or a PSD constraint is not known [60, 61]. If we assume Gaussian distributed inputs, and we assume joint coding and decoding, the capacity of the system with a total power constraint is achieved with an input covariance matrix that is obtained from the water-filling algorithm derived in [62] for a Gaussian vector channel with crosstalks. However, if we do not assume joint coding and decoding over the set of  $M$  sub-channels there is no closed form solution to the power allocation problem (note that in this case the input covariance is diagonal). In this case,

the interference exhibited by each sub-channel is treated as noise by the sub-channel decoder so that the mutual in-out information is not a convex function of the vector of input powers. Therefore, the optimal input power distribution has to be obtained via an exhaustive search, which is clearly unfeasible.

We point out that a large literature exists about similar, but not identical, problems in digital subscriber line (DSL). In DSL, up to 100 subscriber lines can be bundled together to form a DSL binder [63]. Each subscriber deploys DMT modulation over a frequency spectrum common to all the subscribers, thus causing crosstalk interference. A class of algorithms that deals with the crosstalk issues are known as spectrum management techniques. In [64], the authors consider the centralized spectrum management problem, and they find an achievable rate region for the  $N_U$  users weighted sum rate. The weighted sum-rate optimization problem is split into  $M$  sub-problems where each sub-problem considers the weighted sum rate of the  $N_U$  users for a given sub-channel. Thus, considering the use of  $L$  quantized power levels, each sub-problem is solved by doing an exhaustive search for the  $N_U$  power levels to be allocated to a certain sub-channel. The algorithm reduces the computational complexity from an order of  $O(MN_UL^{MN_U})$  to  $O(MN_UL^{N_U}33^{N_U})$ . Unfortunately, this algorithm is not applicable in our context because we deal with  $M$  interfering sub-channels and thus the complexity still remains exponential in  $M$ .

In [63, 65], the interference channel is viewed as a non-cooperative game where the interference experienced by each player is considered as noise (thus single user detection is assumed). In such a case it has been shown that a Nash equilibrium can be reached and it corresponds to a set of competitively optimal power levels. Furthermore, it has been shown that under certain conditions, the equilibrium can be achieved using an iterative water-filling (IWF) algorithm. The conditions for the convergence of this algorithm have been derived in [63] for the two-user case, and in [65] for a general multi-user case. It is worth noting that the IWF presented in [63, 65] renders convex the sum rate optimization problem by splitting it into  $N_U$  convex sub-problems. Once this has been done, water-filling is applied to each user until convergence is

reached. Also this algorithm is not directly applicable to our context because it uses a constraint on the total power transmitted by each user. Therefore, if we treat our  $M$  sub-channels as interfering users, the power constraint coincides with the PSD constraint. Furthermore, the non-cooperative game would yield the trivial solution of a constant power distribution at the PSD level, which in turn, is optimal only when the multi-carrier system does not experience interference.

Inspired by the above results, we consider the problem of the joint allocation of power and CP duration to maximize the system capacity when setting a constraint on the total transmitted power. As stated, a closed form solution to the problem does not exist and the exhaustive search of the optimal values is practically unfeasible. Therefore, we propose a sub-optimal iterative power allocation algorithm jointly with the CP adaptation to see whether capacity improvements can be obtained w.r.t. the conventional choice of a uniform power distribution and a predetermined long CP value that fully equalizes the channel.

The chapter is organized as follows. In Section 6.2, we formulate the joint power and CP optimization problem. Then, in Section 6.3, we propose iterative power allocation algorithms to solve the previous problem, and in Section 6.4, we present the numerical results. Finally, in Section 6.5, we derive the conclusions.

## 6.2 Problem Formulation

We adopt the OFDM system model presented in Section 2.3. According to that model, when the CP is shorter than the channel duration, ISI and ICI components arise. Thus, as equation (2.3) shows, the OFDM system transmits data over a vector interference channel, i.e.,  $M$  parallel sub-channels affected by ISI and crosstalks. The system capacity with a total power constraint, Gaussian additive noise, Gaussian input signals, and assuming optimal joint detection can be computed adapting the formulation in [62]. We are, however, interested in computing the system capacity under the assumption of independent Gaussian distributed input signals and using single tap sub-channel

equalization, i.e., we treat as noise the interference. Therefore, the capacity is obtained by maximizing the input-output mutual information over the CP length and power distribution. To this end, we can formulate the following optimization problem

$$\begin{aligned}
& \max_{\mu, \mathbf{P}_a(\mu)} C(\mu), \\
& \text{s.t.} \quad \sum_{k \in \mathbb{K}_{\text{on}}} P_a^{(k)}(\mu) = \bar{P}, \\
& \quad \quad P_a^{(k)}(\mu) \geq 0, \quad k \in \mathbb{K}_{\text{on}}, \\
& \quad \quad 0 \leq \mu < L_{ch}.
\end{aligned} \tag{6.1}$$

In (6.1),  $C(\mu)$  represents the system capacity. It is defined as:

$$C(\mu) = \frac{1}{(M + \mu)T} \sum_{k \in \mathbb{K}_{ON}} \log_2 \left( 1 + \text{SINR}^{(k)}(\mu) \right), \tag{6.2}$$

where

$$\text{SINR}^{(k)}(\mu) = \frac{P_a^{(k)}(\mu) |H^{(k)}(\mu)|^2}{P_\eta^{(k)} + P_I^{(k)}(\mu)}. \tag{6.3}$$

Furthermore,  $\mathbf{P}_a(\mu) = \{P_a^{(k)}(\mu), \text{ with } k \in \mathbb{K}_{\text{on}}\}$  is the vector of the transmitted powers,  $\bar{P}$  is the total available power, and  $T$  is the sampling period. In (6.3),  $P_I^{(k)}(\mu)$  and  $P_\eta^{(k)}$  respectively denote the interference and the noise power terms on sub-channel  $k$ . Details on their computation can be found in Appendix 11.1. An SNR gap can also be included to take into account the use of modulation and coding schemes [30].

Since the equivalent interference plus noise term, i.e.,  $P_{eq}^{(k)}(\mu) = P_I^{(k)}(\mu) + P_\eta^{(k)}$ , depends on both the vector of the transmitted powers and the CP length, in general, problem (6.1) is neither convex in  $\mu$  nor in  $\mathbf{P}_a(\mu)$ .

A solution to (6.1) could be found doing an exhaustive search on both  $\mu$  and  $\mathbf{P}_a(\mu)$ . However, the exhaustive search in  $\mathbf{P}_a(\mu)$  is practically unfeasible. This is true even supposing to quantize the sub-channel power in a finite number  $L$  of levels. In fact, for each  $\mu$  the exhaustive search would have a

complexity  $O(L^M)$ .

### 6.3 Sub-optimal Power Allocation

If we treat the interference as noise not affected by the input power distribution, conventional power allocation solutions for Gaussian parallel channels can be applied. This is because for a certain value of  $\mu$ , problem (6.1) becomes convex and its solution corresponds to the water-filling power distribution [60]. Besides water-filling (referred to as true water filling), we can also apply the constant power water-filling proposed by Chow [66], or a uniform power allocation at a certain level as specified by a PSD constraint.

These three algorithms are clearly sub-optimal in our context but an improvement can be found if we apply water filling in an iterative fashion. Before describing in detail the proposed iterative water-filling algorithm, we briefly recall the basic power allocation strategies.

#### 6.3.1 True Water-Filling

Let us fix  $\mu$ , then the Lagrangian associated to the primal problem (6.1) is

$$L(\mathbf{P}_a(\mu), \lambda, \boldsymbol{\nu}) = -\frac{1}{NT} \sum_{k \in \mathbb{K}_{ON}} \log_2 \left( 1 + \frac{P_a^{(k)}(\mu) |H^{(k)}(\mu)|^2}{P_{eq}^{(k)}(\mu)} \right) + \lambda \left( \sum_{k \in \mathbb{K}_{on}} P_a^{(k)}(\mu) - \bar{P} \right) - \sum_{k \in \mathbb{K}_{on}} \nu_k P_a^{(k)}(\mu). \quad (6.4)$$

Consequently, we can define the dual problem as

$$g(\lambda, \boldsymbol{\nu}) = \inf_{\mathbf{P}_a(\mu)} L(\mathbf{P}_a(\mu), \lambda, \boldsymbol{\nu}). \quad (6.5)$$

Now, observing that under the hypothesis of an interference plus noise term independent from the transmitted power, the primal (6.1) is convex, it is easy to show that the primal and the dual optimal solutions, namely  $\mathbf{P}_a^*(\mu)$  and  $(\lambda^*, \boldsymbol{\nu}^*)$  can be obtained satisfying the Karush-Kuhn-Tucker (KKT)<sup>1</sup> condi-

<sup>1</sup>see Appendix 11.5 for more details regarding the KKT conditions.

tions [67], i.e.,

$$\begin{aligned}
 P_a^{(k)}(\mu) &\geq 0, \quad k \in \mathbb{K}_{\text{on}}, \\
 \sum_{k \in \mathbb{K}_{\text{on}}} P_a^{(k)}(\mu) - \bar{P} &= 0, \\
 \nu_k &\geq 0, \quad k \in \mathbb{K}_{\text{on}}, \\
 -\nu_k P_a^{(k)}(\mu) &= 0, \quad k \in \mathbb{K}_{\text{on}}, \\
 \lambda - \nu_k - \frac{|H^{(k)}(\mu)|^2}{NT \ln(2) \left( P_{eq}^{(k)}(\mu) + P_a^{(k)}(\mu) |H^{(k)}(\mu)|^2 \right)} &= 0.
 \end{aligned} \tag{6.6}$$

Where, the first and the second condition represent the constraints on the transmitted power, and the third imposes the Lagrangian multipliers associated with the inequality to be non negative. The fourth condition is the so called slackness condition, it implies that if  $P_a^{(k)}(\mu) > 0$  then  $\nu_k = 0$ . Viceversa, if  $P_a^{(k)}(\mu) = 0$  then  $\nu_k > 0$ . The last condition has been obtained computing the gradient of (6.4) w.r.t.  $P_a^{(k)}(\mu)$  and setting it equal to zero.

The solution to (6.6) can be found as follows. Using the slackness condition, i.e.,  $P_a^{(k)}(\mu) > 0$  with  $\nu_k = 0$ , from the last line of (6.6) we can compute the power to be allocated in each sub-channel as

$$P_a^{(k)}(\mu) = \bar{\lambda} - \frac{P_{eq}^{(k)}(\mu)}{|H^{(k)}|^2}, \tag{6.7}$$

with  $\bar{\lambda} = 1/(\lambda NT \ln(2))$ . Now, replacing (6.7) in the first line of (6.6), we obtain  $\bar{\lambda} \geq P_{eq}^{(k)}(\mu)/|H^{(k)}|^2$ .  $\bar{\lambda}$  can be computed replacing (6.7) in the second line of (6.6), i.e.,

$$\bar{\lambda} = \frac{1}{|\mathbb{K}_{\text{on}}|} \left( \bar{P} + \sum_{k \in \mathbb{K}_{\text{on}}} \frac{P_{eq}^{(k)}(\mu)}{|H^{(k)}|^2} \right), \tag{6.8}$$

with  $|\mathbb{K}_{\text{on}}|$  equal to the cardinality of  $\mathbb{K}_{\text{on}}$ . Now, if we set  $P_a^{(k)}(\mu) = 0$  and  $\nu_k > 0$ , we can compute  $\nu_k$  from the last line of (6.6) and replacing it into the third line of (6.6), we obtain  $\bar{\lambda} < P_{eq}^{(k)}(\mu)/|H^{(k)}|^2$ . Therefore the water-filling

solution reads

$$P_a^{(k)}(\mu) = \begin{cases} \bar{\lambda} - \frac{P_{eq}^{(k)}(\mu)}{|H^{(k)}(\mu)|^2} & \text{if } \bar{\lambda} \geq P_{eq}^{(k)}(\mu)/|H^{(k)}(\mu)|^2, \\ 0 & \text{if } \bar{\lambda} < P_{eq}^{(k)}(\mu)/|H^{(k)}(\mu)|^2. \end{cases} \quad (6.9)$$

In (6.8),  $|\mathbb{K}_{\text{on}}|$  indicates the cardinality of  $\mathbb{K}_{\text{on}}$ .

Equation (6.9) yields the water-filling power distribution. This is because if we think to the inverse of the SNRs across sub-channels ( $P_{eq}^{(k)}(\mu)/|H^{(k)}(\mu)|^2$ ) as a bowl, then we can think to pour such a bowl with water (represented by the powers  $P_a^{(k)}(\mu)$ ) to a certain constant level  $\bar{\lambda}$ .

We refer to the solution (6.9) as true water-filling. This is to distinguish (6.9) from the following constant power water-filling algorithm.

### 6.3.2 Constant Power Water-Filling

When the SNR is high, the sum-log in (6.2) weakly depends on the optimal power distribution. This observation has allowed Chow [66] to empirically show that a uniform power distribution has negligible loss w.r.t. true water-filling. Uniform power distribution means to uniformly distribute the overall power (see second line of (6.1)) to the sub-channels where true water-filling allocates positive power, i.e.,

$$P_a^{(k)}(\mu) = \begin{cases} \bar{P}/|\mathbb{K}_{\text{on}}| & \text{if } \bar{\lambda} \geq P_{eq}^{(k)}(\mu)/|H^{(k)}(\mu)|^2, \\ 0 & \text{if } \bar{\lambda} < P_{eq}^{(k)}(\mu)/|H^{(k)}(\mu)|^2, \end{cases} \quad (6.10)$$

with  $\mathbb{K}_{\text{on}} = \left\{ k : \bar{\lambda} \geq P_{eq}^{(k)}(\mu)/|H^{(k)}(\mu)|^2 \right\}$ , and  $\bar{\lambda}$  given by (6.8).

### 6.3.3 Power Allocation with a Constraint on the PSD

Another more simple algorithm consists in uniformly distributing the total power over the set of active sub-channels  $\mathbb{K}_{\text{on}}$ . For instance, with a PSD constraint we can allocate to each active sub-channel a power equal to the PSD level. State-of-the-art broadband PLC (BPLC) systems transmit at a constant PSD level equal to  $-50 \text{ dBm/Hz}$  over the  $2\text{-}28 \text{ MHz}$  band [18, 19, 38]

and some tones are switched off according to a fixed notching mask. This power allocation allows BPLC devices to be compliant with the EN 55022 normative [39]. It is interesting to note that with a PSD constraint the uniform and constant power distribution at the PSD level is optimal only in the absence of interference, which can be easily proved by observing that in the absence of interference capacity is maximized by wasting all available power on each sub-channel.

### 6.3.4 Iterative Water-Filling

As we have previously observed, the three power allocation algorithms above described, are clearly sub-optimal in our context but an improvement can be found if we apply them in an iterative fashion. The following pseudo-code describes the proposed iterative power allocation algorithm.

1. Set the number of maximum iterations  $N_{it}$ .

Set  $iteration = 0$ .

Initialize  $\mathbb{K}_{on}$  equal to the set of active sub-channels given by the power spectral density mask constraint.

Uniformly distribute the power across the active sub-channels at a power  $P_{SD}$  given by the PSD constraint, i.e.,  $P_a^{(k)}(\mu, iteration) = P_{SD}$  with  $k \in \mathbb{K}_{on}$ .

Compute the  $SINR^{(k)}(\mu, iteration)$  with (6.3).

Compute the capacity  $C(\mu, iteration)$  with (6.2).

2. *for*  $iteration = 1, \dots, N_{it}$

- (a) Run true water-filling (6.9) or constant power water-filling (6.10). It gives back  $P_a^{(k)}(\mu, iteration)$  with  $k \in \mathbb{K}_{on}$ . Update  $\mathbb{K}_{on}$  according to the set of active sub-channels computed with one of the water-filling algorithms.

Compute the  $SINR^{(k)}(\mu, iteration)$  with (6.3).

Compute the capacity  $C(\mu, iteration)$  with (6.2).

(b) if  $C(\mu, iteration) < C(\mu, iteration - 1)$

Set  $it_{opt} = iteration - 1$ .

Set  $iteration = N_{it}$ .

end

end

3. Set  $\mathbf{P}_a^*(\mu) = \mathbf{P}_a(\mu, it_{opt})$ .

Set  $C^*(\mu) = C(\mu, it_{opt})$ .

It is worth noting that the algorithm stops if the maximum number of iterations or a local maximum is reached. However, numerical results show that usually the algorithm converges in less than ten steps. This result agrees with the one obtained in [63] where IWF is used to deal with the crosstalk interference typical of DSL multiple access channels.

We now come back to the initial problem (6.1). In order to jointly compute the optimal CP and the power distribution, we can run the IWF for different values of CP length, and we can choose the optimal CP length as the value that maximizes capacity, i.e.,

$$\mu_{opt} = \underset{\mu \in \{0, \dots, \nu-1\}}{\operatorname{argmax}} \{C^*(\mu)\}. \quad (6.11)$$

In the next section, we compare the performance of the proposed algorithm with that obtained adapting the CP length but uniformly allocating the power according to a certain PSD constraint. In this case the optimal CP is obtained as

$$\mu_{opt, PSD} = \underset{\mu \in \{0, \dots, L_{ch}-1\}}{\operatorname{argmax}} \{C(\mu, 0)\}. \quad (6.12)$$

Metric (6.12) has been used in the previous chapter to show that the CP length that maximizes capacity is shorter than the channel duration. Furthermore, we have shown that the adaptation of the CP to the channel realization can significantly improve the system capacity w.r.t. the conventional choice of using a CP as long as the channel duration.

To simplify the complexity given by the exhaustive search done over the values of  $\mu$  in (6.11) or in (6.12), we could use one of the sub-optimal metrics presented in Chapter 3. Therefore, we could first compute the sub-optimal CP length and then run IWF.

## 6.4 Numerical Results

To obtain numerical results, we consider the statistical PLC channel model presented in Section 3.7.1, whose parameters are adjusted in such way that the average PL at zero frequency equals  $\{30, 50, 70\}$  dB. Furthermore, we assume a sampling frequency of 37.5 MHz and transmit in the 2-28 MHz band as it is done by state-of-the-art broadband PLC systems. The number of OFDM sub-channels  $M$  is 384, a quarter of the sub-channels used in HPAV [18].

When the power constraint is imposed on the transmitted signal PSD, we consider a PSD mask of -50 dBm/Hz in 2-28 MHz. Whereas, when the constraint corresponds to the total transmitted power, we set  $\bar{P}$  equal to the integral of the PSD over the band 2-28 MHz.

We assume white Gaussian noise with a PSD of -140 dBm/Hz, which is typical for indoor PLC scenarios. We set an SNR gap of 9 dB in the capacity computation to take into account practical constraints. Since the channel introduces a path loss, with the parameters that we have assumed and taking into account the SNR gap, we obtain three channel scenarios that for a constant transmit PSD at -50 dBm/Hz are characterized by an average SNR (averaged over the transmission band and channel realizations) equal to  $\{46.6, 26.6, 6.6\}$  dB. In the following we use the term SNR to indicate the average SNR.

### 6.4.1 Baseline System

In order to see whether capacity improvements can be obtained with the proposed joint CP and power allocation algorithms, we define a baseline system. It uses a constant CP duration of 5.57  $\mu$ s for all channel realizations, and it transmits in each sub-channel a signal whose power is defined by the PSD level

of  $-50 \text{ dBm/Hz}$ .

### 6.4.2 Simulation Results

We run simulations for 100 channel realizations and for the three SNR cases. Fig. 6.1 shows the capacity obtained using the baseline system, the capacity obtained with iterative true water-filling and with constant power water-filling. Furthermore, we show the capacity achieved by transmitting with constant sub-channel power at the PSD mask level and optimizing the CP length, namely  $C(\mu_{opt,PSD}, 0)$  (see (6.12)). The SNR equals  $6.6 \text{ dB}$ . In Figs. 6.2 and 6.3 we show the same capacity comparisons respectively for an SNR of  $26.6 \text{ dB}$  and  $46.6 \text{ dB}$ . From Figs. 6.1–6.3, we notice that when the SNR is of  $\{6.6, 26.6, 46.6\} \text{ dB}$ , the capacity gains given by the joint CP and power allocation w.r.t. the baseline system are respectively equal to:  $\{29\%, 10\%, 4\%\}$  when using iterative true water-filling,  $\{28\%, 10\%, 4\%\}$  when using constant power IWF, and  $\{22\%, 10\%, 4\%\}$  when we transmit at the PSD level over all the used sub-channels and we optimize the CP.

It is worth noting that for high SNRs, the use of the IWF algorithms does not give improvements w.r.t. the case of transmitting at the PSD level across all the sub-channels. Furthermore, in agreement with the result obtained by Chow [66], we can affirm that also for IWF, for high SNRs, the constant power water-filling has a negligible loss w.r.t. true water-filling.

Fig. 6.4 shows the optimal CP (6.11) and (6.12) cumulative distribution functions (CDFs) for the three SNR values. Regarding (6.11), the optimal CP-CDF is shown for both the IWF algorithms, i.e., for the true water-filling, and for the constant power water-filling. As we can see, only for a low SNR, the optimal CP duration depends on the used power allocation algorithm. Furthermore, the higher the SNR the longer the optimal CP is. This is because, for high SNRs, the interference term dominates the SINR denominator. Thus, a long CP maximizes the capacity (6.2). Consequently, for high SNRs with a long CP, the interference term is small, and therefore, the use of IWF is unnecessary. Summarizing:

- The CP adaptation significantly improves capacity w.r.t. the use of a

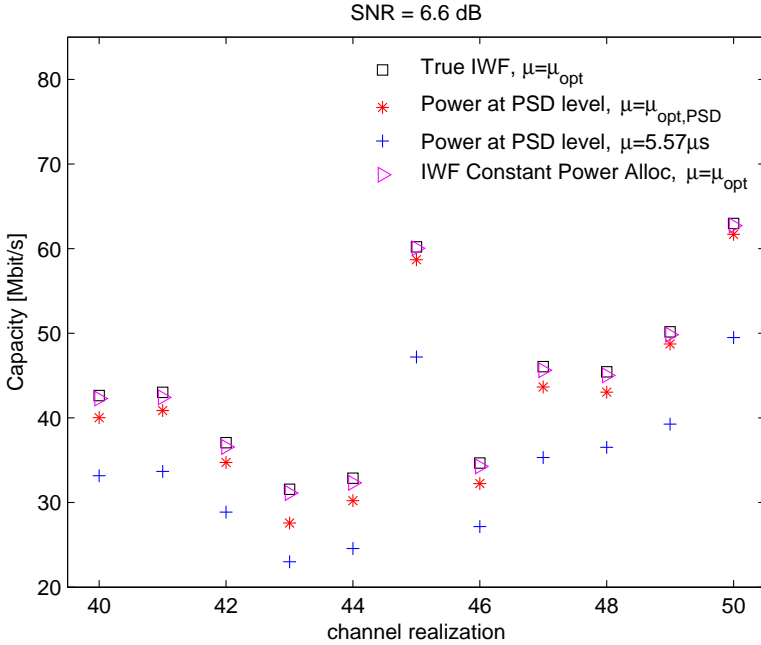


Figure 6.1: Capacities according to the different power allocation algorithms presented in Section 6.3. The SNR is fixed to 6.6 dB. For the sake of readability, only realizations 40 to 50 are shown out of 100.

constant CP of length equal the channel duration.

- Only for low SNRs, the joint adaptation of the power and CP length to the channel realization further improves capacity w.r.t. a uniform power distribution and CP adaptation. The improvements are not significant. This is the reason why we did not consider the power allocation in the previous chapters.
- Constant power IWF gives negligible loss w.r.t. true IWF.
- The optimal CP duration is not appreciably dependent on the used power allocation algorithm.

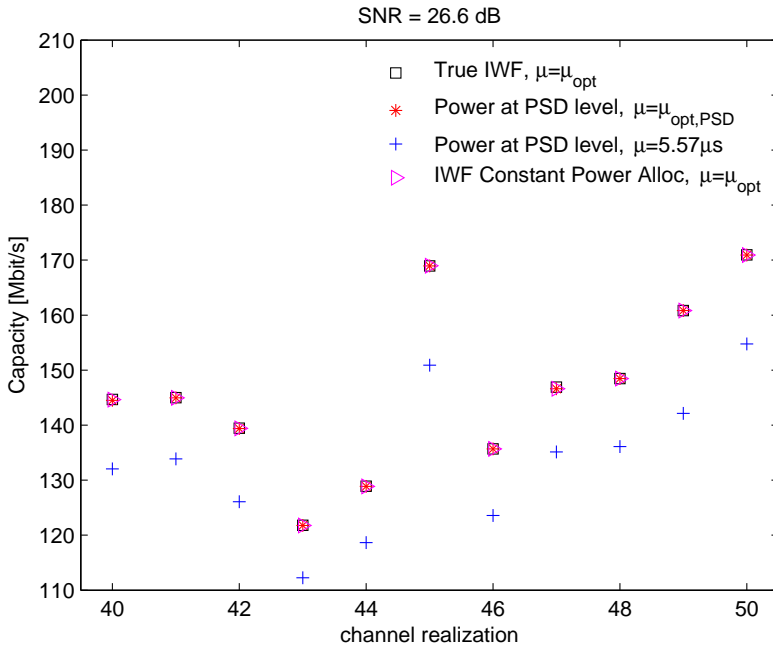


Figure 6.2: Capacities according to the different power allocation algorithms presented in Section 6.3. The SNR is fixed to 26.6 dB. For the sake of readability, only realizations 40 to 50 are shown out of 100.

## 6.5 Main Findings

In this chapter, we have investigated the problem of power allocation and CP length adaptation for the OFDM transmission system. We have shown that, the use of power allocation algorithms based on IWF together with the adaption of the CP can improve the OFDM system capacity for the low SNR region. We have further shown that the optimal CP length does not strongly depends on the power distribution, and that the constant power IWF gives results that are similar to true IWF.

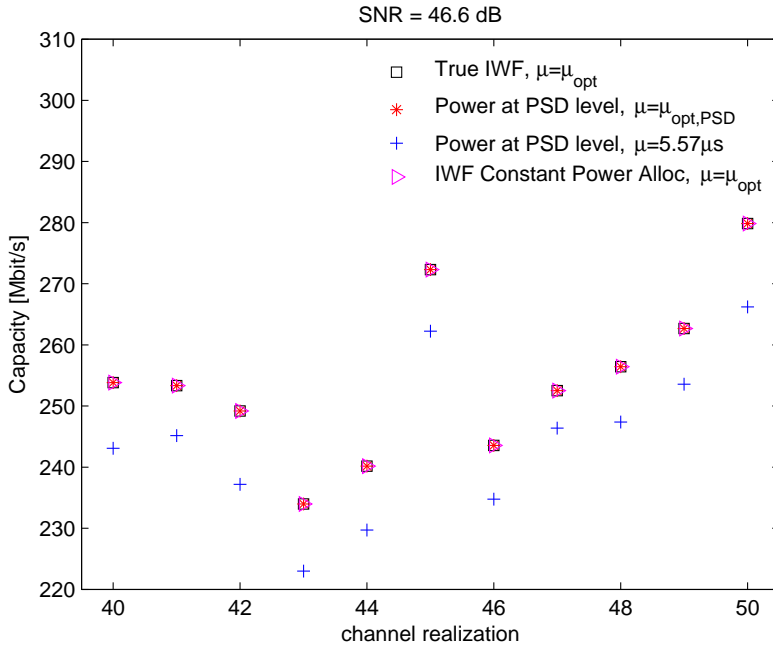


Figure 6.3: Capacities according to the different power allocation algorithms presented in Section 6.3. The SNR is fixed to 46.6 dB. For the sake of readability, only realizations 40 to 50 are shown out of 100.

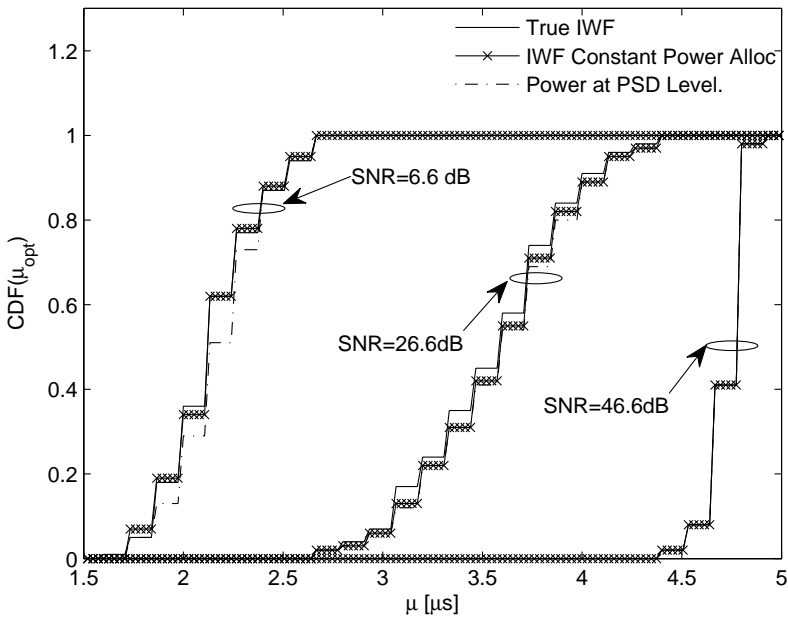


Figure 6.4: Optimal CP CDF for the three proposed power allocation algorithms. The SNR equals  $\{6.6, 26.6, 46.6\}$  dB.

## Adaptation in Hybrid Filter Bank Schemes

In previous chapters, we have proposed to maximize the achievable rate of orthogonal frequency division multiplexing (OFDM) and filtered multitone (FMT) through the adaptation the overhead duration to the channel condition. Numerical results have shown that the adaptation can significantly improve the system performance compared to the corresponding system that uses a single value of overhead.

In this chapter, we present a novel MC architecture that adapts the shape of synthesis and analysis pulses to the channel condition. We refer to this scheme as hybrid FMT (H-FMT). Depending on the channel condition, H-FMT wisely switches between short orthogonal FMT (SO-FMT) and A-OFDM. We propose to use H-FMT to address the energy saving problem in WLAN applications. We show that H-FMT provides a considerable gain in terms of energy efficiency compared to conventional OFDM, yet achieving the same rate. Furthermore, its additional computational complexity is negligible, making this scheme an attractive solution for WLAN applications.

### 7.1 Introduction

In recent years the energy consumption problem of communication devices has had much consideration. Some standards have been developed to cope with the need of energy saving, e.g., the IEEE 802.3az and the HomePlug

Green PHY [68] that are respectively specified for Ethernet and power line communications. Power saving also plays a fundamental role in wireless applications since the communication devices can be battery driven. In this chapter, we consider a WLAN application scenario and we investigate the energy efficiency of a novel hybrid MC modulation scheme [59]. The scheme is referred to as H-FMT. Depending on the channel condition, H-FMT switches between SO-FMT modulation and A-OFDM.

As we have discussed in Chapter 2, the FMT system is a discrete-time implementation of a MC modulation that uses uniformly spaced sub-carriers and identical sub-channel pulses. OFDM can be viewed as an FMT scheme that deploys rectangular prototype pulses. SO-FMT is an FMT system that deploys orthogonal filters designed such that they have length that is equal to the duration of one transmitted symbol, and further they are maximally confined in the frequency domain. Consequently, both ICI and ISI are well mitigated when signaling over a frequency selective channel. Furthermore, the computational complexity is comparable to that of OFDM. The design of the pulse has been described in [59, 69].

In Chapter 3, we have found that over typical WLAN channels, the cyclic prefix (CP) of OFDM has not to be necessarily as long as the channel duration to maximize the achievable rate. Furthermore, for each channel class of the IEEE 802.11n WLAN channel model [49], we have found a nearly optimal value of CP designed according to the statistics of the capacity optimal CP duration. We referred to the OFDM that adapts the CP to the channel condition as A-OFDM.

Thanks to the similarities of the efficient implementation of both SO-FMT and A-OFDM [69], the realization of H-FMT introduces a marginal increase in computational complexity w.r.t. conventional OFDM. Furthermore, in H-FMT single tap equalization is always considered.

In this chapter, we exploit the peculiarities of H-FMT to cope with the problem of energy saving in WLAN applications. Since the H-FMT system is based on A-OFDM and SO-FMT, it generally suffers from interference - making the problem of power allocation not convex. Therefore, it cannot be

solved by conventional methods such as Lagrange multipliers. For this purpose, we present an algorithm that significantly simplifies the power minimization problem. This algorithm allows us to assume convex the power allocation problem assuming that H-FMT suffers of negligible interference.

We compare H-FMT with the OFDM used in the 802.11 standard and we show that H-FMT allows for a considerable gain in terms of energy efficiency compared to OFDM, yet reaching the same rate.

The chapter is organized as follows. In Section 7.2, we recall the system model and the fundamentals of A-OFDM, SO-FMT, and H-FMT. In Section 7.3, we focus on the power minimization problem for H-FMT. In Section 7.4, we present numerical results. Finally, in Section 7.5, the main findings follow.

## 7.2 System Model

We consider the general MC system model described in Section 2.1. According to this model,  $M$  sub-channels low rate data signals  $a^{(k)}(\ell N)$ , with  $k = 0, \dots, M - 1$ , are upsampled by a factor  $N = M + \beta$  ( $\beta$  denotes the overhead (OH) factor), filtered by a sub-channel pulse  $g(n)$ , and exponentially modulated. Then, the sub-channel signals are summed and transmitted over the channel. After channel propagation, the signal  $y(n)$  is processed by an analysis filter bank whose sub-channel pulses are  $h(n)$ . Therefore, the signal received in the  $k$ -th sub-channel, with sampling period  $N$ , can be written as

$$z^{(k)}(\ell N) = a^{(k)}(\ell N)H^{(k)}(\beta) + I^{(k)}(\ell N, \beta) + \eta^{(k)}(\ell N, \beta), \quad (7.1)$$

where  $H^{(k)}(\beta)$  is the amplitude of the data of interest,  $I^{(k)}(\ell N, \beta)$  and  $\eta^{(k)}(\ell N, \beta)$  respectively denote the interference (ISI plus ICI) and the noise term in sub-channel  $k$ .

We use the IEEE 802.11 TGn [49] channel model. This model generates channels belonging to five classes labeled with B,C,D,E,F. Each class is representative of a certain environment, e.g., small office, large open space/office with line of sight (LOS) and non line of sight (NLOS) propagation, and so

on. Both small scale multipath fading and large scale path loss fading as a function of distance are taken into account. For a detailed description of the model, see Section 3.8 and [49].

In order to evaluate the system performances, we assume parallel Gaussian channels and independent and Gaussian distributed input signals, which render ISI and ICI also Gaussian (cf. e.g. [29]). Furthermore, assuming single tap zero forcing equalization, the achievable rate in bit/s for a given channel realization, can be expressed as in equation (2.12), i.e.,

$$C(\beta) = \frac{1}{(M + \beta)T} \sum_{k=0}^{M-1} \log_2 \left( 1 + SINR^{(k)}(\beta) \right), \quad (7.2)$$

where  $T$  is the sampling period, and  $SINR^{(k)} = (1/SNR^{(k)} + 1/SIR^{(k)})^{-1}$  denotes the signal over interference plus noise ratio experienced in sub-channel  $k$ . We denote with  $SNR^{(k)}(\beta) = P_U^{(k)}(\beta)/P_\eta^{(k)}$  and  $SIR^{(k)}(\beta) = P_U^{(k)}(\beta)/P_I^{(k)}(\beta)$  the signal to noise ratio and the signal to interference ratio.  $P_U^{(k)}(\beta)$ ,  $P_I^{(k)}(\beta)$  and  $P_\eta^{(k)}$  respectively are the useful, the interference, and the noise power term on sub-channel  $k$ . Details on their computation can be found in Chapter 2.

As it will be clear in the following, it is convenient to express the SINR as  $SINR^{(k)}(\beta) = P_a^{(k)}\gamma^{(k)}(\beta)$ , where  $P_a^{(k)}$  is the transmitted signal power in the  $k$ -th sub-channel, and  $\gamma^{(k)}(\beta) = |H^{(k)}(\beta)|^2 / (P_I^{(k)}(\beta) + P_\eta^{(k)})$ .

In the next sections, we first briefly recall SO-FMT, we then present H-FMT.

### 7.2.1 Short Orthogonal FMT (SO-FMT)

Differently from OFDM that privileges time confinement using rectangular pulses, in general, FMT schemes privilege the frequency confinement (see Chapter 2). The SO-FMT scheme [69] can be obtained from the general system model simply substituting the prototype pulse  $g(n) = h^*(-n)$  with an FMT orthogonal pulse having minimal length. These pulses satisfy the

orthogonality conditions given by the following system of equations

$$\begin{aligned} \left[ g^{(k)} * h^{(i)} \right] (Nn) &= \delta_n \delta_{i-k}, \\ \forall (k, i) &\in \{0, \dots, M-1\}, \forall n \in \mathbb{Z}, \end{aligned} \quad (7.3)$$

where  $\delta_n$  is Kronecker delta,  $g^{(k)}(n) = g(n)e^{2\pi i f_k n}$ , and  $h^{(i)}(n) = h(n)e^{2\pi i f_i n}$ . The solution of this system is not unique, and thus in [69], it is proposed to parameterize the filter coefficients with a minimal set of parameters  $\theta$ . In order to have maximally frequency confined pulses, the parameters  $\theta$  are chosen to satisfy the minimum square error from a target pulse  $H(f)$ .

$$\arg \min_{\theta} \int_{-0.5}^{0.5} |G(f, \theta) - H(f)|^2 df, \quad (7.4)$$

where  $G(f, \theta)$  is the frequency response of the prototype pulse  $g(n)$  as a function of the parameters  $\theta$ . It is worth noting that the choice of the filter determines the achievable rate (7.2) inasmuch it is proportional to the OH, therefore  $\beta$  can be adapted to the channel condition to maximize the achievable rate. Nevertheless, in order to keep low the system implementation complexity, the family of filters adopted in this chapter has minimal length equal to one symbol duration, i.e.,  $L_g = N$ . Furthermore, numerical results have shown that for SO-FMT the adaptation of  $\beta$  to the channel conditions does not significantly improve the achievable rate, and in general the best performer results to be the filter whose  $N = M + \beta = (9/8)M$ . Therefore, when showing numerical results for SO-FMT, we set the OH  $\beta$  equal to 8 samples with  $M=64$ . More details regarding the filter design of the SO-FMT scheme are reported in [59, 69].

### 7.2.2 Hybrid FMT

We have numerically found that depending on the channel condition it is convenient to use A-OFDM or SO-FMT to maximize the achievable rate (7.2) (see numerical results section).

This can be simply justified observing the following. Firstly, the interference experienced by A-OFDM is always lower than that of SO-FMT if a

further equalization stage is not deployed. Secondly, OFDM suffers of a loss of SNR of a factor equal to  $M/N$  because it does not use a matched filter. Hence, we can understand that, when looking at the SINR of SO-FMT, if it is noise limited, namely if the SNR is lower than the signal to interference ratio (SIR), it is convenient to use SO-FMT. Vice versa, it is convenient to use A-OFDM. Note that the shortest value of CP used by A-OFDM over WLAN channels is equal to 8 samples and it also corresponds to the OH used by SO-FMT. Now, when the SNR is low, both A-OFDM and SO-FMT will likely use an OH of 8 samples but SO-FMT will reach an higher achievable rate than A-OFDM because it does not suffer from the loss of SNR given by the discard of the CP of OFDM.

Clearly, the optimal criterion for switching between A-OFDM and SO-FMT, for each channel realization, should target the achievable rate maximization. Nevertheless, this criterion is not desirable for practical systems where the channel conditions can quickly change. Therefore, in our previous work [70] we have proposed a metric that, based on the estimation of the mean SNR, chooses the scheme to be used. More precisely, numerical results have shown that the average level of the SIR experienced by SO-FMT over WLAN channels is equal to 38 dB (this value is obtained averaging across sub-channels and channel realizations). Thus, if the mean SNR (SNR averaged across sub-channels) is below this value the system uses SO-FMT, otherwise it switches to A-OFDM.

As it will be shown in the numerical results section, the criterion based on the estimation of the mean SNR gives results that are close to that given by the optimal one.

To implement H-FMT we make use of the efficient implementation of a DFT modulated filter bank presented in [69]. Fig. 7.1 shows the H-FMT architecture. More details can be found in [59]. As we can see, at the transmitter the  $M$  data signals  $a^{(k)}(\ell N)$ , with  $k = 0, \dots, M - 1$ , are processed by an  $M$  points inverse discrete Fourier transform (IDFT). The  $N$  output samples from the cyclically extension, are multiplied by the coefficients  $g(n)$ , with  $n = 0, \dots, N - 1$  which corresponds to the prototype synthesis pulse coefficients

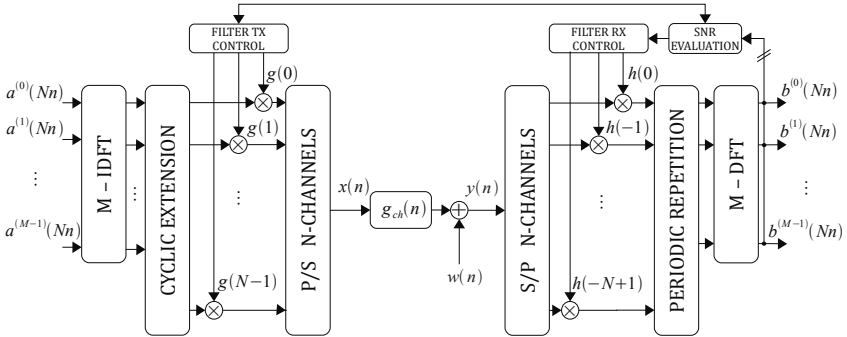


Figure 7.1: Hybrid FMT scheme.

of SO-FMT or A-OFDM. Finally, the outputs are parallel-to-serial converted and transmitted over the channel. The receiver consists in a serial-to-parallel conversion with a converter of size  $N$ . Depending on the modulation scheme used at the transmitter, namely SO-FMT or A-OFDM, the output signals are multiplied by the corresponding prototype analysis pulse coefficients  $h(-n)$  with  $n = 0, \dots, N - 1$ . Then, the periodic repetition with period  $M$  of the block of coefficients of size  $N$  is applied. Finally, the  $M$ -point DFT is performed.

The block SNR Evaluation estimates the mean SNR and feedbacks it to the transmitter. Note that the SNR evaluation can be done sending a known robust training sequence of symbols using OFDM with a conservative long CP. In this case, the received signal results free of interference and the SINR corresponds to the SNR. Furthermore, to adapt the system to the channel condition, the SNR evaluation is done periodically.

Since both SO-FMT and OFDM use filters with almost the same length, the implementation complexity of H-FMT is basically the same of OFDM (see [59, 69] for more details).

### 7.3 Power Allocation

In this section, we propose a practical algorithm to solve the power minimization (PM) problem using H-FMT when a constraint on the power spectral density (PSD) mask is imposed.

The PM problem can be formulated as

$$\begin{aligned} \arg \min_{\mathbf{P}_a} \quad & \sum_{k=0}^{M-1} P_a^{(k)}, & (7.5) \\ \text{s.t.} \quad & 0 \leq P_a^{(k)} \leq \bar{P}, \quad k = 0, \dots, M-1. \\ & \frac{1}{NT} \sum_{k=0}^{M-1} \log_2 \left( 1 + P_a^{(k)} \gamma^{(k)}(\beta) \right) = R, \end{aligned}$$

where  $R$  denotes the target achievable rate in [bit/s],  $\mathbf{P}_a = \{P_a^{(k)}, \text{ with } k = 0, \dots, M-1\}$  is the vector of the transmitted powers, and  $\bar{P}$  is the power constraint given by the PSD limit level.

In general, problem (7.5) is not convex because the interference terms that appear in  $\gamma^{(k)}(\beta)$  are dependent on the transmitted power distribution. A solution to (7.5) could be found doing an exhaustive search on  $\mathbf{P}_a$ . However, this procedure is practically unfeasible. This is true even supposing to quantize the sub-channel power in a finite number  $L$  of levels. In fact, the exhaustive search would have a complexity  $O(L^M)$ . Nevertheless, if we consider the interference term independent from the distribution of the transmitted power, the problem admits an equivalent convex optimization problem. It can be obtained with the change of variable  $P_a^{(k)} = (2^{b_k} - 1)/\gamma^{(k)}$ . The optimal solution of the equivalent convex problem can be computed applying the Karush-Kuhn-Tucker (KKT) conditions. Finally, the optimal solution to the original problem can be found applying the inverse change of variable and it is given by (see Appendix 11.6)

$$P_a^{(k)} = P_a^{(k)}(\nu) = \left[ \nu - 1/\gamma^{(k)}(\beta) \right]_0^{\bar{P}}, \quad (7.6)$$

where

$$[x]_a^b = \begin{cases} b, & x \geq b \\ x, & a < x < b \\ a, & x \leq a, \end{cases} \quad (7.7)$$

and  $\nu$  is given by the solution of the equation

$$\frac{1}{NT} \sum_{k=0}^{M-1} \left(1 + P_a^{(k)}(\nu)\gamma^{(k)}(\beta)\right) = R. \quad (7.8)$$

To solve (7.6),(7.8) we make use of the iterative algorithm presented in [34].

Now the problem is: how does the H-FMT select the modulation to be used? For each channel realization, the optimal approach should target the PM objective. We can have two cases. The first is when the solution to (7.5) exists for both SO-FMT and A-OFDM. In such a case, we should choose the system that transmits less power. The second is when only one system admits a valid solution to (7.5). In this case the choice is trivial. In both cases, the systems in general can be interference limited (i.e., the interference level is higher than that of noise). Thus, (7.5) has to be solved exhaustively and this renders this approach unfeasible.

To diminish the complexity we use the two switching criteria that have been proposed in [70] and summarized in Section 7.2.2. They have been derived considering the dual problem of (7.5), i.e., the achievable rate maximization (RM) under a PSD mask constraint. The first one is optimal for the RM problem in the sense that for each channel realization, it first computes the achievable rate of both SO-FMT and A-OFDM, and consequently chooses the system that maximizes it. The second is sub-optimal, indeed it selects the modulation to be used depending on the experienced mean SNR.

In this way the H-FMT works in a condition where it is always noise limited (i.e., it uses SO-FMT if its interference is lower than the noise, otherwise uses A-OFDM that, thanks to the CP, renders the interference negligible).

It is worth noting that, supposing the interference term independent from the transmitted power distribution, the optimal power allocation that is the

solution of the RM problem is a uniform distribution at the PSD limit level [34]. Therefore, when showing numerical results for the achievable rate obtained using RM power allocation we assume the previous hypothesis verified.

The practical algorithm for the PM of H-FMT can be summarized as follows.

1. *Select the system to be used (SO-FMT or A-OFDM) with one of the criteria proposed for the RM problem.* Namely, the optimal or the mean SNR based criterion.
2. *Compute the coefficients  $\gamma^{(k)}(\beta)$  for  $k = 0, \dots, M - 1$ , setting the transmitted power at the PSD limit level.* Note that in such case the interference is maximal and the corresponding  $\gamma^{(k)}(\beta)$  are the smallest. Therefore, once the power is recomputed through (7.6),  $\gamma^{(k)}(\beta)$  can only increase and the constraints in 7.5 are still satisfied.

Also compute the rate achievable with this power distribution. It is worth noting that it also equals the maximum achievable rate when the interference is negligible.

3. *Set the value for the target rate  $R$ .*
4. *Compute the optimal power allocation (7.6).*

Note that, as done in Section 6.3, we could have computed the power allocation (last step of the previous algorithm) adopting an iterative procedure. Nevertheless, as seen in Section 6.4, the iterative procedure does not give appreciable achievable rate improvements and then we decided to simplify the algorithm by neglecting the iterative procedure.

## 7.4 Numerical Results

To obtain numerical results, we have chosen the following system parameters<sup>1</sup> that essentially are those of the IEEE 802.11 standard [8]. The MC system uses

---

<sup>1</sup>The system parameters that we here use are the same as the ones used in Sections 3.8, and 5.5.

$M = 64$  sub-channels with a transmission bandwidth of  $20 \text{ MHz}$ . The signal is transmitted with a constraint on the PSD limit level of  $-53 \text{ dBm/Hz}$ . At the receiver side, we add white Gaussian noise with PSD equal to  $-168 \text{ dBm/Hz}$ . To show the performance of H-FMT, we use an OFDM baseline system which deploys a fixed CP of  $0.8 \mu\text{s}$  ( $\beta = 16$  samples), that is the value of CP employed by the IEEE 802.11 standard [8].

The H-FMT deploys SO-FMT with fixed OH of  $0.4 \mu\text{s}$  ( $\beta = 8$  samples,  $N = (9/8)M$ ), and A-OFDM with values of CP equal to  $\mathcal{M}_{OFDM} = \{\beta_B^{(99\%)} = 0.4 \mu\text{s}, \beta_C^{(99\%)} = 0.5 \mu\text{s}, \beta_D^{(99\%)} = 0.6 \mu\text{s}, \beta_E^{(99\%)} = 0.9 \mu\text{s}, \beta_F^{(99\%)} = 1.1 \mu\text{s}\}$  (see Section 3.8). Both schemes use single tap zero forcing sub-channel equalization. Fig. 7.2 shows the complementary CDF (CCDF) of the achievable rate obtained using the RM power allocation for SO-FMT, A-OFDM, and the baseline system. For the sake of readability, we only show results for channel classes B, C, and D and for distances between transmitter and receiver equal to  $10 \text{ m}$ ,  $30 \text{ m}$ , and  $60 \text{ m}$ . More results for the baseline OFDM and for A-OFDM can be found in Chapter 3. From Fig. 7.2 we can observe how for high values of distance  $d = \{30, 60\} \text{ m}$ , and thus in the low SNR region, the SO-FMT shows better performance than both A-OFDM and baseline OFDM. On the contrary, for a short distance of  $10 \text{ m}$ , A-OFDM is able to achieve higher rate than SO-FMT. Although not shown, the results obtained with a distance of  $3 \text{ m}$  behave as the ones obtained with a distance of  $10 \text{ m}$ .

It is worth noting that also if not highlighted, in Fig. 7.2 the CCDFs of the achievable rate of H-FMT would correspond to the most right curves.

We now turn our attention to the PM problem (7.5). Fig. 7.3 shows the cumulative distribution functions (CDFs) of the average transmitted power. They have been obtained solving the PM problem (7.5) for H-FMT with the proposed PM algorithm using both the optimal and the mean SNR based switching criteria, and for the baseline system. The results obtained with A-OFDM are also shown. These are meant to show the best performance obtainable using OFDM. The results are obtained drawing the channels randomly among the classes  $\{B, C, D\}$ , and for distances in  $[1, 60] \text{ m}$ . Furthermore, for each channel realization we set the target rate  $R$  equal to the achiev-

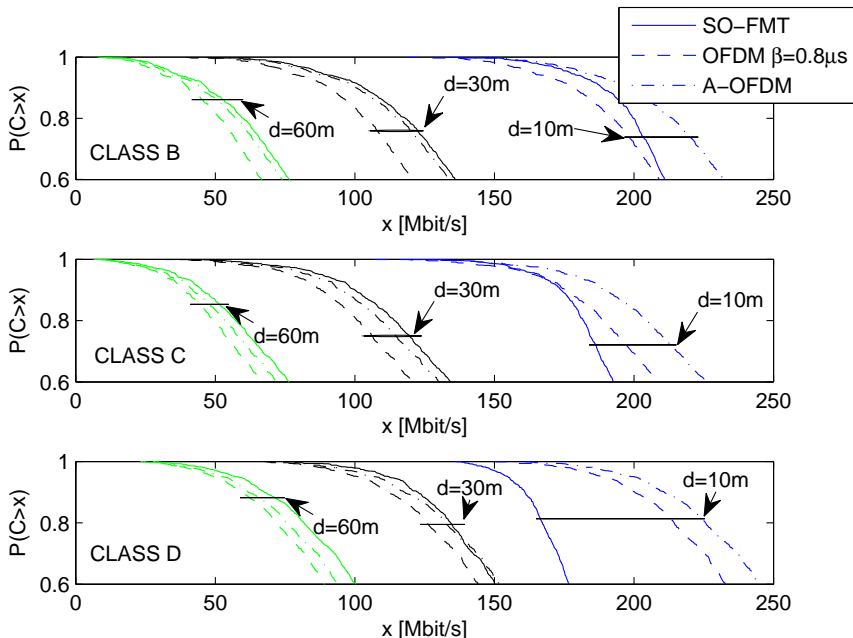


Figure 7.2: Achievable rate CCDF obtained using SO-FMT, A-OFDM, and OFDM with a fixed CP of  $0.8 \mu s$ . The employed channel classes are the B, C, and D. The distance between transmitter and receiver is set to 10 m, 30 m, and 60 m.

able rate of the baseline system (OFDM with fixed CP of  $0.8 \mu s$ ) whose transmitted powers are given by the PSD limit level. This choice is justified observing that the baseline system shows worse performances than both H-FMT and A-OFDM fixing the transmitted power at the PSD level (see Fig. 7.2). Therefore, assuming this value as the target rate, we can first compare the proposed system with the baseline, and further we ensure that a solution to the PM problem exists for both H-FMT and A-OFDM. From Fig. 7.3 we observe the followings.

- The switching criterion based on the mean SNR estimation works close to the optimal one.

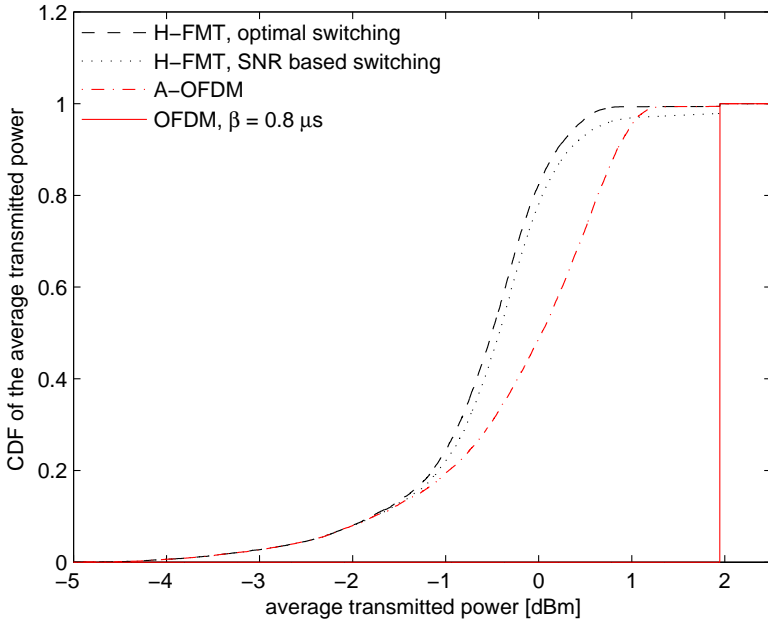


Figure 7.3: CDF of the average transmitted power obtained using the proposed PM algorithm. The comparison is among H-FMT that adopts the optimal and the sub-optimal switching criterion, OFDM with CP equal to  $0.8\mu s$ , and A-OFDM.

- With probability equal to 0.9, H-FMT and A-OFDM respectively transmit with power of about 1.9 and 1.4 dB less than the baseline system, yet achieving the same rate. This translate in a power saving of about 36% and 30% w.r.t. the baseline system.
- There are a 20% of channels where the power saving given by H-FMT equals 3 dB.

## 7.5 Main Findings

We have proposed the use of a hybrid architecture that, to reduce the power transmitted by WLAN devices, wisely exploits the peculiarities of adaptive OFDM and short-orthogonal FMT. Through numerical results, obtained testing the proposed scheme over typical WLAN channels, we have shown that hybrid FMT provides significant power saving gains compared to an OFDM scheme that deploys a fixed CP, yet assuring the same achievable rate. Furthermore, the hybrid FMT efficient implementation only needs a marginal increment of computational complexity w.r.t. OFDM. This makes the proposed scheme suitable for practical implementation.

# Time Slot Design in OFDM-TDMA Systems over Time-Variant PLC Channels

In this chapter, we analyze the resource allocation problem in an indoor power line communication (PLC) system with a physical (PHY) layer based on OFDM, and a medium access control (MAC) layer consisting of a contention region used for best effort traffic and an adaptive time division multiple access (TDMA) region used to provide high quality of service (QoS). A similar scheme is employed in the HomePlug AV standard. In particular, we focus on the optimization of the TDMA region. Differently from the previous chapters, where we have considered both stationary channel and noise, in this chapter, we consider periodically time variant channel and cyclostationary noise. In such a scenario, we compute the optimal time slot duration. It is determined for various amounts of overhead required by the PHY layer. The presented results are suitable for practical systems to perform a fast real-time time slot duration selection and scheduling as a function of the number of active users.

## 8.1 Introduction

PLC channels are frequency selective and time variant. Measurements have shown that they can be modeled as a linear periodically time variant (LPTV) systems with also the presence of additive cyclostationary colored noise [55,71].

As deeply discussed in the previous chapters, in order to mitigate the frequency selectivity of the channel, the state-of-the-art systems employ OFDM at the PHY layer. An attractive feature of OFDM is that it allows practical implementation of the water-filling principle by allocating the power across the sub-channels affected by different attenuations due to the channel frequency selectivity.

The QoS required by multimedia contents can be fulfilled with the use of a Hybrid MAC scheme as the one employed in HomePlug AV (HPAV) [18]. HPAV uses a TDMA scheme to satisfy the QoS based traffic. While, the best effort traffic is served in a non persistent scheduled region or it is left for a contention based region. Nevertheless, in order to improve the overall PLC system performance, a cross-layer optimization between the PHY and the MAC layers has to be considered.

This issue has been previously studied in [72], where the influence of the time slot duration in the performance of an HPAV “like” system is investigated. The differences between our work and the one presented in [72] are the following.

- We take into account the channel response variations, which cause inter-carrier interference (ICI) and inter-symbol interference (ISI) in the OFDM signal, and not only the cyclostationary noise behavior.
- We provide the optimum time slot duration for different overhead lengths.
- We perform the optimization in a multi-user scenario.
- We propose and evaluate a practical resource allocation procedure using linear programming (LP).

In this chapter, we consider a hybrid MAC technique consisting of contention free and contention based regions like the one employed in HPAV. For the contention free region, we propose an algorithm based on LP that allows the computation of the optimal time slot duration and the optimization of the time slots scheduling among the users.

The chapter is organized as follows. In Section 8.2, we describe the PHY layer employed in our simulations. In Section 8.4, we present the hybrid MAC model, and in Section 8.4, we formulate the multi-user resource allocation problem. However, since this problem is not always solvable, a simplified optimization problem is proposed in Section 8.5. Simulations results follow in Section 8.6. Finally, the main findings are summarized in Section 8.7.

## 8.2 PHY Layer Description

The PHY layer is based on multi-carrier transmission using OFDM with  $M$  sub-channels, and a CP length of  $\mu$  samples. The OFDM normalized symbol duration is equal to  $N$  samples and  $N = M + \mu$ . Assuming  $T$  equal to the sampling period, the symbol duration in seconds is equal to  $T_0 = NT$ . The channel model consists of an LPTV filter plus additive cyclostationary noise, both obtained with the simulator described in [73]. Denoting by  $g_{ch}(n; i)$  the channel impulse response at time instant  $n$  to an impulse applied  $i$  time instants before, the received signal can be written as

$$y(n) = \sum_{i=0}^{\nu-1} x(n-i) g_{ch}(n; i) + \eta(n), \quad (8.1)$$

where  $\nu T$  is the impulse response duration,  $x(n)$  is the OFDM transmitted signal, and  $\eta(n)$  is the cyclostationary additive noise. Both, the channel response and the cyclostationary noise have the periodicity of the mains signal (20 ms in Europe). At the receiver, after symbol synchronization, the CP is discarded and an  $M$ -point DFT is computed. The  $k$ -th sub-channel output can be written as

$$z^{(k)}(\ell N) = H^{(k)}(\ell N) a^{(k)}(\ell N) + I^{(k)}(\ell N) + W^{(k)}(\ell N), \quad (8.2)$$

where  $a^{(k)}(\ell N)$  is the  $\ell$ -th data symbol transmitted on that sub-channel,  $H^{(k)}(\ell N)$  is the effective channel transfer function,  $W^{(k)}(\ell N)$  is the noise contribution and  $I^{(k)}(\ell N)$  is the ICI plus ISI term. It must be emphasized

that these distortion terms arise because of the loss of orthogonality due to both an insufficient CP and to channel time variations. The latter effect has been traditionally neglected in PLC [72]. In an OFDM system impaired by Gaussian noise and with neither ISI nor ICI, the receiver determines the bit loading of each sub-channel from its SNR [30]. Provided that the number of sub-channels is sufficiently high, the ISI and ICI can be assumed to have a Gaussian distribution. Hence, once the CP is set, the bit loading can be obtained with one of the algorithms described in Section 3.4. Considering that transmissions are synchronized with the mains and that  $L$  OFDM symbols can be fitted into each mains cycle, the symbol index  $\ell$  can be written as  $\ell = m + Lr$ , where  $0 \leq m \leq L - 1$  and  $r \in \mathbb{Z}$ . Assuming to transmit signals with a constant PSD, the power of all the terms in (8.2) is periodical and the SINR experienced in the  $k$ -th sub-channel at the  $m$ -th time instant can then be expressed as

$$SINR^{(k)}(mN) = \frac{P_U^{(k)}(mN)}{P_W^{(k)}(mN) + P_I^{(k)}(mN)}, \quad (8.3)$$

where

$$\begin{aligned} P_U^{(k)}(mn) &= |H^{(k)}(mn)|^2 E \left[ |a^{(k)}(mN)|^2 \right], \\ P_W^{(k)}(mN) &= E \left[ |W^{(k)}(mN)|^2 \right], \\ P_I^{(k)}(mN) &= E \left[ |I^{(k)}(mN)|^2 \right]. \end{aligned} \quad (8.4)$$

The receiver estimates the sub-channel SINR during the training phase via reception of known training symbols that are periodically sent by the transmitter. The estimate can be refined or updated using a data decision directed mode during data transmission [74].

### 8.3 Hybrid MAC Models

We consider a hybrid MAC protocol that uses contention free and contention based regions, similarly to the one employed in HPAV [18]. It can support

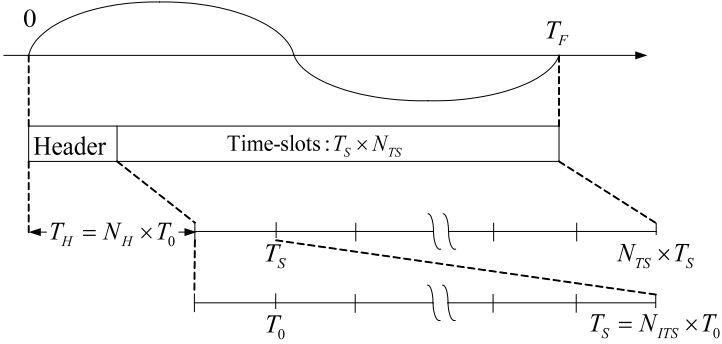


Figure 8.1: Frame Structure.

both the connection oriented traffic and the best effort traffic. Services that require high QoS can be offered using a contention free MAC technique based on TDMA, while best effort traffic can be offered using a contention based scheme as carrier sense multiple access with collision avoidance (CSMA/CA). Similarly to HPAV, we assume to have a node in the network that acts as central coordinator (CCo). The CCo is responsible to allocate resources by collecting information regarding the network state, i.e., number of users, channel conditions, QoS required from each user request, etc. Once the CCo has collected all the information needed, it dynamically allocates the resources among the users. We assume the MAC frame to have duration  $T_F$  equal to a mains cycle, i.e.,  $T_F=20\text{ ms}$ . Fig. 8.1 depicts the frame structure. The MAC frame is divided into two regions. In the first region, referred to as TDMA sub-frame, centralized TDMA is used. Its duration,  $T_{TDMA}$ , depends on the quantity of pending QoS based traffic, and can be expressed as  $T_{TDMA} = N_{TDMA}^{MC} T_F$ , where  $N_{TDMA}^{MC}$  represents an integer number of MAC frames. The TDMA sub-frame comprises a header followed by a number of slots. The header and the slots have a duration equal to an integer number of OFDM symbols duration, i.e., they are equal to  $T_H = N_H T_0$ , and  $T_S = N_{ITS} T_0$ . The MAC frame header carries the following information:

- Time slot duration.

- Scheduling for the time slots. The scheduling is a correspondence between each slot index and the physical address of the node whose slot has been reserved.
- Number of mains cycles where scheduling is valid.

Each slot carries also some overhead (OH) information that is used by the PHY layer for synchronization and channel estimation algorithms. We assume several scheduling algorithms each comprising a given slot format with a different amount of OH. This is discussed in Section 8.4.

### 8.3.1 Example of Parameters

As an example, we assume transmission parameters similar to the ones used by HPAV. The transmission band is 0-37.5 MHz, and the OFDM has  $M=1536$  sub-channels. 1066 sub-channels are used, yielding a useful band in 2-28 MHz. The cyclic prefix duration is equal 6.32  $\mu s$ . Therefore, the OFDM symbol duration is 47.28  $\mu s$ . The signal is transmitted with a power spectral density of -50 dBm/Hz. For simplicity we assume that the contention region is not used. Hence, the number of OFDM symbols in the TDMA sub-frame is equal to 423. We assume a header consisting of 3 OFDM symbols. This results in 420 useful OFDM symbols. The slot duration can vary between a minimum of one OFDM symbol, up to 105 OFDM symbols for a number of nodes (users)  $N_U$  equal to 4. If  $N_U$  equals 3 then the maximum slot length equals 140 OFDM symbols, while if  $N_U$  equals 2 the maximum slot length is 210 OFDM symbols.

## 8.4 MAC Procedures

Before transmission can start, it is necessary to perform resource allocation and scheduling. We focus on the transmission between the CCo and the  $N_U$  nodes and, in particular, in the downlink. This can be viewed for example as the scenario where the CCo distributes data coming from internet, e.g., video streaming to different televisions. Fig. 8.2 shows the considered network. The uplink and the peer-to-peer connection among nodes can work in a similar way.

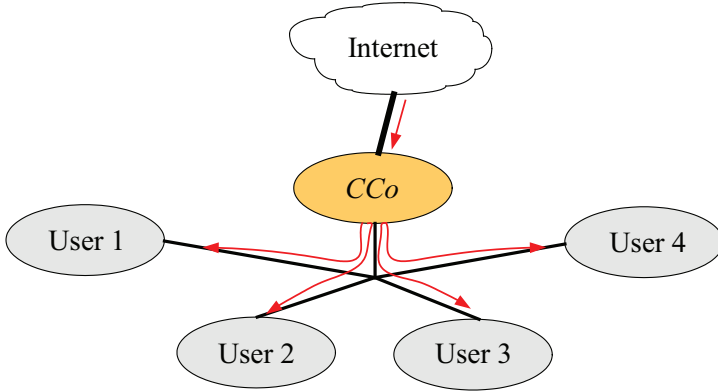


Figure 8.2: Considered network.

The MAC protocol consists of three phases that we refer to as: network state learning, resource allocation, and data exchange. The first two steps have to be performed whenever a new node joins the network or the QoS required by an existing one cannot be fulfilled with the current allocation, e.g. because of a significant channel variation has occurred.

#### 8.4.1 Network State Learning

In this phase, the CCo learns the network state, e.g., the links condition between itself and the nodes, the QoS required by the applications and so on. To accomplish it, the CCo sends training sequences to the users, e.g., the CCo sends known training OFDM symbols modulated using 4-QAM in each sub-channel. All users estimate the SINR that they experience in each sub-channel and OFDM symbol in the TDMA sub-frame. Once estimation of the SINR between the CCo and the nodes is accomplished, the nodes can compute bit-loading for all these symbols. The bit-loading map is denoted with  $b^{(u,k)}(mN)$ , and it provides the number of bits that can be transmitted in the  $k$ -th sub-channel to the  $u$ -th user if the CCo transmits during the  $m$ -th OFDM symbol of the MAC frame.

The bit-loading map is fed back to the CCo by the nodes. It is worth

noting that due to the fact that the channel is LPTV with period equal to the mains cycle, each user has to send only the information regarding a mains cycle, i.e.,  $b^{(u,k)}(mN)$ , with  $m = 0, \dots, L - 1$ . The bit map is computed as follows

$$b^{(u,k)}(mN) = \log_2 \left( 1 + \frac{SINR^{(u,k)}(mN)}{\Gamma} \right), \quad (8.5)$$

where  $SINR^{(u,k)}(mN)$  represents the SINR experienced by the  $u$ -th user in the  $k$ -th sub-channel during the  $m$ -th OFDM symbol of a MAC frame, and  $\Gamma$  is the gap factor that takes into account practical coding/modulation constraints [30, 31]. In our simulations we set  $\Gamma=9$  dB. The values of  $b^{(u,k)}(mN)$  are rounded to the nearest available constellation among 2-PAM, 4, 8, 16, 64, 256 and 1024-QAM. Hence, only 3 bits are needed for the bit-loading map of each sub-channel of an OFDM symbol. Since only 1066 sub-channels are switched on, each user has to send feedback consisting of  $3 \times 1066 \times 423 \approx 1.36$  Mbit/s. By using 4-QAM constellations this requires 319 OFDM symbols, which occupies 75.4% of a MAC frame.

### 8.4.2 Resource Allocation and Scheduling

Once the CCo has received the bit-loading map from the nodes, it is able to determine the resource allocation and scheduling. We point out that the bit-loading information per OFDM symbol is only required by the CCo to perform the time slot duration optimization. If a fixed time slot length is employed, only the bit-loading map per time slot is needed. This may significantly decrease the amount of feedback information. Moreover, when the CCo has just to compute the slots allocation between the network users, e.g., when a peer to peer communication occurs, it only needs to know the achievable rate  $R^{(u)}(mN)$  from/to the  $u$ -th user during the  $m$ -th OFDM symbol of the MAC frame. Clearly, this information is computed using many mains cycles. As said in Section 8.3, we consider four different scheduling procedures for which a different amount of PHY OH is spent in a slot.

**Procedure A.** The slot can have length equal to one symbol and each OFDM symbol uses 10% of the number of sub-channels for OH. In this case,

the throughput reached by the CCo for a transmission to the  $u$ -th user during the  $s$ -th time slot is equal to

$$R_S^{(u)}(N_{ITS}) = \frac{N_{ITS}}{T_F} \sum_{k \in \mathbb{K}_{\text{on}}} \hat{b}_S^{(u,k)}, \quad (8.6)$$

where

$$\hat{b}_S^{(u,k)} = \min_m \left\{ \hat{b}^{(u,k)}(sN_{ITS}N + mN) \right\}, \quad s = 0, \dots, N_{TS}-1, \quad m = 0, \dots, N_{ITS}-1, \quad (8.7)$$

and  $\mathbb{K}_{\text{on}}$  is the set of sub-channel indices employed to transmit useful data (it does not include the ones employed for the overhead). It is worth noting that (8.7) implies the bit-loading to be invariant in each time slot.

**Procedure B.** A full OFDM symbol is spent as PHY OH. This choice was described in [75]. In this case, we may send in the PHY header the bit map as it is done in HPAV. Hence, if the CCo transmits to the  $u$ -th user during the  $s$ -th time slot, the throughput is equal to

$$R_S^{(u)}(N_{ITS}) = \begin{cases} \frac{N_{ITS}-1}{T_F} \sum_{k \in \mathbb{K}_{\text{on}}} \hat{b}_S^{(u,k)} & N_{ITS} > 1, \\ 0 & \text{otherwise.} \end{cases} \quad (8.8)$$

**Procedure C.** As in *Procedure A* but the PHY OH is equal to 10% of the first OFDM symbol in each time slot.

**Procedure D.** In this case, no PHY OH is present. It is here considered to obtain an upper bound in the performances.

Once the CCo has computed the rate that it would achieve transmitting to each user in each time slot  $R_S^{(u)}(N_{ITS})$ , it has to allocate the slots among the users and, further, it has to compute the optimal time slot duration. The problem can be viewed as an optimization problem that can be expressed as

$$\max_{\alpha, N_{ITS}} \sum_{u=1}^{N_U} \sum_{s=0}^{N_{TS}-1} \alpha^{(u,s)} R_S^{(u)}(N_{ITS}),$$

$$\begin{aligned} \text{s.t. } \sum_{u=1}^{N_U} \alpha^{(u,s)} &= 1, \quad s = 0, \dots, N_{ITS} - 1, \\ \sum_{s=0}^{N_{ITS}-1} \alpha^{(u,s)} R_S^{(u)}(N_{ITS}) &\geq \frac{p^{(u)}}{100} \sum_{s=0}^{N_{ITS}-1} R_S^{(u)}(N_{ITS}), \quad u = 1, \dots, N_U, \end{aligned} \quad (8.9)$$

where  $\alpha^{(u,s)}$  denote the binary coefficients equal to 1 if slot  $S$  is allocated to user  $u$ , and zero otherwise.  $p^{(u)}$  is a weighting factor that denotes the percentage of data rate that the  $u$ -th user has to achieve with respect to the one that it would achieve in the corresponding single user scenario. Problem (8.9) can be solved using integer programming (IP) once  $N_{ITS}$  is fixed.

It should be noted that the procedures *A-C* are characterized by a different amount of OH. Therefore, they may have an impact on the robustness of the PHY algorithms that dynamically update synchronization and channel estimation. Nevertheless, according to a previous work [74], the considered OH appears to be sufficient. Clearly, *Procedure C* uses the largest OH that, however, is not required for the PHY algorithms. Furthermore, the inclusion in this OH of the bit map from the CCo to the nodes is not necessary since the receiving nodes are already aware of it. Nevertheless, the HPAV system appears to resend the bit map [75].

## 8.5 Simplified Optimization Problem

In some cases, IP is not able to provide a solution to (8.9) in a reasonable computation time. Moreover, it may also happen that the problem is not solvable satisfying the imposed constraints. In these circumstances, some constraints can be iteratively relaxed until IP gives a solution to the problem. Nevertheless, the problem may still be unsolvable in a reasonable time. To simplify the complexity we propose to use linear programming (LP) [44], once  $N_{ITS}$  is fixed. That is, for each value of  $N_{ITS}$ , the coefficients that give the slots allocation are returned via LP followed by rounding the coefficients  $\alpha^{(u,s)}$ . The optimal time slot duration can be determined by (8.9) varying the time slot length, i.e.,  $N_{ITS}^{opt}$  is the number of OFDM symbols that maximizes the

aggregate rate.

It is interesting to note that in some cases LP followed by rounding the coefficients may give a solution to (8.9) that does not allow all users to transmit. This can happen when the number of time slots that maximizes the aggregate rate  $N_{ITS}^{opt}$  is comparable to  $N_U$ . To solve this problem the following greedy algorithm can be used.

1. Once  $N_{ITS}^{opt}$  has been computed using LP followed by rounding the coefficients, compute  $R^{(u)}(N_{ITS}^{opt}) = \sum_{s=0}^{N_{TS}-1} R_S^{(u)}(N_{ITS}^{opt})$  for each user. If for some users  $R^{(u)}(N_{ITS}^{opt})$  is zero, then decrease  $N_{ITS}^{opt}$ .
2. If  $N_{ITS}^{opt}$  is equal to the minimum slot size, then decrease  $p^{(u)}$  by one and solve (8.9) again. Otherwise, go to the previous step.

## 8.6 Numerical Results

In this section, we present the simulation results obtained with the solution of (8.9) using the simplified algorithm based on LP described in Section 8.5. The simulated network is the one showed in Fig. 8.2, where the data exchange occurs from the CCo to 2, 3 or 4 users. All the combinations CCo-users are considered. Fig. 8.3 and Fig. 8.4 show the aggregate rate for the two-users case obtained using the scheduling procedures described in Section 8.4. It also shows the user rate for the scheduling *Procedure C*. Fig. 8.5 and Fig. 8.6 show the results for the three and four-user cases.

As we can see, the optimal slot duration is always equal to 1 OFDM symbol for the scheduling procedures *A* and *D*. These results are easily explained by noticing that enlarging the time slot always decreases the amount of raw bits transmitted, i.e., without taking into account the OH. This is due to the employed bit-loading procedure presented in (8.7), which does not adapt the constellation size to the channel changes that may occur during the time slot. Since in *Procedure D* there is no OH, increasing the time slot always reduces the bit-rate. In *Procedure A*, this reduction is even larger because the amount of OH increases proportionately to the time slot duration. It is also worth noting that the performance loss of *Procedure B* and, especially *C*, with respect to

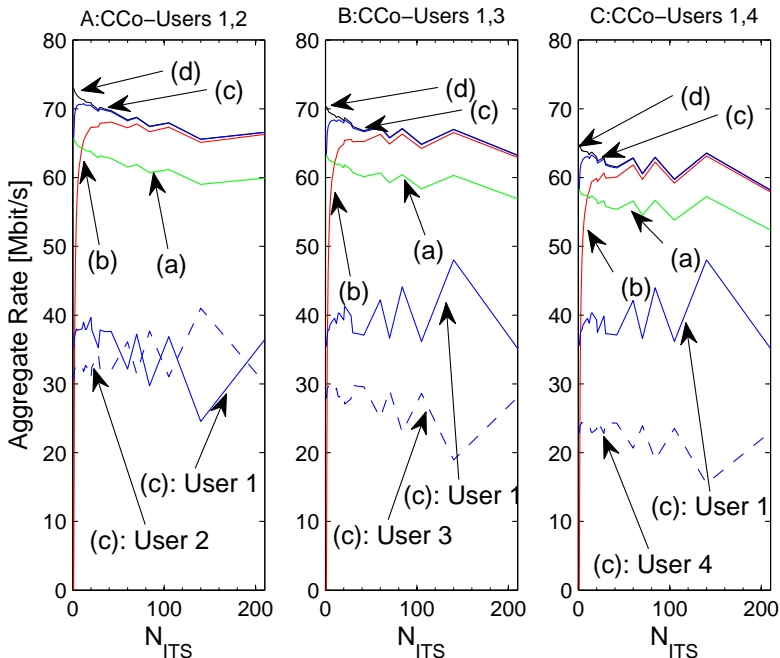


Figure 8.3: **Two users scenario**: Aggregate rates for the 4 scheduling Procedures and single user rates for the Procedure C. Labels (a)-(d) denote Procedures A-D respectively

$D$  is quite reduced. In procedures  $B$  and  $C$  a fixed amount of OH per time slot is introduced. Hence, increasing the time slot length reduces the raw bit-rate but, on the other hand, it increases the transmission efficiency, since the percentage of introduced OH decreases. Therefore, the aggregate rate is, in general, a convex function of the slot duration. Clearly, the optimum time slot duration depends on the rapidity by which the channel and the noise vary. An example can be observed by comparing results in Fig. 8.4.A and in Fig. 8.4.C. In the former one, the characteristics of the involved channels change quite slowly. Hence, the bit-rate loss that occurs because of selecting a longer time slot than the optimum one is quite small. On the other hand,

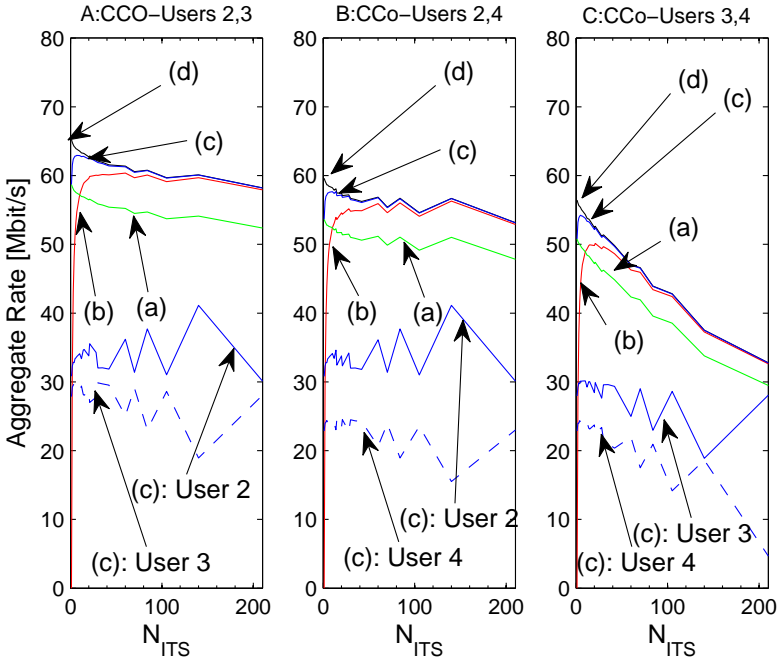


Figure 8.4: **Two users scenario:** Aggregate rates for the 4 scheduling Procedures and single user rates for the *Procedure C*. Labels (a)-(d) denote *Procedures A-D* respectively.

channels involved in the scenario of Fig. 8.4.C exhibit fast time variations, which leads to a severe performance degradation when the time slot duration is increased over its optimum value. Table 8.1 and Table 8.2 list the optimal time slot duration when using procedures *B* and *C*, which are the ones with practical interest, in all the considered scenarios. It can be seen that the optimum values are strongly dependent on the time variation of the involved channels. However, the quite-flat behavior of the aggregate bit-rate curves in Fig. 8.3 to Fig. 8.6 indicates that the performance loss that occurs when a fixed time slot duration is employed in all the scenarios is small.

This can be corroborated by computing the aggregate bit-rate loss that

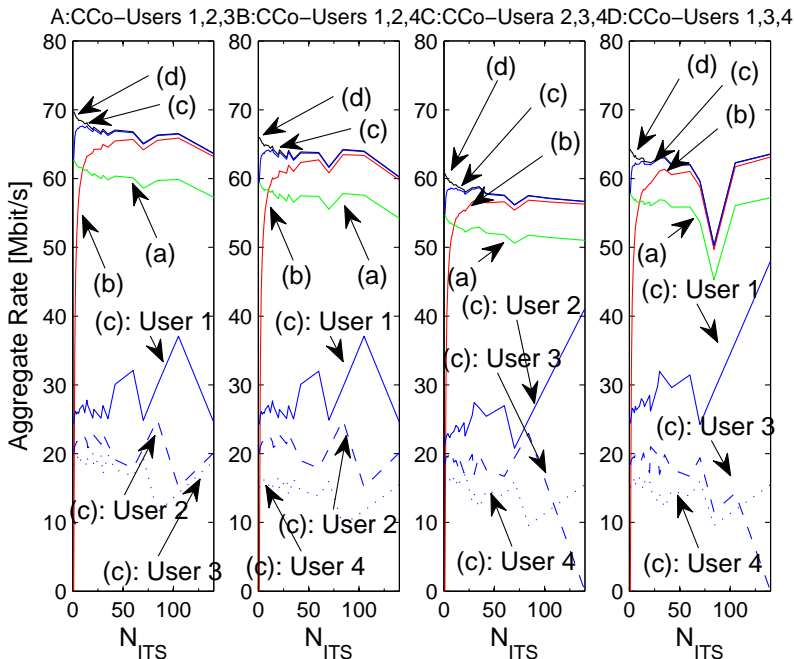


Figure 8.5: **Three users scenario:** Aggregate rates for the 4 scheduling Procedures and single user rates for the *Procedure C*. Labels (a)-(d) denote *Procedures A-D* respectively

occurs in each scenario when a non-optimal time slot duration is employed. Fig. 8.7 and Fig. 8.8 depict these curves for the two-user and the three-user scenario (the four-user scenario gives similar values). It can be noticed that, in general, 50 OFDM symbols could be a trade-off time slot value when using *Procedure B* and 10 OFDM symbols when using *Procedure C*. These lengths lead to aggregate bit-rate loss values smaller than 5%. In practice this loss could be much smaller (it could even be a gain), since employing a fixed time slot length considerably reduces the amount of signaling that the nodes have to transmit to the CCo, as mentioned in Section 8.4.

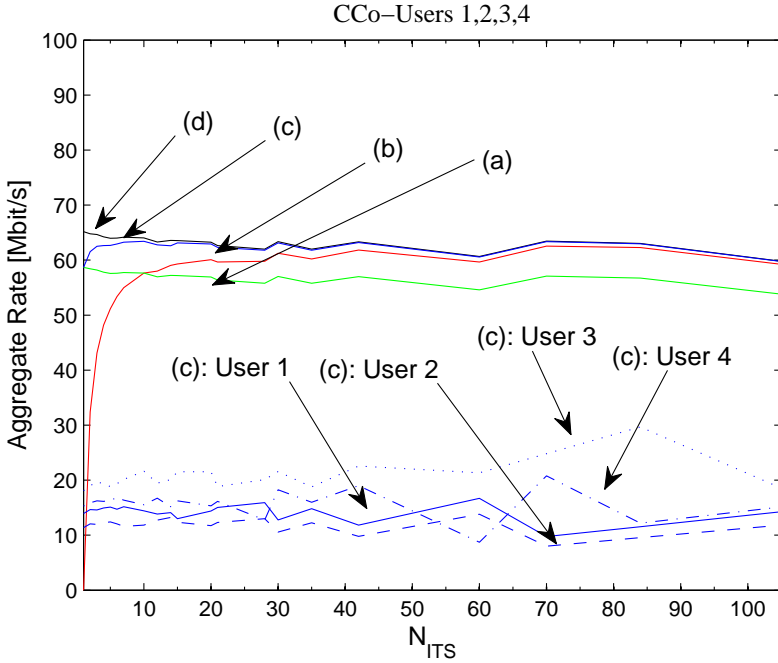


Figure 8.6: **Four users scenario:** Aggregate rates for the 4 scheduling Procedures and single user rates for the *Procedure C*. Labels (a)-(d) denote *Procedures A-D* respectively.

## 8.7 Main Findings

We have studied the resource allocation problem in an indoor PLC system with a physical layer based on OFDM and a medium access control scheme with an adaptive TDMA region. The presented results have been obtained by taking into account both the cyclostationary noise and the cyclic behavior of the channel response. The optimum time slot duration has been determined in a multi-user scenario for three practical scheduling procedures with different amount of PHY layer OH. It has been shown that although the optimum time slot length is strongly dependent on the speed of the channel time vari-

Table 8.1: Optimal time slot duration in number of OFDM symbols obtained in the 2-user scenario using *Procedures B* and *C*.

<b>2-User Scenario</b>						
Users	1-2	1-3	1-4	2-3	2-4	3-4
<i>Proc. B</i>	42	140	140	60	140	21
<i>Proc. C</i>	12	14	140	7	10	5

Table 8.2: Optimal time slot duration in number of OFDM symbols obtained in the 3 and 4 users scenarios using *Procedures B* and *C*.

	<b>3-User Scenario</b>				<b>4-User Scenario</b>
Users	1-2-3	1-2-4	2-3-4	1-3-4	1-2-3-4
<i>Proc. B</i>	105	84	35	140	70
<i>Proc. C</i>	14	14	35	140	10

ations, reasonable trade-off values can be selected. The use of these trade-off values avoids the need for computing the optimum time slot in each particular situation, which considerably reduces the amount of feedback information.

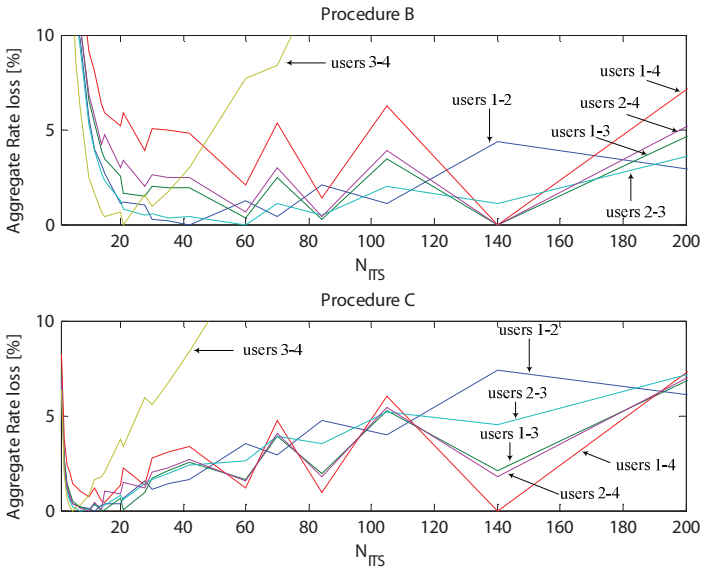


Figure 8.7: Aggregate bit-rate loss for the two-user scenario with *Procedures B* and *C*

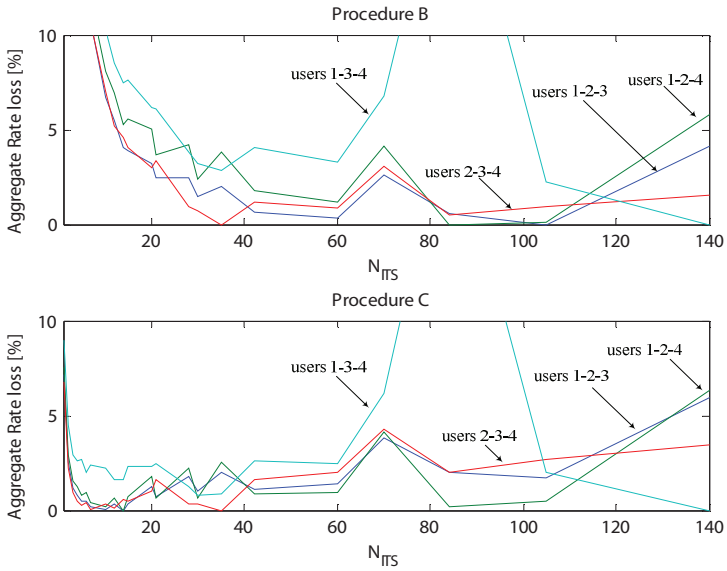


Figure 8.8: Aggregate bit-rate loss for the three-user scenario with *Procedures B* and *C*

## Opportunistic Relaying over PLC Networks

In this chapter, we investigate the use half duplex time division relay protocols to provide capacity improvements, power savings, and coverage extension in home power line communication (PLC) networks. We consider a network where the communication between the source and the destination node follows an opportunistic protocol, namely, the relay is used whenever it allows w.r.t. the direct transmission (DT): a) for capacity improvements, under a power spectral density (PSD) mask constraint; or b) for power saving, under a PSD mask and a rate target constraint. Opportunistic decode and forward (ODF), and opportunistic amplify and forward (OAF) are considered. At the physical layer, we assume the use of multi-carrier modulation.

Under these assumptions, we find the optimal resource allocation, namely, the optimal power and time slot allocation, between the source and the relay nodes that maximizes capacity, or minimizes the total transmitted power for both ODF and OAF. Furthermore, since over in-home PLC networks, the relay can only be placed in accessible points of the network, i.e., in the main panel, or in derivation boxes, or in outlets, for each opportunistic protocol, we also determine the best relay position that maximizes capacity or minimizes the transmitted power.

## 9.1 Introduction

Power saving is playing an important role in future developments of communication devices. Some standards have been developed to cope with this problem, e.g., the IEEE 802.3az and the HomePlug GP (HPGP) [68] that are respectively specified for Ethernet and power line communications (PLCs). Not only power saving, but also high transmission rate has to be granted, as for instance in multimedia applications such as high definition television (HDTV) or 3D virtual video games. It becomes therefore essential to consider advanced communication techniques such as multi-carrier modulation with bit and power loading algorithms, cooperative communication algorithms and cross-layer optimization.

In this chapter, we consider the use of cooperative half duplex time division relay protocols to provide power savings, capacity improvements, and coverage extension in home PLC networks. It is worth noting that the use of relay techniques has been largely treated in the literature that concerns wireless communication systems but only few works have considered the use of relay techniques for PLC. Among them, the first was the work carried out by Lampe and al. in [76].

In the following, we assume that the signal transmitted by the network nodes has to satisfy a PSD mask as it is typically required by state-of-the-art communication standards, e.g., the wireless IEEE 802.11 [8], the power line HomePlug AV [18] or GP [68], the twisted pair xDSLs. In particular, we consider a network where the communication between the source and the destination nodes follows an opportunistic protocol, namely, the relay is used whenever it allows (w.r.t. the DT): a) for capacity improvements under a PSD mask constraint, or b) for power saving under a PSD mask and a rate target constraint. ODF, and OAF are considered. At the physical (PHY) layer we assume the use of multi-carrier modulation, i.e., OFDM.

Under these assumptions, we find the optimal resource allocation, namely, the optimal power and time slot allocation, between the source and the relay nodes that maximizes capacity, or minimizes the total transmitted power for

both ODF and OAF.

The problem of resource allocation in relay networks has been thoroughly treated in the literature. Herein, we mention several papers that have been used as the starting point of our work.

The optimal power and time slot allocation for capacity maximization over Rayleigh fading wireless relay channels has been considered in [77–79].

The power allocation for capacity maximization of OFDM based relay schemes under a total power constraint has been treated in [80–84]. In [80], the authors found a sub-optimal power allocation for the capacity maximization of half duplex amplify and forward (AF) OFDM relay systems under a node total power constraint. The approach alternatively finds the power allocation in one network node (the source or the relay) assuming a given power allocation at the other node. The procedure is implemented in an iterative manner up to convergence. The optimal solution to the previous problem has been found in [81].

In [82], the authors found the power allocation that maximizes the capacity of half duplex AF and decode and forward (DF) OFDM relay schemes under a joint (source-relay) sub-channel total power constraint. Both previous papers assume that the destination node is not directly reachable from the source.

In [83], the full-duplex [77] DF OFDM relay scheme is considered. The approach followed in [82] and [83] to find the optimal power allocation is to pair the OFDM sub-channels between the source and the relay to find an equivalent channel gain and thus obtain the optimal power allocation solving the Karush-Kuhn-Tucker (KKT) conditions [67].

In [84], the authors propose to hybridly use AF, DF, and direct link transmission to maximize the half duplex OFDM relay system capacity.

The main new contributions of our work w.r.t. the ones presented in the literature can be summarized as follows.

- All the results are obtained considering, for each network node, a sub-channel power constraint given by a PSD mask rather than a total power constraint.

- For the capacity maximization problem of ODF, we find the optimal power and time slot allocation. To be more precise, we show that whatever the time slot duration is, the power allocation which maximizes the DF capacity is equal to the one that satisfies the PSD mask. Consequently, we show that the optimal time slot duration is found by the intersection of two linear functions.
- For the power minimization problem of ODF, we show that the joint problem of power and time slot allocation of DF is very hard to be solved and thus implemented. Therefore, to reduce complexity, we propose a simplified algorithm that considers two convex sub-problems. Through numerical results, we show that its performances are very close to the optimal ones.
- For the capacity maximization problem of OAF, we show that the optimal power allocation that maximizes the AF capacity is equal to the one that satisfies the PSD mask.
- We consider the specific and peculiar application of the algorithms to the home PLC scenario. Differently from the wireless case, where the relay can be placed wherever between the source and the destination nodes, over in-home PLC networks, the relay can only be placed in accessible points of the network, i.e., in the main panel, or in derivation boxes, or in outlets. To test the proposed algorithms, we deploy a statistically representative PLC channel generator that uses a home power line topology model together with transmission line theory. For both OAF and ODF, and according to each goal, i.e., capacity maximization or power minimization, we also determine the best position of the relay.

The remainder of the chapter is as follows. In Section 9.2, we present the system model. Then, in Sections 9.3 and 9.4, we respectively consider the resource allocation problem of ODF and OAF. In Section 9.5, we describe the in-home power line application scenario which will be used in Section 9.6 to obtain numerical results. Finally, the main findings follow in Section 9.7.

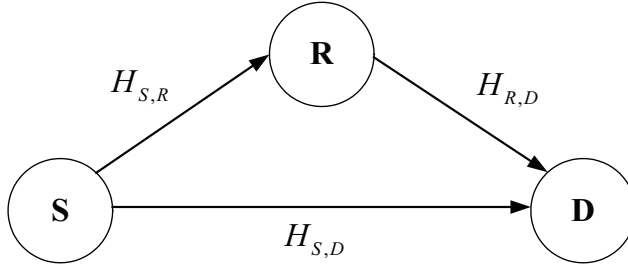


Figure 9.1: Cooperative relay system model.

## 9.2 System Model

We consider a network composed by a source (S), a relay (R) and a destination (D) node as shown in Fig. 9.1. The communication between the source and the destination nodes follows an opportunistic cooperative protocol, namely, the relay is used whenever it allows, according to the goal, for capacity improvements or for power saving w.r.t. the direct transmission. The multiplexing between the source and the relay nodes is accomplished via time division multiple access (TDMA). The time is divided in frames of duration  $T_f$ , and each frame is divided into two time slots whose durations are  $t$  and  $T_f - t$ . When the relay is used, the source transmits its data to the relay and destination nodes during the first slot, whereas, during the second slot, the relay transmits the received data to the destination according to the adopted opportunistic cooperative protocol, i.e., ODF or OAF. When ODF is used, the relay decodes, re-encodes and forwards the received data. Whereas, in OAF, the relay only amplifies and forwards the data. At the physical layer, we assume a multi-carrier scheme with  $M$  sub-channels. The channel frequency response between each pair of nodes is denoted as  $H_{x,y}^{(k)}$ , where the subscripts  $x$  and  $y$  denote the pairs  $\{S,R\}$ ,  $\{S,D\}$  or  $\{R,D\}$ , and  $k$  is the sub-channel index, i.e.,  $k \in \mathbb{K}_{\text{on}}$ , where  $\mathbb{K}_{\text{on}} \subseteq \{0, \dots, M-1\}$  is the sub-set of the used (switched on) sub-channels. Throughout this chapter, we assume the application of a PSD mask constraint for the signal transmitted by the network nodes. As explained in the introduction, this is a practical assumption for both wireless

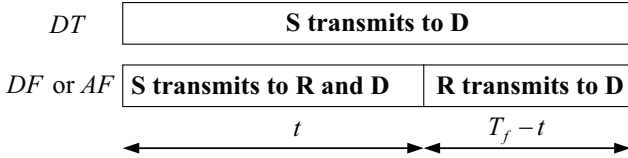


Figure 9.2: DT, DF and AF modes and corresponding time slots allocation.

and wireline communication systems.

### 9.3 Opportunistic Decode and Forward

In ODF [78], the source node sends data to the destination node according to two modes, DT or DF. In DT, S transmits to D occupying all the time frame  $T_f$ . In DF mode, S transmits its data to both R and D during the time slot  $t$ , then in the second slot of duration  $T_f - t$ , R decodes and forwards the same data to D using an independent codebook while the source is silent [77]. Finally, D decodes the message combining the data received in both time slots from both the source and the relay. Fig. 9.2 shows the DT and DF modes, and the corresponding time slots allocation. Recalling that at the physical layer we assume multi-carrier transmission with  $M$  sub-channels, and assuming a frame of normalized duration  $T_f = 1$ , we can compute the capacity of ODF as [78]

$$C_{ODF}(t) = \max \{C_{DT}, C_{DF}(t)\}, \quad (9.1)$$

where  $C_{DT}$  and  $C_{DF}(t)$  respectively denote the capacity of DT and DF modes. They are given by

$$C_{DT} = C_{S,D} \quad (9.2)$$

$$C_{DF}(t) = \min \left\{ \underbrace{tC_{S,R}}_{f_1(t, \mathbf{P}_{S,DF})}, \underbrace{tC_{S,D} + (1-t)C_{R,D}}_{f_2(t, \mathbf{P}_{S,DF}, \mathbf{P}_{R,DF})} \right\}. \quad (9.3)$$

In (9.2) and (9.3),  $C_{S,D}$ ,  $C_{S,R}$  and  $C_{R,D}$  denote the capacity of the links S-D, S-R and R-D, respectively. Assuming Gaussian inputs, a sufficiently large

number of sub-channels and additive Gaussian noise, they are given by [60]

$$C_{x,y} = \frac{1}{MT} \sum_{k \in \mathbb{K}_{\text{on}}} \log_2 \left( 1 + SNR_{x,y}^{(k)} \right),$$

$$\{x, y\} \in \{\{S, D\}; \{S, R\}; \{R, D\}\}, \quad (9.4)$$

where

$$SNR_{x,y}^{(k)} = P_{x,mode}^{(k)} \frac{|H_{x,y}^{(k)}|^2}{P_{w,y}^{(k)}} = P_{x,mode}^{(k)} \eta_{x,y}^{(k)}, \quad (9.5)$$

is the signal to noise ratio (SNR) in sub-channel  $k$  for the link  $x$ - $y$ ,  $T$  is the sampling period, whereas  $P_{x,mode}^{(k)}$  and  $P_{w,y}^{(k)}$  denote the power transmitted by node  $x$  for a given *mode* (DF or DT) and the noise power in sub-channel  $k$  at node  $y$ .  $\eta_{x,y}^{(k)}$  denotes the normalized SNR for the link  $x$ - $y$  in sub-channel  $k$ . Furthermore, in (9.3),  $\mathbf{P}_{S,DF}$  and  $\mathbf{P}_{R,DF}$  denote the vectors (of  $|\mathbb{K}_{\text{on}}|$  elements) of the sub-channel powers at the source and at the relay node respectively. As it will be clear in the following, it is convenient to express the arguments of the minimization in (9.3) through the functions  $f_1$  and  $f_2$ .

To simplify the notation, in (9.4), we do not explicitly show the dependance of the capacity from the transmitted power distribution, which will be done if needed in the following.

From (9.1)-(9.3), it is interesting to note that the direct link is used whenever the capacity  $C_{S,D}$  is greater than  $C_{S,R}$  or  $C_{R,D}$ . This is true for any  $t$ . In the remaining cases, to see whether the communication follows the DT or the DF mode, we need to compute  $C_{DT}$ ,  $C_{DF}(t)$  and compare them as in (9.1) to determine the largest.

In the following Sections 9.3.1 and 9.3.2, we will respectively deal with the power allocation for capacity improvements and power saving of ODF.

### 9.3.1 Capacity Improvements with ODF

From (9.1), we note that the capacity of ODF is a function of both the transmitted power distribution and the time slot allocation. In order to maximize it, when the DT is used, we only need to optimally allocate the power among

the sub-channels of the source node. Contrarily, when the DF mode is used, we need to optimally allocate the power and the time slot of the source and relay.

Assuming that the network nodes have to satisfy a PSD mask constraint, it is known that the sub-channel power allocation that maximizes the capacity for a point-to-point communication corresponds to the one given by the PSD constraint itself [34]. Therefore, for both modes of ODF, we set  $P_{x,mode}^{(k)} = \bar{P}$ , with  $x \in \{S, R\}$ , and  $k \in \mathbb{K}_{\text{on}}$ . Now, to maximize the ODF capacity (9.1), we only need to compute the optimal time slot duration that can be found maximizing (9.3), i.e.,

$$t_{mc}^* = \operatorname{argmax}_{t \in [0,1]} \{C_{DF}(t)\}, \quad (9.6)$$

where we have used the sub-scripts  $mc$  to indicate that  $t_{mc}^*$  is the time slot duration that maximizes the capacity. To solve (9.6), we observe that once the power transmitted by the source and the destination nodes is set, the arguments of the minimization in (9.3) are linear functions of  $t$ . Therefore, the optimal time slot duration is given by the intersection  $f_1(t_{mc}^*, \mathbf{P}_{S,DF}) = f_2(t_{mc}^*, \mathbf{P}_{S,DF}, \mathbf{P}_{R,DF})$ , with  $P_{S,DF}^{(k)} = P_{R,DF}^{(k)} = \bar{P} \forall k \in \mathbb{K}_{\text{on}}$ .

### 9.3.2 Power Saving with ODF

In this section, we propose the use of ODF for power saving and coverage extension. The idea behind is the following. As discussed in the previous sub-section, in ODF the relay is used when the DF capacity is higher than that of DT. Now, let us suppose that the relay is used and we want to achieve a given target rate under a PSD constraint. Then, we can have three cases. The first is when the target rate is reachable either using DT or DF. In such a case, since the DF capacity is higher than that of DT, the amount of power saved lowering the rate of DF to the value of the target rate will be higher than that saved lowering the rate of DT to the target value. The second case is when only the DT capacity is lower than the target rate. In this case, the use of the relay can increase the network coverage. The third case is when the

capacity of both modes is lower than the target rate so that the use of the relay increases the achieved rate possibly toward the target.

To compute the power necessary for ODF when the communication is subject to a target rate  $R$  constraint and to a PSD constraint, we can solve the dual problem of (9.1), i.e.,

$$P_{ODF} = \min \{P_{DT}, P_{DF}\}, \quad (9.7)$$

where  $P_{DT}$  and  $P_{DF}$  respectively denote the minimum power required by the DT and DF modes to achieve a rate  $R$  under a PSD constraint. Therefore,  $P_{DT}$  is the solution to the problem

$$\begin{aligned} P_{DT} &= \min \sum_{k \in \mathbb{K}_{\text{on}}} P_{S,DT}^{(k)} \\ \text{s.t. } C_{S,D} &= R, \\ 0 &\leq P_{S,DT}^{(k)} \leq \bar{P} \quad \forall \quad k \in \mathbb{K}_{\text{on}}, \end{aligned} \quad (9.8)$$

while  $P_{DF}$  is the solution to the problem

$$\begin{aligned} P_{DF} &= \min \sum_{k \in \mathbb{K}_{\text{on}}} tP_{S,DF}^{(k)} + (1-t)P_{R,DF}^{(k)} \\ \text{s.t. } C_{DF}(t) &= \min \{tC_{S,R}, \quad tC_{S,D} + (1-t)C_{R,D}\} = R, \\ 0 &\leq t \leq 1, \\ 0 &\leq P_{S,DF}^{(k)} \leq \bar{P}, \\ 0 &\leq P_{R,DF}^{(k)} \leq \bar{P}, \quad \forall \quad k \in \mathbb{K}_{\text{on}}. \end{aligned} \quad (9.9)$$

Starting from (9.8), we note that its objective and its inequality constraint functions are convex, but its equality constraint is not an affine function. Therefore, (9.8) is not a convex optimization problem (see Appendix 11.5 for the definition of convex optimization problems). Nevertheless, we note that the equivalent problem, obtained considering the change of variables  $P_{S,DT}^{(k)} = (2^{b_{S,DT}^{(k)}} - 1)/\eta_{S,D}^{(k)}$ , where  $b_{S,DT}^{(k)} = \log_2 \left(1 + P_{S,DT}^{(k)}/\eta_{S,D}^{(k)}\right)$ , is a convex

optimization problem. Hence, we can find the solution to (9.8) (assuming that it exists<sup>1</sup>) solving the equivalent problem and applying the inverse change of variables. A solution to the equivalent convex problem can be found applying the KKT conditions [67, pp. 243-244]. The corresponding solution to the original problem is given by (see Appendix 11.6)

$$P_{S,DT}^{(k)} = P_{S,DT}^{(k)}(\nu) = \left[ \nu - 1/\eta_{S,D}^{(k)} \right]_0^{\bar{P}}, \quad (9.10)$$

where

$$[x]_a^b = \begin{cases} b, & x \geq b \\ x, & a < x < b \\ a, & x \leq a, \end{cases} \quad (9.11)$$

and  $\nu$  is equal to the solution of the equality constraint of (9.8), i.e.,

$$\sum_{k \in \mathbb{K}_{\text{on}}} \log_2 \left( 1 + P_{S,DT}^{(k)}(\nu) \eta_{S,D}^{(k)} \right) = MRT. \quad (9.12)$$

Now, turning our attention to problem (9.9), we note that it is more difficult to solve than problem (9.8) inasmuch its objective function is not in general convex. This can be proved observing that the Hessian associated to its objective function, for a given  $k$ , is neither semidefinite positive nor semidefinite negative, consequently, the Sylvester's criterion [85] does not give any information regarding convexity.

In the following, in Section 9.3.2, we discuss the optimal solution to problem (9.9). Then, in Section 9.3.2, we propose a feasible algorithm that gives a sub-optimal solution.

## Optimal DF Power Allocation

To find the optimal solution to (9.9), we observe that for a given value of  $t$ , problem (9.9) can be split into two sub-problems. The first sub-problem is

---

<sup>1</sup>Note that in some cases it is possible that the target rate is not reachable under a PSD constraint and thus the power minimization problem does not admit a solution.

obtained when  $C_{DF}(t) = tC_{S,R}$  and it reads

$$\begin{aligned}
 P_{DF1}(t) &= \min \sum_{k \in \mathbb{K}_{\text{on}}} tP_{S,DF1}^{(k)} + (1-t)P_{R,DF1}^{(k)} \\
 \text{s.t. } \quad &tC_{S,R} = R, \\
 &tC_{S,D} + (1-t)C_{R,D} \geq R, \\
 &0 \leq P_{S,DF1}^{(k)} \leq \bar{P}, \\
 &0 \leq P_{R,DF1}^{(k)} \leq \bar{P}, \quad \forall k \in \mathbb{K}_{\text{on}}.
 \end{aligned} \tag{9.13}$$

In (9.13), we have used the subscript 1 to indicate the first sub-problem.

The second sub-problem is obtained when  $C_{DF}(t) = tC_{S,D} + (1-t)C_{R,D}$  and it reads

$$\begin{aligned}
 P_{DF2}(t) &= \min \sum_{k \in \mathbb{K}_{\text{on}}} tP_{S,DF2}^{(k)} + (1-t)P_{R,DF2}^{(k)} \\
 \text{s.t. } \quad &tC_{S,D} + (1-t)C_{R,D} = R, \\
 &tC_{S,R} \geq R, \\
 &0 \leq P_{S,DF2}^{(k)} \leq \bar{P}, \\
 &0 \leq P_{R,DF2}^{(k)} \leq \bar{P}, \quad \forall k \in \mathbb{K}_{\text{on}}.
 \end{aligned} \tag{9.14}$$

The optimal solution to problems (9.13) and (9.14) would require an exhaustive search that is computationally unfeasible. Nevertheless, it is possible to find a solution to problems (9.13) and (9.14) imposing the KKT conditions. In Section 11.7 we show that the solution to the KKT conditions requires an iterative procedure. Consequently, its complexity is not less than that of conventional methods used for solving inequality constrained minimization problems, e.g., the interior-point method [67, chapter 11]. Therefore, for the numerical results, we use the interior-point method. It should be noted that interior-point methods are in general complex, especially when the dimension of the problem is large.

Now, to compute the DF power allocation, for each value of  $t$ , we can compute  $P_{DF}(t) = \min \{P_{DF1}(t), P_{DF2}(t)\}$ . Therefore, the optimal slot duration

for minimum power can be found as

$$t_{mp}^* = \min_{t \in [0,1]} P_{DF}(t), \quad (9.15)$$

and the minimum power required by DF to reach the rate  $R$  is the one corresponding to  $P_{DF}^* = P_{DF}(t_{mp}^*)$ . Finally, we recall that to compute the power required by ODF to reach the rate  $R$  under the PSD mask constraint, we can replace  $P_{DF}^*$  and (9.10) in (9.7).

### Simplified Algorithm for DF Power Allocation

To reduce complexity, we propose a simplified solution based on the following algorithm. We assume the optimal time slot duration  $t_{mp}^*$  equal to the one computed in (9.6), i.e.,  $t_{mp}^* = t_{mc}^*$ , where we have considered the capacity maximization under a PSD constraint. Furthermore, we impose that for  $t_{mp}^*$  the arguments of the minimization in the second line of (9.9) are equal to  $R$ . Under these assumptions, (9.9) can be divided into two sub-problems where the first allows us to compute the power distribution of the source node independently from the power distribution of the relay node. Once we know the power distribution of the source, we can compute the power distribution of the relay solving the second sub-problem. Fig. 9.3 illustrates the proposed algorithm. Practically, we first find the source power distribution that allows the linear function of  $t$ ,  $f_1(t, \mathbf{P}_{S,DF})$ , to pass through the origin of the axes and the point  $p$  specified by the pair  $\{t_{mp}^*, R\}$ . Then, maintaining this power distribution at the source node, we compute the power distribution at the relay node that allows the function  $f_2(t, \mathbf{P}_{S,DF}, \mathbf{P}_{R,DF})$  to pass through the points  $p$  and the one specified by the pair  $\{1, C_{S,D}\}$ . In particular, the power distribution at the source can be computed solving the following sub-problem of (9.9)

$$\begin{aligned} P_{S,DF} &= \min \sum_{k \in \mathbb{K}_{on}} P_{S,DF}^{(k)} \\ \text{s.t. } t_{mp}^* C_{S,R} &= R, \end{aligned} \quad (9.16)$$

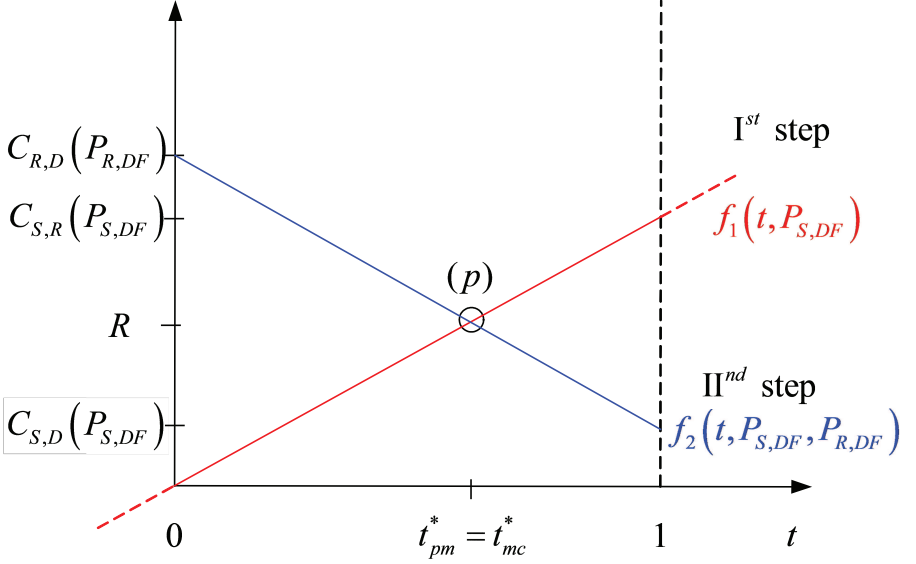


Figure 9.3: Illustration of the proposed power allocation algorithm to minimize the power required by DF to reach a target rate  $R$ .

$$0 \leq P_{S,DF}^{(k)} \leq \bar{P} \quad \forall \quad k \in \mathbb{K}_{\text{on}}.$$

Problem (9.16) can be solved similarly to<sup>1</sup> (9.8). The solution is

$$P_{S,DF}^{(k)} = P_{S,DF}^{(k)}(\nu) = \left[ \nu - 1/\eta_{S,R}^{(k)} \right]_0^{\bar{P}}, \quad (9.17)$$

where  $\nu$  is given by the solution of the second line of (9.16), i.e.,

$$\sum_{k \in \mathbb{K}_{\text{on}}} \log_2 \left( 1 + P_{S,DF}^{(k)}(\nu) \eta_{S,R}^{(k)} \right) = \frac{MRT}{t_{mp}^*}. \quad (9.18)$$

Once the “optimal” power distribution for the source node in DF mode has been computed, it can be used to compute the capacity of the S-D link, namely  $C_{S,D}$  in DF mode. Therefore, we can find the “optimal” power distribution

for the relay node solving the following sub-problem of (9.9)

$$\begin{aligned}
 P_{R,DF} &= \min \sum_{k \in \mathbb{K}_{\text{on}}} P_{R,DF}^{(k)} \\
 \text{s.t. } C_{R,D} &= \hat{R}, \\
 0 &\leq P_{R,DF}^{(k)} \leq \bar{P} \quad \forall k \in \mathbb{K}_{\text{on}}.
 \end{aligned} \tag{9.19}$$

whose solution<sup>1</sup> is

$$P_{R,DF}^{(k)} = P_{R,DF}^{(k)}(\nu) = \left[ \nu - 1/\eta_{R,D}^{(k)} \right]_0^{\bar{P}}, \tag{9.20}$$

with  $\nu$  given by the solution of the second line of (9.19), i.e.,

$$\sum_{k \in \mathbb{K}_{\text{on}}} \log_2 \left( 1 + P_{R,DF}^{(k)}(\nu) \eta_{R,D}^{(k)} \right) = M \hat{R} T, \tag{9.21}$$

where  $\hat{R} = (R - t_{mp}^* C_{S,D}) / (1 - t_{mp}^*)$ , and  $C_{S,D} = 1/(MT) \sum_{k \in \mathbb{K}_{\text{on}}} \log_2(1 + P_{S,DF}^{(k)} \gamma_{S,D}^{(k)})$ .

The power needed by the DF mode to reach the rate  $R$  under the PSD constraint  $\bar{P}$  is

$$P_{DF} = t_{mp}^* P_{S,DF} + (1 - t_{mp}^*) P_{R,DF}. \tag{9.22}$$

Therefore, we solve (9.7) using (9.10) and (9.22). Clearly, there are cases where a solution to the power minimization problem under a target rate and a PSD constraint does not exist for a single or for both modes. In the first case, the algorithm will choose the mode for which the solution exists. Whereas, when the solution does not exist for both modes, the algorithm will choose the mode that achieves the highest rate.

Finally, from (9.10), (9.17), (9.20) we note that the power allocation for the source node in both DT and DF modes, and for the relay node in DF mode follows a typical water-filling shape, where the maximum allowable power in each sub-channel is limited by the power constraint. Therefore, to solve  $\{(9.10),(9.12)\}$ ,  $\{(9.17),(9.18)\}$ , and  $\{(9.20),(9.21)\}$  we can use conventional algorithms for solving power allocation problems when a sub-channel power

constraint is imposed [34].

## 9.4 Opportunistic Amplify and Forward

Like for ODF, in OAF, the relay is used whenever it allows, according to the goal, for capacity improvements or power saving w.r.t. direct transmission. To be more precise, the source node sends data to the destination node according to two modes, DT or AF. In DT, S transmits to D occupying all the time frame  $T_f$ . In AF mode [86, chapter 5], S transmits its data to both R and D during the first half of the frame, then in the second half, R amplifies and forwards the same data to D while the source is silent. Finally, D decodes the message combining the data received in both time slots from both the source and the relay. Fig. 9.2 shows the DT and AF modes, and the corresponding time slot allocation. The capacity of OAF can be then computed as

$$C_{OAF} = \max \{C_{DT}, C_{AF}\}, \quad (9.23)$$

where  $C_{DT}$  is given by (9.2). To compute the capacity of AF, namely  $C_{AF}$ , we make the following assumptions. For all the network nodes, at the physical layer, we assume multi-carrier modulation with  $M$  sub-channels, and the noise at both the relay and destination nodes is considered Gaussian. The frame has normalized duration  $T_f = 1$ . The relay amplifies the signal received in sub-channel  $k$  by the quantity

$$g^{(k)} = \sqrt{\frac{P_{R,AF}^{(k)}}{P_{S,AF}^{(k)} |H_{S,R}^{(k)}|^2 + P_{w,R}^{(k)}}}, \quad (9.24)$$

to assure that the relay transmits the power  $P_{R,AF}^{(k)}$  in sub-channel  $k$  during the second half of the time frame. Finally, we assume the receiver to adopt maximal ratio combining for the data received from the source and the relay. Therefore, assuming Gaussian input signals, the AF capacity can be written

as [80, 82, 86]

$$C_{AF}(\mathbf{P}_{S,AF}, \mathbf{P}_{R,AF}) = \tag{9.25}$$

$$\frac{1}{2MT} \sum_{k \in \mathbb{K}_{on}} \log_2 \left( 1 + P_{S,AF}^{(k)} \eta_{S,D}^{(k)} + \frac{P_{S,AF}^{(k)} \eta_{S,R}^{(k)} P_{R,AF}^{(k)} \eta_{R,D}^{(k)}}{1 + P_{S,AF}^{(k)} \eta_{S,R}^{(k)} + P_{R,AF}^{(k)} \eta_{R,D}^{(k)}} \right).$$

From (9.25), we note that the second and the third arguments of the log function respectively denote the SNR obtained with the direct link, and the one obtained with the relay. Furthermore, the term  $1/2$  accounts for the slot duration.

In Section 9.4.1, we will deal with the power allocation to maximize the OAF capacity. Then, in Section 9.4.2, we will focus on the power saving problem.

### 9.4.1 Capacity Improvements with OAF

Looking at (9.23), we see that the use of OAF can bring capacity improvements w.r.t. the DT. To maximize the capacity of OAF we need to optimally allocate the power for both DT and AF modes.

As explained in Section 9.3.1, assuming that the network nodes have to satisfy a PSD mask constraint, the sub-channel power allocation that maximizes the DT capacity corresponds to the one given by the same PSD constraint, namely, the DT capacity is maximized when  $P_{S,DT}^{(k)} = \bar{P}$ ,  $\forall k \in \mathbb{K}_{on}$ .

To maximize the AF capacity we need to solve the following optimization problem

$$\begin{aligned} & \min \{ -C_{AF}(\mathbf{P}_{S,AF}, \mathbf{P}_{R,AF}) \} \\ & \text{s.t. } 0 \leq P_{S,AF}^{(k)} \leq \bar{P}, \\ & \quad 0 \leq P_{R,AF}^{(k)} \leq \bar{P}, \quad \forall k \in \mathbb{K}_{on}. \end{aligned} \tag{9.26}$$

Looking at problem (9.26), we notice that the Hessian associated to the objective function is not symmetric. Therefore, we can not use the Sylvester's criterion [85], or check the sign of the eigenvalues to see whether the objective

function is convex.

To compute the solution of (9.26) we notice that the objective function is sum of monotonic increasing functions of both the power at the source node and the power at the relay node, further, since we have a constraint on the PSD, we can assert that the optimal power allocation is equal to that given by the same PSD.

Another way to compute the optimal solution of (9.26) is to exploit the notion of invex functions<sup>2</sup> [87]. This is because in 1985, Martin [88] proved the following proposition.

**Proposition 1.** *Besides convex functions, a broader class of functions in which KKT conditions guarantee global optimality are the so called invex functions. So if equality constraints are affine functions, inequality constraints and the objective function are continuously differentiable invex functions then KKT conditions are sufficient for global optimality.*

Therefore, if we show that the objective and the inequality constraint functions of (9.26) are invex, we can find the optimal power distribution just solving the KKT conditions. The definition of an invex function follows. Let us consider a general minimization problem with inequality constraint

$$\min_{x \in \mathbb{S}} f(x), \quad \text{s.t.} \quad g(x) \leq 0, \quad (9.27)$$

where  $x \in \mathbb{R}^n$ ,  $f \in \mathbb{R}$ ,  $g \in \mathbb{R}^m$ ,  $f$  and  $g$  are differentiable on a open set containing the feasible set  $\mathbb{S}$ .

With respect to problem (9.27),  $f(x)$  and  $g(x)$  are Invex at  $u \in \mathbb{S}$  w.r.t. a common function  $\gamma(x, u) \in \mathbb{R}^n$ , if  $\forall x \in \mathbb{S}$

$$f(x) - f(u) \geq \gamma(x, u)^T \nabla f(u), \quad (9.28)$$

$$g_i(x) - g_i(u) \geq \gamma(x, u)^T \nabla g_i(u), \quad i = 1, \dots, m. \quad (9.29)$$

In (9.28),  $\nabla$  denotes the gradient operator. A slight generalization of the

---

<sup>2</sup>Note that the proposed procedure can be applied to the more general case of a constraint on the total transmitted power.

previous definition is Type I Invexity, which, with reference to problem (9.27), is defined as

$$f(x) - f(u) \geq \gamma(x, u)^T \nabla f(u), \quad (9.30)$$

$$-g_i(u) \geq \gamma(x, u)^T \nabla g_i(u), \quad i = 1, \dots, m. \quad (9.31)$$

It is interesting to note that if a function is Type I invex then it is also invex. Now, let us consider the following theorem that is given in [89].

**Theorem 1.** *Suppose that problem (9.27) has a minimal solution at  $u \in \mathbb{S}$ . Suppose also that there is a point  $x \in \mathbb{S}$  such that  $g_i(x) < 0$  for some  $i \in \mathbb{I} = \{i : g_i(u) = 0\}$ . If the Kuhn-Tucker conditions apply at  $u$  and all the Kuhn-Tucker multipliers  $y \in \mathbb{R}^m$  are bounded, then the active constraint functions and the objective function are Type I invex w.r.t. a common nontrivial  $\gamma$  at  $u$ .*

The previous theorem allows us to affirm that if the KKT conditions applied to problem (9.26) give a solution for which the constraints are satisfied and the multipliers are bounded, then the objective function of (9.26) is Type I invex. Note that the inequality constraints in (9.26) are affine functions and thus they are also Type I invex.

In Appendix 11.8, we prove that applying the KKT conditions to problem (9.26), we obtain a solution that satisfies the hypothesis of Theorem 1, and thus the objective function of (9.26) is Type 1 invex. More in detail, we have found that the sub-channel power allocation solution of the KKT conditions for problem (9.26) corresponds to the one given by the PSD constraint for both the source and the relay node, i.e.,  $P_{x,AF}^{(k)} = \bar{P}$ , with  $x \in \{S, R\}$ , and  $k \in \mathbb{K}_{\text{on}}$ . Now, exploiting Proposition 1, we can state that this solution corresponds to the optimal sub-channel power allocation that maximizes the AF capacity under a PSD mask constraint. Therefore, to compute the OAF capacity when the system is subject to a PSD constraint, we can simply compute the DT and the AF capacities obtained setting the powers to  $\bar{P}$ , and then we can choose the mode that gives the highest capacity (9.23).

### 9.4.2 Power Saving with OAF

In Section 9.3.2, we have explained why the use of ODF can potentially bring to power saving w.r.t. the DT. For the same reasons therein listed, also OAF can bring to power saving w.r.t. the DT.

To compute the power used by OAF when the communication is subjected to a target rate  $R$  constraint and to a PSD constraint, we can solve the problem

$$P_{OAF} = \min \{P_{DT}, P_{AF}\}, \quad (9.32)$$

where  $P_{DT}$  and  $P_{AF}$  respectively denote the minimum power required by the DT and the AF modes to achieve a rate  $R$  under a PSD constraint. The optimal power allocation for DT can be found as in (9.8), whereas  $P_{AF}$  is the solution<sup>1</sup> to the problem

$$\begin{aligned} P_{AF} &= \min \frac{1}{2} \sum_{k \in \mathbb{K}_{\text{on}}} \left( P_{S,AF}^{(k)} + P_{R,AF}^{(k)} \right) \\ \text{s.t. } C_{AF} &= R, \\ 0 &\leq P_{S,AF}^{(k)} \leq \bar{P}, \\ 0 &\leq P_{R,AF}^{(k)} \leq \bar{P}, \quad \forall k \in \mathbb{K}_{\text{on}}. \end{aligned} \quad (9.33)$$

Problem (9.33) is not convex because the equality constraint is not an affine function of the transmitted powers. We further report that we have not found a way to reduce the equality constraint to an affine function. Therefore, when showing numerical results, we solve (9.33) using the interior-point method [67, chapter 11].

## 9.5 In-Home Power Line Application Scenario

As discussed in the introduction, we consider the in-home power line scenario to test the proposed resource allocation algorithms.

In the following, in Section 9.5.1, we describe the in-home network topology model here adopted. Then, in Section 9.5.2, we present the statistical chan-

nel generator that we use to obtain the network realizations and the channel frequency responses.

### 9.5.1 Topology Model

In this section, we briefly describe the typical home power line infrastructure. It is characterized by a wiring topology composed of two layers. As it is shown in Fig. 9.4, the outlets are placed at the bottom layer and are grouped and fed by the same “super node”, which is referred to as derivation box. All the outlets fed by the same derivation box are nearby placed. Therefore, the location plan is divided into elements denoted as “clusters” that contain a derivation box with the associated outlets. Each cluster represents a room or a small number of nearby rooms. Different clusters are usually interconnected through their derivation boxes with dedicated cables. This set of interconnections forms the second layer of the topology. We refer to the channels that connect pair of outlets belonging to the same cluster as intracluster channels. Whereas, the channels associated to pairs of outlets that belong to different clusters are referred to as intercluster channels. An intercluster channel example is shown in Fig. 9.4. The main panel (MP) plays a special role inasmuch it connects the home network with the energy supplier network through circuit breakers (CBs). We distinguish two cases. The first case, which we refer to as single-sub-topology network, is when a single circuit breaker (CB) feeds all the derivation boxes of the home network. The second case, which we refer to as multi-sub-topology network, is when many sub-topologies, each comprising a group of derivation boxes, are interconnected through CBs. The latter case can be representative of a multi-floor house, where each floor is a sub-topology. In Fig. 9.4, we report an example of a two-sub-topology network.

In this chapter, we consider the communication between source and destination nodes with the help of a relay. In particular, we consider source-destination channels defined between pair of outlets that do not belong to the same cluster, i.e., intercluster channels. As reported in [90], these channels experience higher attenuations than intracluster channels. Thus, they can have more benefits from the help of a relay. Clearly, these benefits are also depen-

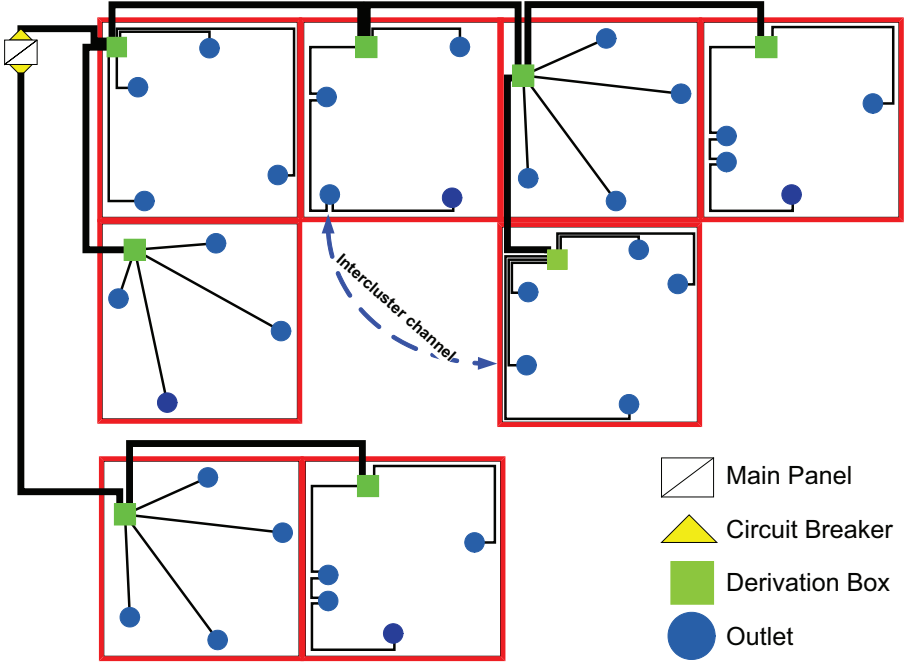


Figure 9.4: Network Architecture with two sub-topologies.

dent on the relay location. To this end, we consider for single-sub-topology networks, the following strategical configurations for the relay.

- *Random derivation box (RDB)*. The relay is located in a randomly selected network derivation box.
- *Backbone derivation box (BDB)*. The relay is located in a randomly selected derivation box that belongs to the backbone between the source and the destination nodes.
- *Source derivation box (SDB)*. The relay is located in the derivation box that feeds the source node. Note that for intercluster channels the path between source and destination includes at least the derivation box that feeds the source and the one that feeds the destination.

- *Destination derivation box (DDB)*. The relay is located in the derivation box that feeds the destination node.
- *Main panel single sub-topology (MPS)*. The relay is located immediately after the CB of the MP.
- *Outlet relay arrangement (ORA)*. The relay is located in randomly selected network outlet.

When considering multi-sub-topology networks, we assume the source and the derivation nodes located into two different sub-topologies. Furthermore, we place the relay between the CBs that feed the sub-topologies, and we model each CB with an attenuation of 5 dB, which is an average value obtained from experimental measurements. We refer to such configuration as *main panel multi-sub-topology (MPM)*.

### 9.5.2 Statistical Channel Generator

According to experimental evidences, a statistically representative channel generator has been developed and described in [90, 91]. It uses a statistical topology model together with the computation of the channel responses through transmission line theory. To be more precise, in [91], a location plan with a given area  $A_f$  contains  $N_c = \lceil A_f/A_c \rceil$  clusters of area  $A_c$ . The outlets are distributed only along the clusters perimeter. The number of outlets belonging to a given cluster is modeled as a Poisson variable with intensity  $\Lambda_o$ . Therefore, the outlets are distributed as the arrivals of a Poisson process along the cluster perimeter. The impact of the loads is also taken into account. In particular, a set of  $N_L$  typical loads for the in-home scenario, such as lamps or computer transformers is considered.

To generate network topologies for the numerical results of the next section, we assume the flat and the cluster areas as uniform distributed random variables, with  $A_f \in \mathcal{U}(100m^2, 300m^2)$ , and  $A_c \in \mathcal{U}(15m^2, 45m^2)$ . We set the probability that no load is connected to a given outlet  $p_v$  to 0.3. The intensity of the Poisson variable  $\Lambda_o$  is set to 0.5 (*outlets/m<sup>2</sup>*), and  $N_L = 10$  loads are

considered. A single and a two-sub-topology arrangement are investigated. Furthermore, unless otherwise stated, we consider 1000 network realizations.

## 9.6 Numerical Results

For the numerical results, we consider a multi-carrier scheme with parameters similar to those employed by the HomePlug AV (HPAV) BPLC system [18]. The system uses  $M=1536$  sub-channels in the frequency band  $0-37.5\text{ MHz}$ , unless otherwise stated. The set  $\mathbb{K}_{\text{on}}$  of switched on sub-channels is defined according to the transmission band  $1-28\text{ MHz}$ . To respect the EMC directive [39], we consider the PSD mask constraint of  $-50\text{ dBm/Hz}$ . Furthermore, we assume that the relay and the destination nodes experience the same level of white Gaussian noise whose PSD is set equal to  $-110\text{ dBm/Hz}$  (worst case) and  $-140\text{ dBm/Hz}$  (best case).

In the following, in Section 9.6.1, we will present numerical results that focus on the capacity improvements that can be led by the use of ODF and OAF. Then, in Section 9.6.2, we will focus on power saving.

### 9.6.1 Capacity Improvements with ODF and OAF

Fig. 9.5-left shows the complementary CDF (CCDF) of the capacity for the DT mode, when no relay is connected to the network, and for the ODF protocol according to the various relay configurations with a single-sub-topology. The time slot  $t$  is optimized according to (9.6), i.e.,  $t = t_{mc}^*$ . The noise PSD is set to  $-110\text{ dBm/Hz}$ . From Fig. 9.5-left, we notice that the relay configuration that maximizes the ODF capacity is the source derivation box (SDB). With probability equal to 0.8, DT and ODF exceed 17 and 48  $Mbit/s$  respectively, allowing for a capacity improvement, w.r.t. DT, equal to 177%. From Fig. 9.5, the relay positions can be ordered from worst to best (at CCDF=0.8) as destination derivation box (DDB), outlet relay arrangement (ORA), random derivation box (RDB), main panel single sub-topology (MPS), backbone derivation box (BDB), and SDB. The same applies for the low noise scenario (Fig. 9.5-right), where we notice that the SDB gain, w.r.t. the DT, equals 40%.

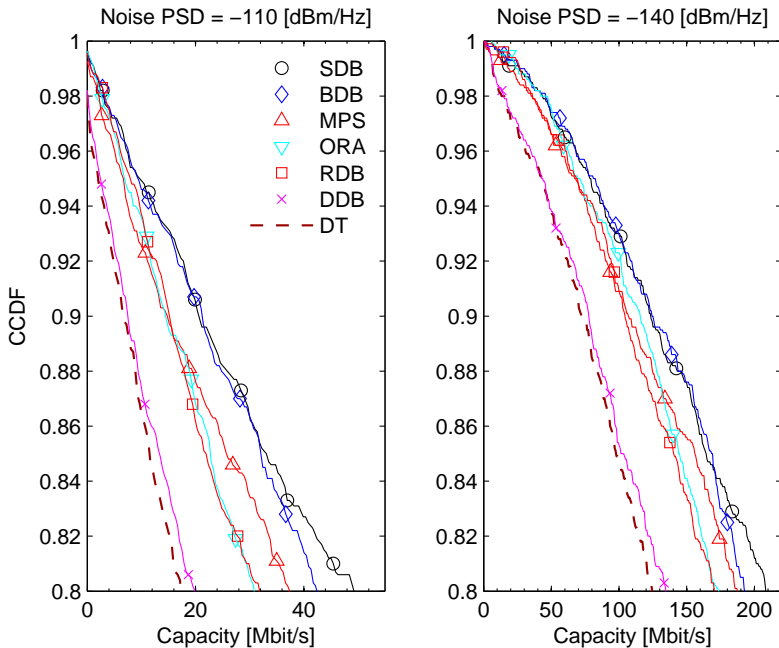


Figure 9.5: CCDFs of capacity obtained using ODF with the relay located according to the various described configurations. The CCDF of capacity obtained assuming DT mode when no relay is connected to the network is also reported.  $M=1536$ .

In Table 9.1, we report the average capacity values obtained using DT and ODF for both noise levels and for all the relay configurations. The percentile usage of the relay is also reported. Note that, as shown in Sections 9.3.1, 9.4.1, the power allocation that maximizes the DT and the DF capacities is given by the PSD limit level. Therefore, all the curves of Fig. 9.5, and all the results of Table 9.1, are obtained on equal transmitted power. Table 9.1 also reports the results for OAF. These will be discussed later. From Table 9.1, we can make the following considerations. The MPS configuration notably gives average capacity values close to that of the SDB configuration. Furthermore, the relay is used in the 100% of the cases when we consider a two-sub-topology network

Table 9.1: Average capacity values using ODF and OAF for the various relay configurations.

Noise PSD= -110 [dBm/Hz]							
Config.	ODF				OAF		
	$C_{S,D}$ [Mbit/s]	$C_{DF}$ [Mbit/s]	$C_{ODF}$ [Mbit/s]	% use of relay	$C_{AF}$ [Mbit/s]	$C_{OAF}$ [Mbit/s]	% use of relay
SDB	101.5	148.2	148.2	99.8	91.7	111.5	58.5
BDB	92.8	132.8	132.8	100	81.1	104.2	50.7
MPS	103.9	140.8	141.2	99.9	86.1	113.2	45.2
ORA	103.4	45.4	114.6	41.9	61.6	105.8	24.5
ADB	95.5	85.1	122.2	69	71.1	103.5	39.3
DDB	100.1	110.1	110.4	99.6	63.8	100.8	8.9
MPM	52.7	99.4	99.4	100	62.9	69.8	71.5
Noise PSD= -140 [dBm/Hz]							
Config.	ODF				OAF		
	$C_{S,D}$ [Mbit/s]	$C_{DF}$ [Mbit/s]	$C_{ODF}$ [Mbit/s]	% use of relay	$C_{AF}$ [Mbit/s]	$C_{OAF}$ [Mbit/s]	% use of relay
SDB	294.6	349.1	349.1	99.9	206.7	297.8	18.5
BDB	276.3	329.9	329.9	100	195.3	285.9	23.2
MPS	295.6	340	341.1	99.9	199.3	301.1	17
ORA	295.5	146.5	315.8	42.5	170.1	298.5	11.9
ADB	280.6	228.5	318.4	70.8	181.2	287.8	18.6
DDB	291.7	303.4	304.2	99.8	166.3	292	1.4
MPM	210.4	276.2	276.2	100	169.4	223.3	34.4

with the main panel multi-sub-topology (MPM) relay configuration. In this scenario, the use of the relay leads to an average capacity gain equal to 88% and 31%, respectively for the high and for the low noise level.

We now turn our attention to the capacity improvements brought by the OAF protocol. Fig. 9.6 shows the CCDFs of the capacity. From Fig. 9.6, we note that in OAF, for both noise levels, there are two relay locations that give similar performance in terms of reliability, namely, minimum capacity value. These are the SDB and the BDB. With probability equal to 0.8 they assure a capacity gain, w.r.t. the DT, equal to 55% and 16% respectively for the high and the low noise levels. This result agrees with what is reported in [92] where it is shown that in low SNR wireless scenarios, the AF protocol does not perform well. This is because the noise is also amplified at the relay. It is

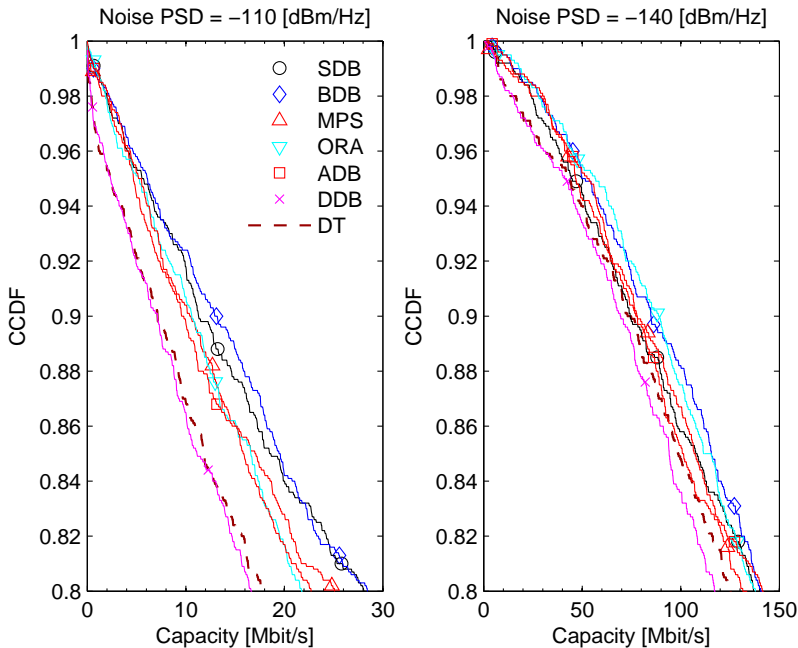


Figure 9.6: CCDFs of capacity obtained using OAF with the relay located according to the various described configurations. The CCDF of capacity obtained assuming DT mode when no relay is connected to the network is also reported.  $M=1536$ .

interesting to note that the SDB and BDB relay configurations are not the ones that give the best performance in terms of average capacity. In fact, looking at Table 9.1, we can see that the relay configuration that yields the highest average capacity for OAF is the MPS. From the previous results we highlight that ODF outperforms OAF. Furthermore, the MPS configuration provides good performance and it is the best suited for a practical relay deployment. This is true for both OAF and ODF.

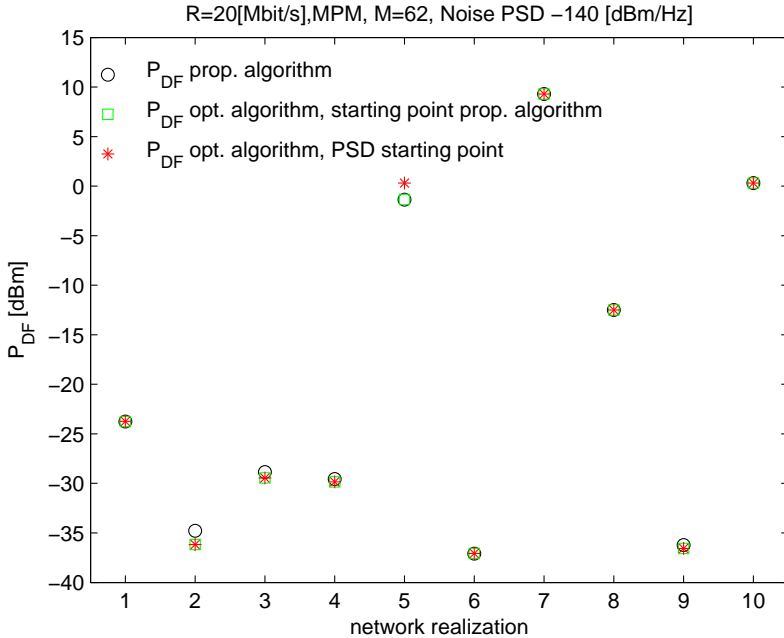


Figure 9.7: Power required by ODF to achieve a target rate  $R$  equal to 20 Mbit/s when using the optimal decode and forward power allocation algorithm and the proposed one. The optimal solution is obtained considering the interior-point algorithms starting from two points, i.e., the power distribution given by the PSD mask and the solution of the proposed algorithm.

### 9.6.2 Power Saving with ODF and OAF

Fig. 9.7 shows the power required by DF to achieve a target rate  $R$  equal to 20 Mbit/s when using the optimal and the simplified decode and forward power allocation algorithm (see Sections 9.3.2, and 9.3.2). Due to the high computational complexity of the optimal solution, we only show the results for ten network realizations, and for  $M=62$  sub-channels. The time slot duration is set equal to  $t_{mc}^*$ . The noise PSD is set to  $-140$  dBm/Hz. The considered relay configuration is the MPM. The optimal solution is obtained considering the interior-point algorithm using as the starting point either the power distri-

bution given by the PSD mask, and the solution of the simplified algorithm. From Fig. 9.7, we note that the proposed DF power allocation algorithm gives results that are almost equal to the optimal ones. Furthermore, we highlight that the cases where the proposed algorithm performs slightly better than the optimal one are due to the numerical precision of the simulation. Therefore, from now on, we only show results for ODF obtained using the proposed DF power allocation algorithm.

In order to assess the performance of the proposed ODF power allocation algorithm (see Section 9.3.2), we set the target rate equal to the capacity of the DT link, i.e.,  $R = C_{DT}$  when  $P_{S,DT}^{(k)} = \bar{P} \forall k \in \mathbb{K}_{\text{on}}$  (see also Fig. 9.5). Fig. 9.8 shows the cumulative distribution function (CDF) of the total transmitted power for DT, and for ODF (9.7) when considering the various relay configurations and both the noise levels. From Fig. 9.8, we can see that, for both noise levels, the best relay position is the SDB. We note that we could have expected this result inasmuch the SDB relay configuration also maximizes the capacity. Furthermore, we also notice that for the high noise level (Fig. 9.8-left), with probability equal to 0.8, the SDB relay configuration allows for saving more than 4 dB, and with the same probability, the BDB and the main panel (MPS) relay configurations allow for saving about 3 dB. Similar results are obtained considering the low noise level (Fig. 9.8-right). In particular, the SDB is the best relay configuration and it leads to a power saving of 3 dB with probability equal to 0.8. Furthermore, the BDB and the MPS allow for saving about 1.5 dB.

In the right sub-plot of Fig. 9.9, we show the results for DT mode, and for the OAF mode. The noise level is set to  $-110$  dBm/Hz. The results obtained using ODF are also reported (Fig. 9.9-left). For fairness of comparison, we set for both schemes  $M = 62$ , and we consider 100 network realizations. From Fig. 9.9, we note that the best relay configurations for power saving with OAF are the SDB and the BDB. Notably, the MPS relay configuration leads to similar power saving. This result agrees with the fact that the previous configurations also lead to the highest capacity values. From Fig. 9.9, we also notice that ODF yields higher power saving than OAF. Finally, it is interesting

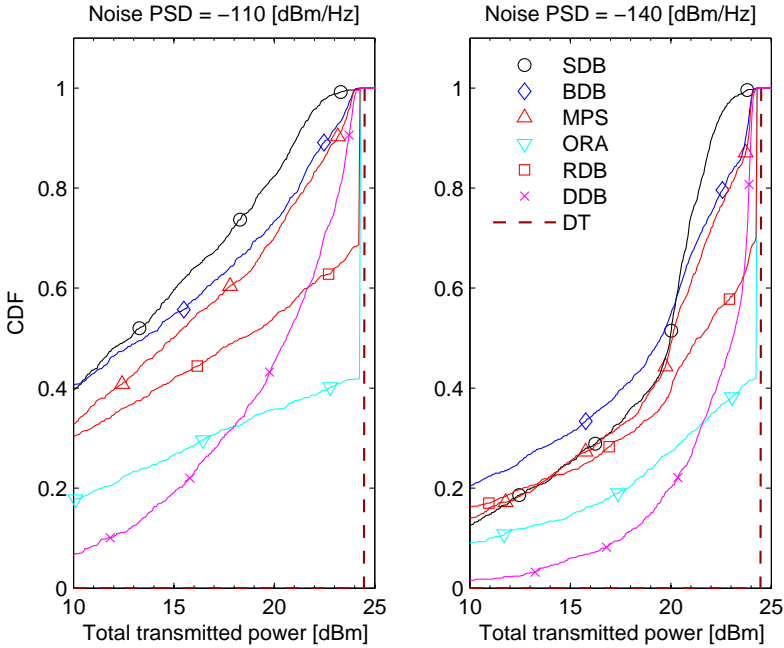


Figure 9.8: CDF of the total transmitted power using ODF, and the direct transmission.  $M=1536$ .

to note that the behaviour of the performance of ODF does not appreciably depend on the number of sub-channels  $M$  (see Figs. 9.8 and 9.9-left).

From the previous results we can say that the main panel is a good and practically deployable relay location with power savings close to the optimal. This is true for both ODF and OAF. We now turn our attention to the network coverage (number of links satisfying the target rate) improvements that can be obtained with the use of a relay. To this end, we consider the MPM relay configuration in a two-sub-topology network. This configuration can be representative of a two-floor house, e.g., networks whose source and destination nodes are associated to outlets that belong to different floors. Since the S-D link experiences high attenuation given by the presence of circuit breakers in

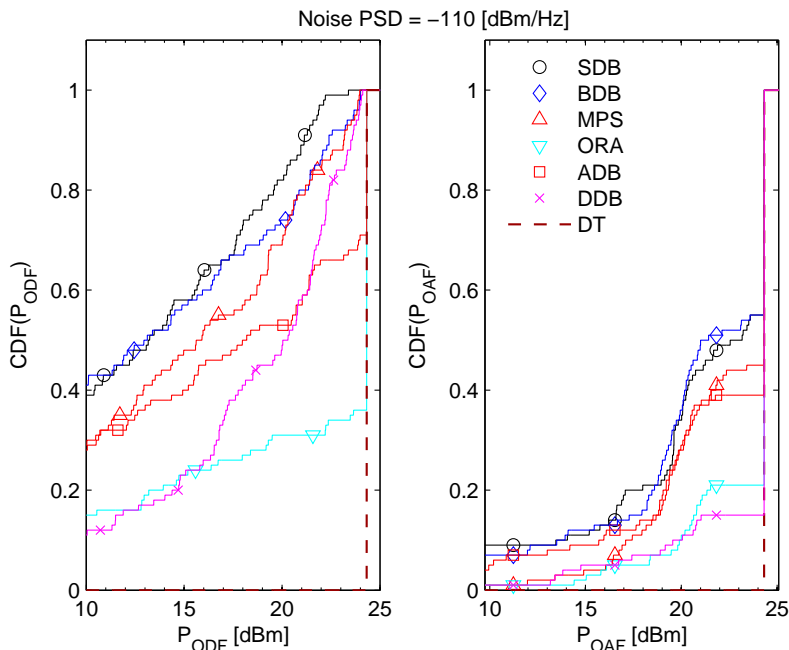


Figure 9.9: CDF of the total transmitted power using (left) ODF and (right) OAF.  $M=62$ .

the main panel, we expect that the use of the relay yields higher coverage extension. To validate our conjecture we consider two scenarios. Firstly, we impose a target rate of  $20 \text{ Mbit/s}$ , e.g., a typical HDTV stream from the living room to the bed room located in an upper floor. Secondly, we increase the target rate to  $50 \text{ Mbit/s}$ , e.g., two HDTV streams plus an Internet connection. In Table 9.2, we report the percentage of links that satisfy the requirements for both scenarios considering DT, and ODF with the MPM relay configuration. We also report the average total transmitted power. We note that with high noise, the use of the relay increases the coverage by 24.8% and 30.4% and it allows for a power saving of 3.7 and 2.7 dB for the first and the second scenario respectively. When the noise level is low, we still have high power

Table 9.2: Percentage of satisfied links and mean transmitted power for two-sub-topology networks using DT and ODF.

Rate Target 20 [Mbit/s]				
	DT		ODF	
Noise PSD [dBm/Hz]	% of satisfied links	$E[P_{DT}]$ [dBm]	% of satisfied links	$E[P_{ODF}]$ [dBm]
-110	57.9	20.8	82.7	17.1
-140	93.1	13.1	99.3	9
Rate Target 50 [Mbit/s]				
-110	38.5	22.6	68.9	19.9
-140	83.7	17	93.6	13

saving using the relay but the gains associated to the coverage extension are reduced below 10%. This is simply explainable observing that for low noise levels the imposed target rates are also achievable using the DT.

Regarding the OAF, we notice that it only allows for a coverage increase of 9% and 5% for the first and the second scenario respectively, and for the high noise level. The corresponding power saving is less than 1 dB. When considering the low noise level, the coverage increase reduces to less than 2% for both the considered scenarios, and the power saving remains less than 1 dB.

## 9.7 Main Findings

We have investigated the use of ODF and OAF relay protocols to provide capacity improvements, power saving, and coverage extension over in home power line communication networks.

We have found the optimal power and time slot allocation that maximizes the ODF capacity with a PSD constraint. Furthermore, considering the power minimization problem of ODF, since it is complex to find the optimal solution, we have proposed a simplified algorithm that is based on the resolution of two convex sub-problems. Through numerical results, we have shown that its

performace is very close to the optimal one. Finally, we have exploited the notion of invex functions to show that the optimal power allocation which maximizes the AF capacity is equal to the one that satisfies the PSD mask.

The specific and peculiar application of the algorithms to the in-home PLC scenario has been considered. For both OAF and ODF, we have found that in most cases the optimal relay location corresponds to the source derivation box. Furthermore, we have shown that a practical relay location, which grants performance close to the optimal one, is the main panel arrangement.

## Conclusions

In this thesis, we have focused on the optimization of MCM schemes. In particular, we have provided parameters design criteria and advanced resource allocation algorithms for adaptive multi-carrier modulation (MCM) schemes whose received signals are affected by interference caused by the signalling over dispersive channels. The extension of the parameters adaptation to the multi-user case has been also considered. In particular, resource allocation algorithms for the downlink case of networks using FDMA and TDMA have been provided.

We also proposed optimal resource allocation algorithms to provide capacity improvements, power savings, and coverage extension in two hops relay networks.

The main achievements are summarized in the following.

### **Parameters Design in OFDM**

We have investigated the problem of CP-length adaptation in OFDM transmission systems, and we have argued that the use of a CP length adjusted to the current transmission conditions is beneficial in terms of achievable data rate. The underlying rationale is that the level of self-interference can be raised in noise-limited systems. We have considered constrained capacity as the pertinent figure of merit, and suggested a number of related, simplified criteria

to select the CP length. Furthermore, we have presented four practical single-user bit-loading algorithms that take into account the CP optimization, and we have outlined extensions to the multiuser transmission scenario using OFDMA and TDMA. Numerical results for typical indoor broadband power line and WLAN channels have shown significant gains due to CP-length adaptation. These gains come from (i) adjusting the CP length according to the instantaneous channel impulse response and (ii) allowing for a controlled amount of self-interference using the proposed optimization criteria.

Finally, we have investigated the problem of the joint power allocation and CP length adaptation for the OFDM transmission system. We have shown that, the use of power allocation algorithms based on iterative water-filling (IWF) together with the adaption of the CP can improve the OFDM achievable rate for the low SNR region. We have further shown that the optimal CP length does not strongly depends on the power distribution, and that the constant power IWF gives results that are similar to true IWF.

### **Parameters Design in PS-OFDM**

We have proposed an adaptive PS-OFDM scheme where the OH parameters (guard interval and roll-off factor) are adapted to jointly maximize capacity and fulfill a desired notching mask. The adaptation can be done when the channel response and/or the notching mask changes. This realizes a form of cognitive PLC system if the notching mask is adapted according to the presence or absence of interferers in the transmission spectrum.

To lower the computational cost, we have also proposed to limit the amount of adaptation, i.e., to use a finite set of OH parameters. The OH values can be computed from the analysis of their distribution function in statistically representative channels. Since a significant change of the OH parameters is caused by a significant change in the SNR, we have considered the design of the OH parameters for a low, a medium, and a high SNR scenario assuming a certain target notching mask. Thus, the adaptation is limited to the computation of the SNR at the receiver, and feedback to the transmitter of the best OH parameters for such an SNR.

---

Several performance results show that both the full adaptation and the limited adaptation provide notable gains compared to the case of using constant suboptimal OH parameters, i.e., a RO that minimizes the number of switched off tones and a GI as long as the channel.

### **Parameters Design in FMT**

We have proposed an adaptive-FMT modulation scheme where the OH parameter (interpolation factor) is adapted to the channel condition to maximize the achievable rate. Through numerical results, obtained over typical WLAN channels, we have seen that the use of adaptive-FMT could further improve the achievable rate w.r.t. the use of adaptive OFDM. This is true for both the single user case and the multi user case that deploys FDMA.

### **Adaptation in Hybrid Filter Bank Schemes**

We have proposed the use of a hybrid architecture that, to reduce the power transmitted by WLAN devices, wisely exploits the peculiarities of adaptive OFDM and short-orthogonal FMT. Through numerical results, obtained testing the proposed scheme over typical WLAN channels, we have shown that hybrid FMT provides significant power saving gains compared to an OFDM scheme that deploys a fixed value of CP, yet assuring the same achievable rate. Furthermore, the hybrid FMT efficient implementation only needs a marginal increment of computational complexity w.r.t. OFDM. This makes the proposed scheme suitable for practical implementation.

### **Time Slot Design in OFDM-TDMA Systems over Time-Variant PLC Channels**

We have studied the resource allocation problem in an indoor PLC system with a physical layer based on OFDM and a medium access control scheme with an adaptive TDMA region. The presented results have been obtained by taking into account both the cyclostationary noise and the cyclic behavior of the channel response. The optimum time slot duration has been determined

in a multi-user scenario for three practical scheduling procedures with different amount of PHY layer OH. It has been shown that although the optimum time slot length is strongly dependent on the speed of the channel time variations, reasonable trade-off values can be selected. The use of these trade-off values avoids the need for computing the optimum time slot in each particular situation, which considerably reduces the amount of feedback information.

### **Opportunistic Relaying**

We have investigated the use of ODF and OAF relay protocols to provide capacity improvements, power saving, and coverage extension over in home power line communication networks.

We have found the optimal power and time slot allocation that maximizes the ODF capacity with a PSD constraint. Furthermore, considering the power minimization problem of ODF, since it is complex to find the optimal solution, we have proposed a simplified algorithm that is based on the resolution of two convex sub-problems. Through numerical results, we have shown that its performance is very close to the optimal one. Finally, we have exploited the notion of convex functions to show that the optimal power allocation which maximizes the AF capacity is equal to the one that satisfies the PSD mask.

The specific and peculiar application of the algorithms to the in-home PLC scenario has been considered. For both OAF and ODF, we have found that in most cases the optimal relay location corresponds to the source derivation box. Furthermore, we have shown that a practical relay location, which grants performance close to the optimal one, is the main panel arrangement.

## Appendices

### 11.1 Derivation of the Useful and the Interference Power

The signal at the output of the  $i$ -th analysis pulse (or equivalently the  $i$ -th DFT output for OFDM or PS-OFDM) at time instant  $\ell N$ , in the absence of noise and with the channel model in (2.2), can be written as

$$z_{signal}^{(i)}(\ell N + \Delta) = \sum_{m \in \mathbb{Z}} \sum_{p=0}^{v-1} \sum_{k \in K_{ON}} \alpha_p a^{(k)}(mN) r_{gh}^{(k,i)}(\beta, \ell N - mN + \Delta - p) \times e^{j2\pi \frac{k\ell N}{M}} e^{-j2\pi \frac{i(\ell N + \Delta)}{M}} \quad (11.1)$$

with

$$r_{gh}^{(k,i)}(\beta, n) = g^{(k)}(n) * h^{(i)}(n), \quad (11.2)$$

and

$$g^{(k)}(n) = \bar{g}(n) e^{j2\pi \frac{kn}{M}}, \quad h^{(i)}(n) = h(n) e^{j2\pi \frac{in}{M}}. \quad (11.3)$$

In (11.1),  $\Delta$  denotes the synchronization phase. In (11.2) we have explicitly indicated the dependence of the crosstalk impulse response term  $r_{gh}^{(k,i)}(\beta, n)$  at the instant  $n$  on the parameter  $\beta$ .

The useful signal term can be obtained setting in (11.1)  $k = i$  and  $m = \ell$ ,

i.e.,

$$z_U^{(i)}(\ell N + \Delta) = a^{(i)}(\ell N) \sum_{p=0}^{\nu-1} \alpha_p r_{gh}^{(i,i)}(\beta, \Delta - p) e^{-j2\pi \frac{i\Delta}{M}} \quad (11.4)$$

$$= a^{(k)}(\ell N) H^{(k)}(\beta, \Delta). \quad (11.5)$$

The interference term  $I^{(k)}(\beta, \ell N + \Delta)$  can be computed setting in (11.1)  $k \neq i$  and  $m \neq \ell$ .

The total power of the received sub-channel signal (11.1), i.e.,  $P_{TOT}^{(i)}(\beta, \Delta)$  =  $E[|z_{signal}^{(i)}(\ell N + \Delta)|^2]$ , depends on the OH parameters and on  $\Delta$ . It can be computed assuming the data symbols to be independent, with zero mean and power  $P_a^{(k)}$ . The calculation yields:

$$\begin{aligned} P_{TOT}^{(i)}(\beta, \Delta) &= \sum_{\ell \in \mathbb{Z}} \sum_{k \in K_{ON}} \sum_{p, p'=0}^{\nu-1} P_a^{(k)} \alpha_p (\alpha_{p'})^* \\ &\quad \times r_{gh}^{(k,i)}(\beta, \ell N - mN + \Delta - p) \\ &\quad \times \left( r_{gh}^{(k,i)}(\beta, \ell N - mN + \Delta - p') \right)^*. \end{aligned} \quad (11.6)$$

If we set in (11.6),  $k = i$  and  $m = \ell$ , we obtain the power of the useful received signal in the  $k$ -th sub-channel, i.e.,

$$P_U^{(k)}(\beta, \Delta) = \sum_{p, p'=0}^{\nu-1} P_a^{(k)} \alpha_p (\alpha_{p'})^* r_{gh}^{(k,k)}(\beta, \Delta - p) \left( r_{gh}^{(k,k)}(\beta, \Delta - p') \right)^*. \quad (11.7)$$

The interference power can be computed as the difference between the total and the useful power.

## 11.2 Capacity Bound Criteria

In this appendix, we provide the details for the derivation of the capacity lower and upper bounds used in Section 3.3.2. The lower bound is obtained by the application of the Bernoulli inequality [93]  $(1+x)^r > 1+rx$ , for  $r > 1$  and  $x > 0$ , to the capacity formula (3.5), which results in

$$\begin{aligned}
 C(\mu) &= \frac{1}{(M+\nu)T} \sum_{k \in \mathbb{K}_{\text{on}}} \log_2 \left( 1 + \frac{\text{SINR}^{(k)}(\mu)}{\Gamma} \right)^{\frac{M+\nu}{M+\mu}} \\
 &> \frac{1}{(M+\nu)T} \sum_{k \in \mathbb{K}_{\text{on}}} \log_2 \left( 1 + \frac{(M+\nu)\text{SINR}^{(k)}(\mu)}{(M+\mu)\Gamma} \right) \\
 &> \frac{1}{(M+\nu)T} \sum_{k \in \mathbb{K}_{\text{on}}} \log_2 \left( \frac{(M+\nu)\text{SINR}^{(k)}(\mu)}{(M+\mu)\Gamma} \right) \\
 &= \frac{1}{(M+\nu)T} \sum_{k \in \mathbb{K}_{\text{on}}} \log_2 \left( \frac{P_{\text{U}}^{(k)}(\mu)}{P_{\eta}} \right) \\
 &\quad - \frac{1}{(M+\nu)T} \sum_{k \in \mathbb{K}_{\text{on}}} \log_2 \left( \frac{(M+\mu)\Gamma}{M+\nu} \left( 1 + \frac{P_{\text{I}}^{(k)}(\mu)}{P_{\eta}} \right) \right). \quad (11.8)
 \end{aligned}$$

Defining  $P_{\text{U},\min} = \min_{k \in \mathbb{K}_{\text{on}}, \mu} \{P_{\text{U}}^{(k)}(\mu)\}$  and thus  $\sum_{k \in \mathbb{K}_{\text{on}}} \log_2 (P_{\text{U}}^{(k)}(\mu)/P_{\eta}) \geq \sum_{k \in \mathbb{K}_{\text{on}}} \log_2 (P_{\text{U},\min}/P_{\eta}) = M_{\text{on}} \log_2 (P_{\text{U},\min}/P_{\eta})$ , (11.8) can further be bounded by

$$\begin{aligned}
 C(\mu) &> \frac{M_{\text{on}}}{(M+\nu)T} \log_2 (P_{\text{U},\min}/P_{\eta}) \\
 &\quad - \frac{1}{(M+\nu)T} \sum_{k \in \mathbb{K}_{\text{on}}} \log_2 \left( \frac{(M+\mu)\Gamma}{M+\nu} \left( 1 + \frac{P_{\text{I}}^{(k)}(\mu)}{P_{\eta}} \right) \right). \quad (11.9)
 \end{aligned}$$

Finally, applying Jensen's inequality [94] to the second term of (11.9), we obtain the final result (3.7). It should be noted that the bound is not necessarily tight as an arbitrary factor  $F > M + \nu$  could have been introduced in (11.8). However, the resulting criterion is independent of this factor and thus also

applies to  $F$  producing the tightest possible approximation.

The application of the inequality  $\log_b(x) \leq (x - 1) \log_b(e)$ ,  $\forall x \in \mathbb{R}^+$ ,  $b > 1$ , to  $C(\mu)$  in (3.5) leads to the capacity upper bound

$$C(\mu) \leq \frac{1}{\Gamma(M + \mu)T} \log_2(e) \sum_{k \in \mathbb{K}_{\text{on}}} \text{SINR}^{(k)}(\mu), \quad (11.10)$$

which, considering (3.10) is the result in (3.9).

### 11.3 Interference Power in OFDM with Uniform Power Distribution

In this section, we compute the total interference power experienced by OFDM when the transmitted power is uniformly distributed among the sub-channels, i.e.,  $P_a^{(k)} = P_a \forall k \in \mathbb{K}_{\text{on}}$ .

Let us define the synthesis and the analysis pulses as

$$g(n) = A \times r\left(\frac{n}{N}\right), \text{ and } h(n) = B \times r\left(-\frac{n + \mu}{M}\right), \quad (11.11)$$

where  $r(n/X)$  is the rect function equal to 1 for  $n = 0, \dots, X - 1$ , and zero otherwise.

To compute the total interference power, we can first compute the total received power, and then we can subtract the useful power.

From (11.6), we can write the total power in sub-channel  $k$  as

$$\begin{aligned} P_{TOT}^{(k)} = & P_a \sum_{\ell, n, n' \in \mathbb{Z}} \sum_{i=0}^{M-1} \sum_{p, p'=0}^{\nu-1} \alpha_p (\alpha_{p'})^* g(n) (g(n'))^* h(\ell N - p - n) \\ & \times (h(\ell N - p' - n'))^* e^{j2\pi f_i(n-n')} e^{j2\pi f_k(p'-p+n'-n)}, \end{aligned} \quad (11.12)$$

where we have omitted the dependance of the total power from the overhead  $\beta$  and we have imposed  $\Delta = 0$ . Using the relation  $\sum_{i=0}^{M-1} e^{j2\pi f_i(n-n')} = M \sum_{i \in \mathbb{Z}} \delta(n - n' - iM)$ , (11.12) becomes

$$\begin{aligned} P_{TOT}^{(k)} = & MP_a \sum_{\ell, n, n' \in \mathbb{Z}} \sum_{i \in \mathbb{Z}} \sum_{p, p'=0}^{\nu-1} \alpha_p (\alpha_{p'})^* g(n) (g(n'))^* h(\ell N - p - n) \\ & \times (h(\ell N - p' - n'))^* \delta(n - n' - iM) e^{j2\pi f_k(p'-p+n'-n)}. \end{aligned} \quad (11.13)$$

We can now compute the total received power as

$$\begin{aligned} P_{TOT} = & \sum_{k=0}^{M-1} P_{TOT}^{(k)} = M^2 P_a \sum_{\ell, n, n' \in \mathbb{Z}} \sum_{i, k \in \mathbb{Z}} \sum_{p, p'=0}^{\nu-1} \alpha_p (\alpha_{p'})^* g(n) (g(n'))^* \\ & \times h(\ell N - p - n) (h(\ell N - p' - n'))^* \end{aligned}$$

$$\times \delta(n - n' - iM)\delta(p' - p + n' - n - kM). \quad (11.14)$$

Now, observing that in order to have (11.14) different from zero, it has to jointly be  $n - n' = iM$  and  $n - n' = p' - p - kM$ , and this happens if and only if  $i = -k$  and  $p' = p$ , we can simplify (11.14) as follows

$$\begin{aligned} P_{TOT} &= M^2 P_a \sum_{\ell, n, n', k \in \mathbb{Z}} \sum_{p=0}^{\nu-1} |\alpha_p|^2 g(n) (g(n'))^* h(\ell N - p - n) (h(\ell N - p - n'))^* \\ &\quad \times \delta(n - n' + kM) \\ &= (ABM)^2 P_a \sum_{\ell, k \in \mathbb{Z}} \sum_{n, n'=0}^{N-1} \sum_{p=0}^{\nu-1} |\alpha_p|^2 r\left(\frac{n}{N}\right) r\left(\frac{n'}{N}\right) r\left(\frac{n+p+\mu-\ell N}{M}\right) \\ &\quad \times r\left(\frac{n'+p+\mu-\ell N}{M}\right) \delta(n - n' + kM). \end{aligned} \quad (11.15)$$

In order to have (11.15) different from zero, we need to consider three cases:  $k = \{-1, 0, 1\}$ . It can be shown that (11.15) is not null only for  $k = 0$ . In such a case, (11.15) becomes

$$\begin{aligned} P_{TOT} &= (ABM)^2 P_a \sum_{\ell \in \mathbb{Z}} \sum_{n=0}^{N-1} \sum_{p=0}^{\nu-1} |\alpha_p|^2 r\left(\frac{n+p+\mu-\ell N}{M}\right) \\ &= (ABM)^2 P_a \sum_{p=0}^{\nu-1} |\alpha_p|^2 (p - \mu) S_{p-\mu}, \end{aligned} \quad (11.16)$$

where  $S_x = 1$  if  $x \geq 0$ , and zero otherwise.

We can now compute the useful power in sub-channel  $k$  expliciting (11.7). It is equal to

$$\begin{aligned} P_U^{(k)} &= P_a \sum_{n, n' \in \mathbb{Z}} \sum_{p, p'=0}^{\nu-1} \alpha_p (\alpha_{p'})^* g(n) (g(n'))^* h(-p - n) \\ &\quad \times (h(-p' - n'))^* e^{j2\pi \frac{k}{M}(p' - p)}. \end{aligned} \quad (11.17)$$

Therefore, the total useful power can be computed as

$$\begin{aligned}
 P_U &= \sum_{k=0}^{M-1} P_U^{(k)} = P_a \sum_{k=0}^{M-1} \sum_{n, n' \in \mathbb{Z}} \sum_{p, p'=0}^{\nu-1} \alpha_p (\alpha_{p'})^* g(n) (g(n'))^* h(-p-n) \\
 &\quad \times (h(-p' - n'))^* e^{j2\pi \frac{k}{M}(p'-p)} \\
 &= MP_a \sum_{k \in \mathbb{Z}} \sum_{n, n' \in \mathbb{Z}} \sum_{p, p'=0}^{\nu-1} \alpha_p (\alpha_{p'})^* g(n) (g(n'))^* h(-p-n) (h(-p' - n'))^* \\
 &\quad \times \delta(p' - p - kM) \\
 &= MP_a \sum_{n, n' \in \mathbb{Z}} \sum_{p=0}^{\nu-1} |\alpha_p|^2 g(n) (g(n'))^* h(-p-n) (h(-p-n'))^* \\
 &= MP_a \sum_{p=0}^{\nu-1} |\alpha_p|^2 \left| \sum_{n \in \mathbb{Z}} g(n) h(-p-n) \right|^2 = MP_a \sum_{p=0}^{\nu-1} |\alpha_p|^2 |r_{gh}(-p)|^2 \\
 &= M(AB)^2 P_a \sum_{p=0}^{\nu-1} |\alpha_p|^2 \left| \sum_{m=0}^{N-1} r \left( \frac{m+p-\mu}{M} \right) \right|^2 \\
 &= M(AB)^2 P_a \sum_{p=0}^{\nu-1} |\alpha_p|^2 |M - (p-\mu)\delta_{p-\mu}|^2. \tag{11.18}
 \end{aligned}$$

The total interference power can be computed as the difference between the total power and the total useful power, i.e.,

$$P_I = P_{TOT} - P_U = (MAB)^2 P_a \sum_{p=0}^{\nu-1} |\alpha_p|^2 \left[ M - \frac{|M - (p-\mu)\delta_{p-\mu}|^2}{M} \right]. \tag{11.19}$$

### 11.4 Fourier Transform of the Raised Cosine Window

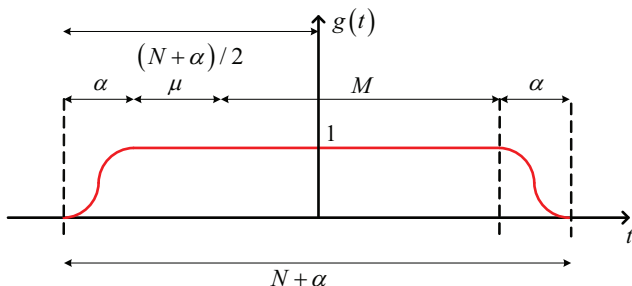


Figure 11.1: Raised cosine window.

Let us consider the raised cosine window  $g(t)$  represented in Fig. 11.1. It is defined as

$$g(t) = \begin{cases} \frac{1}{2} + \frac{1}{2} \cos\left(\frac{\pi}{\alpha} \left(|t| - \frac{N-\alpha}{2}\right)\right), & t \in \left[-\frac{N+\alpha}{2}, -\frac{N-\alpha}{2}\right] \cup \left[\frac{N-\alpha}{2}, \frac{N+\alpha}{2}\right], \\ 1, & t \in \left[-\frac{N-\alpha}{2}, \frac{N-\alpha}{2}\right] \\ 0, & \text{otherwise.} \end{cases} \tag{11.20}$$

The Fourier transform of (11.20) can be computed as

$$\begin{aligned} G(f) &= \int_{-\infty}^{+\infty} g(t) e^{-j2\pi ft} dt = \int_{-\infty}^{+\infty} g(t) [\cos(2\pi ft) + j\sin(2\pi ft)] dt = \\ &= \int_{-\infty}^{+\infty} g(t) \cos(2\pi ft) dt = 2 \int_0^{+\infty} g(t) \cos(2\pi ft) dt = \tag{11.21} \\ &= \underbrace{2 \int_0^{(N-\alpha)/2} \cos(2\pi ft) dt}_{\mathbf{A}} + \underbrace{2 \int_{(N-\alpha)/2}^{(N+\alpha)/2} g(t) \cos(2\pi ft) dt}_{\mathbf{B}}. \end{aligned}$$

The solution of integrals **A** and **B** is

$$\mathbf{A} = (N - \alpha) \operatorname{sinc}(f(N - \alpha)), \tag{11.22}$$

$$\mathbf{B} = \frac{N + \alpha}{2} \text{sinc}(f(N + \alpha)) - \frac{N - \alpha}{2} \text{sinc}(f(N - \alpha)), \quad (11.23)$$

where  $\text{sinc}(x) = \sin(\pi x)/(\pi x)$ . Therefore,  $G(f)$  can be computed as the sum of (11.22) and (11.23). The result is

$$G(f) = \frac{N}{1 - (2\alpha f)^2} \text{sinc}(fN) \cos(\pi f\alpha). \quad (11.24)$$

## 11.5 Karush Kuhn Tucker Conditions

In this section we give the definition of the Karush-Kuhn-Tucker (KKT) conditions. The interested reader can refer to [67, 95] for a detailed derivation.

Let us consider an optimization problem in standard form:

$$\begin{aligned} \min \quad & f_0(\mathbf{x}), \\ \text{s.t.} \quad & f_i(\mathbf{x}) \leq 0, \quad i = 1, \dots, m \\ & h_i(\mathbf{x}) = 0, \quad i = 1, \dots, p, \end{aligned} \tag{11.25}$$

with variable  $\mathbf{x} \in \mathbb{R}^n$ , and domain  $\mathcal{C} = \bigcap_{i=1}^m \text{dom } f_i \cap \bigcap_{i=1}^p \text{dom } h_i$  not empty.

The **Lagrangian**  $L : \mathbb{R}^n \times \mathbb{R}^m \times \mathbb{R}^p \rightarrow \mathbb{R}$  associated to problem (11.25) is defined as

$$L(\mathbf{x}, \boldsymbol{\lambda}, \boldsymbol{\nu}) = f_0(\mathbf{x}) + \sum_{i=1}^m \lambda_i f_i(\mathbf{x}) + \sum_{i=1}^p \nu_i h_i(\mathbf{x}), \tag{11.26}$$

with  $\text{dom } L = \mathcal{D} \times \mathbb{R}^m \times \mathbb{R}^p$ ,  $\lambda_i$  the Lagrange multiplier associated to the  $i$ -th inequality, and  $\nu_i$  the Lagrange multiplier associated to the  $i$ -th equality. The vectors  $\boldsymbol{\lambda}$  and  $\boldsymbol{\nu}$  are called *dual variable* or *Lagrangian vector associated with the primal problem*.

The **Lagrange dual function**  $g : \mathbb{R}^m \times \mathbb{R}^p \rightarrow \mathbb{R}$  is defined as the minimum value of the Lagrangian over  $\mathbf{x}$ : for  $\lambda \in \mathbb{R}^m$ ,  $\nu \in \mathbb{R}^p$ , i.e.,

$$g(\boldsymbol{\lambda}, \boldsymbol{\nu}) = \inf_{\mathbf{x} \in \mathcal{D}} L(\mathbf{x}, \boldsymbol{\lambda}, \boldsymbol{\nu}). \tag{11.27}$$

When the Lagrangian is unbounded below in  $\mathbf{x}$ , the dual function takes on the value  $-\infty$ . It is worth noting that since the dual function is the pointwise infimum of a family of affine functions of  $(\boldsymbol{\lambda}, \boldsymbol{\nu})$ , it is concave, even when the problem (11.26) is not convex.

The **Lagrangian dual problem** is defined as

$$\begin{aligned} \max \quad & g(\boldsymbol{\lambda}, \boldsymbol{\nu}), \\ \text{s.t.} \quad & \lambda_i \geq 0, \quad i = 1, \dots, m. \end{aligned} \tag{11.28}$$

Problem (11.28) is said *dual feasible* if exists a pair  $(\boldsymbol{\lambda}, \boldsymbol{\nu})$  with  $\boldsymbol{\lambda} \geq 0$  and  $g(\boldsymbol{\lambda}, \boldsymbol{\nu}) > -\infty$ .

Now, let us indicate with  $\mathbf{x}^*$  the optimal solution to problem (11.25), with the pair  $(\boldsymbol{\lambda}^*, \boldsymbol{\nu}^*)$  the optimal solution to the dual problem, and with  $d^*$  the corresponding value of  $g$ , namely  $g(\boldsymbol{\lambda}^*, \boldsymbol{\nu}^*) = d^*$ . We can then define the **duality gap** as  $f_0(\mathbf{x}^*) - d^*$ . It is said that the **strong duality** holds when the optimal duality gap is zero.

Assuming  $f_0, \dots, f_m, h_1, \dots, h_p$  differentiable,  $\mathbf{x}^*$  and  $(\boldsymbol{\lambda}^*, \boldsymbol{\nu}^*)$  be any primal and dual optimal points with zero duality gap, the Karush Kuhn Tucker conditions can be expressed as:

$$\begin{aligned} f_i(\mathbf{x}^*) &\leq 0, \quad i = 1, \dots, m \\ h_i(\mathbf{x}^*) &= 0, \quad i = 1, \dots, p, \\ \lambda_i^* &\geq 0, \quad i = 1, \dots, m \\ \lambda_i^* f_i(\mathbf{x}^*) &= 0, \quad i = 1, \dots, m \end{aligned} \tag{11.29}$$

$$\nabla f_0(\mathbf{x}^*) + \sum_{i=1}^m \lambda_i^* \nabla f_i(\mathbf{x}^*) + \sum_{i=1}^p \nu_i^* \nabla f_i(\mathbf{x}^*) = 0.$$

In (11.29), the lines, from the first to the sixth denote: the inequality constraints, the equality constraints, the non negativity condition of the Lagrange multipliers associated with the inequality constraints, the slackness conditions, and the condition that the gradient of the Lagrangian in the optimal point has to be null.

Therefore, we can summarize saying that for any optimization problem with differentiable objective and constraint functions for which strong duality obtains, any pair of primal and dual optimal points must satisfy the KKT conditions (11.29).

### 11.5.1 KKT Conditions for Convex Problems

Sufficient, although not necessary [96], conditions to have a primal problem (11.25) **convex** are

- the objective function is convex,
- the inequality constraint functions are convex,
- the equality constraint functions are affine.

When the primal problem is convex, the KKT conditions are also sufficient for the points to be primal and dual optimal. In other words, if  $f_i$  are convex and  $h_i$  are affine, and  $\mathbf{x}^*$ , and  $(\boldsymbol{\lambda}^*, \boldsymbol{\nu}^*)$  are any points that satisfy the KKT conditions then  $\mathbf{x}^*$ , and  $(\boldsymbol{\lambda}^*, \boldsymbol{\nu}^*)$  are primal and dual optimal, with zero duality gap.

## 11.6 Multi-Carrier Power Minimization under a PSD Constraint

Let us consider the general multi-carrier (MC) scheme that has been presented in Section 2.1. According to that model a set of  $M$  parallel data signals, each having power  $P_a^{(k)}$ , where  $k = 0, \dots, M - 1$ , is transmitted over a frequency selective channel.

In this section, we want to find the power allocation among the  $M$  sub-channels, which minimizes the total transmitted power, and allows the system to achieve a given target rate  $R$  under a power spectral density (PSD) mask constraint. This is a power minimization (PM) problem that in our case can be formulated as

$$\begin{aligned} \arg \min_{\mathbf{P}_a} \quad & \sum_{k \in \mathbb{K}_{\text{on}}} P_a^{(k)}, & (11.30) \\ \text{s.t.} \quad & 0 \leq P_a^{(k)} \leq \bar{P}, \quad k \in \mathbb{K}_{\text{on}}. \\ & \frac{1}{NT} \sum_{k \in \mathbb{K}_{\text{on}}} \log_2 \left( 1 + P_a^{(k)} \gamma^{(k)} \right) = R, \end{aligned}$$

where  $R$  denotes the target achievable rate in [bit/s],  $\mathbf{P}_a = \{P_a^{(k)}\}$ , with  $k = 0, \dots, M - 1$  is the vector of the transmitted powers,  $\bar{P}$  is the power constraint given by the PSD limit level, and  $\mathbb{K}_{\text{on}}$  is the set of used sub-channels, i.e.,  $\mathbb{K}_{\text{on}} \subseteq \{0, \dots, M - 1\}$ .

In the following, we suppose the coefficients  $\gamma^{(k)}$  to be independent from the transmitted power vector.

According to the definition given in Appendix 11.5, in general, Problem (11.30) is not a convex optimization problem inasmuch the equality constraint is not an affine function. Nevertheless, if we apply the change of variable  $P_a^{(k)} = (2^{(b_k)} - 1) / \gamma^{(k)}$ , the obtained problem is equivalent<sup>1</sup> to Problem (11.30), and it is a convex optimization problem. Now, since the problems are equivalent, also their solutions are equivalent [67, pp. 130]. Therefore, a way to find the solution to problem (11.30) is to solve the KKT conditions for the equivalent convex problem. Then, the optimal solution of (11.30) can be ob-

<sup>1</sup>See [67, pp. 130] for the definition of equivalent problems.

tained applying the inverse change of variables. The solution to the equivalent convex problem is well known and it is given by [34]

$$b_k = b_k(\bar{\nu}) = \left[ \bar{\nu} - \log_2 \left( 1/\gamma^{(k)} \right) \right]_0^{\bar{b}}, \quad (11.31)$$

where

$$[x]_a^b = \begin{cases} b, & x \geq b \\ x, & a < x < b \\ a, & x \leq a, \end{cases} \quad (11.32)$$

and  $\bar{\nu}$  is given by the solution of the equation

$$\frac{1}{NT} \sum_{k=0}^{M-1} b_k(\bar{\nu}) = R. \quad (11.33)$$

The solution to problem (11.30), namely the optimal power distribution, can be found applying the change of variables, and it is equal to

$$P_a^{(k)} = P_a^{(k)}(\nu) = \left[ \nu - 1/\gamma^{(k)} \right]_0^{\bar{P}}, \quad (11.34)$$

where  $\nu$  is given by the solution of the equation

$$\frac{1}{NT} \sum_{k=0}^{M-1} \left( 1 + P_a^{(k)}(\nu) \gamma^{(k)} \right) = R. \quad (11.35)$$

Another way to find a solution to Problem (11.30) is to solve the KKT conditions. As it is well known, the solution to the KKT conditions gives in general the stationary points of the minimization problem. Now, the stationary points are minima (in general local minima) if some regularity conditions (or constraints qualification) are satisfied. In our case, the constraints satisfy the constant rank constraint qualification [97]. Therefore, the stationary points that we will find imposing the KKT conditions are local minima. Consequently, the global minimum can be found by doing an exhaustive comparison among the local minima. Clearly, if the KKT solution is unique, the minimum is also

global. To solve the KKT conditions associated to Problem (11.30), we first compute the Lagrangian, i.e.,

$$\begin{aligned}
 L(\mathbf{P}_a, \boldsymbol{\lambda}, \boldsymbol{\mu}, \nu) &= \sum_{k \in \mathbb{K}_{\text{on}}} P_a^{(k)} + \sum_{k \in \mathbb{K}_{\text{on}}} \lambda_k \left( P_a^{(k)} - \bar{P} \right) \\
 &\quad - \sum_{k \in \mathbb{K}_{\text{on}}} \mu_k P_a^{(k)} + \nu \left[ \frac{1}{NT} \sum_{k \in \mathbb{K}_{\text{on}}} \log_2 \left( 1 + P_a^{(k)} \gamma^{(k)} \right) - R \right].
 \end{aligned} \tag{11.36}$$

$$\tag{11.37}$$

We can now derive the KKT conditions as:

$$\begin{aligned}
 1 + \lambda_k - \mu_k + \nu \frac{\gamma^k}{NT \ln(2) \left( 1 + P_a^{(k)} \gamma^{(k)} \right)} &= 0, \\
 P_a^{(k)} - \bar{P} &\leq 0, \\
 -P_a^{(k)} &\leq 0, \\
 \frac{1}{NT} \sum_{k=0}^{M-1} \log_2 \left( 1 + P_a^{(k)} \gamma^{(k)} \right) - R &= 0, \\
 \lambda_k &\geq 0, \\
 \mu_k &\geq 0, \\
 \lambda_k \left( P_a^{(k)} - \bar{P} \right) &= 0, \\
 \mu_k P_a^{(k)} &= 0, \\
 \forall k \in \mathbb{K}_{\text{on}}.
 \end{aligned} \tag{11.38}$$

In (11.38), the first line represents the condition that the partial derivative of the lagrangian w.r.t.  $P_a^{(k)}$  has to be null. The second and the third represent the inequality constraints. The fourth is the equality constraint. The fifth and sixth express the non negative condition of the Lagrange multipliers associated to the inequalities constraints, and the last two conditions are the slackness conditions.

The KKT conditions can be solved studying the cases where  $P_a^{(k)}$  is equal to zero, to  $\bar{P}$ , or belongs to the set  $]0, \bar{P}[$ .

It is easy to show that only one solution satisfies the KKT conditions and it is equal to the solution (11.34) that we have found solving the equivalent problem.

## 11.7 Power Allocation in DF for Power Minimization

Let us consider the first sub-problem associated to problem (9.9), i.e.,

$$\begin{aligned}
 P(t) &= \min \sum_{k \in \mathbb{K}_{\text{on}}} tP_S^{(k)} + (1-t)P_R^{(k)} \\
 \text{s.t. } \quad &tC_{S,R} = R, \\
 &tC_{S,D} + (1-t)C_{R,D} \geq R, \\
 &0 \leq P_S^{(k)} \leq \bar{P}, \\
 &0 \leq P_R^{(k)} \leq \bar{P}, \quad \forall k \in \mathbb{K}_{\text{on}},
 \end{aligned} \tag{11.39}$$

where we have omitted the subscripts *DF1* for easiness of the following treatment.

Problem (11.39) is not convex inasmuch the equality constraint is not affine.

To find a solution to Problem (11.39), we can impose the KKT conditions (see Section 11.5). To this end, we first compute the Lagrangian associated with problem (11.39) that reads:

$$\begin{aligned}
 L(\mathbf{P}_S, \mathbf{P}_R, \boldsymbol{\lambda}_S, \boldsymbol{\lambda}_R, \boldsymbol{\mu}_S, \boldsymbol{\mu}_R, \nu, \gamma) &= \tag{11.40} \\
 &\sum_{k \in \mathbb{K}_{\text{on}}} tP_S^{(k)} + \sum_{k \in \mathbb{K}_{\text{on}}} (1-t)P_R^{(k)} + \sum_{k \in \mathbb{K}_{\text{on}}} \lambda_S^{(k)} (P_S^{(k)} - \bar{P}) + \sum_{k \in \mathbb{K}_{\text{on}}} \lambda_R^{(k)} (P_R^{(k)} - \bar{P}) \\
 &- \sum_{k \in \mathbb{K}_{\text{on}}} \mu_S^{(k)} P_S^{(k)} + \sum_{k \in \mathbb{K}_{\text{on}}} \mu_R^{(k)} P_R^{(k)} \\
 &+ \gamma \left[ R - \frac{t}{MT} \sum_{k \in \mathbb{K}_{\text{on}}} \log_2 \left( 1 + P_S^{(k)} \eta_{S,D}^{(k)} \right) - \frac{1-t}{MT} \sum_{k \in \mathbb{K}_{\text{on}}} \log_2 \left( 1 + P_R^{(k)} \eta_{R,D}^{(k)} \right) \right] \\
 &+ \nu \left[ \frac{t}{MT} \sum_{k \in \mathbb{K}_{\text{on}}} \log_2 \left( 1 + P_S^{(k)} \eta_{S,R}^{(k)} \right) - R \right].
 \end{aligned}$$

From (11.39) and (11.40), we can derive the KKT condition as:

$$\begin{aligned}
 tC_{S,D} + (1-t)C_{R,D} &\geq R, \\
 tC_{S,R} &= R,
 \end{aligned}$$

$$\begin{aligned}
 \lambda_S^{(k)} \geq 0, \quad \lambda_R^{(k)} \geq 0, \quad \mu_S^{(k)} \geq 0, \quad \mu_R^{(k)} \geq 0, \quad \gamma \geq 0, \\
 \lambda_S^{(k)} \left( P_S^{(k)} - \bar{P} \right) = 0, \quad \lambda_R^{(k)} \left( P_R^{(k)} - \bar{P} \right) = 0, \\
 \mu_S^{(k)} P_S^{(k)} = 0, \quad \mu_R^{(k)} P_R^{(k)} = 0,
 \end{aligned} \tag{11.41}$$

$$\gamma [tC_{S,D} + (1-t)C_{R,D} - R] = 0,$$

$$t + \lambda_S^{(k)} - \mu_S^{(k)} - \gamma \frac{t\eta_{S,D}^{(k)}}{MT \ln(2)} \frac{1}{1 + P_S^{(k)}\eta_{S,D}^{(k)}} + \nu \frac{t\eta_{S,R}^{(k)}}{MT \ln(2)} \frac{1}{1 + P_S^{(k)}\eta_{S,R}^{(k)}} = 0$$

$$1 - t + \lambda_R^{(k)} - \mu_R^{(k)} - \gamma \frac{(1-t)\eta_{R,D}^{(k)}}{MT \ln(2)} \frac{1}{1 + P_R^{(k)}\eta_{R,D}^{(k)}} = 0,$$

$$\forall k \in \mathbb{K}_{\text{on}}.$$

In (11.41), from the first to the last line we have: the inequality constraint, the equality constraint, the condition on the non negativity of the Lagrange multipliers, the slackness conditions (lines 3-5), the gradient of the Lagrangian equal to zero (lines 7-8).

Now, to solve the KKT conditions, we can consider the cases where both  $P_S^{(k)}$  and  $P_R^{(k)}$  belong to the set  $\{0, (0, \bar{P}), \bar{P}\}$ . Therefore we need to consider nine cases.

After many algebraic manipulations, it can be shown that the solution to the KKT conditions is given by:

$$P_S^{(k)} = \begin{cases} 0, & \bar{\nu} \leq \frac{1-\bar{\gamma}\eta_{S,D}^{(k)}}{\eta_{S,R}^{(k)}} \\ x, & \frac{1-\bar{\gamma}\eta_{S,D}^{(k)}}{\eta_{S,R}^{(k)}} < \bar{\nu} < \frac{1+\bar{P}\eta_{S,R}^{(k)}}{\eta_{S,R}^{(k)}} \left( 1 + \frac{\bar{\gamma}\eta_{S,D}^{(k)}}{1+\bar{P}\eta_{S,d}^{(k)}} \right) \\ \bar{P}, & \bar{\nu} \geq \frac{1+\bar{P}\eta_{S,R}^{(k)}}{\eta_{S,R}^{(k)}} \left( 1 + \frac{\bar{\gamma}\eta_{S,D}^{(k)}}{1+\bar{P}\eta_{S,d}^{(k)}} \right), \end{cases} \tag{11.42}$$

$$P_R^{(k)} = \left[ \bar{\gamma} - \frac{1}{\eta_{R,D}^{(k)}} \right]_{\bar{P}}^{\bar{P}}. \tag{11.43}$$

In (11.42),(11.43),  $\bar{\gamma} = \gamma/(MT \ln(2))$ , and  $\bar{\nu} = -\nu/(MT \ln(2))$ . Further-

more, in (11.42),  $x$  is the solution of the equation

$$\eta_{S,R}^{(k)}\eta_{S,D}^{(k)}x^2 + \left[ \eta_{S,R}^{(k)} + \eta_{S,D}^{(k)} + \eta_{S,R}^{(k)}\eta_{S,D}^{(k)}(\bar{\gamma} + \bar{\nu}) \right] x - \bar{\gamma}\eta_{S,D}^{(k)} - \bar{\nu}\eta_{S,R}^{(k)} + 1 = 0, \quad (11.44)$$

whereas  $\bar{\gamma}$  and  $\bar{\nu}$  can be computed imposing the conditions of the first two lines of (11.41).

Looking at (11.42),(11.43), and (11.44), it is clear that we need to adopt an iterative algorithm to find a solution to the KKT condition. Consequently, its complexity would be not less than that of conventional methods used for solving inequality constrained minimization problems, e.g., the interior-point method [67]. This is why in Section 9.3.2 we decided to solve the power minimization problem of decode and forward using the interior-point method.

Finally, we note that the second sub-problem (equation (9.14)) of (9.9) can be solved with the same procedure used to solve (11.39). Again, the computation of the solution to the KKT conditions requires an iterative algorithm.

## 11.8 Power Allocation in AF for Capacity Maximization

The Lagrangian associated to problem (9.26) is given by

$$\begin{aligned}
 L(\mathbf{P}_{S,AF}, \mathbf{P}_{R,AF}, \mu_S, \mu_R, \lambda_S, \lambda_R) = & \\
 & - C_{AF}(\mathbf{P}_{S,AF}, \mathbf{P}_{R,AF}) - \sum_{k \in \mathbb{K}_{on}} \mu_S^{(k)} P_{S,AF}^{(k)} \\
 & + \mu_R^{(k)} P_{R,AF}^{(k)} - \lambda_S^{(k)} (P_{S,AF}^{(k)} - \bar{P}) - \lambda_R^{(k)} (P_{R,AF}^{(k)} - \bar{P}). \quad (11.45)
 \end{aligned}$$

From (9.26) and (11.45), we can derive the KKT conditions as [67, pp. 243]

$$\frac{\partial L}{\partial P_{S,AF}^{(k)}} = 0, \quad \frac{\partial L}{\partial P_{R,AF}^{(k)}} = 0, \quad (11.46)$$

$$P_{S,AF}^{(k)} - \bar{P} = 0, \quad P_{R,AF}^{(k)} - \bar{P} = 0, \quad -P_{S,AF}^{(k)} \leq 0, \quad -P_{R,AF}^{(k)} \leq 0, \quad (11.47)$$

$$\mu_S^{(k)} \geq 0, \quad \mu_R^{(k)} \geq 0, \quad \lambda_S^{(k)} \geq 0, \quad \lambda_R^{(k)} \geq 0, \quad (11.48)$$

$$\begin{aligned}
 \lambda_S^{(k)} (P_{S,AF}^{(k)} - \bar{P}) = 0, \quad \lambda_R^{(k)} (P_{R,AF}^{(k)} - \bar{P}) = 0, \quad \mu_S^{(k)} P_{S,AF}^{(k)} = 0, \quad \mu_R^{(k)} P_{R,AF}^{(k)} = 0, \\
 \forall k \in \mathbb{K}_{on} \quad (11.49)
 \end{aligned}$$

To solve the KKT conditions, we can consider the cases where both  $P_{S,AF}^{(k)}$  and  $P_{R,AF}^{(k)}$  belong to the set  $\{0, (0, \bar{P}), \bar{P}\}$ . Therefore we need to consider nine cases. It is easy to show that the only case for which all the KKT conditions are satisfied is when  $P_{S,AF}^{(k)} = P_{R,AF}^{(k)} = \bar{P} \forall k \in \mathbb{K}_{on}$ . In such a case all the Lagrange's multipliers are non negative and bounded. Therefore, for Theorem 1 of Chapter 9, the objective function of (9.26) is Type 1 invex.

# Bibliography

- [1] M. L. Doelz, E. T. Heald, and D. L. Martin, “Binary Data Transmission Techniques for Linear Systems,” *Proc. of IRE*, vol. 45, pp. 529–540, May 1957.
- [2] H. C. Ferreira, L. Lampe, J. Newbury, and T. G. Swart, *Power Line Communications: Theory and Applications for Narrowband and Broadband Communications over Power Lines*. NY: Wiley & Sons, 2010.
- [3] S. Weinstein and P. Ebert, “Data Transmission by Frequency-Division Multiplexing using the Discrete Fourier Transform,” *IEEE Trans. Commun. Technol.*, vol. 19, pp. 628 – 634, May 1971.
- [4] F. Sjoberg, R. Nilsson, M. Isaksson, P. Odling, and P. Borjesson, “Asynchronous Zipper,” in *Proc. of IEEE Int. Conf. of Commun. (ICC 1999)*, (Vancouver, BC, Canada), pp. 231–235, June 1999.
- [5] G. Cherubini, E. Eleftheriou, and S. Olcer, “Filtered Multitone Modulation for Very High-Speed Digital Subscriber Lines,” *IEEE J. Select. Areas Commun.*, vol. 20, pp. 1016–1028, June 2002.
- [6] S. D. Sandberg and M. A. Tzannes, “Overlapped Discrete Multitone Modulation for High Speed Copper Wire Communications,” *IEEE J. Select. Areas Commun.*, vol. 13, pp. 1571–1585, Dec. 1995.

- [7] International Telecommunication Union, “Section 1: ISM Applications,” *online at <http://life.itu.ch/radioclub/rr/art01.htm>*, Oct. 2009.
- [8] IEEE Std.802.11, *Wireless LAN Medium Access Control and Physical Layer Specification*. IEEE, June 2007.
- [9] IEEE Std. 802.16e, *Air Interface for Fixed and Mobile Broadband Wireless Access Systems*. IEEE, Feb. 2006.
- [10] M. Hamon and et. al, *FP7 OMEGA Project - Deliverable D2.1, “Technical Requirements”*. available at <http://www.ict-omega.eu>, 2008.
- [11] J. Zyren, “Overview of the 3GPP Long Term Evolution Physical Layer,” in *white paper of Freescale Semiconductor*, July 2007.
- [12] DVB Consortium, *DVB Fact Sheet: Digital Terrestrial Television*. DVB Project Office, July 2009.
- [13] DVB Consortium, *DVB Fact Sheet: Second Generation Digital Terrestrial Television*. DVB Project Office, Mar. 2010.
- [14] G. Abdalla, M. A. Abu-Rgheff, and S. M. Senouci, “Current Trends in Vehicular Ad Hoc Networks,” *Special Issue of Ubiquitous and Commun. Journal*, 2007.
- [15] ERDF, *PLC G3 Physical Layer Specification*.
- [16] PRIME Alliance Technical Working Group, *Draft Standard for PowerLine Intelligent Metering Evolution*.
- [17] V. Oksman and J. Zhang, “G.HNEM: the new ITU-T standard on narrowband PLC technology,” *IEEE Commun. Mag.*, vol. 49, pp. 36–44, Dec. 2011.
- [18] HomePlug Powerline Alliance, *HomePlug AV System Specifications, Version 1.0.09*. HomePlug, Feb. 2007.

- [19] S. Galli and O. Logvinov, "Recent Developments in the Standardization of Power Line Communications within the IEEE," *IEEE Commun. Mag.*, vol. 46, pp. 64–71, July 2008.
- [20] V. Oksman and S. Galli, "G.hn: The New ITU-T Home Networking Standard," *IEEE Commun. Mag.*, vol. 47, pp. 138–145, Oct. 2009.
- [21] P. Macaulay, "Broadband Technology Update," in *Presentation at the DSL Forum 2007*, 2007.
- [22] T. Starr and J. Cioffi, *Understanding Digital Subscriber Line Technology*. Prentice Hall, 1998.
- [23] A. M. Tonello, "Asynchronous Multicarrier Multiple Access: Optimal and Sub-Optimal Detection and Decoding," *Bell Labs Tech. Journal, special issue: Wireless Radio Access Networks*, vol. 7, no. 3, pp. 191–217, 2003.
- [24] A. Tonello, "A Concatenated Multitone Multiple Antenna Air-Interface for the Asynchronous Multiple Access Channel," *IEEE J. Sel. Areas Commun.*, vol. 24, Mar. 2006.
- [25] A. M. Tonello and F. Pecile, "Efficient Architectures for Multiuser FMT Systems and Application to Power Line Communications," *IEEE Trans. on Commun.*, vol. 57, no. 5, pp. 1275–1279, 2009.
- [26] F. Pecile and A. M. Tonello, "On the Design of Filter Bank Systems in Power Line Channels Based on Achievable Rate," in *Proc. of IEEE Int. Sym. on Power Line Commun. and its Applications (ISPLC 2009)*, (Dresden, Germany), Mar. 2009.
- [27] A. Tonello and F. Pecile, "Analytical Results about the Robustness of FMT Modulation with Several Prototype Pulses in Time-Frequency Selective Fading Channels," *IEEE Trans. Wireless Commun.*, vol. 7, pp. 1634 – 1645, May 2008.
- [28] A. Peled and A. Ruiz, "Frequency Domain Data Transmission Using Reduced Computational Complexity Algorithms," in *Proc. of IEEE*

- Int. Conf. on Acoustic, Speech, and Signal Processing (ICASSP 1980)*, pp. 964–967, Apr. 1980.
- [29] J. Seoane, S. Wilson, and S. Gelfand, “Analysis of Intertone and Interblock Interference in OFDM when the Length of the Cyclic Prefix is Shorter than the Length of the Impulse Response of the Channel,” in *Proc. of IEEE Global Telecommun. Conf. (GLOBECOM 1997)*, (Phoenix, AZ, USA), pp. 32–36, Nov. 1997.
- [30] I. Kalet, “The Multitone Channel,” *IEEE Trans. Commun.*, vol. 37, pp. 119–124, Feb. 1989.
- [31] J. Cioffi, *Lecture notes: Advanced Digital Communication, Chapter 4*. available at <http://www.stanford.edu/class/ee379c/reader.html>, 2008.
- [32] C. Wong, R. Cheng, K. Letaief, and R. Murch, “Multiuser OFDM with Adaptive Subcarrier, Bit, and Power Allocation,” *IEEE J. Select. Areas Commun.*, vol. 17, pp. 1747–1758, Oct. 1999.
- [33] R. Sonalkar and R. Shively, “An Efficient Bit-Loading Algorithm for DMT Applications,” *IEEE Commun. Lett.*, vol. 4, pp. 80–82, Mar. 2000.
- [34] N. Papandreou and T. Antonakopoulos, “Bit and Power Allocation in Constrained Multi-carrier Systems: The Single-User Case,” *EURASIP Journal on Advances in Signal Processing*, vol. 2008, no. Article ID 643081, 2008.
- [35] M. Batarieri, K. Baum, and T. Krauss, “Cyclic Prefix Length Analysis for 4G Systems,” in *Proc. of IEEE Vehicular Technology Conf. (VTC Fall)*, (Los Angeles, CA, USA), pp. 543–547, Sept. 2004.
- [36] E. Viterbo and K. Fazel, “How to Combat Long Echoes in OFDM Transmission Schemes: Sub-channel Equalization or More Powerful Channel Coding,” in *Proc. of IEEE Global Telecommun. Conf. (GLOBECOM 1995)*, (Singapore, Republic of Singapore), pp. 2069–2074, Nov. 1995.

- [37] Z. Zhao-yang and L. Li-feng, "A Novel OFDM Transmission Scheme with Length-Adaptive Cyclic Prefix," *Journal of Zhejiang University SCIENCE*, vol. 2004, pp. 1336–1342, 2004.
- [38] Universal Powerline Association, *UPA Digital Home Specification White Paper*. UPA, 2006.
- [39] M. Tlich, R. Razaferson, G. Avril, and A. Zeddami, "Outline about the EMC Properties and Throughputs of the PLC Systems up to 100 MHz," in *IEEE Int. Symp. on Power Line Commun. and its Appl. (ISPLC)*, (Jeju Island, Korea), pp. 259–262, Apr. 2008.
- [40] S. Mishra, R. Brodersen, S. Brink, and R. Mahadevappa, "Detect and Avoid: an Ultra-Wideband/WiMAX Coexistence Mechanism," *IEEE Commun. Mag.*, vol. 45, pp. 68–75, June 2007.
- [41] A. Goldsmith, *Wireless Communications*. Cambridge University Press, 2005.
- [42] K.-B. Song, A. Ekbal, S. Chung, and J. M. Cioffi, "Adaptive Modulation and Coding (AMC) for Bit-Interleaved Coded OFDM (BIC-OFDM)," *IEEE Trans. Wireless Commun.*, vol. 5, pp. 1685–1694, July 2006.
- [43] C. Sung, S.-Y. Chung, J. Heo, and I. Lee, "Adaptive Bit-Interleaved Coded OFDM With Reduced Feedback Information," *IEEE Trans. Commun.*, vol. 55, pp. 1649–1655, Sept. 2007.
- [44] D. Luenberger, *Linear and Nonlinear Programming*. Addison-Wesley, 1984.
- [45] M. Tlich, A. Zeddami, F. Moulin, and F. Gauthier, "Indoor Powerline Communications Channel Characterization up to 100 MHz - Part I: One-Parameter Deterministic Model," *IEEE Trans. Power Delivery*, vol. 23, pp. 1392–1401, July 2008.

- [46] A. M. Tonello, F. Versolatto, and B. Béjar, “A top-down random generator for the in-home plc channel,” in *proc. of IEEE Global Telecommun. Conf. (GLOBECOM 2011)*, (Houston - Texas, USA), Dec. 2011.
- [47] M. Zimmermann and K. Dostert, “A Multipath Model for the Powerline Channel,” *IEEE Trans. Commun.*, vol. 50, pp. 553–559, Apr. 2002.
- [48] A. Tonello, “Wideband Impulse Modulation and Receiver Algorithms for Multiuser Power Line Communications,” *EURASIP Journal on Advances in Signal Processing*, vol. 2007, no. Article ID 96747, 2007.
- [49] V. Erceg, L. Shumacher, and al., *IEEE P802.11 Wireless LANs, TGn Channel Models, doc.: IEEE 802.11-03/940r4 (2004)*. IEEE, 2004.
- [50] H. Latchman, K. Afkhamie, S. Katar, B. Mashburn, R. Newman, and L. Yonge, “High speed multimedia home networking over powerline,” *NCTA Technical Papers*, pp. 9–22, Apr. 2005.
- [51] J. Proakis, *Digital Communications*. New York: McGraw Hill, 4th ed., 2001.
- [52] T. M. Schmidl and D. C. Cox, “Robust frequency and Time Synchronization for OFDM,” *IEEE Trans. on Commun.*, vol. 45, Dec. 1997.
- [53] T. Pollet and M. Peeters, “Synchronization with DMT modulation,” *IEEE Commun. Mag.*, vol. 37, Apr. 1999.
- [54] P. Pagani, M. Tlich, A. Zeddani, A. Tonello, F. Pecile, S. D’Alessandro, G. Mijic, and K. Kriznar, “PLC Channel Transfer Function Models for the OMEGA ICT Project,” in *Proc. of ICT-Mobile Summit 2009*, (Santander, Spain), June 2009.
- [55] F. J. Cañete, J. A. Cortés, L. Díez, and J. T. Entrambasaguas, “Analysis of the Cyclic Short-Term Variation of Indoor Power Line Channels,” *IEEE J. Select. Areas Commun.*, vol. 24, pp. 1327–1338, July 2006.

- 
- [56] A. Tonello, S. DAlessandro, and al., *FP7 OMEGA Project: Deliverable D3.4 Performance Report of Optimized PHY Algorithms*. available at <http://www.ict-omega.eu>, 2010.
- [57] H. Afkhamie, H. Latchman, L. Yonge, T. Davidson, and R. Newman, “Joint Optimization of Transmit Pulse Shaping, Guard Interval Length, and Receiver Side Narrow-Band Interference Mitigation in the HomePlugAV OFDM System,” in *Proc. of IEEE Int. Workshop on Signal Processing Advances for Wireless Commun. (SPAWC 2005)*.
- [58] F. Pecile, *PhD Thesis: Filtered Multitone Modulation (FMT): Efficient Implementation, Synchronization and Robustness*. University of Udine, Apr. 2009.
- [59] N. Moret, *Ph.D. Thesis - Filter Bank Tranceiver Systems: Design and Performance Analysis*. University of Udine, Apr. 2012.
- [60] T. M. Cover and J. A. Thomas, *Elements of Information Theory*. NY: Wiley & Sons, 2006.
- [61] E. Calvo, J. R. Fonollosa, and J. Vidal, “On the Totally Asynchronous Iterative Channel with Single-User Receivers,” in *Proc. of IEEE Int. Sym. on Inf. Theory (ISIT 2009)*.
- [62] W. Yu, W. Rheem, S. Boyd, and J. M. Cioffi, “Iterative Water-filling for Gaussian Vector Multiple Access Channels,” *IEEE Trans. Inform. Theory*, vol. 50, pp. 145–152, Jan. 2004.
- [63] W. Yu, G. Ginis, and J. M. Cioffi, “Distributed Multiuser Power Control for Digital Subscriber Lines,” *IEEE J. Select. Areas Commun.*, vol. 20, pp. 102–111, June 2002.
- [64] R. Cendrillon and et. al., “Optimal Multiuser Spectrum Balancing for Digital Subscriber Lines,” *IEEE Trans. Commun.*, vol. 54, pp. 102–111, May 2006.

- [65] S. T. Chung, S. J. Kim, J. Lee, and J. M. Cioffi, "A Game-Theoretic Approach to Power Allocation in Frequency-Selective Gaussian Interference Channels," in *Proc. of IEEE Int. Sym. on Inf. Theory*, (Yokohama, Japan), June 2003.
- [66] W. Yu and J. Cioffi, "Constant-Power Waterfilling: Performance Bound and Low-Complexity Implementation," *IEEE Trans. Commun.*, vol. 54, pp. 23–28, Jan. 2006.
- [67] S. Boyd and L. Vandenberghe, "Convex Optimization," *Cambridge University Press*, 2004.
- [68] HomePlug Powerline Alliance, *Home Plug Green PHY The Standard For In-Home Smart Grid Powerline Communications*. HomePlug, June 2010.
- [69] N. Moret and A. M. Tonello, "Design of Orthogonal Filtered Multitone Modulation Systems and Comparison among Efficient Realizations," *EURASIP Journal on Advances in Signal Processing*, 2010.
- [70] S. D'Alessandro, N. Moret, and A. M. Tonello, "Hybrid Filtered Multitone Architecture for WLAN Applications," in *to appear in Proc. of IEEE Personal, Indoor, and Mobile Radio Conf. (PIMRC 2010)*, (Istanbul, Turkey), Sept. 2010.
- [71] M. Katayama, T. Yamazato, and H. Okada, "A Mathematical Model of Noise in Narrowband Power Line Communication Systems," *IEEE J. Select. Areas Commun.*, vol. 24, pp. 1267–1276, July 2006.
- [72] S. Katar, B. Mashburn, K. Afkhamie, H. Latchman, and R. Newman, "Channel adaptation based on cyclo-stationary noise characteristics in plc systems," in *proc. of IEEE Int. Sym. on Power Line Commun. and Its Applications (ISPLC 2006)*, (Orlando, USA), Mar. 2006.
- [73] S. Sancha, F. J. Cañete, L. Díez, and J. T. Entrambasaguas, "A Channel Simulator for Indoor Power-line Communications," in *Proc. of IEEE Int. Sym. on Power Line Commun. and Its Applications (ISPLC 2007)*, (Pisa, Italy), Mar. 2007.

- 
- [74] J. A. Cortés, A. M. Tonello, and L. Díez, “Comparative Analysis of Pilot-based Channel Estimators for DMT Systems Over Indoor Power-line Channels,” in *Proc. of IEEE Int. Sym. on Power Line Commun. and Its Applications (ISPLC 2007)*, (Pisa, Italy), Mar. 2007.
- [75] S. Guk and S. Bahk, “Rate Adaptation Scheme in Power Line Communication,” in *proc. of IEEE Int. Sym. on Power Line Commun. and Its Applications (ISPLC 2008)*, (Jeju Island, South Korea), Apr. 2008.
- [76] L. Lampe, R. Schober, and S. Yiu, “Distributed Space-Time Coding for Multihop Transmission in Power Line Communication Networks,” *IEEE J. Select. Areas Commun.*, vol. 24, pp. 1389–1400, July 2006.
- [77] A. Host-Madsen and J. Zhang, “Capacity Bounds and Power Allocation for the Wireless Relay Channel,” *IEEE Trans. Inform. Theory*, vol. 51, pp. 2020–2040, June 2005.
- [78] D. Gündüz and E. Erkip, “Opportunistic Cooperation by Dynamic Resource Allocation,” *IEEE Trans. Wireless Commun.*, vol. 6, pp. 1446–1454, Apr. 2007.
- [79] L. Xie and X. Zhang, “TDMA and FDMA Based Resource Allocations for Quality of Service Provisioning Over Wireless Relay Networks,” in *proc. of IEEE Int. Conf. on Commun. (ICC 2007)*, June 2007.
- [80] I. Hammerström and A. Wittneben, “On the Optimal Power Allocation for Nonregenerative OFDM Relay Links,” in *proc. of IEEE Int. Comm. Conf. (ICC 2006)*, (Istanbul, Turkey), June 2006.
- [81] W. Zhang, U. Mitra, and M. Chiang, “Optimization of Amplify-and-Forward Multicarrier Two-Hop Transmission,” *IEEE Trans. Commun.*, vol. 59, pp. 1434–1445, May 2011.
- [82] Y. Li, W. Wang, J. Kong, and M. Peng, “Subcarrier Pairing for Amplify-and-Forward and Decode-and-Forward OFDM-Relay Links,” *IEEE Commun. Lett.*, vol. 13, Apr. 2009.

- [83] W. Ying, Q. Xin-Chun, W. Tong, and L. Bao-Ling, "Power Allocation and Subcarrier Pairing Algorithm for Regenerative OFDM Relay System," in *proc. of IEEE Vehicular Tech. Conf. (VTC-Spring 2007)*, (Dublin, Ireland), Apr. 2007.
- [84] X. Li, J. Zhang, and J. Huang, "Power Allocation for OFDM Based Links in Hybrid Forward Relay," in *proc. of IEEE Vehicular Tech. Conf. (VTC 2009 Spring)*, June 2009.
- [85] E. W. Weisstein, *Sylvester's Criterion*.
- [86] G. Kramer, I. Maric, and R. Yates, "Cooperative Communications," *Foundation and Trends in Networking*, 2007.
- [87] A. Ben-Israel and B. Mond, "What is Invexity?," *Journal Aust. Math. Soc.*, pp. 1–9, 1986.
- [88] D. H. Martin, "The essence of invexity," *Journal of Optimization Theory and Applications*, vol. 47, no. 1, pp. 65–76, 1985.
- [89] G. Giorgi, "Remarks on M. A. Hanson's Paper "Invexity and the Kuhn-Tucker Theorem"," *Int. Journal of Optimization: Theory, Methods and Applications*, vol. 1, no. 1, pp. 72–74, 2009.
- [90] A. M. Tonello and F. Versolatto, "Bottom-Up Statistical PLC Channel Modeling - Part II: Inferring the Statistics," *IEEE Trans. Power Delivery*, vol. 25, pp. 2356–2363, Oct. 2010.
- [91] A. M. Tonello and F. Versolatto, "Bottom-Up Statistical PLC Channel Modeling - Part I: Random Topology Model and Efficient Transfer Function Computation," *IEEE Transactions on Power Delivery*, vol. 26, pp. 891–898, Apr. 2010.
- [92] J. Laneman, D. Tse, and G. Wornell, "Cooperative Diversity in Wireless Networks: Efficient Protocols and Outage Behavior," *IEEE Trans. Inform. Theory*, vol. 50, no. 12, pp. 3062–3080, 2004.

- [93] E. Weisstein, *Bernoulli Inequality*. From MathWorld—A Wolfram Web Resource. <http://mathworld.wolfram.com/BernoulliInequality.html>.
- [94] I. Gradshteyn and I. Ryzhik, *Table of Integrals, Series, and Products*. Academic Press, 1980.
- [95] H. W. Kuhn and A. W. Tucker, “Nonlinear Programming,” in *proc. of Second Berkeley Symp. on Math. Statist. and Prob.* (U. of Calif. Press, ed.), pp. 481–492, 1951.
- [96] J. Dattorro, “Convex Optimization and Euclidean Distance Geometry,” *Meboo Publishing*, 2005.
- [97] R. Andreani, C. Echague, and M. Schuverdt, “Constant-Rank Condition and Second-Order Constraint Qualification,” *Springer, J. Optim Theory Appl.*, Feb. 2010.